University of South-Eastern Norway
Faculty of Technology, Natural Sciences and Maritime Studies

Doctoral dissertation no. 44
2019

Asanthi Jinasena

Models and Estimators for Flow of Topside Drilling Fluid

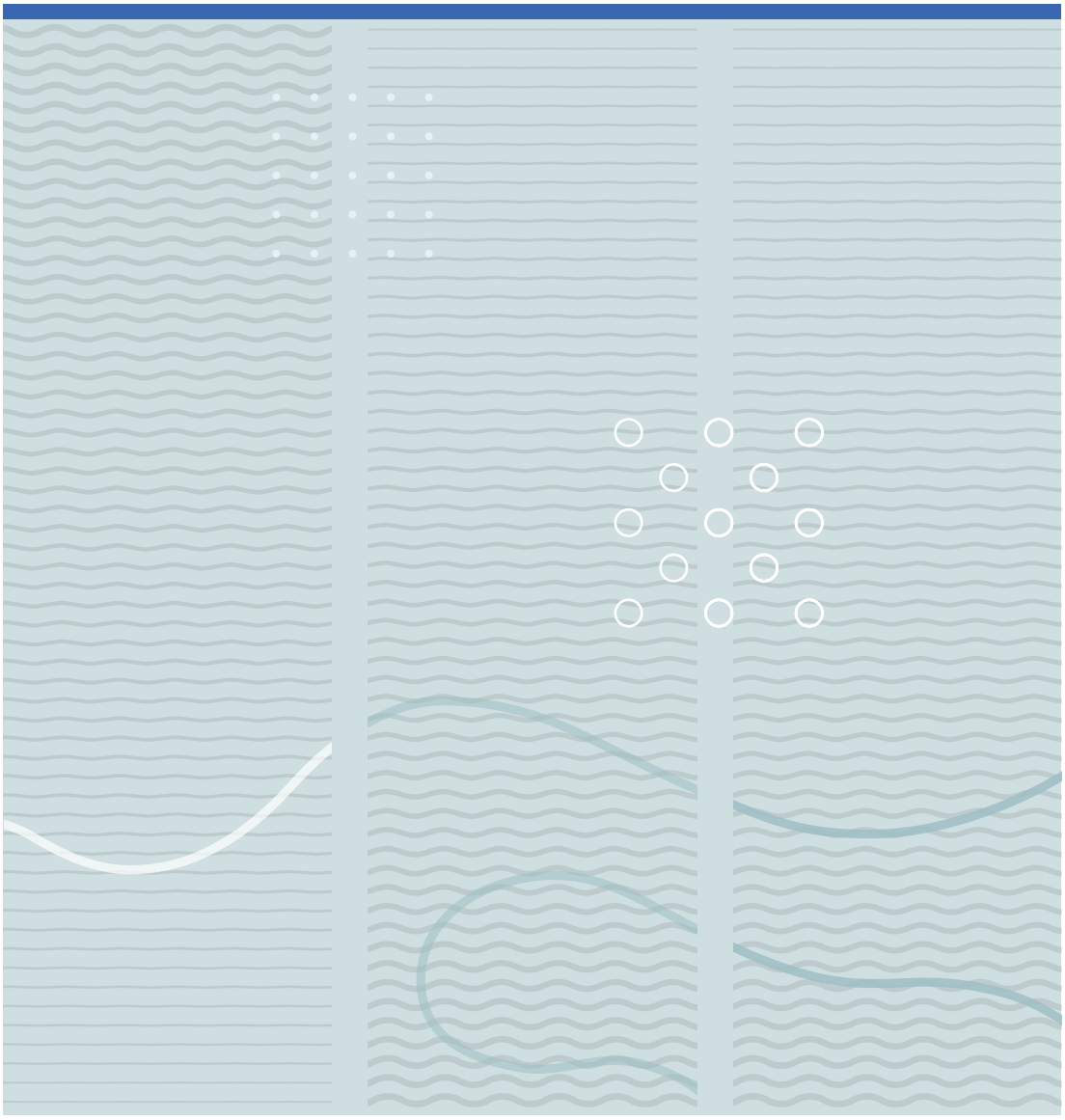

Asanthi Jinasena

Models and Estimators for Flow of Topside Drilling Fluid

A PhD dissertation in
Process, Energy and Automation Engineering

Faculty of Technology, Natural Sciences and Maritime Studies
University of South-Eastern Norway
Porsgrunn, 2019

Doctoral dissertations at the University of South-Eastern Norway no. 44

ISSN: 2535-5244 (print)
ISSN: 2535-5252 (online)

ISBN: 978-82-7206-529-3 (print)
ISBN: 978-82-7206-530-9 (online)

Print: University of South-Eastern Norway

මේ පුදුම පොත කාහට?

දෙමාපිය දෙදෙනට
සෝයුරුද සෝයුරියට
සොඳුරු තරුවට හිරුවට
පුදමි වෙන හැර කාහට!

Dedicated to You!
Yes, YOU!

Preface

This dissertation is written to fulfill the graduation requirements of the degree of Doctor of Philosophy at the Faculty of Technology, Natural Sciences and Maritime Studies at the University of South–Eastern Norway (USN). The dissertation contains the work of the study on mathematical model based real-time flow rate measurement of the return flow and the estimation of fluid losses on the topside of an oil drilling process. It is presented with two main parts, where Part I gives an insight into the background and introduction of the research problem, while Part II contains the main contributions as a compendium of scientific publications.

For the aforementioned achievement, I would like to thank my main supervisor, Roshan Sharma (Associate Professor, USN) and co-supervisor, Glenn–Ole Kåsa (CEO, Kelda Drilling Controls) for their direction, inspiration, guidance, support and the thought-provoking ideas given throughout this work. My gratitude is extended to Christian Leuchtenberg, for initiating the idea of using a Venturi meter for the return flow measurement, which then gave the birth to the project Semi–kidd. The valuable comments and inputs given by the Semi–kidd members led by Bernt Lie (Professor, USN), the financial aid provided by the Research Council of Norway and Equinor ASA, and the industrial visits to Equinor given by Geir Elseth (Project Leader, Equinor) are highly admired. Further, all the partners of the project Semi–kidd are kindly acknowledged. Moreover, It was a pleasure to work at Kelda Drilling Controls AS, Porsgrunn as an intern, under the support and guidance of Glenn–Ole Kåsa (CEO), Geir Arne Evjen (CTO), Christian Berg (Research Engineer) and the cordial fellowship of the entire staff.

I express my appreciation to my co-authors, Ali Ghaderi (Associate Professor, USN) and Ivan Pirir (Ph.D. Student, NTNU) for their valuable inputs, ideas, and insightful discussions. The technical knowledge and the support extended for the operation of the experimental rig, given by Khim Chhantyal (Ph.D., USN), Per Kristian Fylkesnes (Senior Engineer, USN), and Om Prakash Chapagain (M.Sc., USN) are much obliged.

Further, I am grateful for the help and support extended by the staff at USN throughout the project, especially the Department of Electrical Engineering, IT and Cybernetics led by Svein Thore Hagen (HoD) and Randi Toreskås Holta (Former HoD). My thanks to Anushka Perera for the critical input, and Wathsala Jinadasa, Wathsala Perera and Thamali Jayawickrama for the help given during the thesis

writing process. I deeply cherish my colleagues and friends who helped me in many ways, especially Morten Hansen Jondahl, Prasanna Welahettige, and Håvard Holta.

I hope you enjoy your reading!

23rd September 2019

Asanthi Jinasena

Porsgrunn, Norway

Abstract

The reduction of risk and non-productive time in oil drilling is a key research interest in the oil and gas industry. The early detection of kick and loss is a crucial part in safe well control operations, thus, it plays a major role in this regard. Early kick and loss detection is done by incorporating the available pressure data of the bottom side of the well with the available data at the surface on the topside. The data on the topside is mainly the return flow rate and the mud pit level. There are advanced flow measurement techniques available for the clean flow going into the well, which is comparatively easy to measure. On the contrary, the return flow consists of drill cuttings and gases which makes flow measurement difficult and inaccurate. Although there exist many flow meters that can measure the return flow rate, most of the on-shore and off-shore oil rigs still use conventional drilling systems. These conventional drilling processes use intermittent or online return flow rate and density measurements together with mud pit levels for kick and loss detection. There are various flow meters used in these processes, but most of the time paddle flow sensors are used. These have comparatively less accuracy as well as repeatability. In most of the conventional oil rigs, this is just an indicator rather than a real-time flowmeter, thus early kick and loss detection cannot be expected. Advances in flow metering technology will provide accurate differential flow measurements. Therefore, the development of cost-effective, accurate and online sensors for early kick and loss detection is vital.

The development of an efficient model based real-time estimator of the flow rate of the return flow using an open Venturi channel is studied in this research work, such that it can be used as a return flowmeter for early kick detection in conventional drilling. Different mathematical models are investigated for this purpose, and a suitable numerical solver for the models are developed based on the orthogonal collocation for real-time implementation. The effect of different types of drilling fluids and different geometries of channels are studied. The flow rate and various parameters like the friction factors are estimated in real-time using different estimators. The models and estimators are tested against a well-known numerical scheme and verified using experimental results from a test flow loop.

Further, the combination of two kick detection indicators, the return flow rate and the active mud pit level, are investigated in a modeling environment. For this, a combined model which includes both the bottomside and the topside of an oil well drilling process is developed and simulated to study the behavior of these indicators

for different drilling operation scenarios. The model is able to show the bottomside pressure dynamics and the corresponding topside flow dynamics at once. This gives rise to a complete closed-loop model of an oil well drilling. The drilling fluid losses that can occur during the removal of drill cuttings using the solid removal equipment are estimated from these models. With the availability of real-time estimation of drill fluid losses at the top side, the replenishing of the lost mud could potentially be automated.

Keywords: return flow sensor, real-time estimation, open channel hydraulics, reduced order model

List of Publications

Articles: Published and under Review

1. Jinasena, A., Kaasa, G.-O., and Sharma, R. (2017). Use of Orthogonal Collocation Method for a Dynamic Model of the Flow in a Prismatic Open Channel: For Estimation Purposes. In Proceedings of the 58th Conference on Simulation and Modelling (SIMS 58), pages 90–96, Reykjavik, Iceland. Linköping University Electronic Press. https://doi.org/10.3384/ecp1713890

2. Jinasena, A., Ghaderi, A., and Sharma, R. (2018). Modeling and Analysis of Fluid Flow through a Non-Prismatic Open Channel with Application to Drilling. Modeling, Identification and Control, 39(4):261–272. https://doi.org/10.4173/mic.2018.4.3

3. Jinasena, A. and Sharma, R. (2018). Model based Real-Time Flow Rate Estimation in Open Channels with Application to Conventional Drilling. In 18th International Conference on Control, Automation and Systems (ICCAS 2018), pages 546–551, PyeongChang, Korea. http://www.dbpia.co.kr/Journal/ArticleDetail/NODE07549683

4. Jinasena, A., Kaasa, G.-O., Sharma, R. (2019). Improved Real–Time Estimation of Return Flow Rate of Drilling Fluids by Model Adaptation for Friction Parameter. IEEE Sensors Journal, 19(20):9314–9323. https://doi.org/10.1109/JSEN.2019.2923854

5. Jinasena, A., Sharma, R., Adaptive Moving Horizon Estimator for Flow Rate Estimation using Fluid Levels of a Venturi Channel, Under review at IEEE Access

6. Pirir, I., Jinasena, A., and Sharma, R. (2018). A Dynamic Model for Drain Back to Active Mud Pit Combined with a Well Model During Drilling. Journal of Petroleum Science and Engineering, 167:803–818. https://doi.org/10.1016/j.petrol.2018.04.057

7. Jinasena, A., Sharma, R., Estimation of Drilling Fluid Losses during the Removal of Drill Cuttings in Topside of a Drilling Operation, Submitted to SPE Journal

Other Contributions

1. Pirir, I., Jinasena, A., and Sharma, R. (2017). Model Based Flow Measurement using Venturi Flumes for Return Flow during Drilling. Modeling, Identification and Control, 38(3):135–142. https://doi.org/10.4173/mic.2017.3.3

Contents

List of Figures

List of Tables

List of Acronyms and Symbols

Acronyms

ADP	Annular Discharge Pressure
AI	Artificial Intelligence
BHP	Bottomhole Pressure
BOP	Blowout Preventer
ECD	Equivalent Circulating Density
EKD	Early Kick Detection
EKF	Extended Kalman Filter
KDV	Kick Detection Volume
KP	Kurganov–Petrova Method
LKF	Linear Kalman Filter
LO	Linear Observer
MHE	Moving Horizon Estimator
MPD	Managed Pressure Drilling
OC	Orthogonal Collocation
ODE	Ordinary Differential Equations
OSPAR	Protection of the Marine Environment of the North-East Atlantic
PDE	Partial Differential Equations
PVT	Pit Volume Totalizer

RMSE	Root Mean Squared Error
SPP	Standpipe Pressure
SVE	Saint–Venant Equations
SWE	Shallow Water Equations
UKF	Unscented Kalman Filter

Greek Symbols

α	Average Coriolis/energy coefficient
β	Momentum correction coefficient
ν	Kinematic viscosity
θ	Channel slope angle with the horizontal axis

Roman Symbols

A	Wetted cross sectional area of flow in the channel
A_m	cross-sectional area of the mud pit
f	Fanning friction factor
Fr	Froude number
g	Acceleration of gravity
h	Depth of flow
h_c	Critical fluid level
h_m	Mud pit level
I_1	First moment of area
I_2	Second moment of area
L	Length of the channel
L_c	Characteristic length
Q	Volumetric flow rate in the channel

q	Lateral in or out flow rate
q_{in}	Inflow rate of the mud pit
q_{out}	Outflow rate of the mud pit
Re	Reynolds number
S_b	Channel bed slope
S_f	Friction slope
t	Time
u	Mean velocity
u_p	Velocity at a certain point
w	Width of the channel at an arbitrary level $\bar{z}$
x	Differential length along the flow direction
z	Absolute fluid level
$\bar{z}$	An arbitrary level

Part I

Overview

1 Introduction

1.1 Background

Oil well drilling operations are prone to high risks. Especially, the high risks are associated with offshore and deepwater drilling operations. Dealing with high operational pressures, temperatures, and the presence of uncertainty are some of the main factors which make drilling very risky. Generally, pressure related problems in drilling are high contributors for both risk and cost. Hence, reduction of risk and cost in oil drilling is a key research interest in the oil and gas industry.

1.2 System Description

A typical oil well drilling process is shown in Figure 1.1. The drilling is done by penetrating a rotating drill bit into the rock formation, creating a wellbore. The formation is a high pressure and temperature environment. Therefore, a liquid known as drilling mud is continuously circulated through the wellbore. This circulation process is usually divided into two parts; bottomside and topside. The bottomside is the wellbore and the connected sections, whereas the topside is the section on the surface. The topside consists of the mud pump, standpipe, mud line, shale shaker, and mud tanks. The mud line is also known as the return flowline or drain back flowline. The drilling mud coming out of the wellbore contains the broken rock formations known as drill cuttings. These drill cuttings are separated through shale shakers in order to clean the drilling mud before circulating back. Therefore, the shale shakers and the connected equipment are known as the solids control system. The clean mud tank which is connected to the mud pump is known as the active mud pit.

One of the main purposes of using drilling mud is to maintain the pressure inside the wellbore. Normally, the wellbore pressure is created by the pressure exerted by the drilling mud column. This wellbore pressure can fluctuate due to drilling operations, especially due to the start and stop of the mud pump and due to sudden vertical movements of the drill pipe.

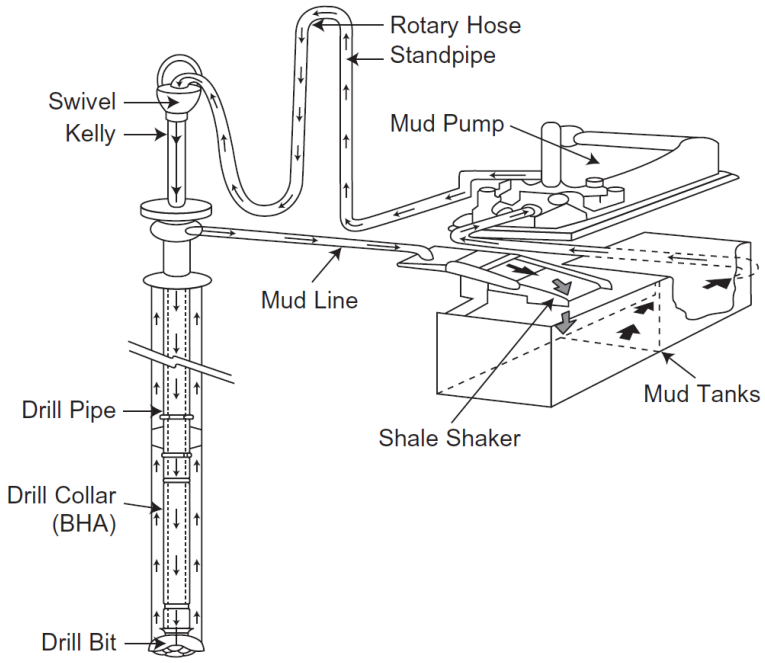

Figure 1.1: A typical drilling mud circulating system (Figure 1.1 in Guo and Liu, 2011, p. 4). Here BHA is the bottomhole assembly.

The pressure in the wellbore needs to be maintained within a pressure window for safe operation. When the wellbore pressure becomes lower enough than the formation fluid pressure, formation gas or liquid may suddenly enter into the wellbore. This phenomenon is commonly referred to as a 'kick' which could result in a catastrophic blowout if not controlled properly. If the wellbore pressure increases than the fracture pressure of the formation, the drilling mud may seep into the formation, which is known as a 'loss'. This phenomenon could result in wellbore damages and loss of the drilling mud by potentially reducing the productivity of the formation, which leads to both financial and environmental problems.

1.3 Importance of Return Fluid Flow Measurements

The early detection of kick and loss is a crucial part of safe well control operations. A recent study done in the Norwegian Continental Shelf shows that 13 % of the causes for well control incidents are due to technical failures of, or imperfect kick detection (Carlsen et al., 2011).

The most common kick and loss detection method that is used today is the delta flow measurement together with the mud pit gain (Fu et al., 2015). The delta flow is the net difference between the flow pumped into the well and the flow coming out of the well through the drain back flowline (see Figure 1.2). The delta flow has a direct

relationship with the wellbore pressure, thus effective as a kick and loss detection method.

There are advanced flow measurement techniques available for the clean mud pumped into the well, which is comparatively easy to measure since its rheological properties are known in advance. On the contrary, the outflow (also known as the return flow) consists of drill cuttings and gases which makes flow measurement difficult and inaccurate. There are flow metering technologies that can accurately measure the return flow, such as Coriolis flowmeters. However, these are expensive and may not be accurate enough for return flow in the presence of gasses. Although there are advanced drilling systems such as the managed pressure drilling (MPD) that uses the Coriolis flowmeters as return flowmeters, most of the onshore and offshore oil rigs still use conventional drilling systems. These conventional drilling processes use intermittent or online return flow rate and density measurements together with mud pit levels for kick and loss detection. There are various flowmeters used in these processes, but most of the time paddle flow sensors are used. These have comparatively less accuracy as well as repeatability. In most of the conventional oil rigs, the paddle flow sensor is just an indicator rather than a real-time flowmeter, thus early kick and loss detection cannot be expected. Advances in flow metering technology can provide accurate differential flow measurements. Therefore, the development of cost-effective, accurate and online sensors for early kick and loss detection is vital.

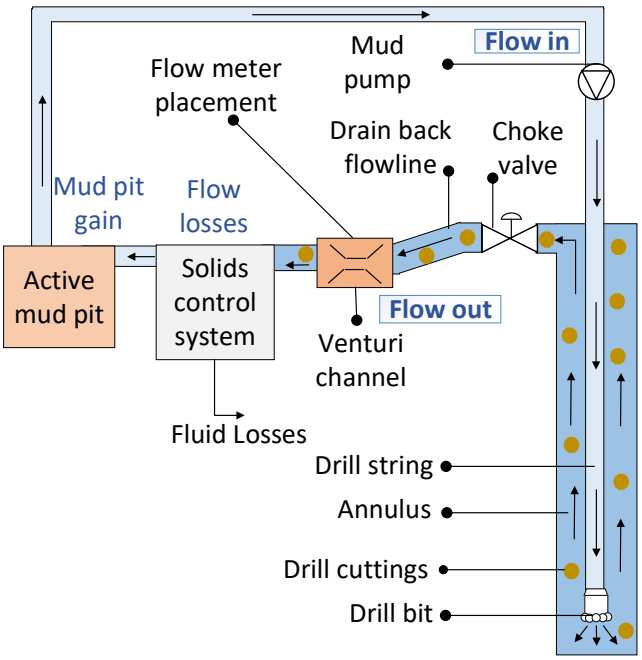

Figure 1.2: The placement of a Venturi channel as an outflow meter in the topside of a drilling mud circulating system.

Thus, real-time estimation of the return fluid is important for kick and loss detection algorithms. Equally, it is important to study the dynamics of the fluid flow in the drain back flowline. This PhD study focuses on the development of models and estimators for monitoring and measuring the return flow of drill mud at the topside of an oil well drilling. Figure 1.2 shows a suitable placement of a flow sensor on the drain back flowline. Although in general, the return flow line is a closed circular pipe, the fluid flow through this line normally operates under atmospheric pressure. Hence, the return flowline can be considered as an open channel flow.

1.4 Research Objectives

This PhD study which is a part of the project Semi–kidd (Sensors and models for improved kick/loss detection in drilling) focuses on developing novel flow measuring methods for oil drilling. This probably can enable enhanced control and monitoring during oil well drilling, allow the development of early problem detection, and reduce non-productive time in drilling operations. The project has been funded by the Research Council of Norway and Equinor ASA, and lead by the University of South–Eastern Norway.

The central idea proposed in this project is the use of an open Venturi channel as an alternative to existing flow meters as shown in Figure 1.2. The Venturi flowmeter can be used to accurately measure the return flow rate in real-time. The information about the return flow rate can potentially be used as an online soft sensor for early kick and loss detection. For sections with higher flow rates, the Venturi meter could provide a more accurate volumetric flow rate than the paddle flow meters. Further, the Venturi channel is non-intrusive and easy to maintain. Therefore, a Venturi flowmeter has the potential to replace the existing flow meters in conventional drilling processes. The possibility of developing an online flow sensor with the use of Venturi effect in open channel flow has been studied recently by Berg et al. (2015); Chhantyal et al. (2016b); Chhantyal (2018); Welahettige et al. (2018); Chhantyal et al. (2018). Thus, the development of an efficient, model-based, real-time estimator for the flow rate of the return flow is the main aim of this research task.

The main objectives are as follows.

- Development of a mathematical model that can be used for estimation of the flow rate through a Venturi channel.
- Development of a suitable estimator for the estimation of flow rate using the level measurements of the Venturi channel. The estimator should be adapted for unknown and time-varying parameters such as the friction factor.

- Development of a topside model for fluid flow which can be combined with the model of the oil well at the bottomside. The model should be used for studying the flow dynamics at the topside when the dynamics at the bottomside change due to various drilling operations.
- Development of a suitable estimator for the estimation of drilling fluid losses during the drill cuttings removal.

1.5 Main Contributions

The work done to achieve the stated objectives is listed here. Each main contribution is presented as one or more articles in Part II. Whenever the articles do not contain all the necessary details, the additional details are presented before each article.

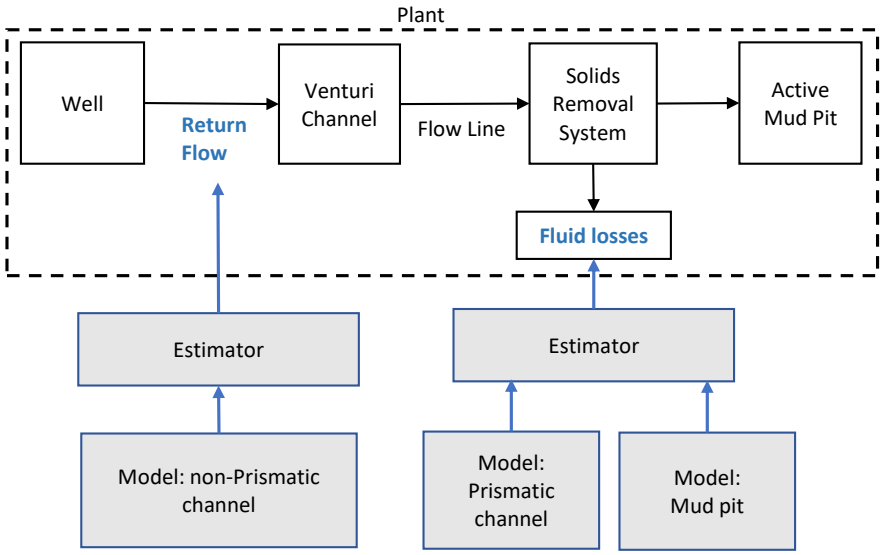

Figure 1.3: An illustration that shows the interconnections of different contributions that are included in the thesis.

1. Development of a numerical method to reduce a mathematical model of fluid flow of a prismatic channel, such that it can be used in real-time flow rate estimation: Article A

   Orthogonal collocation (OC) method was used to reduce the model, with different numbers of discretization points and positions. The model is validated using the full order model solved by the Kurganov-Petrova (KP) method.

2. Development of a numerical method to reduce a mathematical model of fluid flow of a Venturi channel (non-prismatic channel), such that it can be used in real-time flow rate estimation: Article B

The OC method was used to develop the reduced order model with selected discretization positions and different numbers of discretization points. The model is validated using the full order model solved by the KP method (for two possible flow conditions and different boundary conditions). Further, a sensitivity analysis was done for both OC and KP methods. Both methods are validated using the experimental results.

3. Estimation of the fluid flow rate using the reduced order model of the Venturi channel: Article C

   Different model-based estimators were developed based on the reduced order mathematical model and the results were validated using experimental data.

4. Fluid flow rate and friction parameter estimation using a modified model of the Venturi channel: Article D and E

   The Venturi channel model is modified by using different Newtonian and non-Newtonian friction models and an unscented Kalman filter (UKF) was developed for each friction model. The validation of estimators was done using experimental data. A moving horizon estimator (MHE) was developed for selected friction models (for Newtonian and non-Newtonian fluids) with constraints on each friction parameter and the results were validated using experimental data. Further, the effect of the most sensitive parameter (channel bottom slope) on the results were tested.

5. Development of a mathematical model for top flow loop including the bottomside of the well: Article F

   Developed a model for the entire top flow loop for a MPD system including the bottomside, drain back flowline, solids removal system, and mud pit. The models are simulated for different drilling operations.

6. State and parameter estimation using the topside flow model: Article G

   The topside flow model is modified with the inclusion of fluid losses from the solids removal system, OC method is developed for the flowline and is validated using KP method. A UKF and MHE are developed for the topside model for estimating fluid losses and the return flow rate (excluding the bottom side from estimation) and simulated for different drilling operations.

1.6 Structure of the Thesis

The PhD thesis is presented as a compendium of scientific publications, which consists of two main parts. Part I is the synopsis of the research work, that comprises of five chapters to provide a broad overview of the research. Chapter 1 of Part I

includes a system description, the research problem, and the main objectives. The main contributions are also listed in this chapter. A literature review on previous work and background knowledge on the rotary drilling process, kick detection, open channel flow and estimation are included in detail in Chapter 2. The methods and approaches of model development, solution methods, and estimation methods are summarized in Chapter 3. The detailed description of the experimental setup and procedure is given in Chapter 4 of Part I. The conclusions that are drawn from the research work, the limitations of the study and recommendations for improvement are stated in Chapter 5, followed by the Bibliography.

Part II, which is the main part of the thesis is a collection of scientific articles that have either been already published or are currently under review. Before each article, additional information regarding the respective article is presented for a better understanding.

2 Literature Review

2.1 Introduction

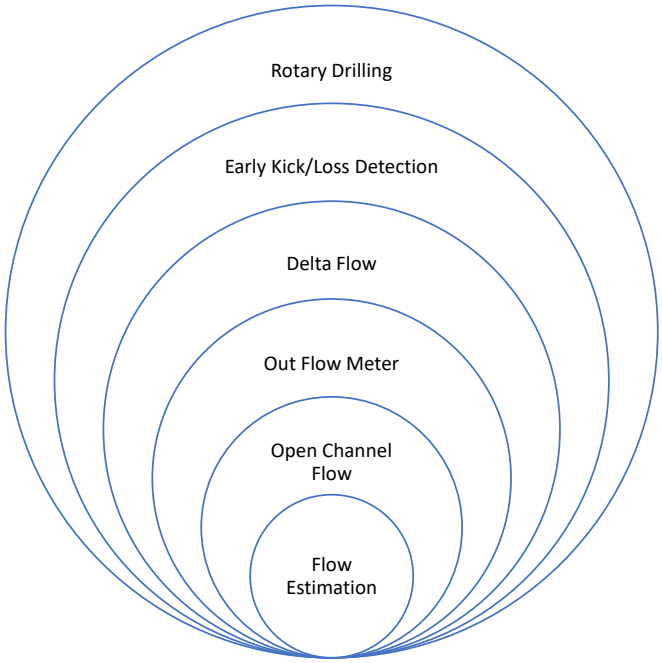

Figure 2.1: A graphical map for the contents of literature review.

The chapter is composed as shown in Figure 2.1 focusing on the necessary background knowledge. Drilling is widely considered as one of the oldest technologies in the world. Petroleum drilling is the main branch of drilling as petroleum products still are the driving force of today's energy sector in the world. Since the start of the oil drilling in the mid-1800s, petroleum drilling technologies have advanced throughout history, economically, efficiently and sustainably. This is a brief insight into these technologies.

Usually, the life cycle of petroleum products starts from exploration, drilling, completion, production and then to refining and transportation to the end user. There are different types of drilling wells in the drilling stage.

Exploration wells First, the exploration is done by making a few exploration wells to determine the viability of the reservoir. It is the well that helps to determine the presence of hydrocarbons. On average, only one in eight North Sea exploration wells are successful (Hossain and Al-Majed, 2015).

Appraisal wells If exploration well is successful, then drilling of the appraisal wells will be commenced to establish the extent of the reservoir.

Abandonment wells If no hydrocarbons are found, the exploration well or the appraisal well needs to be sealed and closed to prevent possible environmental disaster and this is called an abandonment well.

Development wells If hydrocarbons are found and the size is estimated, then finally, the development wells will be commenced to extract the hydrocarbons. The development well is drilled in a production field or in an area to extract natural gas or crude oil. From here onwards, the words 'drilling' and 'well' refer to the drilling of the development wells.

Generally, the drilling sequence contains three major steps; *i.e.* 1) the initiation and acceleration of the drilling of a hole on the surface of the earth, 2) the casing and cementing operations to fix the hole, and 3) the completion of the well. Usually, drilling of a well in the petroleum industry is done by different techniques such as rotary drilling, percussion or cable drilling and jet drilling. Percussion or cable drilling is largely obsolete in oil drilling, although it is still used to drill water wells (Patel, 2019). Jet drilling is an emerging technology, where a high-pressure liquid or gas jet is used to drill the rock formations (Fang and Duan, 2014; Khan and Islam, 2007). Rotary drilling, on the other hand, is conventional and yet still largely used in the industry. Rotary drilling uses a sharp rotating drill bit to drill and a fluid is used to remove the drill cuttings. The rotary drilling process is stated in detail under different topics of interest.

2.2 The Rotary Drilling Process

A rotary drilling system consists of multiple subsystems of various specific tasks. An overview of some of the equipment and systems on a conventional rotary drilling rig is shown in Figure 2.2, showing the hoisting system, the drill string with the bottomhole assembly and drill bit, the drilling fluid circulation system and the blowout preventer (BOP). The hoisting system; a crane and a pulley system are used to lift and lower the rotating drill bit from and into the ground. The drill bit is attached to the bottom-hole assembly, that consists of a drill string which is a

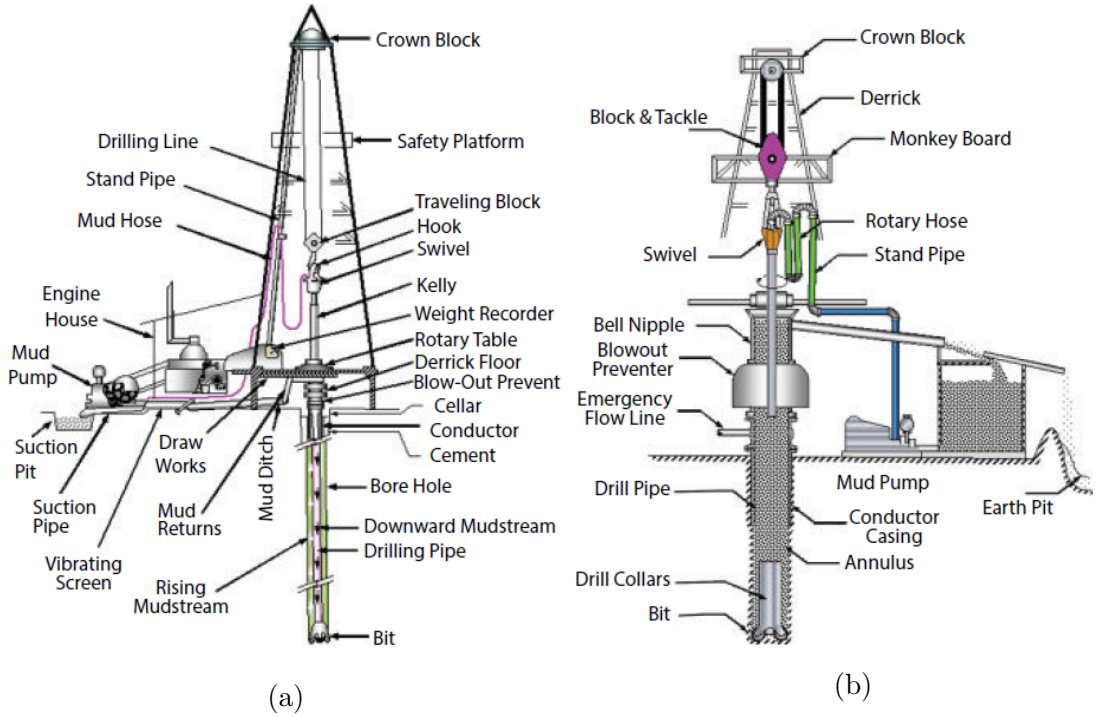

Figure 2.2: A conventional rotary drilling rig showing different components (a) on top of the surface and (b) under the rotary table (Figure 2.4 in Hossain and Al-Majed, 2015, p. 21).

drill pipe and a drill collar. These are rotated by the rotary table. As the drilling progresses, new sections of drill pipe assembly are added on the rig floor. When the drill bit wears out, the drill bit is replaced by pulling out the entire drill string. The BOP is a large valve installed on the wellhead to control the pressure in the annular space between the casing and drill pipe. The BOP is one of the main safety features in a drilling rig, where it stops influxes from the formation releasing to the surface. Usually, BOP acts as the second barrier for influxes and a series of BOPs are stacked together to allow the drill string to move through a closed well (Willersrud, 2015). The drilling rig must also be able to perform the other necessary functions such as circulating drilling fluids.

Most of these components in a rotary drilling rig can be categorized into four different subsystems which are interconnected and drives the whole drilling operation, named as the power system, the hoisting system, the circulation system, and the rotary system (Hossain and Al-Majed, 2015). The draw-works, mud pumps and rotary table are the main components of the power system, while the swivel, kelly/top drive, rotary table, rotary drive, drill pipe, and drill collars fall under the rotary system. The main components of a hoisting system are derrick and substructure, draw-works, and block and tackle. The circulation system is the closed-loop drilling fluid flowing system from mud pumps to the bottom-hole through the drill bit and then up to the surface and back to mud pump through various cleaning equipment.

More details on this circulation system will be explained in further topics.

2.2.1 Different Drilling Processes

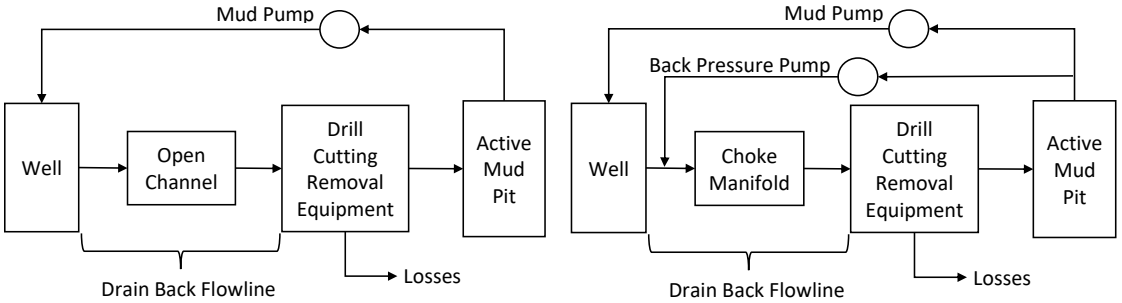

Figure 2.3: Block diagrams of (a) a conventional drilling and (b) a MPD process

Usually, the drilling systems are categorized into conventional and unconventional drilling, based on the methods of control of the bottomhole pressure (BHP). In conventional drilling, the well is open to the atmosphere at the top and the pressure is maintained using mainly the hydrostatic and circulating pressures of the drilling fluid. If the well is drilled with a BHP above the pore pressure, it is drilled overbalanced, which is the conventional way of drilling. If the well pressure is intentionally kept lower than formation pore pressure, the well is drilled underbalanced.

The topside is the surface section of a drilling rig with the exclusion of the bottomhole activities, thus the pressure control devices are operated from the topside. The main components in a conventional and MPD topside drilling processes can be seen in Figure 2.3. The flow of the drilling fluid is the main focus here, where the drain back/return flowline from the bell nipple, the solids control system, and the mud pit are the major components. Since the conventional drilling doesn't have any pressure control other than the hydrostatic pressure, pump and the friction pressure by circulating the drilling fluid, the drilling fluid directly flows into the return/drain back flowline after the bell nipple. However, in the MPD system, the BHP is controlled by the back pressure pump and a choke assembly. Therefore, right after the bell nipple, the drilling fluid flows through the choke manifold before the return flowline. This is based on the handling of the BHP in various drilling systems.

2.2.2 Bottomhole Pressure

The pressure at the bottom of the wellbore, which is usually known as the bottomhole pressure needs to be properly controlled/maintained for a safe drilling operation.

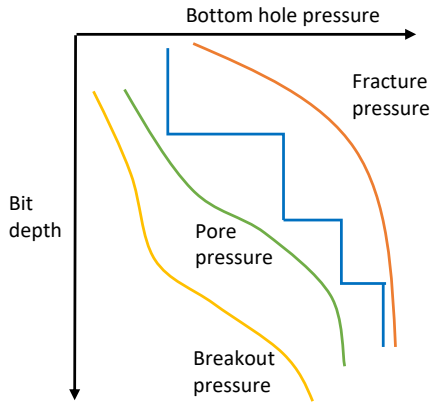

Figure 2.4: A drilling window.

Therefore, the drilling must be performed by maintaining the BHP to lie inside a drilling window which is shown in Figure 2.4. To prevent any inflow of formation fluids the BHP must exceed the pore pressure, which is the pressure exerted by the fluids in the pores of the formation. The pore pressure depends on the depth of the porous formation, the density of the formation fluids and the geological conditions. The BHP must also be higher than the breakout pressure of the formation, to avoid any collapsing of formation into the hole that was just drilled. If BHP exceeds the fracture pressure, the formation could fracture causing the drilling fluid losing into the fractures (Caenn et al., 2017). The wells are designed in a way that each time this drilling window becomes narrowed down closer to zero, a new casing string is set. This allows targeting a particular group of formations at a given time, where predetermined hydrostatic and circulating pressure profiles can be maintained not to exceed the defined drilling window boundaries.

In a conventional drilling system, there are two main pressure profiles, the static pressure due to the hydrostatic pressure of the drilling fluid and the dynamic or circulating pressure due to the hydrostatic pressure plus the pump pressure necessary to circulate the fluid into the wellbore. This is also known as the equivalent circulating density (ECD). Because the two main pressure profiles have limitations, conventional drilling cannot operate in narrow drilling windows. Apart from these two, pipe rotation, cuttings load and the drill bit depth can affect the BHP. These pressure profiles are shown in Figure 2.5.

However, MPD has the ability to adjust the surface pressure in order to fit the BHP profile within the drilling window, which allows drilling through narrow drilling windows. The conventional hydrostatic pressure is no longer a constraint as extra pressure can be applied to BHP from the topside (such as back pressure and/or choke pressure), creating a different pressure profile when pumps are off, which is known as equivalent static density (Chin, 2012). For both conventional and MPD systems, the drilling fluid needs to be properly maintained for a successful operation.

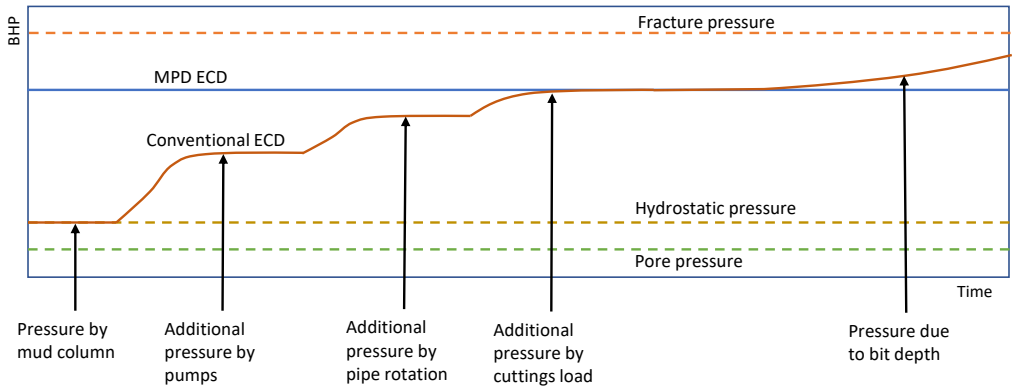

Figure 2.5: The changes of conventional ECD according to various factors. MPD ECD is also shown here and kept at the desired level by changing the back pressure pump.

2.2.3 Drilling Fluid

The principal purposes of the drilling fluid in a rotary drilling system can be listed as follows (Caenn et al., 2017; ASME Shale Shaker Committee, 2005),

1. Keep the wellbore pressure within the required pressure limits to prevent the kicks and losses: This is controlled by the density of the fluid and the ECD. The ECD is a combination of the hydrostatic pressure exerted by the fluid column in the wellbore and the added pressure that is needed to pump the fluid up the annulus of the wellbore.

2. Lift and transport the drill cuttings to the surface and allow cuttings to be separated from the liquid: This is done by manipulating the viscosity of the fluid in order to obtain a good transport efficiency in the wellbore annulus and to ensure good efficiency of solids control equipment.

3. Suspend solids: This is controlled by the effective viscosity and gel strength of the fluid to minimize settling of particles under both static and dynamic flow conditions.

4. Form a thin film which can seal any openings in the permeable formation that is being penetrated by the drill bit: This is done by monitoring the particle size distribution of the solids and maintaining the proper wellbore strengthening materials in the fluid.

5. Maintain the stability of the uncased sections of the wellbore: This is done by monitoring the mud weight and mud/wellbore chemical reactivity to maintain the integrity of the wellbore until the next casing is placed.

The use of fluids in the drilling process has the following added advantages,

- Lubricate the drill string and drill pipe particularly when it wears against the sides of the well,
- Cool and clean the drill bit, and
- Transport the data and information from the wellbore to the surface.

Composition of Drilling Fluids

These drilling fluids consist of a base fluid, solids, and additives. The base fluid is either a water-based, non-aqueous based (oil or synthetic) liquid or a pneumatic fluid (see the classification in Figure 2.6), while solids can be either active or inert. The type of solids and its concentration in mud influences many factors such as drilling rate, hydraulics, dilution rate, torque and drag, surge and swab pressures, differential sticking, lost circulation, hole stability, and balling of the bit and the bottomhole assembly (ASME Shale Shaker Committee, 2005). The additives are used to control the mud weight, viscosity, fluid losses, and the chemical reactivity of the fluid system. Some of the additives for water-based, brine-based and oil-based fluids can be tabulated as shown in Table 2.1, according to the fluid property that is meant to be controlled by adding the stated additives (Caenn et al., 2017).

There exists a large number of drilling fluid formulations. However, a suitable drilling fluid for a particular drilling system will be selected after careful considera-

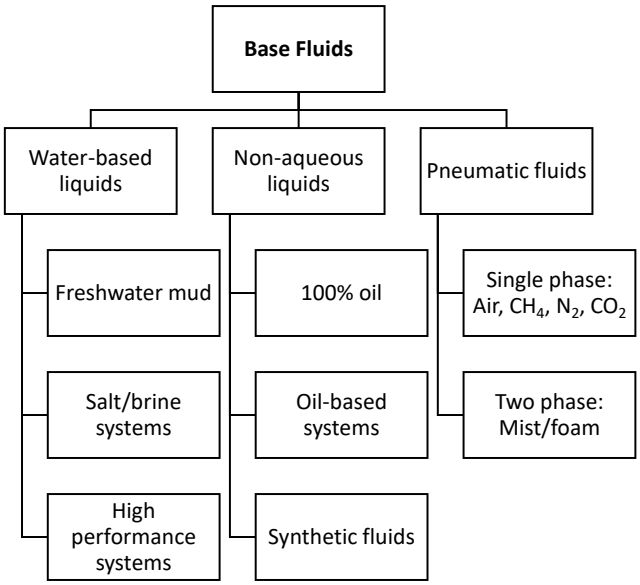

Figure 2.6: Classification of drilling fluid systems by their base fluid (Caenn et al., 2017).

Table 2.1: Different drilling fluid formulations: Additives for water-based, brine-based and oil-based fluids

Base fluid	**Mud weight**	**Viscosity**	**Fluid loss**	**Chemical reactivity**
Clear water, bentonite, calcium based, potassium based	barite, calcium carbonate	bentonite, polymers, thinners, flocculants, deflocculants	bentonites, polymers	pH, alkalinity, lubricity, contamination control, surfactants
Chlorides, sodium, potassium, calcium, sea water, lime, silicates	Barite, calcium carbonate, salt	pre-hydrated clay, attapulgite, xanthen gum, modified starch	pre-hydrated clay, calcium carbonate, starch, microcellulose	caustic soda, surfactants, emulsifiers, lubricants, defoamers
Diesel oil, mineral oil, vegetable oil, olephins	Barite, hematitie, illmenite, calcium carbonate, formates	organophyllic clay, fatty acids, sulphonated polystyrene	organophyllic lignite, asphalt, calcium carbonate, microcellulose	brine water, lime, emulsifiers, wetting agents, surfactants

tion of the well costs, formation evaluation, productivity and the risk of catastrophes, such as wellbore instability, stuck drill pipe, loss of circulation, and gas kicks.

Rheology of Drilling Fluids

Most of the drilling fluids are non–Newtonian in behavior, specially shear-thinning (pseudoplastic) behavior. Generally, non–Newtonian models which use two or three parameters are used to model these fluids. Commonly used three-parameter models in the drilling industry are Robertson– Stiff, Collins–Graves, and Herschel-Bulkley models (Gjerstad and Time, 2015; Weir and Bailey, 1996; Bailey and Weir, 1998). However, other models such as the Newtonian model, the Bingham plastic model, the power law or Ostwald–de Waele model are also being used by drilling engineers to approximate the drilling fluid behavior (Mitchell and Miska, 2011). Some of these models are represented graphically in the rheogram shown in Figure 2.7. There is no general rheological model which will suit all types of drilling fluids. However, the Herschel- Bulkley model has a wide acceptance throughout the industry and have the American Petroleum Institute recommendation (API RP 13D) (Gjerstad and Time, 2015).

Further, drilling fluids are usually dependent on shear time (thixotropic) (Mitchell and Miska, 2011). The thixotropic behavior of drilling fluids is rarely modeled mathematically. Livescu (2012) has reviewed the mathematical modeling done on thixotropic drilling fluids so far. However, these studies are based on well conditions and/or pipe flow (Reed and Pilehvari, 1993; Negrão et al., 2011; Mitchell and Miska,

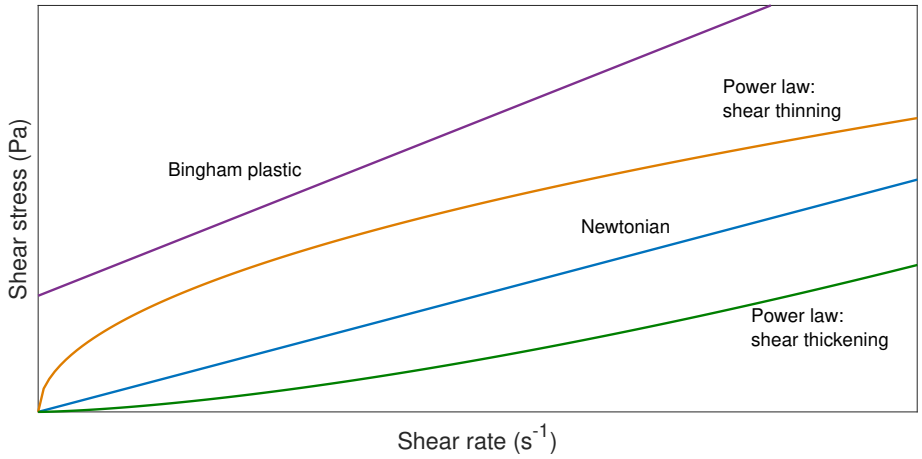

Figure 2.7: A typical rheogram for general drilling fluids.

2011; Livescu, 2012; Gjerstad and Time, 2015), and there are no explicit models developed for open flow. Usually, complex rheological models are accepted as more accurate when predicting the rheological behavior of drilling fluids (Livescu, 2012).

2.2.4 Solids Control System

The ability to predict, maintain and control the fluid densities and rheologies are critical for keeping wellbore integrity intact, thus improving the drilling efficiency and overall performance. This fluid consistency is ensured by the effective operation of the solids control system. The solids control system is the process of cleaning and recovering the drilling mud before returning it back to the drilling system. This is also known as the 'solids removal system' or 'solids handling system' in the industry. The purpose of a solids control system is to remove drill cuttings from the drilling fluid in order to maintain the required rheology of the drilling fluid. Fine particles that are created due to the breakdown of larger drill cuttings when they pass through various separation equipment, contaminate the drilling fluid. Therefore, the solids control system limits the mechanical degradation of the cuttings and maximizes the removal of solids from the drilling fluid. This helps to lower fluid dilution rates, decrease the volume of required additives, achieve higher flow rates, and reduce fluid degradation, which would result in a holistic reduction of the cost of fluid property maintenance and reduction of transportation and disposal of solid and liquid waste.

The equipment for solid removal is selected based on the drilling fluid, formation characteristics, equipment available on the rig, and the specific cuttings disposal requirements (Charles and Sayle, 2010). The process consists of a series of separation equipment which is designed to remove coarse to fine-grained solids, sequentially.

Table 2.2: Classification of solids particles in a drilling fluid (Table 2.2 in ASME Shale Shaker Committee, 2005, p. 26).

Category	**Size (μm)**	**Types of solids**
Colloidal	< 2	Bentonite, clays, ultra-fine drilled solids
Silt	2–74	Barite, silt, fine drilled solids
Sand	74–2000	Sand, drilled solids
Gravel	> 2000	Drilled solids, gravel, cobble

The solids in drilling fluid are categorized into different types based on their particle size as shown in Table 2.2. The type of equipment that can be used for each particle size is different (see the Figure 2.8). In general, these equipment are shale shakers, centrifuges, de-silters, de-sanders, dryers, Gumbo removal equipment, cyclones, de-watering, and de-gassing systems. These equipment are installed on top of the series of mud tanks as shown in the typical solids control system in Figure 2.9. Usually, to improve the efficiency, a series of shale shakers are used which are called primary, secondary and/or tertiary shale shakers. The term shale shaker in a drilling system can mean a shaking screen, vibrating screen, oscillating screen or a combination of these (Guo and Liu, 2011; ASME Shale Shaker Committee, 2005; American Association of Drilling Engineers, 1999).

The amount of retention fluid that adheres to the drill cuttings depends on the solids control equipment and their efficiency, the particle size of the cuttings, and the type of drilling fluid. The methods of determining the quantity of drilling fluids that are lost on drilled cuttings are limited in the current industry. Usually, a bulk measurement is taken by the retort on the retention of mud on cuttings, but this method is of limited accuracy and chemical specificity (Hughes et al., 1991).

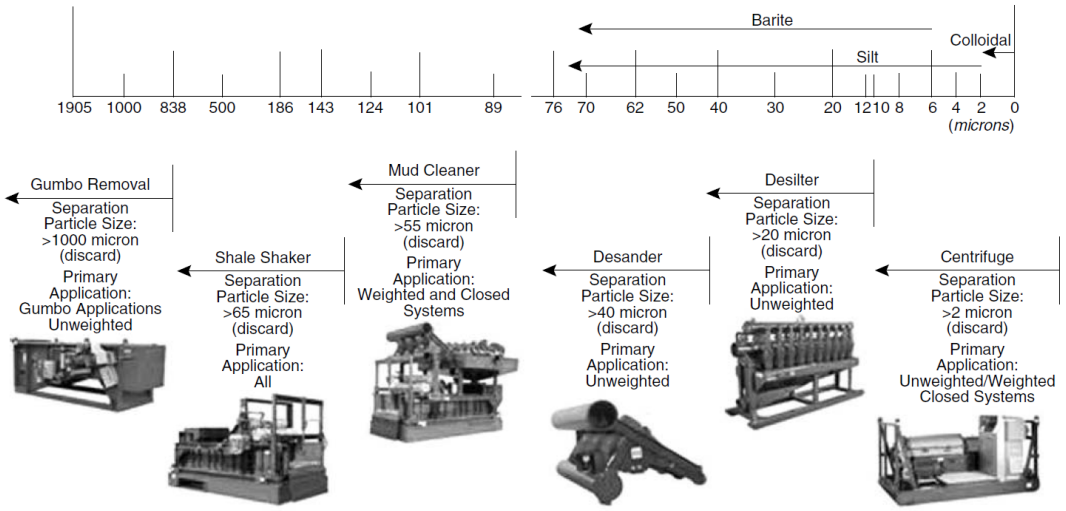

Figure 2.8: The capabilities of general solids control equipment (Figure 5.2 in ASME Shale Shaker Committee, 2005, p. 97).

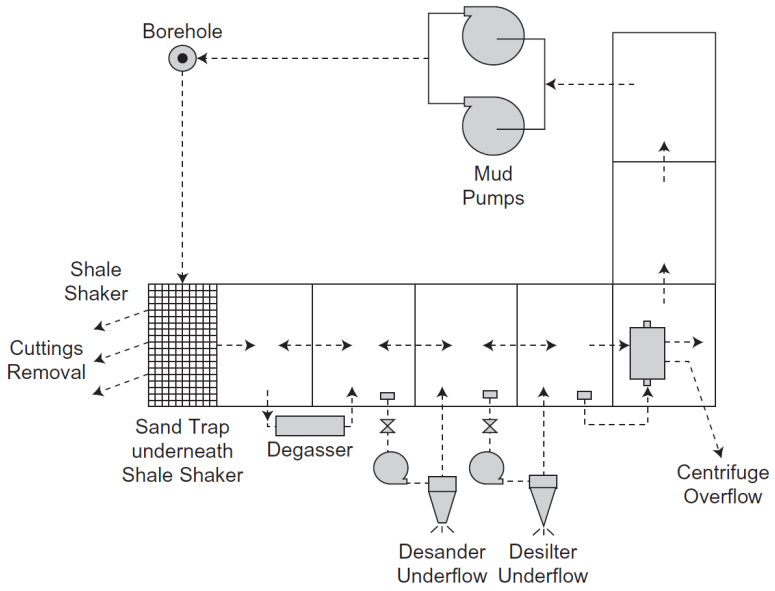

Figure 2.9: Solids removal equipment in a typical solids control system (Figure 1.12 in Guo and Liu, 2011, p. 11).

The cuttings are further treated to remove the drilling mud that is attached after the solids control system before discharging. How much drill mud is removed from treatment is based on the discharge standards. There are different discharge standards in place for different countries under international and regional conventions related to environmental control and regulations, such as the convention for the protection of the marine environment of the North-East Atlantic (OSPAR convention), marine emergency mutual aid centre (MEMAC) and Barcelona convention. It is generally permissible to release cuttings with water-based drilling fluids. However, according to OSPAR convention, cuttings with synthetic and oil-based drilling mud should be treated before discharge. In Norway, oil-based drill cuttings are allowed to be discharged, if the cuttings have less than 1 % oil weight attached to the dry cuttings. In recent years, Norway has stopped discharging oil-based cuttings into the sea, as a result of establishing a zero-discharge target in 1997, for hazardous substances released by petroleum activities (Caenn et al., 2017; Veil, 2002; Taylor et al., 2018).

2.2.5 Drilling Incidents

The smooth drilling operation via proper BHP maintenance or control is generally associated with different drilling operations and incidents, because these can cause pressure variations inside the well.

Influx of formation fluids (kick)

An influx can occur when the BHP drops below the formation pore pressure. The fluid is forced through the permeable pore structure into the well. If it contains gases, the density of the drilling fluid could change significantly. The gases tend to travel upwards where the pressure reduces gradually, which can cause the gas volume to increase and thereby further reduce the fluid density. With reduced density, the BHP will reduce further causing more influx from the formation into the well, which is known as 'drawdown' (Willersrud, 2015). A kick is a severe incident that needs to be either prevented or identified early and controlled.

If a kick is detected the actions that need to be taken are shutting the well in, stopping the pump and closing the BOP around the drill string. Then the kick handling operation must take place, which includes circulating the kick out and replacing the drilling fluid with a heavier kill mud (Willersrud, 2015). An uncontrollable kick is known as a blowout, which is catastrophic.

Lost circulation (loss)

Loss of fluid into the formation is known as lost circulation, which occurs due to too high BHP than the fracture pressure. Loss can also occur if fractured formations are encountered during drilling. Lost circulation is one of the most common and troublesome problems in drilling, because of the loss of drilling fluid and the reduction of productivity of the reservoir if the drilling fluid enters the reservoir.

Ballooning (breathing)

Sometimes when higher BHPs are exerted over a formation (such as turning mud pumps on), some of the drilling fluid can flow into the formation and when the pumps are stopped and the BHP reduces, the formation fluids can enter into the wellbore. This happens due to an anomaly in formation, where the circulating frictional pressure forces the drilling fluid into the microfissures of the rock formation, which open only enough to contain the fluid, but not enough to permanently fracture the rock. When the pumps are stopped and the circulating pressure ceases, the overburden of the rock forces the contained fluid back into the wellbore. This effect is commonly referred to as Ballooning or breathing because of the similarity of the effect of inflation and deflation. Identifying ballooning is critical since it is hard to differentiate with the initiation of a kick or loss.

Pipe connection

The drill strings are segments of 27–30 feet in length. Once this length has been drilled, a new segment of the drill string is added. The procedure of adding a new segment of the drill string is called pipe connection. During a pipe connection, the mud pumps are stopped, therefore, the BHP has the risk of falling down to dangerously low levels, if it is not controlled properly.

Surge and swab

The up and down movements of the drill string inside the well can change the BHP and could cause the mud to flow in and out of the well. When the drill string is moved upwards from the well causing the pressure to drop, it is known as a swab. The opposite, when the drill string is pushed down causing a sudden increase of the pressure is known as a surge. The surge and swab will cause the mud to flow out and into the topside to compensate for the sudden pressure changes, respectively.

Tripping

The complete removal of the drill string from the wellbore by pulling it out and then running it back in the hole is known as tripping or a round trip. This operation is done to replace or repair the drill bit after wear. The drill string is removed by 90 feet sections at a time, by unscrewing every third drill pipe. Then depending on the situation a new drill bit is selected based on the failure mechanism and attached to the drill string and lowered into the bottomhole. The duration for the entire operation depends on the total depth of the well and the skill of the drill crew.

Proper differentiation and identification among these incidents need to be practiced for a safe and effective drilling.

2.3 Early Kick Detection

For a safe drilling operation, the impact of drilling incidents needs to be minimized. Kick is a critical incident and the main reasons that can cause a kick are having a mud weight less than the formation pore pressure, failure to keep the hole full while tripping, swabbing while tripping, lost circulation and having a mud cut by gas, water or oil (Grace et al., 1994). Detecting and classifying the kick or loss as soon as possible is crucial to initiate counter actions which can reduce the risk of escalation of an abnormal situation. This process is generally known as early kick detection (EKD).

2.3.1 Kick Detection Methods

Usually, there will be one or several warning signs if a kick is about to happen. These warnings (also known as indicators) are; a sudden increase in drilling rate, an increase in fluid volume at the surface, a change in pump pressure, a reduction in drill pipe weight or gas, oil, or water in return mud (Grace et al., 1994).

Sudden increase in drilling rate

Usually, the first indication of a kick is a sudden increase in drilling rate, sometimes known as a 'drilling break'. This shows that the formation may have been penetrated. The drilling crew must have the knowledge to limit the length of open hole to a minimum in an event of drilling break.

Increase in fluid volume at the surface

A sudden increase of flow at surface is shown as a pit level increase or a return flow rate increase. Usually, this will be known after knowing a drilling break. However, sometimes a variation of drill bit could mask a drilling break, thus an increase of flow volume will be the first indicator. The influx could be rapid or virtually imperceptible based on the productivity of the formation. Therefore, any change of fluid volume at the surface should not be ignored.

Change in pump pressure

A decrease in pump pressure during an influx will happen if the hydrostatic pressure in the annulus is reduced. Most of the time, this will be evident after the other two indicators.

Usually, the reduction in drillpipe weight and a gas, oil, or water in mud will be detected after the other warnings.

There are different types of EKD methods that are used in the industry, which are based on these warnings. Generally, the EKD systems in MPD systems are faster than the EKD methods used in conventional systems (Reitsma, 2010).

Mud Logging

Mud logging is one of the oldest methods of EKD and still a popular method in conventional drilling. Mud logging is continuous observing of the down-hole conditions, and monitoring and evaluation of certain parameters, at the surface. Some of these parameters are, total gas, mud pit volume, connection flow back, pump pressure, drill break, return flow, rate of penetration, trip tank and trip sheets (Grace, 2003; Nayeem et al., 2016). Here, 'total gas' is the measurement of the total combustible hydrocarbon gasses which are present in the mud out flow and rate of penetration is the speed at which the drill bit can break the rock formation. A 'trip tank' is a low-volume, calibrated tank that can be isolated from the circulation system and used to keep track of fluid volumes while tripping (Ahmed et al., 2016). Monitoring the mud pit gain is the most common method out of these. However, the interpretation of active pit volume variations alone could be difficult during drilling, due to the changes in the inflow to the well and the fact that a large amount of mud is buffered in the return flowline and the solids control system prior reaching the mud pits. Further, any change of the pit configuration could affect the total active volume making it difficult to understand the variations and the direct addition of base oil or additives into the active pit may look like a gain or vice versa. There should be clear connections with other indicators to avoid false alarms (Cayeux and Daireaux, 2013; Nayeem et al., 2016). An example of a mud pit volume indicator for different drilling incidents including a kick is shown in Figure 2.10.

Delta Flow

The difference of the flow rate going in and out of the well (delta flow) is a direct and reliable indication of a kick or a loss, where a positive value indicates a kick and a

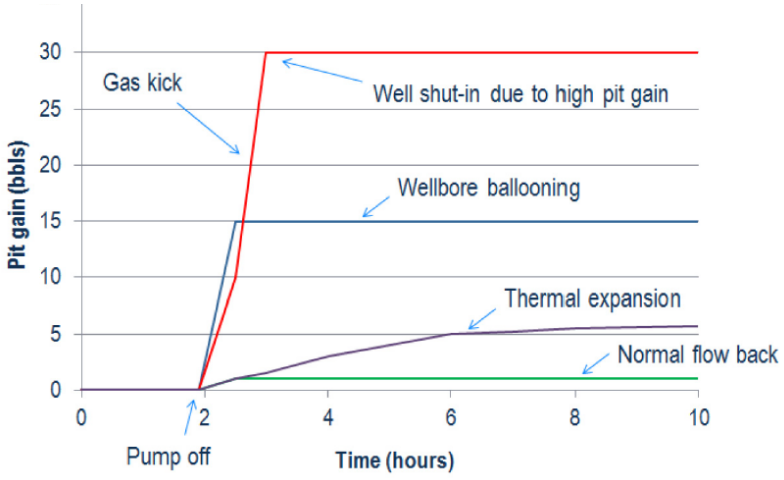

Figure 2.10: Mud pit gain as an indicator (Figure 3 in Yuan et al., 2016, p. 6).

negative value indicates a fluid loss. However, it requires accurate flow measurements for both the inflow and outflow. Usually, in conventional drilling the outflow is observed using a paddle flowmeter, which is an indicator rather than a flowmeter. However, MPD systems use accurate flow meters such as Coriolis flow meters for out flow, thus the delta flow monitoring is used in most MPD systems (Orban et al., 1987; Schafer et al., 1992; Cayeux and Daireaux, 2013; Nayeem et al., 2016). However, the delta flow can generate false alarms during starting and stopping of mud pumps or during axial movements of the drill string (Speers and Gehrig, 1987).

Standpipe Pressure

Standpipe pressure (SPP) is also a common kick indicator, where the pressure of the standpipe (the pipe in between the mud pump and the kelly/top drive, which provides a high pressure pathway for the drilling mud to travel up the derrick) is monitored. SPP can detect any abrupt change but difficult to interpret alone, because of the pressure changes from other sources, such as mud motors, pump problems, washouts and rotation in slim-hole wells (a smaller bore hole than regular). Further, smaller influxes are difficult to detect due to the low resolution of the sensor in SPPs (Reitsma, 2010; Cayeux and Daireaux, 2013; Nayeem et al., 2016).

Bottomhole Pressure using Logging-While-Drilling or Pressure-While-Drilling

This is quite similar to a SPP and the BHP is measured through a logging-while-drilling or pressure-while-drilling tool. Having known the actual BHP, is easier to interpret kicks and hole conditions than using SPP while the pumps are on. Both SPP and this method are effective at detecting influxes where there is a measurable increase in ECD and surface piping. However, when using the mud pulse telemetry to transfer the signal to the topside, the data can be obtained only when the pumps are off. Further, the sensors could become faulty due to the down-hole conditions, therefore, the accuracy, repeatability and reliability could reduce (Reitsma, 2010).

Annular Discharge Pressure

Annular discharge pressure (ADP) is measured right after the rotating control device where the drilling fluid leaves the annulus, and before the choke valve in a MPD system. A highly accurate pressure sensor is needed for accurate measurements (Reitsma, 2010). Usually the SPP and ADP need to be analyzed together to identify an incident. For example, a simultaneous increase of both the SPP and ADP is an indication of a kick while an increase of SPP together with a decrease of ADP is a typical characteristic of a plugged drill string or annulus bridging. However, this

method can only be applied in steady state flow conditions to avoid false alarms (Cayeux and Daireaux, 2013).

The Figure 2.11 shows an example of a kick detection incident in a MPD system (Reitsma, 2010). First an increase of delta flow was detected and the driller was informed. The driller was monitoring only the SPP not the delta flow and interpreted the event as a pump problem. At 5 minutes the choke was closed to 30 % to reduce the influx rate. However, at the time it was difficult to decide whether the influx has been stopped or not because ADP continued to increase but delta flow decreased and then became steady. Without checking the SPP, which was still decreasing, which means more gas is entering the annulus the crew decided that the kick is under control and resumed drilling. This is evident in the increase in SPP and a temporary decrease in ADP and delta flow at approximately 24 minutes. The resumption of drilling caused more reservoir to be exposed to the bottom-hole, and delta flow and ADP increased again. Then the well was shut-in using the well control system (Reitsma, 2010).

Although there are many methods available for EKD in MPD systems, the key detection methods for conventional drilling systems are the mud pit gain and the delta flow.

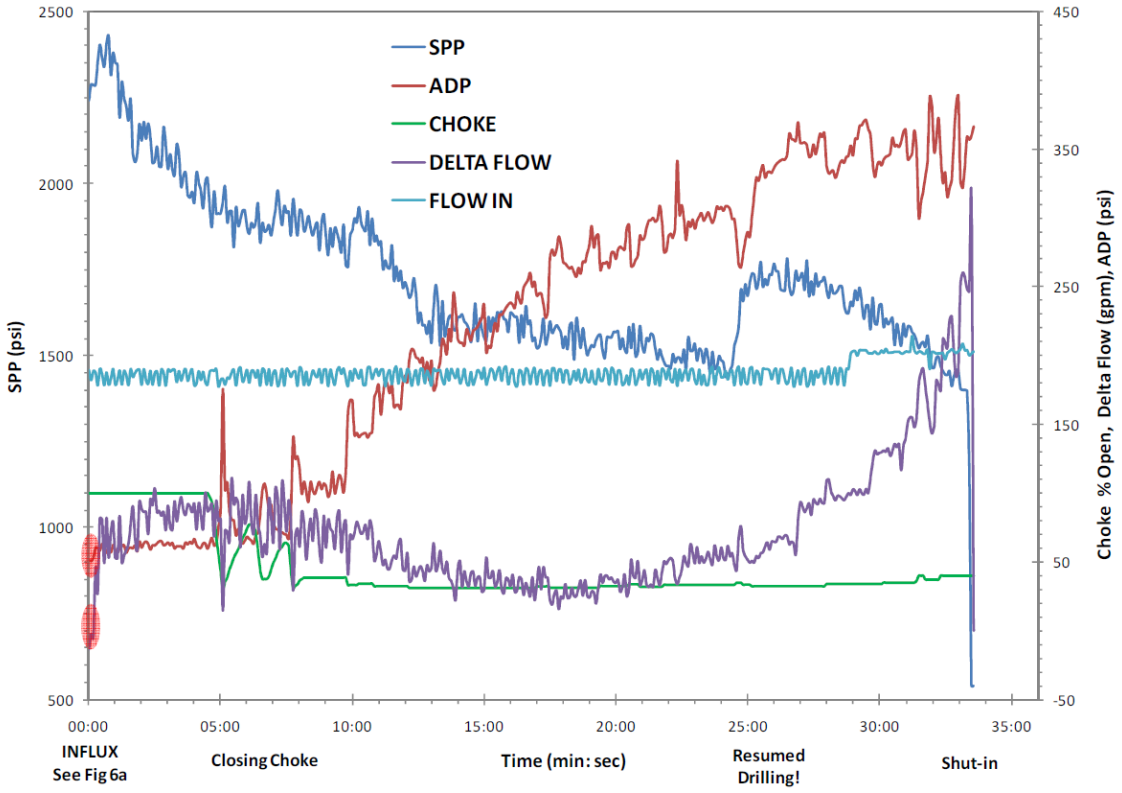

Figure 2.11: An example of the use and comparison of various kick detection methods (Figure 12 in Reitsma, 2010, p. 16). The time is in minutes. The kick started at 0 minutes.

2.3.2 Early Kick Detection in Conventional Drilling

Usually, different EKD indicators or combinations are used for different drilling operations and incidents in conventional drilling. The primary kick indicators for drilling or circulation are an increase of mud return flow rate compared to the mud flow in and the mud pit gain. For the pipe connections, the continuation of return flow rate when the mud pumps are off, and the pit gain are the primary indicators. Further, for the tripping, the continuation of return flow rate and trip tank gain compared to the expected gain would be the primary indicators for kick detection (Brakel et al., 2015). Outflow sensors that are used in conventional drilling platforms are usually qualitative and requires an additional indicator support before positively identifying a kick. Pit gain or pit volume totalizer (PVT) indications are limited by the relatively large size of the pit tanks. Generally, the reliable detection limit of PVT is estimated to be in the order of 10 bbls. Even though, this much of a PVT acts alone as an indicator, it is a common practice to conduct a flow check to confirm the flow is from the well (Fraser et al., 2014). The trip tanks are quite smaller than the mud pits. Usually, trip tanks can detect changes of $\approx 1/4$ of a barrel, hence the most accurate kick detector in a conventional rig. However, this indicator can only be used when the flow is not circulating (Fraser et al., 2014). In order to detect a kick or loss successfully using delta flow, the required accuracy of the delta flow should be in the range of 25–50 gpm (Orban et al., 1987).

To use the delta flow method as a EKD method, the conventional drilling rigs need an accurate outflow meter for measuring the return flow rate. The importance of an outflow meter for EKD is summarized in Table 2.3.

Normally, the outflow is sensitive to slight changes such as rig heave or the manner the pumps are started and stopped, hence might show up noticeable changes in the outflow meter. Therefore, compensation for rig heave and other standard practices are needed for such a meter (Fraser et al., 2014). According to Orban et al. (1987), a flowmeter for kick loss detection in drilling should have an accuracy of 1.5–3 l/s for flow rates up to 75 l/s in a normal drilling operational environment. Further, it requires the reliability and accuracy of measurements over the full range of flow and the accuracy should be maintained for any type of drilling fluid in a viscosity range of 1–200 **cP** and a density range of 1000–2160 $\frac{\text{kg}}{\text{m}^3}$ (Orban et al., 1987). Moreover, there are some complexities that needs to be considered for an outflow meter, such as variable flow rate due to stop–start process, the variable cuttings load and gas cut during drilling.

2.3.3 State of the Art Flow Meters in Drilling

There exists many novel and advanced flow metering techniques for petroleum industry, especially for multiphase flow metering (Falcone et al., 2014). Therefore,

Table 2.3: A comparison of early kick detection operations (Table 1 in Fraser et al., 2014, p. 3).

	Operation	**Tripping out**	**Connection**	**Drilling ahead**	**Out of the hole**	**Plug and abandon**
Conventional drilling	Primary kick indicators	trip tank	PVT, flow indicator	PVT, flow indicator	visual, trip tank	PVT, flow indicator
	estimated KDV	≈3 bbl	> 10 bbl	> 10 bbl	≈5 bbl	> 10 bbl
Conventional drilling with outflow meter	Primary kick indicators	trip tank, flowmeter*	flowmeter, boost pump strokes	flowmeter, pump strokes	visual, flowmeter	flowmeter, pump strokes
	estimated KDV	≈1 bbl	> 5 bbl	> 3 bbl	≈5 bbl	> 5 bbl

KDV–Kick Detection Volume
* – if the flowmeter is upstream of the trip tank

different types of flow meters with its own characteristics and applications are available for the EKD purpose. The inflow is a comparatively clean fluid with known rheological properties, thus many flowmeter types can be used to measure the inflow rate accurately. Some of the inflow meters that are used in the industry are mud pump stroke counter, pump rotary speed transducer, magnetic and Doppler ultrasonic flow meters (Schafer et al., 1992). However, the outflow or the return fluid is contaminated with drill cuttings, wear material and sometimes even gasses and other formation fluids. Due to this harsh condition only a limited number of flowmeter types can be used such as Coriolis, electromagnetic, ultrasonic and open channel flow meters.

Since most of the current operating drilling rigs are still conventional, the popular industry standard for outflow meter is the flow paddle (Cayeux and Daireaux, 2016; Brezina, 2016). The flow paddle is only an indicator which requires human interpretation to convert into flow rate, thus cannot be used for online monitoring. Instead of a flow paddle, a more precise magnetic flowmeter can be used. However, it can only be used with electrically conductive fluids such as water based drilling mud (Schafer et al., 1992; Le Blay et al., 2012). On the other hand, Coriolis meters are highly accurate and the current state-of-the-art for pressure controlled systems such as managed pressure drilling. However, the high footprint (large size, need for bypass lines and pressure limitations) and cost make this less feasible for conventional drilling systems. Further, these have shown certain systematic bias during pipe connections (Cayeux and Daireaux, 2013), and inaccurate measurements in the presence of gasses (Chhantyal et al., 2018). Out of the ultrasonic flow meters, the most suitable type for outflow is Doppler ultrasonic flow meters. This type is suitable for conventional drilling systems, however it is less accurate than the Coriolis or magnetic flow meters and the accuracy is affected by the mechanical and electrical noise in the drilling environment (Schafer et al., 1992; Zhou et al., 2017).

The open channel flow meters can be either placed in contact with the fluid when flowing in an open channel such as the flow paddle, rolling float meter, or a level sensor can be placed above the open channel such as Venturi flowmeter. These are low in cost, easy to install and specially the Venturi flow meters are easy to maintain because of the non-intrusive nature of the level sensors (Schafer et al., 1992; Brezina, 2016). The main disadvantage of this Venturi meter is that the temperature and the composition of air in the return flowline can affect the echo time of the level sensors, thus the measurement needs to be corrected (Schafer et al., 1992). Typical Venturi flumes are designed according to the ISO 4359:2013 standards and performs best for steady or slowly varying flow conditions. These flume equations need one level measurement and empirical coefficients based on the geometry (International Organization for Standardization [ISO], 2013; Basu, 2019). Hence, these flume equations are not suitable for a rapidly changing fluid flow environment such as a return flow during drilling. Therefore, to overcome this problem, a model based method which can be used with dynamic flow conditions needs to be investigated.

2.4 Open Channel Flow

An open channel flow is a flow which has a free surface (subjected to atmospheric pressure) and the driving force of the fluid motion is gravity. Open channel flow can be classified into many types as shown in Figure 2.12. Flow conditions in open channels are often complicated, because the position of the free surface could change with respect to time, space, and other factors such as the depth of flow, discharge, and the slopes of the channel bottom. The channel types are categorized based on the geometry as either prismatic or non-prismatic. A prismatic channel is a channel with uniform cross-sectional area and a uniform bottom slope, which are independent of the longitudinal distance along the flow direction. If the cross-sectional area or the bottom slope is not uniform, then it is a non-prismatic channel. Based on the time, it is classified as either steady flow or unsteady flow. Uniform flow and varied flow is defined based on the space. Varied flow is further divided into two as rapidly or gradually varied flow (Chow, 1959).

2.4.1 Flow Conditions

Further, the flow can be categorized as laminar, turbulent or transitional according to the Reynolds number (Re). According to the Froude number (Fr), the flow can be classified as critical flow ($Fr = 1$), sub-critical or fluvial flow ($Fr < 1$) or super-critical or torrential flow ($Fr > 1$) (Chow, 1959). Reynolds number can be written

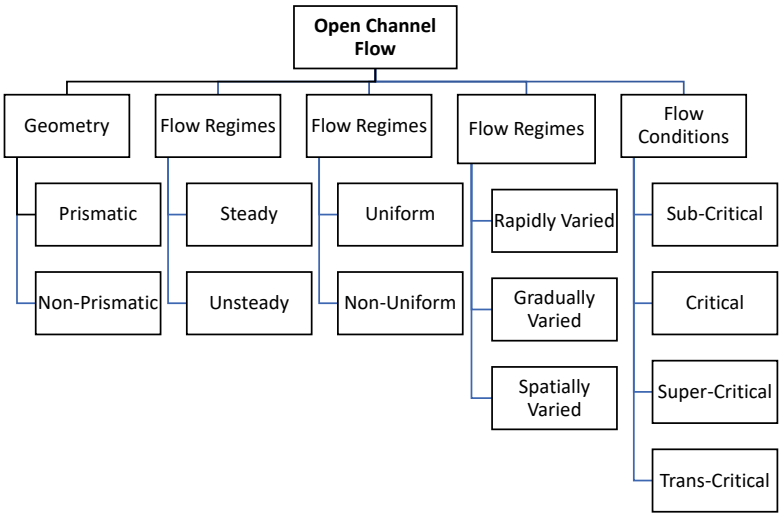

Figure 2.12: Open channel flow classifications.

as the ratio of inertial forces relative to the viscosity forces,

$$\mathrm{Re} = \frac{uL_c}{\nu}, \tag{2.1}$$

where L_c is the characteristic length and ν is the kinematic viscosity. The Froude number is the ratio of inertial forces relative to the gravitational forces,

$$\mathrm{Fr} = \frac{u}{\sqrt{gL_c}}, \tag{2.2}$$

where u is the mean velocity of the flow and g is the gravitational acceleration.

At critical flow, the flow velocity equals the wave celerity, which is the speed of a small wave on the liquid surface relative to the speed of the liquid. A critical flow can happen at a sudden contraction created by a lift in the bottom and/or a narrowing of the width of the channel, or by a sudden change in the slope of the channel bottom. Any disturbance to the surface at this point will not be propagated. The depth at this point is known as critical depth. The transition from a rapid flow to a slow flow is known as hydraulic jump. This is also expressed as an energy transition where a super-critical flow cannot be sustained, and then becomes sub-critical flow by dissipating energy in terms of a hydraulic jump (Chow, 1959; Chanson, 2004; Basu, 2019). There are different types of hydraulic jumps based on the Froude number (Fr) such as undular jumps (Fr: 1–1.7), weak jumps (Fr: 1.7–2.5), oscillating jumps (Fr: 2.5–4.5), steady jumps (Fr: 4.5–9) and strong jumps (Fr: 9) (Basu, 2019; Chaudhry, 2008). Hydraulic jumps help to achieve higher fluid levels at downstream.

2.4.2 Flow Measurement methods

The flow measurement proposition using open channels is quite complex than the flow in conduits, especially because there are many variables associated with these flow channels, mainly the change of free surface. However, for most of the cases it is possible to approximate and express these variables utilizing the continuity and energy equations of fluid mechanics. There exist a number of established approaches for open channel flow measurement, mostly based on steady flow conditions and are listed as follows (Basu, 2019).

Hydraulic Structure

A hydraulic structure, usually, a weir or a control flume, is used to create a critical flow, and the flow rate is calculated from a relationship with the fluid height before the hydraulic structure. This is one of the most common methods to determine the flow rate by calculations based entirely on water depth upstream. This essentially obstructs the flow, thus create problems for any solids present in the fluid and loss of pressure will occur.

Hydraulic Radius and Slope

This method is based on the principle of depth and velocity, and the flow rate is computed by using the Manning's equation. This contains a few empirical parameters, which are assumed to be constants and most of the time the values for these parameters are available only for water.

Area velocity method

Here, the flow rate is computed by multiplying the area of the flow by its average velocity that is measured using various methods. Both the fluid level and the velocity is measured.

Volumetric Tank Method

In this method, the time required to fill a tank of a known volume is used to compute the flow rate. However, this is effective only for smaller flow rates and the accuracy is highly dependent on personnel.

Different Flow Models

Further, empirical equations for prismatic open channels such as the Chezy equation or Manning equation (Chanson, 2004; Chow, 1959; Chaudhry, 2008) for Newtonian fluids and Haldenwang equations (Haldenwang and Slatter, 2006; Burger et al., 2010, 2015a,b; Haldenwang et al., 2010) for non-Newtonian fluids are used in literature. These equations use one level measurement from the channel, and are developed for steady flows for specific geometrical channels. For non-prismatic channels, especially for Venturi channels, a steady flow equation based on the Bernoulli principle can be derived for two level measurements with several empirical coefficients that needs to be tuned (Pirir et al., 2017; Chhantyal, 2018). Flume equations based on one level measurement and empirical coefficients developed for specific Venturi flumes that are designed according to the ISO 4359:2013 standards are available (International Organization for Standardization [ISO], 2013; Basu, 2019; Chhantyal, 2018; Baker, 2016). However, these perform best for steady or slowly varying flow conditions only. Flow equations can be developed based on the critical level of the channel, yet these are quite impractical because the critical level position can vary along the channel due to the changes in the flow rate and flow conditions (Chhantyal, 2018; Chhantyal et al., 2017a). Similar techniques and equations are discussed in detail in (Boiten, 2002; Basu, 2019; Baker, 2016; Henderson, 1966; Alderman and Haldenwang, 2007).

Most of these methods are quite specific and only works for certain types of fluids and flow conditions. Therefore, a versatile, complete and dynamic open channel flow model should be investigated.

Other Models

In addition to mathematical models, black-box and grey-box models, transfer function models, and neural network models have been used for shallow water applications. A nonlinear black-box model is used by Elfawal-Mansour et al. (2000) with an optimal control approach to find the control trajectories by minimizing the energy consumption in a water channel. A grey-box model incorporated with a mass balance has been used with parameter identification for a natural river basin (Weyer, 2001; Ooi and Weyer, 2001). A neural network model is proposed for a river system to identify the plant (Toudeft and Gallinari, 1997). Different artificial intelligence (AI) techniques have been used including fuzzy logic, neural networks and support vector regression to estimate the flow rate of a Venturi channel (Chhantyal et al., 2018; Chhantyal, 2018; Chhantyal et al., 2017b, 2016b).

2.4.3 Shallow Water Equations

The shallow water equations (SWE) are commonly used to model free surface flows provided that it is a shallow water flow; *i.e.* the representative vertical dimensions (characteristic height) are small with respect to the horizontal dimensions (characteristic length). These are a set of hyperbolic (or parabolic, if viscous shear is considered) partial differential equations (PDE) depending on the case and are derived from the Navier-Stokes equations by depth integration. Although, the general SWEs are in 3-D, only the 1-D equations are discussed in here. A sketch of the considered open channel is shown in Figure 2.13. The SWEs for a non-prismatic channel with a general cross-section is written as follows (Garcia-Navarro et al., 2008; Chow, 1959; Chanson, 2004; Chaudhry, 2008; Khan and Lai, 2017).

$$\frac{\partial A}{\partial t} + \frac{\partial Q}{\partial x} = q \tag{2.3}$$

$$\frac{\partial Q}{\partial t} + \frac{\partial}{\partial x}\left(\frac{\beta Q^2}{A} + gI_1 \cos\theta\right) = gI_2 + gA(S_b - S_f) \tag{2.4}$$

Here, $A(x,h,t)$ is the wetted cross sectional area normal to the flow, $h(x,t)$ is the depth of flow, $Q(x,t)$ is the volumetric flow rate, and q is the lateral in or out flow rate. I_1, the first moment of area represents the hydrostatic pressure term and I_2 represents the pressure forces in the fluid volume, which occur from the longitudinal width and slope variations. I_1 and I_2 are defined as follows,

$$I_1(x,A) = \int_0^{h(x,A)} \{h(x,A) - \bar{z}\}\, w(x,\bar{z}) d\bar{z}, \quad \text{and} \tag{2.5}$$

$$I_2(x,A) = \int_0^{h(x,A)} \{h(x,A) - \bar{z}\} \frac{\partial w(x,\bar{z})}{\partial x} d\bar{z}, \tag{2.6}$$

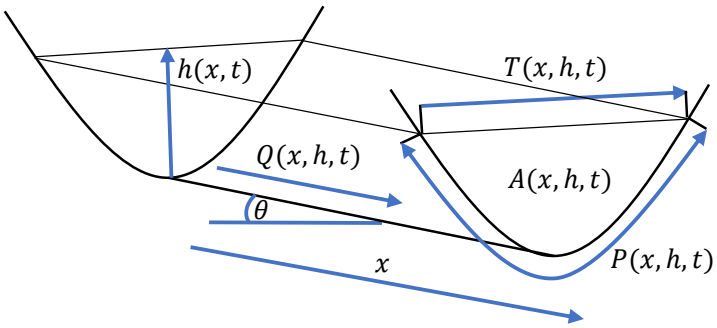

Figure 2.13: Open channel flow along a longitudinal axis x. The fluid level $h(x,t)$, wetted cross-sectional area $A(x,h,t)$ and the discharge $Q(x,h,t)$ which is defined as $Q(x,h,t) = A(x,h,t)v(x,t)$ are shown here with the geometrical parameters; top width $T(x,h,t)$ and wetted perimeter $P(x,h,t)$.

where $w(x,\bar{z})$ is the width of the channel at an arbitrary level $\bar{z}$. g is the gravitational acceleration, t is the time and x is the distance along the flow direction (Chow, 1959; Chaudhry, 2008). β is known as the momentum correction coefficient or the Boussinesq coefficient and corresponds to the deviations of the local velocity over the mean velocity of the flow and defined as follows,

$$\beta = \frac{\int u_p^2 dA}{u^2 \int dA}, \tag{2.7}$$

where u_p is the velocity at a certain point and u is the mean velocity of the liquid Chow (1959); Chanson (2004); Chaudhry (2008). The channel bed slope $S_b(x)$ is calculated by $-\frac{\partial z}{\partial x}$ (z is the absolute fluid level above a datum) or $\sin\theta$, where it is considered positive when sloping downwards. S_f is the friction slope, and usually is defined by the Gauckler–Manning–Strickler formulae for Newtonian fluids (Chow, 1959).

SWE presented in (2.3) and (2.4) are given in the conservative form as the continuity and momentum conservation equations, respectively. It is possible to expand the derivatives in the second and third terms of (2.4) using the product rule to simplify further. However, it will loose the conservative form of the equation.

A special case of SWEs with various assumptions are widely used as Saint–Venant Equations (SVE), which is derived by the French engineer, Adhémar Jean Claude Barré de Saint–Venant in 1871 (de Saint-Venant, 1871). The main assumptions for the SVEs can be listed as follows (Chaudhry, 2008; Litrico and Fromion, 2009).

- The pressure distribution is hydrostatic.
- The velocity of the flow is uniform over the cross section of the channel.
- The channel is prismatic *i.e.* the cross sectional area perpendicular to the flow and the channel bed slope do not change with the direction of the flow.
- The channel bed slope is small *i.e.* the cosine of the angle it makes with the horizontal axis may be replaced by unity.
- The head losses in unsteady flow (due to the effect of boundary friction and turbulence) can be calculated through resistance laws analogous to those used for steady flow.
- No lateral inflow rates are considered ($q = 0$).

$$\frac{\partial A}{\partial t} + \frac{\partial Q}{\partial x} = 0 \tag{2.8}$$

$$\frac{\partial Q}{\partial t} + \frac{\partial}{\partial x}\left(\frac{Q^2}{A}\right) = gA\left(-\frac{\partial z}{\partial x} + S_b - S_f\right) \tag{2.9}$$

The 1-D SWEs and the SVEs are capable of approximating most of the dynamic flow conditions including the complex hydraulic jumps to a certain extent. However, there are two major limitations to the 1-D SWEs, which are the inability to handle dry channels; *i.e.* when the fluid flows are stopped, zero fluid levels and zero flow rates cannot be used to solve the equations, and the inability to handle the back water flows due to channel constrictions. It is possible to approximate the back water flows in limited cases, using continuity, momentum and energy principles under the assumption that normal boundary friction losses are zero (Chow, 1959). Limitations of the SVE applications include shallow-water flood plains where the flow is nearly 2-D, undular and wavy flows, and the propagation of sharp discontinuities (Chanson, 2004).

A closed form analytical solution of these equations is not available except for very simplified cases. Therefore, numerical methods are used for their integration (Chaudhry, 2008).

2.4.4 Numerical Methods

Various types of numerical methods have been used to solve SWEs in the literature, such as the finite volume methods, finite element methods, finite difference methods, and method of characteristics (Chanson, 2004; Chaudhry, 2008).

Initially, 1-D numerical schemes were based mostly on central difference methods. They are known to be heavily dependent on the flow conditions. The more recent numerical schemes tend to focus on high-resolutions and handling discontinuities. First or second order upwind schemes and total variation diminishing techniques of this category are commonly used in hydrological applications (Garcia-Navarro et al., 2008).

Generally, there are two ways of describing fluid motion as Lagrangian and Eulerian. Lagrangian ways follow the particles' individual history, while the Eulerian ways are focused on fixed points in space instead of individual particles. Similarly, the numerical techniques are also categorized as such. Lagrangian discretization uses a finite number of particles of known positions and Eulerian discretization uses a fixed set of spatial points called a grid. A mix of these two techniques are called semi-Lagrangian. Commonly used numerical schemes of these categories are stated here.

Lax-Friedrichs Scheme This is a central finite difference technique of first order. Since this is easy to implement, robust and conservative, it is used in solving SWEs extensively (Garcia-Navarro et al., 2008; Garcia et al., 1992). But this method suffers from numerical diffusion.

Lax-Wendroff Scheme This is an explicit second order method, more stable and accurate in shock capturing. Although this is a classical shock-capturing scheme, it has shown some difficulties in handling source terms in the discretization while keeping the second order accuracy (Lax and Wendroff, 1960; Garcia-Navarro et al., 2008; Burguete and García-Navarro, 2001).

Preissmann Scheme This is a commonly used implicit finite difference method for SWEs, which is stable and robust (Georges et al., 2000; Venutelli, 2002; Zhuan and Xia, 2007; Litrico and Fromion, 2009; Sart et al., 2010). This is widely used for sub-critical flows, and also well suited for fully super-critical flows, nevertheless, not valid for trans-critical flows (Sart et al., 2010).

Kurganov-Petrova Schemes These are well developed, semi-discrete, second order and central upwind schemes, which has specifically been used to solve SVEs (Kurganov, 2018; Kurganov et al., 2017; Kurganov and Petrova, 2007; Bernstein et al., 2016; Bollermann et al., 2013; Vytvytskyi et al., 2015b,a; Jinasena et al., 2018; Pirir et al., 2017). The schemes are well-balanced and positivity preserving *i.e.* the method will guarantee that the computed water depth are non-negative at all times. Although, the validity of the SVE in the presence of dry areas is questionable, being able to operate at near zero fluid levels/flow rates is practically important, especially in drilling.

Discontinuous Galerkin Methods These are finite element methods which use discontinuous piecewise polynomial space as the solution and test function spaces. It contain advantages of both finite element and finite volume methods, thus has been successfully used in a wide range of SWEs applications. Some of these advantages are the accuracy, high parallel efficiency, flexibility for hp-adaptivity and arbitrary geometry and meshes (Lozovskiy et al., 2017; Carlberg et al., 2017; Safarzadeh Maleki and Khan, 2015; Khan and Lai, 2014; Xing et al., 2010; Di Martino et al., 1999). Several positivity preserving, high order, accurate, and well-balanced discontinuous Galerkin methods have been developed recently (Xing et al., 2010).

Collocation Methods Collocation method is a special case of the weighted-residual methods, commonly used in chemical engineering applications and computational physics (Mofid and Peyrett, 1993; Arora et al., 2006; Fromme and Golberg, 1981; Fletcher, 1984). However this method has not been investigated much in hydraulics systems until recently. Collocation method leads to very simple solutions, with very little computation effort, hence suitable for online or real-time estimation and control applications related to SWEs. Most of the studies with orthogonal collocation have used Lagrange or Spline polynomial approximations (Jinasena et al., 2017, 2018;

Costabile and Napoli, 2011; Arora et al., 2005; Ouarit et al., 2003; Layton, 2003; Botella, 2002; Georges et al., 2000).

2.5 Estimations in Oil Drilling and in Open Channel Flow

A short introduction to estimation and different types of estimators used in oil well drilling and for open channel flows are summarized in this chapter.

2.5.1 Introduction

In a process, some states or parameters may not always be measurable due to lack of appropriate measuring devices or due to high priced sensors. In order to estimate the unmeasured states, various estimation principles and methods are available. Luenberger observer and Kalman filter are known as classical estimation principles and many of the other estimators that are used in practice, are mostly the extensions of these two principles. An observer is a deterministic way of estimating an unmeasured state, where the process noise and the measurement noise are not taken into consideration. It is usually based on the stability analysis of the error dynamics. Development of observers has not been the focus of this PhD study. Kalman filter (and its variants) is a stochastic way of estimating an unmeasured state, where the process and measurement noises are taken into consideration with statistical analysis. Some of the well-known Kalman filter variants are extended Kalman filter (EKF), UKF and ensemble Kalman filter. The Kalman filter is used for linear systems where the EKF and UKF are usually used for nonlinear systems. Kalman filters fall under the category of Bayesian method for estimation. Another Bayesian method that has been used in this study is the MHE, which is based on optimization.

2.5.2 Estimation in Drilling

Most of the literature on the development and use of estimators for oil well drilling are focused on the bottomside dynamics. Taking measurements at high pressure and high temperature environment at the bottomside of a drilling operation is comparatively difficult than the topside. Therefore, various estimators have been developed for bottomside, especially for the estimation of BHP, flow rate and various parameters at the bottomside. Some of the recent studies on estimations in oil drilling operations are tabulated in Table 2.4.

Table 2.4: Some of the recent estimation studies of oil drilling operations.

Estimator	Estimate	Remarks	Reference
Adaptive observer	BHP, friction factor, density, effective bulk modulus	A Simplified hydraulic model for a MPD system. A recursive least-squares estimation is incorporated with the observer to estimate the bulk modulus.	Kaasa et al. (2012)
Adaptive observer	BHP and flow rate, reservoir pressure	A swapping based observer for kick detection and attenuation of a MPD system.	Holta et al. (2018)
Adaptive observer	Topside pressure, liquid holdup, gas velocity	An observer based on backstepping method for an underbalanced drilling operation.	Di Meglio et al. (2014)
Adaptive observer	Drill bit velocity, friction factor	Estimation done using only the surface measurements. A linear observer is combined with an update law of friction factors used in a nonlinear friction model.	Aarsnes et al. (2019)
Infinite dimensional observer	Pressure and flow rate through drill bit, Lost circulation rate	A nonlinear adaptive observer for a MPD system based on backstepping method.	Hasan et al. (2017)
MHE	Pressure and flow rate at annulus	Used a hydraulic model of a MPD system. Friction factor is taken as a tuning parameter.	Hasan and Imsland (2014)
Reduced order observer	BHP, density and friction	Observer is adapted to friction and density at annulus.	Stamnes et al. (2008)
UKF	Pressure factors at annulus, drill string, and bit Outlet flow rate factor	The factors are the ratio between a gas kick and normal operation. The estimates are used in a gas kick detection algorithm.	Jiang et al. (2019)
UKF and EKF	Production parameters, slip parameters	A simplified drift-flux model is used.	Nikoofard et al. (2015)

2.5.3 Open Channel Flow Estimation

Open channel fluid flow related literature on state and parameter cover a wide variety of industries. Some of the examples for applications of open channel flow and the use of various estimators in irrigation, aerospace, oil drilling, and hydropower industry are shown in Table 2.5. Most of the estimators are used for control purposes. Studies on the development and use of estimators with open channel flows are comparatively limited in the drilling industry. A few other mathematical model-based and AI-based estimators in return flow estimation in drilling can be found in detail in Chhantyal et al. (2018, 2016b,a); Berg et al. (2015).

Table 2.5: Examples of estimations in open channel flow applications.

Estimate	**Estimator**	**Remarks**	**Reference**
Fluid flow velocity	Sliding mode observer	A proper orthogonal decomposition based nonlinear estimator is developed. Observer is used to estimate the Galerkin coefficients.	Mackunis et al. (2011)
Fluid flow rate	AI-based estimators	Applied to a Venturi channel with an array of ultrasonic level sensors. Fuzzy logic, neural networks and support vector regression algorithms are used.	Chhantyal et al. (2017b)
Fluid flow rate	Ensemble Kalman filter	Applied to a Venturi channel. The estimator is based on SVE.	Agu and Lie (2014)
Fluid flow rate	Nonlinear observer	Applied to an irrigation canal system. SVE are used with various numerical schemes.	Georges (1994, 1995)
Discharge and infiltration variables	linear unknown input observer and a nonlinear sliding mode disturbance observer	Applied to a cascaded open channel irrigation canal system subjected to unknown infiltrations.	Pillosu et al. (2012)
Infiltration flow along a canal and flow rate in the middle	Linear and high gain observers	A water level control design for irrigation canals or dam-river systems. Based on SVE with collocation.	Besancon et al. (2001)
Actuator faults	Unknown input observer	Designed for linear delayed systems with unknown input and time-varying delays. A fault detection and isolation scheme is incorporated.	Koenig et al. (2005)

3 Methods and Approaches

3.1 Mathematical Models

The development of mathematical models for the flow of topside of drilling fluid can be categorized into two main sections: (a) the open channel flow models and (b) topside models. The open channel flow models are for the Venturi channel to estimate the return flow rate and for the drain back flowline to study the return flow dynamics. These are non-prismatic and prismatic channels, respectively. Therefore, two different types of SWEs are used. The topside model consists of models for the drain back flowline and the active mud pit. The overall model development, solution methods, and the validation methods that are used can be seen from the graphical representation in Figure 3.1.

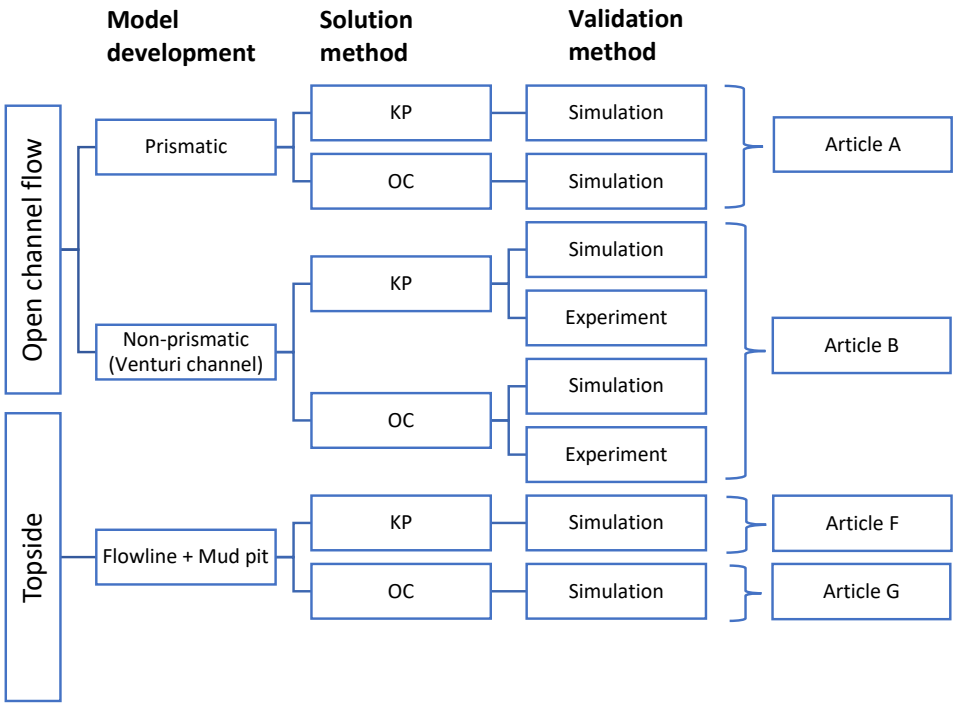

Figure 3.1: The graphical representation of the approaches and methods for developing models for the flow of topside drilling fluid.

The prismatic model was developed at first using SVEs as shown in simplified form in (3.1) and (3.2). The friction slope S_f is approximated using a Newtonian friction model for a horizontal channel. The detailed model development for a trapezoidal channel is stated in Article A of Part II of the thesis. Only the main equations are listed here as follows.

$$\frac{\partial A}{\partial t} + \frac{\partial Q}{\partial x} = 0 \tag{3.1}$$

$$\frac{\partial Q}{\partial t} + \frac{\partial (Q^2/A)}{\partial x} + gA\frac{\partial z}{\partial x} = gAS_b - gAS_f \tag{3.2}$$

The prismatic model for a Newtonian fluid using SVEs for a circular pipe (circular channel) which is the flow model for the drain back flowline is the same as (3.1) and (3.2), but with a modification in (3.2) to represent an angled channel as shown in (3.3). The detailed model development is described in Article F.

$$\frac{\partial Q}{\partial t} + \frac{\partial}{\partial x}\left(\frac{Q^2}{A} + gI_1\cos\theta\right) = gA\sin\theta - gAS_f \tag{3.3}$$

The model for the drain back flowline is further modified and improved using a non-Newtonian friction model as shown in (3.4) and is used for state estimation in Article G. Here, f in the friction term is the Fanning friction factor.

$$\frac{\partial Q}{\partial t} + \frac{\partial}{\partial x}\left(\frac{Q^2}{A} + gI_1\cos\theta\right) = gA\sin\theta - \frac{fPQ|Q|}{2A^2} \tag{3.4}$$

The non-prismatic model for channels with lower slope or smaller inclination angle for a Newtonian fluid is shown in (3.5) and (3.6). The equations are derived from the SWEs for a flow with no lateral inflow. The model is used for a specific Venturi channel with a trapezoidal cross-section and the details of model derivation are shown in Article B. This model is further expressed in terms of fluid level by replacing the cross-sectional area of the flow A by the relationship of fluid level h for direct use of level measurements in Article C.

$$\frac{\partial A}{\partial t} + \frac{\partial Q}{\partial x} = 0 \tag{3.5}$$

$$\frac{\partial Q}{\partial t} + \frac{\partial (\beta Q^2/A + gI_1)}{\partial x} = gI_2 + gA\left(S_b - S_f\right) \tag{3.6}$$

The same non-prismatic model is used in Articles D and E, with different non-Newtonian friction models for the friction term gAS_f in (3.6).

The mud pit model used in the topside model is obtained from simple mass balance as follows,

$$\frac{dh_m}{dt} = \frac{1}{A_m}\left(q_{in} - q_{out}\right), \tag{3.7}$$

where h_m is the mud pit level, A_m is the cross-sectional area of the mud pit, and q_{in}, q_{out} are the inlet and outlet fluid flow rates of the mud pit, respectively.

The bottomside model to be used together with the topside model is a well-known, simple and high fidelity model developed by Kaasa et al. (2012). The model development is described in detail in Kaasa et al. (2012); Stamnes (2007), and the key equations that are needed for the topside model are summarized in Article F in Part II of the thesis.

3.2 Numerical Methods

Two solution methods are used for solving the models described in Section 3.1. One is a well developed, semi-discrete, second order and central-upwind scheme developed by Kurganov and Petrova (2007), which is known as the KP scheme. The KP scheme is used extensively for solving the SVEs. The details of the numerical method can be found in (Kurganov, 2018; Kurganov et al., 2017; Kurganov and Petrova, 2007) and summarized in various articles in Part II, for example in Article A.

The second method is the orthogonal collocation method which is written as the OC method in short. The OC method is used to efficiently reduce the PDEs given by the SVEs into a reduced order model described by a set of ordinary differential equations (ODE). The OC method is used with a Lagrange polynomial approximation over different numbers of in-equispaced spatial points. These spatial points are known as collocation points and selected using shifted Legendre polynomials. Detailed development of the OC method for the prismatic model is stated in Article A whereas for the non-prismatic model it is stated in Article B. The models are solved using Runge-Kutta fourth order method or Euler method and the results are validated either through simulations or by using experimental data and are shown in Figure 3.1.

3.3 Estimation Methods

The open channel flow models and the topside model are used to develop different estimators for estimating flows and some unknown parameters like the friction factor. A brief introduction to the estimators are given in Section 2.5.1. The estimators for this study are selected based on the application suitability and simplicity. The used estimators are linear observer (LO), linear Kalman filter (LKF), EKF, UKF, and MHE. The detailed development of LO, and the algorithms of LKF, EKF, and UKF are shown in Article C in detail. The detailed development of MHE is stated in Article E. Each estimator is then validated by simulation and/or experiments, as

shown in the overview of the estimator development in Figure 3.2. The results, the performance of the estimators and their limitations are discussed in the respective articles.

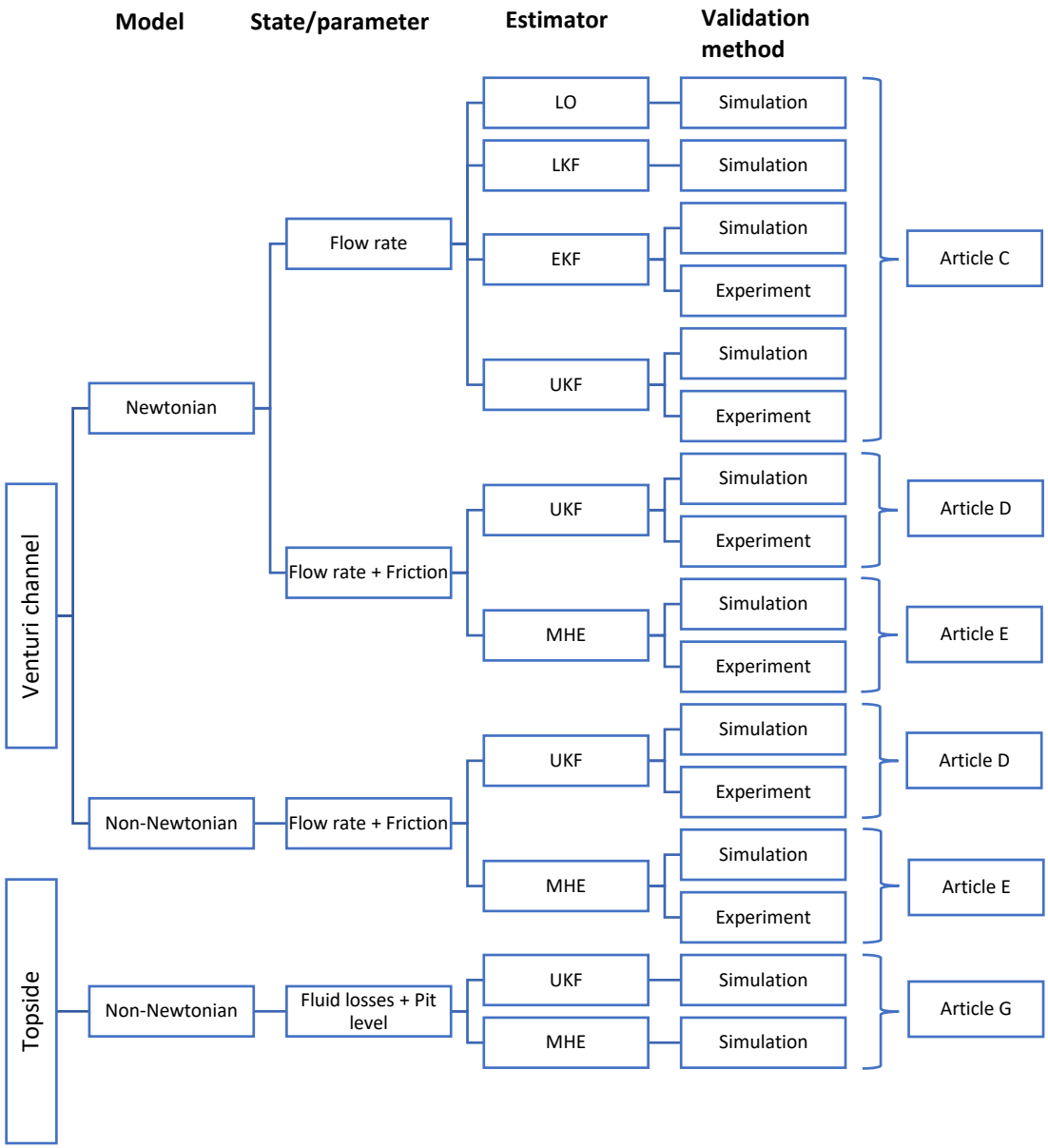

Figure 3.2: An overview of the approaches and methods for developing estimators for the flow of topside drilling fluid.

4 Experimental Setup and Procedures

4.1 Experimental Setup

An experimental setup of a closed loop fluid circulation system is available at the University of South–Eastern Norway. The block diagram of the experimental flow loop is shown in Figure 4.1. The system consists of a fluid tank, a pump, an open Venturi channel and a control system and different types of sensors.

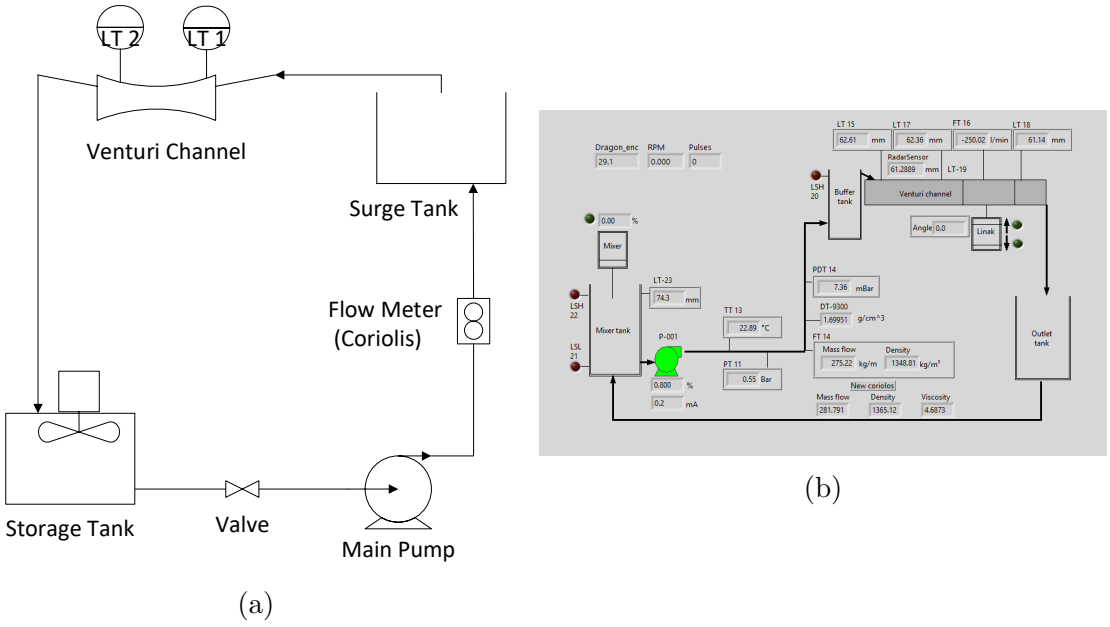

Figure 4.1: (a) The block diagram of the test flow loop. Two of the level sensors (LT-level transducer) are indicated above the Venturi channel. (b) A snapshot of the graphical user interface during operation

4.1.1 Experimental Procedure

Synthetic drilling fluids are prepared separately and stored in separate storage tanks. A separate manual pump system (not shown in Figure 4.1) is available for pumping the desired fluid into the fluid storage tank in the flow loop. Once the fluid is pumped

into the tank, the main pump can be started. The Coriolis flowmeters are placed right after the pump. The storage tank, valve and the main pump are located at the ground floor, while the Venturi channel and the surge tank are located on the first floor. The fluid will flow through the Coriolis flowmeters up to the floor above and into the surge tank, then to the open Venturi channel. The surge tank is placed to reduce the turbulence of the flow at the start of the Venturi channel. The channel is pivoted in one end, to be able to move up and down to change the channel bottom slope. Different types of level meters are placed above the channel. These level sensors can be moved along the horizontal axis of the channel to get measurements at different positions along the center line of the channel. Further, the level sensors are mounted to the channel in a way that the level measurement will be the fluid level perpendicular to the bottom of the channel so that no corrections are needed to get the exact fluid depth when the channel is not horizontal. After the channel, the fluid flows down a pipe back to the storage tank.

If a different fluid needs to be circulated, then the circulation has to be stopped. The existing fluid in the storage tank is emptied, and the entire circulation system is washed by circulating water in the loop, and then the desired fluid needs to be filled again. Some pictures of the Venturi channel during its operation are shown in Figure 4.2.

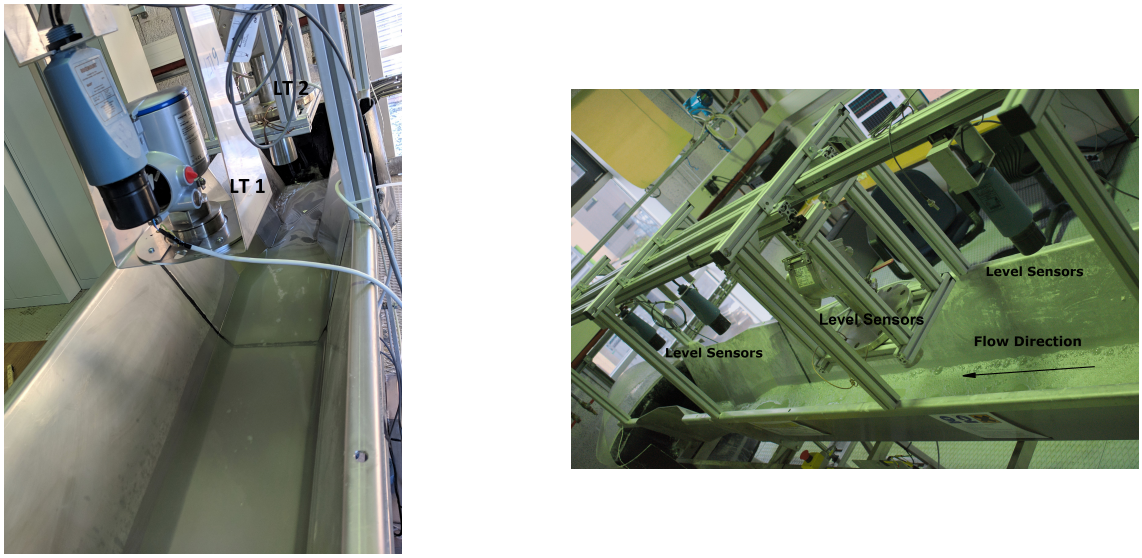

Figure 4.2: Venturi channel at the rig during the flow loop operation

The experiments were carried out by the author and no major changes were done to the experimental set up during the research time period, except for setting up and calibrating the radar level sensors. A number of experiments were carried out for different fluids, for different flow conditions, and with different dynamics. Whenever experimental data is used for validation, the experimental details are clearly stated in each article.

4.1.2 Details of Sensors

The levels of the fluid at different positions along the Venturi channel are used to estimate the fluid flow rate. Therefore, the mass flow rate obtained from the Coriolis meter is used as a reference flow rate which is only used for validation. The density measured by the Coriolis flowmeter is used to convert the volumetric flow rates into mass flow rates and vice versa. The channel bottom slope angle and the viscosity is also measured. The details about the sensors including the accuracy and the type are tabulated in Table 4.1. The experimental data is recorded at either 0.1 s or 1 s intervals. The radar level sensors were not available for the early studies, hence only the ultrasonic level sensors were used, and the details of the used sensors are stated in each relevant article.

Table 4.1: Details of the available sensors that are used

Sensor	**Type**	**Measuring range**	**Accuracy**	**Other**
Level	radar: Krohne Optiwave 7500	0–100 m	± 2 mm	W–band 80 GHz frequency range
Level	radar: Krohne Optiwave 8300 C	0.2–40 m	$<$ 2 mm	24 GHz frequency range
Level	ultrasonic: Rosemount 3108	0.3–3.3 m	± 2.5 mm	4–20 mA with HART output
Level	radar: Rosemount 5300	0–50 m	± 3 mm	Guided wave radar
Mass flow	Coriolis: Promass 63F (Endress +Hauser)	0–180 $\frac{\text{t}}{\text{h}}$	± 0.1 %	range and accuracy for liquid only
Density	Coriolis: Promass 63F (Endress +Hauser)	900–1600 $\frac{\text{kg}}{\text{m}^3}$	± 0.0005 $\frac{\text{g}}{\text{cc}}$	
Viscosity	Coriolis: Promass 83I (Endress +Hauser)	0–20000 cP	± 5%	for Newtonian fluids
Inclination Angle	INY030D-F99-I2E2 (Pepperl +Fuchs)	-15–15°	$\leq$ 0.2°	2-axis with high shock resistance

4.2 Venturi Channel

The Venturi channel is a non-prismatic channel with an isosceles trapezoidal cross-section and a Venturi contraction. The channel is designed according to the standard dimensions to ensure a critical flow at the contraction. The plan and side views of the channel is shown in Figure 4.3. The total length L of the channel is 3.7 m. The bottom width of the channel varies between 0.1 m and 0.2 m with the narrowest width at the Venturi section. The channel bed slope S_b is adjustable between 0 to 2°.

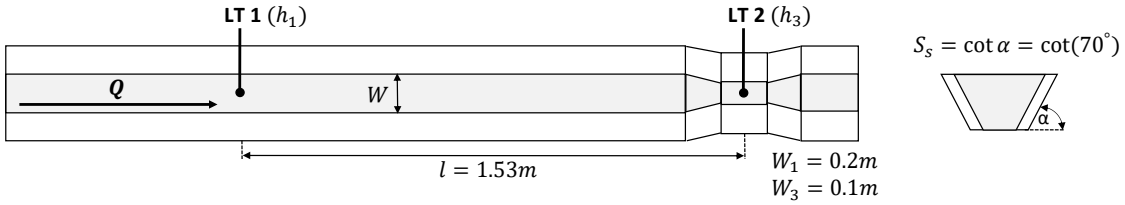

Figure 4.3: Plan view and the side elevation of the Venturi channel. The measurements are given in meters. The flow direction is from left to right.

4.3 Tested Drilling Fluid Types and Properties

Different water-based synthetic drilling fluids are available for the experiments. These drilling fluids are synthesized to have the same density and viscosity as the industrial drilling fluids, hence are expected to mimic the behavior of the industrial drilling fluids. These fluids are a mixer of potassium and calcium carbonates (as densifying agent) and xanthan gum (as the viscosifier) dissolved in water. The mixtures are made of different compositions to create a few different fluid types. All the synthetic drilling mud used in the experiments are non-Newtonian. Water is used as the Newtonian fluid for the experiments.

5 Conclusions and Recommendations

5.1 Conclusions

The mathematical models of fluid flow through both prismatic and non-prismatic open channels were developed by using a set of hyperbolic PDEs. By using the OC method, the models were efficiently reduced into lower order models of ODEs. Three collocation points which give six ODEs were sufficient to obtain a good accuracy with the reduced order model. A significant reduction in the computational time is observed with the use of the reduced order model, with respect to the use of more complex KP scheme for solving the PDE models.

These mathematical models are used with different estimators to estimate the flow rate through the open Venturi channel using only two level measurements along the channel. For model-based estimators, two collocation points are sufficient for obtaining relatively accurate estimates. The model adaptation for friction parameters to suit non-Newtonian fluid types was done with both UKF and MHE. The estimations with UKF had the least root mean squared error (RMSE) out of the tested models of 4.1 $\frac{\text{l}}{\text{min}}$ (=1.465 % = 0.068 $\frac{\text{l}}{\text{s}}$) and the MAPE (Mean Absolute Percentage Error) of 0.1655, which is superior to the recorded values of similar cases in the literature. Further, the effect of change of bottom slope of the channel when the channel is placed on vibrating platforms is also investigated. The results show that the estimator is capable of handling the noise and the errors created by the false fluid levels due to small variations in the channel slope. The collective results show that this method holds tremendous potential for real-time estimation of drill mud flowing out of the well during oil well drilling. From this research work, it has been shown that a cost-effective and simple solution for measuring the return drilling mud flow using an open Venturi channel is indeed possible. Thus, replacing the less reliable existing flowmeter by a Venturi meter based on open channel flow on the return flowline can potentially be realized in practice for a conventional drilling system.

Further, a dynamic model for the closed loop circulation of drilling mud from the mud pumps into the well and back again to the mud pits was developed. It is a simple model and relatively easy to solve and implement. More importantly, it shows the dynamic behavior of both the bottom side and the topside of a drilling operation simultaneously. Moreover, the model is reduced by the orthogonal collocation and

used for state and parameter estimation, to estimate the return flow rate and the drilling mud losses during the removal of drill cuttings at the solids control system. The reduced order model of the drain back flowline is capable of showing the fluid transport delay through the flowline, and thus the mud pit dynamics with a time delay is observed. Accurate and fast estimation of the flow rate of fluid through the drain back flowline and the changes in the mud pit volume hopefully will be useful for early detection of kick or loss. In addition, being able to estimate the loss of drilling mud during the solids removal process in real-time can be used for automating the replenishing procedure which is currently performed manually.

5.2 Limitations and Recommendations

The mathematical model for the non-prismatic channel has a few limitations. One is the fact that the momentum correction coefficient (β) acts as a tuning parameter. This parameter is based on the position of the last collocation point of the channel, usually where the second level sensor is placed on the throat section. This position changes according to the number of collocation points that are used in the model. Hence, this parameter needs to be calibrated for a known flow rate, if the number of collocation points or the position of the last collocation point is changed.

The reduced order model of the Venturi channel is not capable of handling the backflow created by the sudden contraction at the throat during transient flow conditions. During the backflow, the fluid level before the contraction is higher than the fluid level at the upstream, which suggests the model that the flow direction is changed. If the difference in levels is comparatively small, the model has the ability to recover, once the transients are over. If the level differences are comparatively higher, for example during a start up process from a completely dry channel, the flow estimations can become unrealistically negative values. Analytical and empirical approximations of backwater profiles have been developed for uniform flows (Litrico and Fromion, 2004; Ashpis et al., 1993; White, 2011). The ability to handle backflow during transients need to be studied, especially for start up conditions.

Further, the model is not suitable for completely dry channels (approximately less than 3 mm fluid levels) unless a flow constraint is specified while solving the model. There are a few numerical schemes that are capable of handling dry channels, especially in dam-break applications. Most of the numerical methods are based on the discontinuous Galerkin method (Safarzadeh Maleki and Khan, 2015; Lai and Khan, 2012; Chang et al., 2011; Bollermann et al., 2013). The ability to handle completely dry channel conditions are needed for a flow meter in drilling especially during pipe connections where the mud pump is shut down and no liquid is flowing for a considerable time. Hence, this needs to be studied further.

Offshore floating oil rigs are often subjected to heave due to ocean waves. The effect of heave on the fluid levels of the Venturi channel is an interesting study to embark on, as an especial application. The behavior of the flow estimation for drilling fluids with solids particles is also a key aspect that needs to be studied.

Further studies can be done to improve the estimation, by full order model based estimators, by sensor fusion, by incorporation of AI-based models, and by the inclusion of more accurate non-Newtonian friction models. Furthermore, the estimators need to be tested in a pilot scale experimental set up. Moreover, the topside model can be tested together with a more detailed hydraulic model of the bottomside and with plant/experiment data for validation.

Bibliography

Aarsnes, U. J. F., Auriol, J., Di Meglio, F., and Shor, R. J. (2019). Estimating Friction Factors While Drilling. *Journal of Petroleum Science and Engineering*, 179:80–91.

Agu, C. E. (2014). *Model Based Estimation of Drilling Mud Flow Using a Venturi Channel*. Msc, Telemark University College.

Agu, C. E. and Lie, B. (2014). Smart Sensors for Measuring Fluid Flow Using a Venturi Channel. In *55th Conference on Simulation and Modelling (SIMS 55)*, pages 21–22, Aalborg, Denmark.

Ahmed, M. A., Hegab, O. A., and Sabry, A. (2016). Early Detection Enhancement of the Kick and Near-Balance Drilling using Mud Logging Warning Sign. *Egyptian Journal of Basic and Applied Sciences*, 3(1):85–93.

Alderman, N. J. and Haldenwang, R. (2007). A Review of Newtonian and Non-Newtonian Flow in Rectangular Open Channels. In *Hydrotransport 17: The 17th International Conference on the Hydraulic Transport of Solids*, pages 1–20, Cape Town, South Africa.

American Association of Drilling Engineers (1999). *Shale Shakers and Drilling Fluid Systems*. Butterworth-Heinemann, Texas, USA.

Arora, S., Dhaliwal, S. S., and Kukreja, V. K. (2005). Solution of Two Point Boundary Value Problems Using Orthogonal Collocation on Finite Elements. *Applied Mathematics and Computation*, 171(1):358–370.

Arora, S., Dhaliwal, S. S., and Kukreja, V. K. (2006). Simulation of Washing of Packed Bed of Porous Particles by Orthogonal Collocation on Finite Elements. *Computers and Chemical Engineering*, 30(6-7):1054–1060.

Ashpis, D. E., Gatski, T. B., and Hirsh, R. (1993). *Instabilities and Turbulence in Engineering Flows*. Springer Science.

ASME Shale Shaker Committee (2005). *Drilling Fluids Processing Handbook*. Gulf Professional Publishing, Oxford, UK.

Bailey, W. J. and Weir, I. S. (1998). Investigation of Methods for Direct Rheological Model Parameters Estimation. *Journal of Petroleum Science and Engineering*, 21:1–13.

Baker, R. C. (2016). *Flow Measurement Handbook: Industrial designs, operation principles, performance and applications*. Cambridge University Press, New York, 2nd edition.

Basu, S. (2019). Open-Channel Flow Measurement. In Basu, S., editor, *Plant Flow Measurement and Control Handbook*, chapter III, pages 257–331. Academic Press.

Berg, C., Malagalage, A., Agu, C. E., Kaasa, G.-O., Vaagsaether, K., and Lie, B. (2015). Model-based Drilling Fluid Flow Rate Estimation Using Venturi Flume. *IFAC-PapersOnLine*, 48(6):171–176.

Bernstein, A., Chertock, A., and Kurganov, A. (2016). Central-Upwind Scheme for Shallow Water Equations with Discontinuous Bottom Topography. *Bulletin of the Brazilian Mathematical Society*, 47(1):91–103.

Besancon, G., Dulhoste, J.-F., and Georges, D. (2001). Nonlinear Observer Design for Water Level Control in Irrigation Canals. In *Proceedings of the 40th IEEE Conference on Decision and Control*, volume 5, pages 4968–4973, Orlando, FL, USA.

Boiten, W. (2002). Flow Measurement Structures. *Flow Measurement and Instrumentation*, 13(5-6):203–207.

Bollermann, A., Chen, G., Kurganov, A., and Noelle, S. (2013). A Well-Balanced Reconstruction of Wet/Dry Fronts for the Shallow Water Equations. *Journal of Scientific Computing*, 56(2):267–290.

Botella, O. (2002). On a Collocation B-Spline Method for the Solution of the Navier-Stokes Equations. *Computers and Fluids*, 31(4-7):397–420.

Brakel, J. D., Tarr, B. A., Cox, W., Jorgensen, F., and Straume, H. V. (2015). SMART Kick Detection: First step on the well-control automation journey. *Spe Drilling & Completion*, 30(3):233–242.

Brezina, B. (2016). *Analysis of Flow Behavior in Mud Return Lines of Open System Drilling Rigs*. Msc thesis, University of Leoben, Austria.

Burger, J., Haldenwang, R., and Alderman, N. (2010). Friction Factor-Reynolds Number Relationship for Laminar Flow of Non-Newtonian Fluids in Open Channels of Different Cross-Sectional Shapes. *Chemical Engineering Science*, 65(11):3549–3556.

Burger, J. H., Haldenwang, R., and Alderman, N. J. (2015a). Laminar and Turbulent Flow of Non-Newtonian Fluids in Open Channels for Different Cross-Sectional Shapes. *Journal of Hydraulic Engineering*, 141(4):04014084–1–12.

Burger, J. H., Haldenwang, R., Chhabra, R. P., and Alderman, N. J. (2015b). Power Law and Composite Power Law Friction Factor Correlations for Laminar and Turbulent Non-Newtonian Open Channel Flow. *Journal of the Brazilian Society of Mechanical Sciences and Engineering*, 37(2):601–612.

Burguete, J. and García-Navarro, P. (2001). Efficient Construction of High-Resolution TVD Conservative Schemes for Equations with Source Terms: Application to shallow water flows. *International Journal for Numerical Methods in Fluids*, 37(2):209–248.

Caenn, R., Darley, H. C. H., and Gray, G. R. (2017). *Composition and Properties of Drilling and Completion Fluids*. Gulf Professional Publishing, Oxford, UK, 7th edition.

Carlberg, K., Barone, M., and Antil, H. (2017). Galerkin v. Least-Squares Petrov–Galerkin Projection in Nonlinear Model Reduction. *Journal of Computational Physics*, 330:693–734.

Carlsen, I. I., Hauge, S., Tinmannsvik, R. K., and Okstad, E. (2011). Causes and Measures Related to Well Control Incidents in Norwegian Petroleum Activities. In Tuntland, Ø., editor, *Risikonivå i Petroleumsvirksomheten Hovedrapport 2011, Norsk Sokkel*, chapter 10, pages 1–261. Petroleum Safety Authority Norway.

Cayeux, E. and Daireaux, B. (2013). Precise Gain and Loss Detection Using a Transient Hydraulic Model of the Return Flow to the Pit. In *SPE/IADC Middle East Drilling Technology Conference and Exhibition*, pages 1–24, Dubai, UAE. Society of Petroleum Engineers.

Cayeux, E. and Daireaux, B. (2016). Insights Into the Physical Phenomena That Influence Automatic Gain/Loss Detection During Drilling Operations. *SPE Drilling & Completion*, 32(01):13–24.

Chang, C. T. and Chen, J. W. (1995). Implementation Issues Concerning the EKF-Based Bault Diagnosis Techniques. *Chemical Engineering Science*, 50(18):2861–2882.

Chang, T.-J., Kao, H.-M., Chang, K.-H., and Hsu, M.-H. (2011). Numerical Simulation of Shallow-Water Dam Break Flows in Open Channels Using Smoothed Particle Hydrodynamics. *Journal of Hydrology*, 408(1-2):78–90.

Chanson, H. (2004). *The Hydraulics of Open Channel Flow: An introduction*. Elsevier Butterworth-Heinemann, Burlington, 2nd edition.

Charles, M. and Sayle, S. (2010). Offshore Drill Cuttings Treatment Technology Evaluation. In *SPE International Conference on Health, Safety and Environment in Oil and Gas Exploration and Production*, pages 1–11, Rio de Janeiro, Brazil. Society of Petroleum Engineers.

Chaudhry, M. H. (2008). *Open-Channel Flow*. Springer, New York, 2nd edition.

Chhantyal, K. (2018). *Sensor Data Fusion Based Modelling of Drilling Fluid Return Flow through Open Channels*. Phd, University of South-Eastern Norway.

Chhantyal, K., Jondahl, M. H., and Viumdal, H. (2018). Upstream Ultrasonic Level Based Soft Sensing of Volumetric Flow of non-Newtonian Fluids in Open Venturi Channels. *IEEE Sensors Journal*, 18(12):5002–5013.

Chhantyal, K., Viumdal, H., and Mylvaganam, S. (2017a). Online Drilling Fluid Flowmetering in Open Channels with Ultrasonic Level Sensors Using Critical Depths. In *Proceedings of the 58th Conference on Simulation and Modelling (SIMS 58)*, pages 385–390, Reykjavik, Iceland. Linköping University Electronic Press.

Chhantyal, K., Viumdal, H., and Mylvaganam, S. (2017b). Soft Sensing of Non-Newtonian Fluid Flow in Open Venturi Channel Using an Array of Ultrasonic Level Sensors—AI Models and Their Validations. *Sensors (Switzerland)*, 17(11):1–19.

Chhantyal, K., Viumdal, H., Mylvaganam, S., and Elseth, G. (2016a). Estimating Viscosity of Non-Newtonian Fluids Using Support Vector Regression Method: Rheological parameters of drilling fluids using data fusion. *SAS 2016 - Sensors Applications Symposium, Proceedings*, pages 285–290.

Chhantyal, K., Viumdal, H., Mylvaganam, S., and Elseth, G. (2016b). Ultrasonic Level Sensors for Flow Metering of Non-Newtonian Fluids in Open Venturi Channels: Using data fusion based on artificial neural network and support vector machines. In *2016 IEEE Sensors Applications Symposium (SAS)*, pages 1–6, Catania.

Chin, W. C. (2012). *Managed Pressure Drilling: Modeling, Strategy and Planning*. Gulf Professional Publishing, Oxford, UK.

Chow, V. T. (1959). *Open-Channel Hydraulics*. McGraw-Hill, New York.

Costabile, F. and Napoli, A. (2011). A Class of Collocation Methods for Numerical Integration of Initial Value Problems. *Computers and Mathematics with Applications*, 62(8):3221–3235.

de Saint-Venant, A. J. C. B. (1871). Théorie du mouvement non-permanent des eaux, avec application aux crues des rivières et è l'introduction des marées dans leur lit. *Comptes Rendus de l'Académie des Sciences*, 73:147–154 and 237–240.

Di Martino, B., F. J. Chatelon, F. J., and Orenga, P. (1999). The Nonlinear Galerkin Method Applied To Shallow Water Equations. *Mathematical Models and Methods in Applied Sciences*, 9(6):825–854.

Di Meglio, F., Bresch-Pietri, D., and Aarsnes, U. J. F. (2014). An Adaptive Observer for Hyperbolic Systems with Application to Under Balanced Drilling. In *19th World Congress (IFAC)*, pages 11391–11397, Cape Town, South Africa. IFAC.

Elfawal-Mansour, H., Georges, D., and Ohnishi, N. (2000). Optimal Control of an Open Channel Irrigation System Based on Nonlinear Models. In *2000 TENCON Proceedings. Intelligent Systems and Technologies for the New Millennium (Cat. No.00CH37119)*, volume 2, pages 308–313, Kuala Lumpur, Malaysia. IEEE.

Falcone, G., Hewitt, G., Alimonti, C., and Harrison, B. (2014). Multiphase Flow Metering: Current trends and future developments. *Journal of Petroleum Technology*, 54(04):77–84.

Fang, H. and Duan, M. (2014). Special Problems of Deep-Sea Oil and Gas Engineering. In *Offshore Operation Facilities*, chapter 4, pages 537–686. Gulf Professional Publishing, Boston, USA.

Fletcher, C. A. J. (1984). *Computational Galerkin Methods*. Springer, Berlin, Heidelberg.

Fraser, D., Lindley, R., Moore, D., Staak, M. V., and Corp, H. (2014). Early Kick Detection Methods and Technologies. In *SPE Annual Technical Conference and Exhibition*, pages 1–7, Amsterdam. Society of Petroleum Engineers.

Fromme, J. A. and Golberg, M. A. (1981). Convergence and Stability of a Collocation Method for the Generalized Airfoil Equation. *Applied Mathematics and Computation*, 8(4):281–292.

Fu, J., Su, Y., Jiang, W., and Xu, L. (2015). Development and testing of kick detection system at mud line in deepwater drilling. *Journal of Petroleum Science and Engineering*, 135:452 – 460.

Garcia, A., Hubbard, M., and De Vries, J. J. (1992). Open Channel Transient Flow Control by Discrete Time LQR Methods. *Automatica*, 28(2):255–264.

Garcia-Navarro, P., Brufau, P., Burguete, J., and Murillo, J. (2008). The Shallow Water Equations : An example of hyperbolic system. *Monographias de la Real Academia de Ciencias de Zaragoza*, 31:89–119.

Georges, D. (1994). Non Linear Model Identification and State-Observer Design for Water Distribution Systems. In *International Conference on Control*, volume 2, pages 887–894, Coventry, UK.

Georges, D. (1995). Nonlinear Implicit State-Observer Design for the Monitoring of Open-Channel Hydraulic Systems. In *Systems, Man and Cybernetics, 1995. Intelligent Systems for the 21st Century., IEEE International Conference on*, pages 3772–3777, Vancouver, BC.

Georges, D., Dulhoste, J.-f., and Besançon, G. (2000). Modelling and Control of Water Flow Dynamics via a Collocation Method. *Math. Theory of Networks and Systems*.

Gjerstad, K. and Time, R. (2015). Simplified Explicit Flow Equations for Herschel-Bulkley Fluids in Couette-Poiseuille Flow For Real-Time Surge and Swab Modeling in Drilling. *SPE Journal*, 20(03):610–627.

Grace, R. D. (2003). *Blowout and Well Control Handbook*. Gulf Professional Publishing, New York.

Grace, R. D., Cudd, B., Carden, R. S., and Shursen, J. L. (1994). *Advanced Blowout and Well Control*. Gulf Publishing Company, Texas, USA.

Guo, B. and Liu, G. (2011). *Applied Drilling Circulation Systems : Hydraulics, calculations, and models*. Elsevier, New York.

Haldenwang, R. and Slatter, P. (2006). Experimental Procedure and Database for Non-Newtonian Open Channel Flow. *Journal of Hydraulic Research*, 44(2):283–287.

Haldenwang, R., Slatter, P. T., and Chhabra, R. P. (2010). An experimental study of non-Newtonian fluid flow in rectangular flumes in laminar, transition and turbulent flow regimes. *Journal of the South African Institution of Civil Engineering*, 52(1):11–19.

Hasan, A. and Imsland, L. (2014). Moving Horizon Estimation in Managed Pressure Drilling Using Distributed Models. *2014 IEEE Conference on Control Applications, CCA 2014*, (978):605–610.

Hasan, A., Imsland, L., and Hauge, E. (2017). Design and Experimental Validation of Nonlinear Infinite-Dimensional Adaptive Observer in Automated Managed Pressure Drilling. *Journal of Dynamic Systems, Measurement and Control, Transactions of the ASME*, 139(11).

Haseltine, E. L. and Rawlings, J. B. (2005). Critical Evaluation of Extended Kalman Filtering and Moving-Horizon Estimation. *Industrial and Engineering Chemistry Research*, 44(8):2451–2460.

Henderson, F. M. (1966). *Open Channel Flow*. Macmillan Publishing Co., New York.

Holta, H., Anfinsen, H., and Aamo, O. M. (2018). Improved Kick and Loss Detection and Attenuation in Managed Pressure Drilling by Utilizing Wired Drill Pipe. *IFAC-PapersOnLine*, 51(8):44–49.

Hossain, M. E. and Al-Majed, A. A. (2015). *Fundamentals of Sustainable Drilling Engineering*. Scrivener, New Jersy.

Hughes, T., Jones, T., Tomkins, P., Gilmour, A., Houwen, O., and Sanders, M. (1991). Chemical Monitoring of Mud Products on Drilled Cuttings. In *International Conference on Health, Safety and Environment*, number 13, pages 391–402, The Hauge, Netherlands. Society of Petroleum Engineers.

International Organization for Standardization [ISO] (2013). Flow measurement structures – rectangular, trapezoidal and u-shaped flumes. Standard ISO 4359:2013, International Organization for Standardization.

Isaacson, E. and Keller, H. B. (1966). *Analysis of Numerical Methods*. John Wiley & Sons, New York, 2nd edition.

Jiang, H., Liu, G., Li, J., Zhang, T., Wang, C., and Ren, K. (2019). Numerical Simulation of a New Early Gas Kick Detection Method Using UKF Estimation and GLRT. *Journal of Petroleum Science and Engineering*, 173:415–425.

Jinasena, A., Ghaderi, A., and Sharma, R. (2018). Modeling and Analysis of Fluid Flow Through a Non-Prismatic Open Channel with Application to Drilling. *Modeling, Identification and Control*, 39(4):261–272.

Jinasena, A., Kaasa, G.-O., and Sharma, R. (2017). Use of Orthogonal Collocation Method for a Dynamic Model of the Flow in a Prismatic Open Channel : For estimation purposes. In *Proceedings of the 58th Conference on Simulation and Modelling (SIMS 58)*, pages 90–96, Reykjavik, Iceland. Linköping University Electronic Press.

Kaasa, G.-O., Stamnes, Ø. N., Aamo, O. M., and Imsland, L. (2012). Simplified Hydraulics Model Used for Intelligent Estimation of Downhole Pressure for a Managed-Pressure-Drilling Control System. *SPE Drilling & Completion*, 27(1):127–138.

Khan, A. A. and Lai, W. (2014). *Modeling Shallow Water Flows Using the Discontinuous Galerkin Method*. Taylor & Francis, London.

Khan, A. A. and Lai, W. (2017). One-Dimensional Shallow Water flow in Non-Rectangular Channels. In Khan, A. A. and Lai, W., editors, *Modeling Shallow Water Flows Using the Discontinuous Galerkin Method*, chapter 5, pages 83–110. CRC Press, New York, 1st edition.

Khan, M. I. and Islam, M. R. (2007). Drilling and Production Operations. In *The Petroleum Engineering Handbook: Sustainable Operations*, chapter 4, pages 79–134. Gulf Publishing Company, Texas, USA.

Koenig, D., Bedjaoui, N., and Litrico, X. (2005). Unknown Input Observers Design for Time-Delay Systems Application to an Open-Channel. *Proceedings of the 44th IEEE Conference on Decision and Control, and the European Control Conference, CDC-ECC '05*, 2005:5794–5799.

Kolås, S., Foss, B., and Schei, T. (2009). Noise Modeling Concepts in Nonlinear State Estimation. *Journal of Process Control*, 19(7):1111–1125.

Kurganov, A. (2018). Finite-Volume Schemes for Shallow-Water Equations. *Acta Numerica*, 27:289–351.

Kurganov, A. and Petrova, G. (2007). A Second-Order Well-Balanced Positivity Preserving Central-Upwind Scheme for the Saint-Venant System. *Communications in Mathematical Sciences*, 5(1):133–160.

Kurganov, A., Prugger, M., and Wu, T. (2017). Second-Order Fully Discrete Central-Upwind Scheme for Two-Dimensional Hyperbolic Systems of Conservation Laws. *SIAM Journal on Scientific Computing*, 39(3):A947–A965.

Lai, W. and Khan, A. A. (2012). A discontinuous Galerkin Method for Two-Dimensional Shallow Water Flow. *International Journal for Numerical Methods in Fluids*, 70:939–960.

Lax, P. and Wendroff, B. (1960). Systems of Conservation Laws. *Communications on Pure and Applied Mathematics*, 13(2):217–237.

Layton, A. T. (2003). A Semi-Lagrangian Collocation Method for the Shallow Water Equations on the Sphere. *SIAM Journal on Scientific Computing*, 24(4):1433–1449.

Le Blay, F., Villard, E., Hilliard, S. C., and Gronas, T. (2012). A New Generation of Well Surveillance for Early Detection of Gains and Losses When Drilling Very High Profile Ultradeepwater Wells, Improving Safety, and Optimizing Operating Procedures. In *SPETT 2012 Energy Conference and Exhibition*, pages 1–10, Trinidad. Society of Petroleum Engineers.

Litrico, X. and Fromion, V. (2004). Analytical Approximation of Open-Channel Flow for Controller Design. *Applied Mathematical Modelling*, 28(7):677–695.

Litrico, X. and Fromion, V. (2009). *Modeling and Control of Hydrosystems*. Springer.

Livescu, S. (2012). Mathematical Modeling of Thixotropic Drilling Mud and Crude Oil Flow in Wells and Pipelines-A review. *Journal of Petroleum Science and Engineering*, 98-99:174–184.

Lozovskiy, A., Farthing, M., and Kees, C. (2017). Evaluation of Galerkin and Petrov–Galerkin Model Reduction for Finite Element Approximations of the Shallow Water Equations. *Computer Methods in Applied Mechanics and Engineering*, 318:537–571.

Mackunis, W., Drakunov, S. V., Reyhanoglu, M., Ukeiley, L., Beach, D., and Facility, E. E. (2011). Nonlinear Estimation of Fluid Flow Velocity Fields. In *50th IEEE Conference on Decision and Control and European Control Conference (CDC-ECC)*, pages 6931–6935, Orlando, FL, USA.

Mason, J. C. and Handscomb, D. C. D. C. (2003). *Chebyshev Polynomials*. Chapman & Hall/CRC.

Mitchell, R. F. and Miska, S. Z. (2011). *Fundamentals of Drilling Engineering*, volume 12. Society of Petroleum Engineers, Texas, USA.

Mofid, A. and Peyrett, R. (1993). Stability of the Chebyshev Collocation Approximation to the Advection-Diffusion Equation. *Computers and Fluids*, 22(4-5):453–465.

Nayeem, A. A., Venkatesan, R., and Khan, F. (2016). Monitoring of Down-Hole Parameters for Early Kick Detection. *Journal of Loss Prevention in the Process Industries*, 40:43–54.

Negrão, C. O., Franco, A. T., and Rocha, L. L. (2011). A Weakly Compressible Flow Model for the Restart of Thixotropic Drilling Fluids. *Journal of Non-Newtonian Fluid Mechanics*, 166:1369–1381.

Nikoofard, A., Aarsnes, U. J. F., Johansen, T. A., and Kaasa, G.-O. (2015). Estimation of States and Parameters of a Drift-Flux Model with Unscented Kalman Filter. *IFAC-PapersOnLine*, 28(6):165–170.

Ooi, S. K. and Weyer, E. (2001). Closed Loop Identification of an Irrigation Channel. In *Proceedings of the 40th IEEE Conference on Decision and Control (Cat. No.01CH37228)*, volume 5, pages 4338–4343, Orlando, FL. IEEE.

Orban, J., Zanner, K., and Orban, A. (1987). New Flowmeters for Kick and Loss Detection During Drilling. In *62nd Annual Technical Conference and Exhibition of the Society of Petroleum Engineers*, pages 151–161, Dallas, Texas. Society of Petroleum Engineers.

Ouarit, H., Lefèvre, L., Georges, D., and Begovich, O. (2003). A Way to Deal with Nonlinear Boundary Conditions in Open-Channel Optimal Control Problems. In *42nd IEEE International Conference on Decision and Control*, number 1, pages 336–341, Hawaii.

Patel, A. (2019). *Geotechnical Investigations and Improvement of Ground Conditions*. Woodhead Publishing.

Pillosu, S., Pisano, A., and Usai, E. (2012). Unknown-Input Observation Techniques for Infiltration and Water Flow Estimation in Open-Channel Hydraulic Systems. *Control Engineering Practice*, 20(12):1374–1384.

Pirir, I., Jinasena, A., and Sharma, R. (2017). Model Based Flow Measurement Using Venturi Flumes for Return Flow During Drilling. *Modeling, Identification and Control*, 38(3):135–142.

Quarteroni, A. and Valli, A. (2008). *Numerical Approximation of Partial Differential Equations*. Springer, Berlin, 1st edition.

Reed, T. D. and Pilehvari, A. A. (1993). A New Model for Laminar, Transitional, and Turbulent Flow of Drilling Muds. *SPE Production Operations Symposium*, pages 469–482.

Reitsma, D. (2010). A Simplified and Highly Effective Method to Identify Influx and Losses During Managed Pressure Drilling Without the Use of a Coriolis Flow Meter. In *SPE/IADC Managed Pressure Drilling and Underbalanced Operations Conference and Exhibition*, pages 1–16, Kuala Lumpur, Malaysia.

Rivlin, T. J. (1974). *The Chebyshev Polynomials*. Wiley.

Romanenko, A., Santos, L. O., and Afonso, P. A. (2004). Unscented Kalman Filtering of a Simulated pH System. *Industrial and Engineering Chemistry Research*, 43(23):7531–7538.

Runge, C. (1901). Über empirische Funktionen und die Interpolation zwischen äquidistanten Ordinaten. *Zeitschrift für Mathematik und Physik*, 46:224–243.

Safarzadeh Maleki, F. and Khan, A. A. (2015). Effect of Channel Shape on Selection of Time Marching Scheme in the Discontinuous Galerkin Method for 1-D Open Channel Flow. *Journal of Hydrodynamics*, 27(3):413–426.

Sart, C., Baume, J.-P., Malaterre, P.-O., and Guinot, V. (2010). Adaptation of Preissmann's Scheme for Transcritical Open Channel Flows. *Journal of Hydraulic Research*, 48(4):428–440.

Schafer, D., Loeppke, G., Glowka, D., Scott, D., and Wright, E. (1992). An Evaluation of Flowmeters for the Detection of Kicks and Lost Circulation During Drilling. In *IADC/SPE Drilling Conference*, pages 783–792, New Orleans.

Speers, J. and Gehrig, G. (1987). Delta Flow: An Accurate, Reliable System for Detecting Kicks and Loss of Circulation During Drilling. *SPE Drilling Engineering*, 2(4):359–363.

Stamnes, Ø. N. (2007). *Adaptive Observer for Bottomhole Pressure During Drilling*. Msc, Norwegian University of Science and Technology.

Stamnes, Ø. N., Zhou, J., Kaasa, G.-O., and Aamo, O. M. (2008). Adaptive Observer Design for the Bottomhole Pressure of a Managed Pressure Drilling System. In *2008 47th IEEE Conference on Decision and Control*, pages 2961–2966. IEEE.

Szegö, G. (1939). *Orthogonal Polynomials*, volume 23. American mathematical society, 4th edition.

Taylor, A., Madsen, E., Nielsen, H. B., Machetanz, K., Cronin, M., van Vliet, R., and Rønning, I. (2018). Discharges, Spills and Emissions from Offshore Oil and Gas Installations in 2016. Technical report, OSPAR Commission, London.

Toudeft, A. and Gallinari, P. (1997). Neural and Adaptive Controllers for a Non-Minimum Phase Varying Time-Delay System. *Artificial Intelligence in Engineering*, 11(4):431–439.

Veil, J. A. (2002). Drilling Waste Management: Past, present, and future. In *SPE Annual Technical Conference and Exhibition*, pages 1–7, Texas, USA. Society of Petroleum Engineers.

Venutelli, M. (2002). Stability and Accuracy of Weighted Four-Point Implicit Finite Difference Schemes for Open Channel Flow. *Journal of Hydraulic Engineering*, 128(3):281–288.

Vytvytskyi, L., Sharma, R., Granström, I., and Lie, B. (2015a). Modeling for Control of Run-of-River Power Plant Grnvollfoss. In *Proceedings of the 56th SIMS*, pages 237–246, Linköping, Sweden.

Vytvytskyi, L., Sharma, R., and Lie, B. (2015b). Model Based Control for Run-of-River System. Part 1: Model implementation and tuning. *Modeling, Identification and Control*, 36(4):237–249.

Wan, E. A. and Merwe, R. V. D. (2000). The Unscented Kalman Filter for Nonlinear Estimation. In *Proceedings of IEEE Symposium Adaptive Systems for Signal Processing, Communications, and Control*, pages 153–158, Alberta.

Weir, I. S. and Bailey, W. J. (1996). A Statistical Study of Rheological Models for Drilling Fluids. *SPE Journal*, 1:473–486.

Welahettige, P., Vaagsaether, K., and Lie, B. (2018). A Solution Method for One-Dimensional Shallow Water Equations Using Flux Limiter Centered Scheme for Open Venturi Channels. *Journal of Computational Multiphase Flows*, 10(4):228–238.

Weyer, E. (2001). System Identification of an Open Water Channel. *Control Engineering Practice*, 9(12):1289–1299.

White, F. M. (2011). *Fluid Mechanics*. McGraw-Hill, New York, 7th edition.

Whittaker, E. and Watson, G. (1920). Legendre Functions. In *A Course of Modern Analysis*, chapter XV, pages 302–336. Cambridge University Press, 3rd edition.

Willersrud, A. (2015). *Model-Based Diagnosis of Drilling Incidents*. Phd, Norwegian University of Science and Technology.

Xing, Y., Zhang, X., and Shu, C.-W. (2010). Positivity-Preserving High Order Well-Balanced Discontinuous Galerkin Methods for the Shallow Water Equations. *Advances in Water Resources*, 33(12):1476–1493.

Yuan, Z., Morrell, D., Mayans, A. G., Adariani, Y. H., and Bogan, M. (2016). Differentiate Drilling Fluid Thermal Expansion, Wellbore Ballooning and Real Kick during Flow Check with an Innovative Combination of Transient Simulation and Pumps off Annular Pressure While Drilling. In *IADC/SPE Drilling Conference and Exhibition*, pages 1–14, Texas, USA.

Zarei, J. and Poshtan, J. (2010). Design of Nonlinear Unknown Input Observer for Process Fault Detection. *Industrial and Engineering Chemistry Research*, 49(22):11443–11452.

Zhou, Q., Zhao, H., He, Y., Li, S., Jiang, S., and Zhang, H. (2017). Research on Mud Flow Rate Measurement Method Based on Continuous Doppler Ultrasonic Wave. *International Journal of Optics*, 2017:1–12.

Zhuan, X. and Xia, X. (2007). Models and Control Methodologies in Open Water Flow Dynamics: A survey. In *Africon 2007*, pages 1–7, Windhoek.

Part II

Scientific Publications

Article A

Use of Orthogonal Collocation Method for a Dynamic Model of the Flow in a Prismatic Open Channel: For Estimation Purposes

Jinasena, A., Kaasa, G.-O., and Sharma, R. (2017). Use of Orthogonal Collocation Method for a Dynamic Model of the Flow in a Prismatic Open Channel: For Estimation Purposes. In Proceedings of the 58th Conference on Simulation and Modelling (SIMS 58), pages 90–96, Reykjavik, Iceland. Linköping University Electronic Press. https://doi.org/10.3384/ecp1713890

Overview

The paper contains a dynamic mathematical model development for a 1–D open channel flow through a prismatic channel, the model reduction using orthogonal collocation method and the validation with the Kurganov–Petrova (KP) method. The paper is presented at the 58th Conference on Simulation and Modeling (SIMS 58) held at Reykjavik, Iceland from 25th to 27th September, 2017. The paper is published in the conference proceedings.

Additional Information for Article A

Lagrange interpolating polynomial

The Lagrange interpolating polynomial is as follows (Szegö, 1939; Isaacson and Keller, 1966),

$$f(x) = \sum_{i=1}^{n} L_i(x) f(x_i). \tag{A.1}$$

$L_i(x)$ is known as the basis function for the polynomial function.

$$L_i(x) = \prod_{\substack{j=1 \\ j \neq i}}^{n} \frac{x - x_j}{x_i - x_j} \tag{A.2}$$

Here, x is a set of n number of specific points selected from the entire domain. $f(x)$ is the $(n-1)^{\text{th}}$ order polynomial function and $f(x_i)$ is the original function at the i^{th} point.

An example of a polynomial interpolation of four points by the cubic Lagrange polynomial is shown in Figure A.1. Here, each weighted basis function is shown as $L_i f(x_i)$ and the interpolation polynomial has become the summation of each basis function. The summation of basis functions, the interpolation polynomial, passes through all four control points. Each basis polynomial passes through its respective control point and at all the other control points its value is zero (pointed by the dashed lines). Therefore, the orthogonality of these basis functions can be clearly seen from Figure A.1.

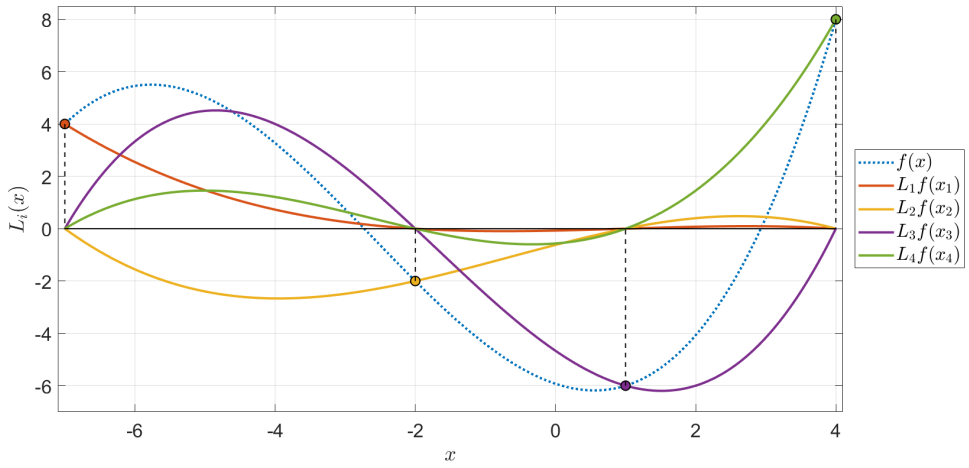

Figure A.1: An example of a polynomial interpolation by the cubic Lagrange polynomial for random four points. The interpolated function $f(x)$ is shown in a continuous line. Each basis function is shown as $L_i f(x_i)$, where $i = 1, 2, 3, 4$.

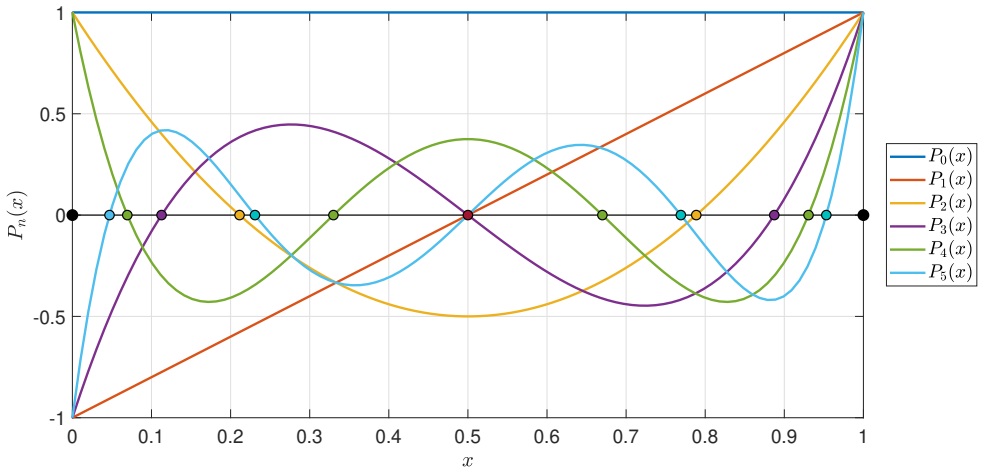

Figure A.2: The first six shifted Legendre polynomials. The different colored points indicate the position of CPs with respect to the degree of each polynomial.

Shifted Legendre polynomials

Shifted Legendre polynomial of the first kind in general form is written using the Rodrigues' formulae (Whittaker and Watson, 1920; Isaacson and Keller, 1966; Quarteroni and Valli, 2008) as follows,

$$P_n(x) = \frac{1}{n!}\frac{d^n}{dx^n}\left\{(x^2-x)^n\right\}. \tag{A.3}$$

The first six shifted Legendre polynomials can be derived from (A.3) as follows,

$$\begin{aligned}
P_0(x) &= 1, && n=0,\\
P_1(x) &= 2x-1, && n=1,\\
P_2(x) &= 6x^2-6x+1, && n=2,\\
P_3(x) &= 20x^3-30x^2+12x-1, && n=3,\\
P_4(x) &= 70x^4-140x^3+90x^2-20x+1, && n=4,\\
P_5(x) &= 252x^5-630x^4+560x^3-210x^2+30x-1, && n=5.
\end{aligned} \tag{A.4}$$

The six polynomials are shown in Figure A.2, and it can be clearly seen how the collocation points (CP) are clustering towards the edges when the degree of the polynomial is increased.

Shifted Chebyshev polynomials

Similarly, the shifted Chebyshev polynomial of the first kind can be derived from the Rodrigues' formulae (Rivlin, 1974; Isaacson and Keller, 1966; Mason and Hand-

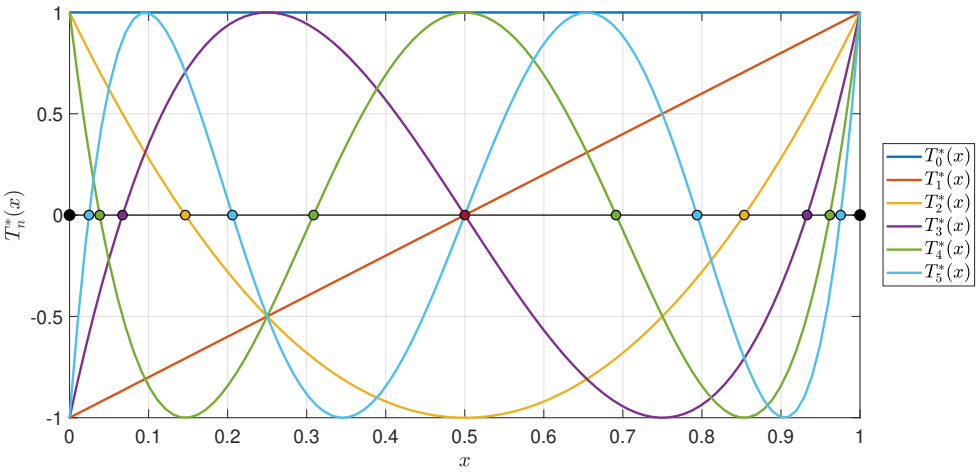

Figure A.3: The first six shifted Chebyshev polynomials. The different colored points indicate the position of CPs with respect to the degree of each polynomial.

scomb, 2003) as follows,

$$T_n^*(x) = T_n(2x-1). \tag{A.5}$$

The first six shifted Chebyshev polynomials can be derived from (A.5) as follows,

$$\begin{aligned}
T_0^*(x) &= 1, && n=0,\\
T_1^*(x) &= 2x-1, && n=1,\\
T_2^*(x) &= 8x^2-8x+1, && n=2,\\
T_3^*(x) &= 32x^3-48x^2+18x-1, && n=3,\\
T_4^*(x) &= 128x^4-256x^3+160x^2-32x+1, && n=4,\\
T_5^*(x) &= 512x^5-1280x^4+1120x^3-400x^2+50x-1, && n=5.
\end{aligned} \tag{A.6}$$

The six Chebyshev polynomials are shown in Figure A.3, and it can be similarly seen how the CPs are positioned with the degree of the polynomial.

Usually, the number of collocation points are stated as either the number n used in the polynomial function or the total number of points including the two endpoints which is $n+2$. Throughout the study, the number of collocation points is interpreted as the total number of points. For example, the linear interpolation by $T_1^*(x)$ or $P_1(x)$ is interpreted as 3 collocation points in this study.

Runge's phenomenon

Runge's phenomenon is a common problem in polynomial interpolation. When interpolating with high degree polynomials over a set of equally spaced (equispaced)

interpolation points, oscillations occur closer to the endpoints, (see Figure A.4), thus increasing the degree of the polynomial may not always improve the accuracy (Runge, 1901). This was discovered by Carl David Tolmé Runge in 1901, while exploring the behavior of various errors in polynomial interpolation. This problem can be avoided by using in-equispaced interpolation points, such as the interpolation points given by Legendre or Chebyshev polynomials.

In the example shown in Figure A.4, the true function is approximated by a 15^{th}-degree polynomial, within the shown interval. Figure A.4.(a) shows the polynomial interpolation at equally spaced points, where it fits with the true function in the middle points but deviates towards the endpoints. To avoid Runge's phenomenon, in-equispaced points are used for the same interpolating polynomial as shown in Figure A.4.(b). The points are the solutions of the Chebyshev polynomial of the first kind (of degree 15), which are known as Chebyshev nodes.

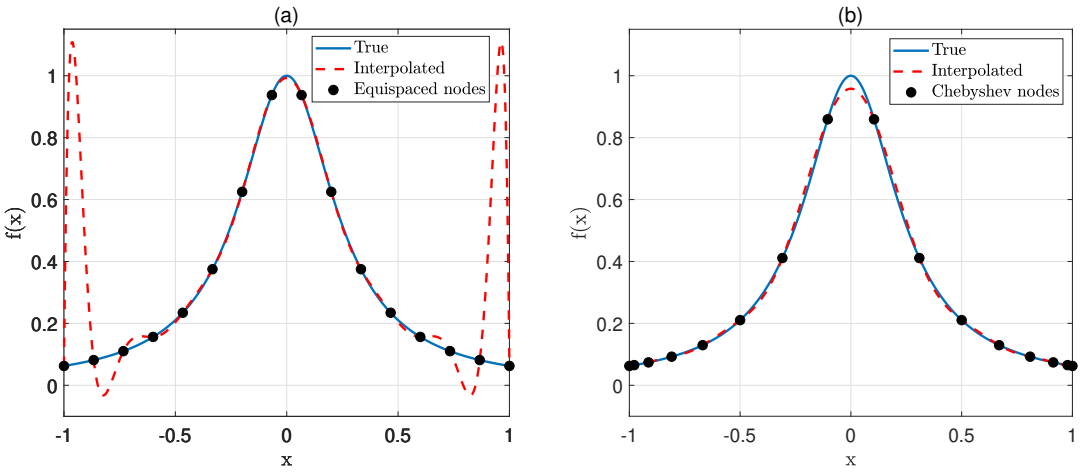

Figure A.4: An example of the Runge's phenomenon. Here, (a) shows the interpolation by a 15^{th}-degree polynomial using equispaced points, while (b) shows the interpolation by the same polynomial using Chebyshev nodes.

Use of Orthogonal Collocation Method for a Dynamic Model of the Flow in a Prismatic Open Channel: For Estimation Purposes

Asanthi Jinasena[1] Glenn–Ole Kaasa[2] Roshan Sharma[1]

[1]Faculty of Technology, Natural Sciences and Maritime Sciences, University College of Southeast Norway, Norway
asanthi.jinasena@usn.no, roshan.sharma@usn.no
[2]Kelda Drilling Controls A/S, Porsgrunn, Norway, gok@kelda.no

Abstract

The modeling and simulation of free surface flows are complex and challenging. Especially, the open channel hydraulics are often modeled by the well–known and efficient Saint–Venant equations. The possibility of efficiently reducing these partial differential equations into ordinary differential equations with the use of orthogonal collocation method is studied with the goal of application in estimations. The collocation method showed the flexibility of choosing the boundary conditions with respect to the flow behavior. The results were comparable enough to the selected finite volume method. Further, a significant reduction in computational time in the collocation method is observed. Therefore, the collocation method shows a good possibility of using it for the real–time estimation of flow rate in an open channel.

Keywords: orthogonal collocation, open channel, prismatic, flow estimation, dynamic modeling

1 Introduction

The real–time estimation of flow rates in fluid flows with the use of mathematical models is a widely known practice in the industry, especially in oil drilling processes, hydro power industry and in agricultural industries. The simplicity and the robustness of the mathematical model are influential in estimation. However, the modeling and simulation of free surface flows are complex and challenging. Especially, the open channel hydraulics are often modeled by the well known and efficient shallow water equations, which are also known as the *Saint–Venant Equations* (SVEs). These are a set of nonlinear, hyperbolic *Partial Differential Equations* (PDEs). These equations are widely used throughout the history, yet the discretization remains tricky which makes it difficult to solve.

Although the classical methods such as *finite difference* and *finite volume* methods are of high precision, it needs numerous spatial discretization points to obtain a realistic solution and consumes a considerable amount of computational time. Hence, these numerical solvers could create complications in applications of online state and parameter estimation. On the contrary, the collocation method, which is a special case of the weighted residual method, could lead to simple solutions with less computational time. This method is commonly used in computational physics for solving PDEs and in chemical engineering for model reduction.

Therefore, the main aim of this work is to study the possibility of reducing the PDEs into *Ordinary Differential Equations* (ODEs) efficiently, with a future goal of an application in estimations. This paper describes the numerical approach which is taken to solve the 1-D shallow water equations in the reduced ODE form. Further, it includes the verification of the used numerical approach in comparison to the other well–known and accurate numerical schemes for selected case studies.

In this paper, the orthogonal collocation method is used for converting the PDEs into ODEs, and then the ODEs are solved using the Runge–Kutta fourth order numerical scheme (for the discretization in the time domain). The Lagrange interpolating polynomials are used for the approximation of the shallow water equations and the shifted Legendre polynomials are used for the selection of collocation points. For the case study, a prismatic channel with a trapezoidal cross–section along the length is selected as the open channel. Different numbers of collocation points were tested and the results are compared with the numerical simulation results obtained from a classical finite volume method. The finite volume method used in this study is a semi-discrete, second order and a central upwind scheme developed by Kurganov and Petrova (Kurganov and Petrova, 2007) for the spatial discretization and the Runge–Kutta fourth order numerical scheme for the temporal discretization.

2 Mathematical Model

There are a large number of versions of the SVEs, based on the physical natures those are assumed upon (Chalfen and Niemiec, 1986; Chaudhry, 2008). The SVEs are a set of hyperbolic, non–linear PDEs, and the used version of the SVEs in this study are derived with the assumptions listed below (Chaudhry, 2008; Litrico and Fromion, 2009).

- The pressure distribution is hydrostatic.
- The velocity of the flow is uniform over the cross section of the channel.

- The channel is prismatic *i.e.* the cross sectional area perpendicular to the flow and the channel bed slope do not change with the direction of the flow.
- The channel bed slope is small *i.e.* the cosine of the angle it makes with the horizontal axis may be replaced by unity.
- The head losses in unsteady flow (due to the effect of boundary friction and turbulence) can be calculated through resistance laws analogous to those used for steady flow.
- No lateral inflow rates are considered.

The Equations for a 1D, unsteady, prismatic, open channel system, can be expressed as,

$$\frac{\partial A}{\partial t}+\frac{\partial Q}{\partial x}=0, \quad (1)$$

$$\frac{\partial Q}{\partial t}+\frac{\partial (Q^2/A)}{\partial x}+Ag\left(\frac{\partial z}{\partial x}+S_f-S_b\right)=0, \quad (2)$$

where $A(x,h,t)$ is the wetted cross sectional area normal to the flow, $h(x,t)$ is the depth of flow, $Q(x,t)$ is the volumetric flow rate, $S_f(Q,x,h)$ is the friction slope, z is the absolute fluid level, which changes with the geometry of the channel, g is the gravitational acceleration, t is the time and x is the distance along the flow direction (Chow, 1959; Chaudhry, 2008). The channel bed slope $S_b(x)$ is calculated by $-\frac{\partial z}{\partial x}$, which is considered positive when sloping downwards. The friction slope S_f is calculated from the Gauckler–Manning–Strickler formulae as shown in Equation 3 (Chow, 1959),

$$S_f=\frac{Q|Q|n_M^2}{A^2R^{\frac{4}{3}}}, \quad (3)$$

where n_M is the Manning friction coefficient $\left(\frac{1}{k_s}\right)$ and R is the hydraulic radius given by $\frac{A}{P}$. Here, k_s is the Strickler friction coefficient and P is the wetted perimeter. The analytical solution for these equations exists only for the simplified cases (Chalfen and Niemiec, 1986; Chung and Kang, 2004; Bulatov, 2014), therefore, these are generally solved by numerical methods. Two different numerical methods are considered in this study, the orthogonal collocation method and the Kurganov and Petrova (KP) Scheme, which are described in the following sections 2.1 and 2.2.

2.1 The Orthogonal Collocation Method

The states A and Q in the SVEs can be approximated by the general polynomial interpolation, using the Lagrange interpolating polynomial (Isaacson and Keller, 1966). The Lagrange interpolating polynomial of n^{th} order for a general function $f(x)$, at $n+1$ data points, is given by (Szegö, 1939),

$$f_n(x)=\sum_{i=0}^{n}L_i(x)f(x_i), \quad (4)$$

where,

$$L_i(x)=\prod_{\substack{j=0\\ j\neq i}}^{n}\frac{x-x_j}{x_i-x_j}. \quad (5)$$

Here, $L_i(x)$ is a weighting function, which is considered as the basis function for the Lagrange function. Now, the approximated states can be defined as A_a and Q_a, where,

$$A_a(x,t)=\sum_{i=0}^{n}L_i(x)A_i(t), \quad \text{and} \quad (6)$$

$$Q_a(x,t)=\sum_{i=0}^{n}L_i(x)Q_i(t). \quad (7)$$

Using these approximations in the SVEs, the Equations 1 and 2 can be re–written as follows,

$$\frac{\partial A_a}{\partial t}+\frac{\partial Q_a}{\partial x}=R_1, \quad (8)$$

$$\frac{\partial Q_a}{\partial t}+\frac{\partial (Q_a^2/A_a)}{\partial x}+A_ag\left(\frac{\partial z}{\partial x}+S_f-S_b\right)=R_2, \quad (9)$$

where $R_1(x,\bar{A},\bar{Q})$ and $R_2(x,\bar{A},\bar{Q})$ are the residuals and $\bar{A}$ and $\bar{Q}$ are the vectors of the coordinates of A_a and Q_a, respectively.

The spatial length x is divided into $n-1$ inequidistant spaces for n nodes, which are named as the *collocation points*. Two of these collocation points will be placed at the boundaries. When the residuals are closer to zero, the unknowns ($\bar{A}$ and $\bar{Q}$) can be computed for each collocation point x_i^c.

$$R_1(x_i^c,\bar{A},\bar{Q})\approx 0, \quad i=1,2,...,n \quad (10)$$

$$R_2(x_i^c,\bar{A},\bar{Q})\approx 0, \quad i=1,2,...,n \quad (11)$$

The corresponding collocation points x_i^c, can be found by choosing the points carefully. When the points are at the roots of any orthogonal polynomial such as the Legendre or Chebyshev polynomial, the approximation error can be minimized (Isaacson and Keller, 1966; Quarteroni and Valli, 2008). The Legendre polynomials are selected in this study. As the number of points are increased, these collocation points cluster towards the two endpoints of the selected total length. This prevents the formation of Runge's phenomenon, which occurs when the nodes are equispaced.

When the residuals are closer to zero, the Equations 8 and 9 can be re–written as follows,

$$\frac{\partial A_a}{\partial t}+\frac{\partial Q_a}{\partial x}\approx 0, \quad (12)$$

$$\frac{\partial Q_a}{\partial t}+\frac{\partial (Q_a^2/A_a)}{\partial x}+A_ag\left(\frac{\partial z}{\partial x}+S_f-S_b\right)\approx 0. \quad (13)$$

Further, the Equation 13 can be simplified as,

$$\frac{\partial Q_a}{\partial t}+\frac{2Q_a}{A_a}\frac{\partial Q_a}{\partial x}-\frac{Q_a^2}{A_a^2}\frac{\partial A_a}{\partial x}+A_ag\left(\frac{\partial z}{\partial x}+S_f-S_b\right)\approx 0. \quad (14)$$

From the Equations 6 and 7, the derivatives are expressed as,

$$\frac{\partial A_a}{\partial x} = \sum_{i=0}^{n} L_{ij}^{'} A_i, \quad \text{and} \tag{15}$$

$$\frac{\partial Q_a}{\partial x} = \sum_{i=0}^{n} L_{ij}^{'} Q_i, \tag{16}$$

where

$$L_{ij}^{'}(x_i) = \frac{\partial L_i(x)}{\partial x}. \tag{17}$$

The substitution of this expression in the Equations 12 and 14 will give two ODEs.

$$\frac{dA_a}{dt} + \sum_{i=0}^{n} L_{ij}^{'} Q_i \approx 0, \tag{18}$$

$$\frac{dQ_a}{dt} + \frac{2Q_a}{A_a} \sum_{i=0}^{n} L_{ij}^{'} Q_i - \frac{Q_a^2}{A_a^2} \sum_{i=0}^{n} L_{ij}^{'} A_i + A_a g \left(\frac{dz}{dx} + S_f - S_b \right) \approx 0. \tag{19}$$

At the selected collocation points, the approximated value is the same as the functional value,

$$A_a(x = x_i, t) = \sum_{i=0}^{n} L_i A_i(t) = A_i(x = x_i, t) \quad \text{and} \tag{20}$$

$$Q_a(x = x_i, t) = \sum_{j=0}^{n} L_i Q_j(t) = Q_i(x = x_i, t). \tag{21}$$

Therefore, the approximated Equations 18 and 19 become as follows,

$$\frac{dA_i}{dt} + \sum_{i=0}^{n} L_{ij}^{'} Q_i = 0 \text{ and} \tag{22}$$

$$\frac{dQ_i}{dt} + \frac{2Q_i}{A_i} \sum_{i=0}^{n} L_{ij}^{'} Q_i - \frac{Q_i^2}{A_i^2} \sum_{i=0}^{n} L_{ij}^{'} A_i + A_i g \left(\frac{dz}{dx} + S_f - S_b \right) = 0. \tag{23}$$

which produces a set of ODEs as shown in Equations 24 and 25.

$$\dot{A}_i = -\sum_{i=0}^{n} L_{ij}^{'} Q_i \tag{24}$$

$$\dot{Q}_i = -\frac{2Q_i}{A_i} \sum_{i=0}^{n} L_{ij}^{'} Q_i + \frac{Q_i^2}{A_i^2} \sum_{i=0}^{n} L_{ij}^{'} A_i - A_i g \left(\frac{dz}{dx} + S_f - S_b \right), \quad i = 0, 1, ..., n \tag{25}$$

Two more equations can be build up using the boundary conditions, which we can choose according to the condition of the flow. For sub–critical flows, one boundary can be chosen from the upstream and the other from the downstream. For super–critical flows, both the boundaries have to be on the upstream (Georges et al., 2000).

To obtain a stable solution, the discretized time Δt, should satisfy the 'current number condition' Cr (Dulhoste et al., 2004),

$$Cr = \frac{\Delta t}{\Delta x} \leq \frac{1}{|v| + c}, \tag{26}$$

where v is the velocity and c is the celerity. The celerity for a trapezoidal channel is defined as $\sqrt{g\frac{A}{T}}$, where T is the top width of the free surface of the channel.

2.1.1 Selection of Collocation Points for Different Number of Points (n)

The points are selected using the Legendre polynomials. The Legendre functions of the first kind is selected over the Chebyshev polynomials of the first kind, due to the less numerical oscillations given by the Legendre functions.

The Legendre polynomials are a set of orthogonal polynomials, which are the solutions to the Legendre differential equations (Whittaker and Watson, 1920). The Legendre polynomials are in the range of $x \in [-1, 1]$ and the shifted Legendre polynomials are analogous to the Legendre polynomials, but are in the range of $x \in [0, 1]$. Therefore, the shifted Legendre polynomials are selected in this study, due to the easiness in converting the collocation points over the selected channel. The shifted Legendre polynomials of the first kind can be generated from the Rodrgues' formulae (Equation 27) (Whittaker and Watson, 1920; Isaacson and Keller, 1966; Quarteroni and Valli, 2008),

$$P_n(x) = \frac{1}{n!} \frac{d^n}{dx^n} \left\{ (x^2 - x)^n \right\}. \tag{27}$$

2.1.2 Development of the ODEs for a Sample Set of Collocation Points

The polynomials $P_n(x)$ for n from 3 to 5 can be derived from the Equation 27 as follows,

$$\begin{aligned} P_1(x) &= 2x - 1, & n = 3, \\ P_2(x) &= 6x^2 - 6x + 1, & n = 4, \\ P_3(x) &= 20x^3 - 30x^2 + 12x - 1, & n = 5. \end{aligned} \tag{28}$$

Each collocation point x_i, lies at the roots of these polynomials along the normalized length of the channel. For a channel with a length of l, the positions of the collocation points can be expressed as follows,

$$\begin{aligned} x_i &\in [0, 0.5l, l], & i = 1, 2, 3 \\ x_i &\in [0, 0.2113l, 0.7887l, l], & i = 1, 2, 3, 4 \\ x_i &\in [0, 0.1127l, 0.5l, 0.8873l, l]. & i = 1, 2, 3, 4, 5 \end{aligned} \tag{29}$$

For a case of three collocation points ($n = 3$), the corresponding Lagrange interpolating polynomial coefficients,

$L^{'}$, can be calculated by differentiating $L(x)$ with respect to x from the Equation 5,

$$L_1^{'}(x) = \frac{d}{dx}\left(\frac{x-x_2}{x_1-x_2}\times\frac{x-x_3}{x_1-x_3}\right) = \frac{(x-x_3)+(x-x_2)}{(x_1-x_2)(x_1-x_3)},$$
$$L_2^{'}(x) = \frac{d}{dx}\left(\frac{x-x_1}{x_2-x_1}\times\frac{x-x_3}{x_2-x_3}\right) = \frac{(x-x_3)+(x-x_1)}{(x_2-x_1)(x_2-x_3)},$$
$$L_3^{'}(x) = \frac{d}{dx}\left(\frac{x-x_1}{x_3-x_1}\times\frac{x-x_2}{x_3-x_2}\right) = \frac{(x-x_2)+(x-x_1)}{(x_3-x_1)(x_3-x_2)}.$$

The coefficient matrix $L^{'}$ at each collocation point x_i, can be calculated by solving $L_i^{'}$ at each point ($L_i^{'}(x=x_i)$), using the position values from Equation 29. The coefficient matrix for the case of the three collocation points is as follows,

$$L^{'} = \begin{bmatrix} L_1 \\ L_2 \\ L_3 \end{bmatrix}^T = \frac{1}{l}\begin{bmatrix} -3 & 4 & -1 \\ -1 & 0 & 1 \\ 1 & -4 & 3 \end{bmatrix}.$$

Similarly, for $n=4$,

$$L^{'} = \frac{1}{l}\begin{bmatrix} -7.0005 & 8.1964 & -2.1959 & 1 \\ -2.7326 & 1.7328 & 1.73190 & -0.7321 \\ 0.7321 & -1.7319 & -1.7328 & 2.7326 \\ -1 & 2.1959 & -8.1964 & 7.0005 \end{bmatrix},$$

and for $n=5$,

$$L^{'} = \frac{1}{l}\begin{bmatrix} -13.0001 & 14.7884 & -2.6666 & 1.8783 & -1 \\ -5.3239 & 3.8731 & 2.0656 & -1.2910 & -0.6762 \\ 1.5 & -3.2275 & 0 & 3.2275 & -1.5 \\ -0.6762 & 1.291 & -2.0656 & -3.8731 & 5.3239 \\ 1 & -1.8783 & 2.6666 & -14.7884 & 13.0001 \end{bmatrix}.$$

The substitution of the $L^{'}$ in Equations 24 and 25, will give the corresponding set of ODEs. The ODEs for the case of the three collocation points are as follows,

$$\dot{A_1} = \frac{1}{l}(-3Q_1+4Q_2-Q_3), \tag{30}$$
$$\dot{A_2} = \frac{1}{l}(-Q_1+Q_3), \tag{31}$$
$$\dot{A_3} = \frac{1}{l}(Q_1-4Q_2+3Q_3), \tag{32}$$
$$\dot{Q_1} = -\frac{2Q_1}{A_1 l}(-3Q_1+4Q_2-Q_3)+\frac{Q_1^2}{A_1^2 l}(-3A_1+4A_2-A_3) - A_1 g\left(\frac{dz}{dx}+S_{f_1}-S_b\right), \tag{33}$$
$$\dot{Q_2} = -\frac{2Q_2}{A_2 l}(-Q_1+Q_3)+\frac{Q_2^2}{A_2^2 l}(-A_1+A_3) - A_2 g\left(\frac{dz}{dx}+S_{f_2}-S_b\right), \tag{34}$$
$$\dot{Q_3} = -\frac{2Q_3}{A_3 l}(Q_1-4Q_2+3Q_3)+\frac{Q_3^2}{A_3^2 l}(A_1-4A_2+3A_3) - A_3 g\left(\frac{dz}{dx}+S_{f_3}-S_b\right). \tag{35}$$

One or two equations from the above set of equations, can be replaced by the chosen boundary conditions.

2.2 The Kurganov and Petrova (KP) Scheme

The KP scheme (Kurganov and Petrova, 2007) is a well balanced scheme which utilizes a central upwind scheme. Further, it does not have the Reimann problem. To illustrate this scheme, the SVEs stated in Equations 1 and 2 are re–written as follows,

$$\frac{\partial U}{\partial t}+\frac{\partial F}{\partial x} = S, \tag{36}$$

where,

$$U = \begin{bmatrix} A \\ Q \end{bmatrix}, \tag{37}$$
$$F = \begin{bmatrix} Q \\ \frac{Q^2}{A} \end{bmatrix}, \quad \text{and} \tag{38}$$
$$S = \begin{bmatrix} 0 \\ -Ag\left(\frac{\partial z}{\partial x}+S_f-S_b\right) \end{bmatrix}. \tag{39}$$

The space is discretized in to a grid for a finite volume cell of a cell size of Δx and $x_{j-\frac{1}{2}} \le x_j \le x_{j+\frac{1}{2}}$ in a uniform grid. The KP scheme for the given Equation 36, can be written as the following set of ODEs,

$$\frac{d\bar{U}_j(t)}{dt} = -\frac{H_{j+\frac{1}{2}}(t)-H_{j-\frac{1}{2}}(t)}{\Delta x}+\bar{S}_j(t), \tag{40}$$

where $H_{j\pm\frac{1}{2}}(t)$ are the central upwind numerical fluxes at the cell interfaces (Kurganov and Petrova, 2007; Sharma, 2015; Vytvytskyi et al., 2015). More details in this scheme is included in (Kurganov and Petrova, 2007). The time step Δt is restricted by the standard Courant–Friederich–Levy (CFL) condition as follows (Kurganov and Petrova, 2007; Bollermann et al., 2013),

$$\text{CFL} = \frac{\Delta t}{\Delta x}\max_j\left|a^{\pm}_{j+\frac{1}{2}}\right| \le \frac{1}{2}, \tag{41}$$

where $a^{\pm}_{j\pm\frac{1}{2}}$ is a one sided local speed of propagation.

2.3 The Parameters of the Open Channel

The selected open channel is a prismatic channel with a trapezoidal cross section. The total length l of the channel is 2.95 m. The bottom width of the channel is 0.2 m, with a zero channel bed slope S_b. The Strickler friction coefficient, k_S is taken as 42 $\frac{\text{m}^{1/3}}{\text{s}}$.

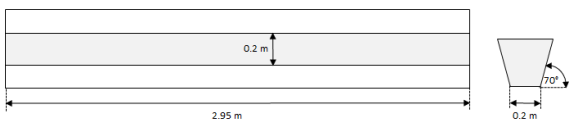

Figure 1. Plan View and the Side Elevation of the Prismatic Channel

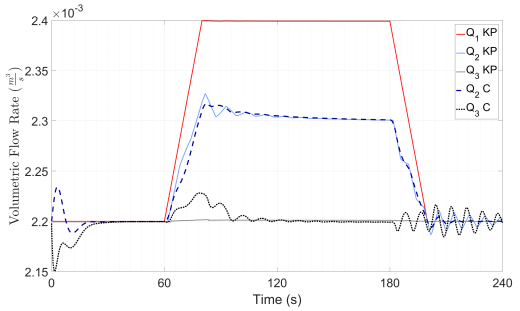

Figure 2. Comparison of the Flow Rates between the KP method and OC Method, at the Three Collocation Points. 'KP ': Results from KP, 'C ': Results from OC

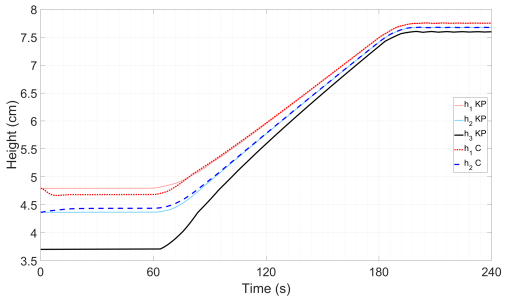

Figure 3. Comparison of the Fluid Levels between the KP method and the OC Method, at the Three Collocation Points. 'KP ': Results from KP, 'C ': Results from OC

3 Simulation, Results and Discussion

A prismatic channel is selected for the dynamic simulations in MATLAB(9.0.1), with three cases of different number of collocation points. For the collocation method, the selected boundary conditions are the flow rate into the channel and the wetted cross sectional area out of the channel. For the simulations with KP, the two boundaries are the flow rates into and out of the channel. For both the methods, the sets of ODEs are solved by the use of Runge Kutta fourth order numerical scheme with a fixed step length.

3.1 Simulation Setup

The simulations for the KP method were started from a steady state, and after 60 seconds, the volumetric flow rate at the inlet was changed from 0.0022 to 0.0024 $\frac{m^3}{s}$ within 20 seconds. This increased flow rate was maintained for about 120 seconds, and then it was reduced back to the previous value within 20 seconds. The flow rate at the end of the channel was kept at the same value of 0.0022 $\frac{m^3}{s}$, throughout the simulations.

The inlet flow rate conditions of the KP method and the outlet wetted cross section area resulted from the simulations, were used as the boundary conditions for the simulations of the collocation method.

3.2 Results and Discussion

Three case studies were simulated using the orthogonal collocation (OC) method. Those results are compared with the results from the KP method and are described in the sections 3.2.1, 3.2.2 and 3.2.3.

3.2.1 Case 1: Three Collocation Points (n=3)

The results from the simulations of the KP scheme are compared with the results from the method with three collocation points. The volumetric flow rates and the heights of the fluid level at the three points are shown in Figures 2 and 3, respectively.

The flow rates obtained from the collocation method are similar to the results from the KP method, but with a few numerical oscillations. At the start of the simulation, the numerical oscillations can be observed due to the unsteady state conditions in the collocation method. These deviations can also be clearly seen in the deviations of the heights in Figure 3 at the beginning. During the transient conditions, the flow rate at the middle of the channel, which is obtained by the collocation method, *i.e.* Q_2 *C* in Figure 3 after 60 seconds, has less numerical

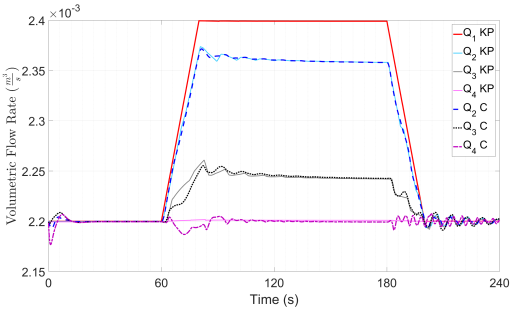

Figure 4. Comparison of the Flow Rates between the KP method and the OC Method, at the Four Collocation Points. 'KP ': Results from KP, 'C ': Results from OC

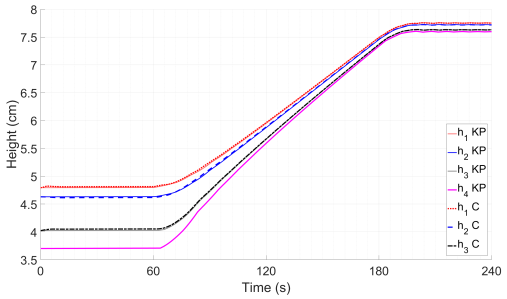

Figure 5. Comparison of the Fluid Levels between the KP method and the OC Method, at the Four Collocation Points. 'KP ': Results from KP, 'C ': Results from OC

oscillations than the same from the KP method, but the flow rate at the end of the channel *i.e.* Q_3 C has more oscillations than from the KP method.

3.2.2 Case 2: Four Collocation Points (n=4)

The volumetric flow rates and the heights of the fluid level at the selected four points, are shown in Figures 4 and 5, respectively.

The results of the simulation from the OC method with four collocation points are more comparable with the results from the KP method, than the same with the three collocation points. Although the amplitude of the oscillations are reduced, the frequency of the oscillations are increased than in the previous case (in section 3.2.1). The reason could be the dual effect of the better approximation due to the increase of the number of collocation points, and the oscillatory behavior of the polynomial approximation due to the increase of the order of the polynomial. This could be observed further by increasing the number of collocation points to five.

3.2.3 Case 3: Five Collocation Points (n=5)

The results for the five collocation points are shown in Figures 6 and 7, respectively. The better approximation due to the increase of the number of collocation points has dominated over the oscillatory behavior caused by the increase of the order of the polynomial, as shown in Figure 6. The oscillations in OC method are the same as from KP, except for Q_5 C, which is at the end of the channel.

3.2.4 Selection of an Orthogonal Polynomial for the Collocation Points

A comparison between the Legendre and Chebyshev polynomials of the first kind was done to justify the selection of the Legendre polynomial. The simulations were done for the case of five collocation points. As shown in the zoomed areas of the Figure 8, it can be justified that the Legendre polynomials tend to produce less oscillations compared to the Chebyshev polynomials.

The OC method is accurate enough with four or more collocation points, as oppose to the numerous discretization points (100) in the KP method. Therefore, to satisfy the CFL condition, the time step Δt of the KP scheme has to be small due to the small Δx. On the contrary, to satisfy the different Current number condition, the OC method allows a larger time step due to the comparatively bigger Δx. Altogether, the computational time taken for the OC method was about 5-20 times less than the computational time taken by the KP method. Handling the ODEs that are

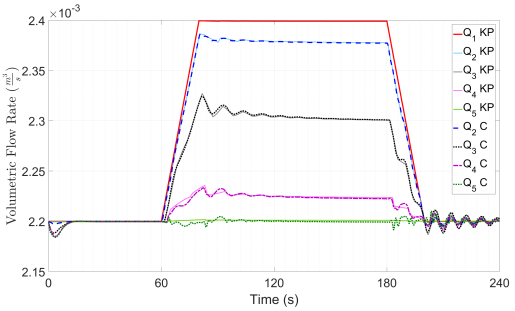

Figure 6. Comparison of the Flow Rates between the KP method and the OC Method, at the Five Collocation Points. 'KP ': Results from KP, 'C ': Results from OC

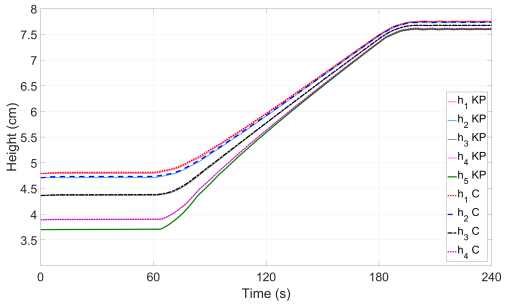

Figure 7. Comparison of the Fluid Levels between the KP method and the OC Method, at the Five Collocation Points. 'KP ': Results from KP, 'C ': Results from OC

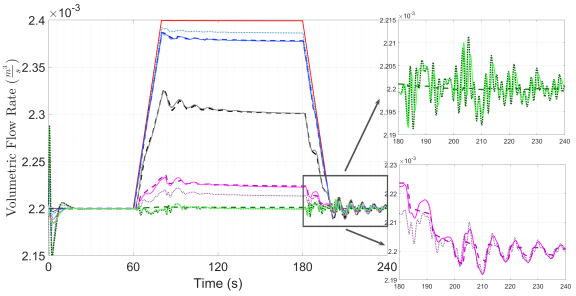

Figure 8. Comparison of the Legendre and Chebyshev polynomials of the first kind. (dashed lines: Results from KP at different collocation points, dotted lines: Results from the OC using Chebyshev polynomials, solid lines: Results from OC using Legendre polynomials.

generated by the OC method is computationally simpler than the KP method. Further, it has a considerably similar accuracy, specially takes much less computational time, which makes the use of OC method in the application of online state and parameter estimation, to be promising.

4 Conclusion

The possibility of efficiently reducing the PDEs into ordinary differential equations (ODEs) using orthogonal col-

location method, is studied with the goal of application in state and parameter estimations in real–time. The collocation method showed the flexibility of choosing the boundary conditions with respect to the flow behavior. The results were comparable enough to the selected finite volume method, which is a widely used, central–upwind scheme. Further, a significant reduction in the computational time in the collocation method is observed. Therefore, the collocation method shows a promising potential of using it in the estimation of state and parameters of open channel flows.

5 Acknowledgment

The economic support from The Research Council of Norway and Statoil ASA through project no. 255348/E30 'Sensors and models for improved kick/loss detection in drilling (Semi–kidd)'is gratefully acknowledged.

References

Andreas Bollermann, Guoxian Chen, Alexander Kurganov, and Sebastian Noelle. A Well-Balanced Reconstruction of Wet/Dry Fronts for the Shallow Water Equations. *Journal of Scientific Computing*, 56(2):267–290, 2013. doi:10.1007/s10915-012-9677-5.

O. V. Bulatov. Analytical and Numerical Riemann Solutions of the Saint Venant Equations for Forward– and Backward–Facing Step Flows. *Computational Mathematics and Mathematical Physics*, 54(1):158–171, 2014. doi:10.1134/S0965542514010047.

Mieczyslaw Chalfen and Andrzej Niemiec. Analytical and Numerical Solution of Saint-Venant Equations. *Journal of Hydrology*, 86:1–13, 1986.

M. Hanif Chaudhry. *Open–Channel Flow*. Springer, New York, 2nd edition, 2008. ISBN 9780387301747.

V. T. Chow. *Open–Channel Hydraulics*. McGraw-Hill, New York, 1959. ISBN 0070107769.

W. H. Chung and Y. L. Kang. Analytical Solutions of Saint Venant Equations Decomposed in Frequency Domain. *Journal of Mechanics*, 20(03):187–197, 2004. doi:10.1017/S1727719100003403.

Jean-François Dulhoste, Didier Georges, and Gildas Besançon. Nonlinear Control of Open–Channel Water Flow Based on Collocation Control Model. *Journal of Hydraulic Engineering*, 130(3):254–266, 2004. doi:10.1061/(ASCE)0733-9429(2004)130:3(254).

Didier Georges, Jean-françois Dulhoste, and Gildas Besançon. Modelling and Control of Water Flow Dynamics via a Collocation Method. *Math. Theory of Networks and Systems*, 2000.

Eugene Isaacson and Herbert Bishop Keller. *Analysis of Numerical Methods*. John Wiley & Sons, New York, 2nd edition, 1966. ISBN 9780486680293.

Alexander Kurganov and Guergana Petrova. A Second–Order Well–Balanced Positivity Preserving Central–Upwind Scheme for the Saint–Venant System. *Communications in Mathematical Sciences*, 5(1):133–160, 2007. doi:10.4310/CMS.2007.v5.n1.a6.

Xavier Litrico and Vincent Fromion. *Modeling and Control of Hydrosystems*. Springer, 2009. ISBN 9781848826236.

Alfino Quarteroni and Alberto Valli. *Numerical Approximation of Partial Differential Equations*. Springer, Berlin, 1st edition, 2008. ISBN 9783540852674.

Roshan Sharma. Second order scheme for open channel flow. Technical report, Telemark University College, 2015. URL `http://hdl.handle.net/11250/2438453`.

Gabor Szegö. *Orthogonal Polynomials*, volume 23. American mathematical society, 4th edition, 1939. ISBN 9780821810231.

Liubomyr Vytvytskyi, Roshan Sharma, and Bernt Lie. Model Based Control for Run-of-river System. Part 1: Model Implementation and Tuning. *Modeling, Identification and Control*, 36(4):237–249, 2015. doi:10.4173/mic.2015.4.4.

E.T. Whittaker and G.N. Watson. Legendre Functions. In *A Course of Modern Analysis*, chapter XV, pages 302–336. Cambridge University Press, 3rd edition, 1920.

Article B

Modeling and Analysis of Fluid Flow through a Non–Prismatic Open Channel with Application to Drilling

Jinasena, A., Ghaderi, A., and Sharma, R. (2018). Modeling and Analysis of Fluid Flow through a Non-Prismatic Open Channel with Application to Drilling. Modeling, Identification and Control, 39(4):261–272. https://doi.org/10.4173/mic.2018.4.3

Overview

The article contains a dynamic mathematical model development and validation by simulations for a 1–D open channel flow through a non–prismatic Venturi channel. Two different flow conditions are tested. A sensitivity and uncertainty analysis is also included to analyze the sensitivity of the parameters and the effect of noise in the input signal. The article is published at the Modeling, Identification and Control journal.

Additional Information for Article B

Validation of the schemes with experimental values

The article contains model validation using the advanced KP numerical scheme as the reference, similar to Article A. Further, the KP scheme is validated using experimental results in Pirir et al. (2017). However, this article in itself does not contain any model validation using experimental results.

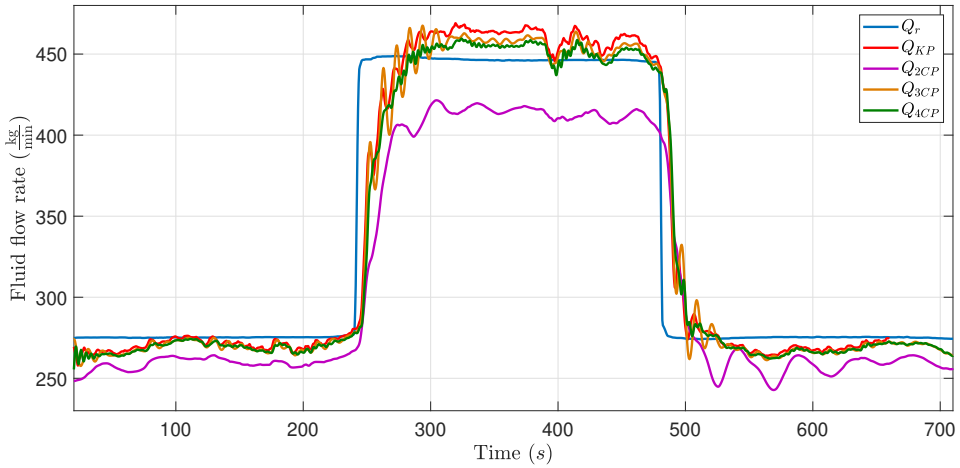

Figure B.1: The model validation using experimental results. Q_r: reference mass flow rate from the experiment, Q_{KP}: mass flow rate from KP scheme, Q_{2CP}, Q_{3CP} and Q_{4CP}: mass flow rates from collocation models with 2, 3 and 4 collocation points.

Therefore, the experimental validation for both KP scheme and the orthogonal collocation method is presented here as shown in Figure B.1. The experiments are done at the experimental rig stated in Chapter 4. The flow conditions are subcritical as explained in section 4.1 in Article B. The supercritical conditions are difficult to measure in the Venturi channel due to the inability of getting reliable level measurements of the hydraulic jump at the throat section. As evident from Figure B.1, the KP scheme and the collocation method with 3 and 4 CPs are comparative with the real flow rate. However, the model with 2 CPs has a considerable amount of offset with real values. This is also evident from the results shown in Paper B.

The fluid flow rates throughout Article B are presented as mass flow rates for the sake of comparison. The mass flow rates are calculated by using the volumetric flow rate from the models and the average density.

The importance of a dynamic model

The importance of dynamic models for an open Venturi flow for the purpose of return flow rate estimation has been studied in detail (Pirir et al., 2017; Chhantyal et al., 2016b; Chhantyal, 2018; Agu, 2014). In these studies, the Bernoulli's equation, the steady state solution of the SVEs and empirical equations were tested with different dynamic mathematical models and data driven models such as artificial neural network and support vector machine models.

The requirement of using a dynamic model is not discussed in Article B. Therefore, two of the aforementioned steady state equations are used to demonstrate the usefulness of a dynamic model for determining the flow rate using a Venturi channel.

The Bernoulli's equation and the steady state solution of the SVEs in simplified form is selected as the steady state equations.

The flow rate based on the Bernoulli's equation for a horizontal channel can be written as follows (Chow, 1959; Chanson, 2004),

$$Q = A_1 A_2 \sqrt{\frac{2g\left(h_2 - h_1\right)}{\alpha\left(A_2^2 - A_1^2\right)}}. \tag{B.1}$$

Here, α is the average Coriolis or energy coefficient for the channel which needs to be tuned. The subscripts 1 and 2 indicate the upstream and downstream positions of the channel, where the level measurements are taken.

The flow rate based on the steady state solution of the SVEs can be written as follows,

$$Q = \sqrt{\frac{g\left(h_c^2 S_s + W h_c\right)^3}{\beta\left(2h_c S_s + W\right)}}, \tag{B.2}$$

using the critical fluid level h_c at the critical point where the flow becomes critical (Chhantyal, 2018). Although the critical point changes with different flow rates and different fluid types, the level measurement taken at the throat is assumed as the critical fluid level.

Two level measurements are taken from the Venturi channel for known flow rates for 3 different non–Newtonian fluid types. More details on the experimental data are given in Article D. The real flow rate from the experiments are plotted together

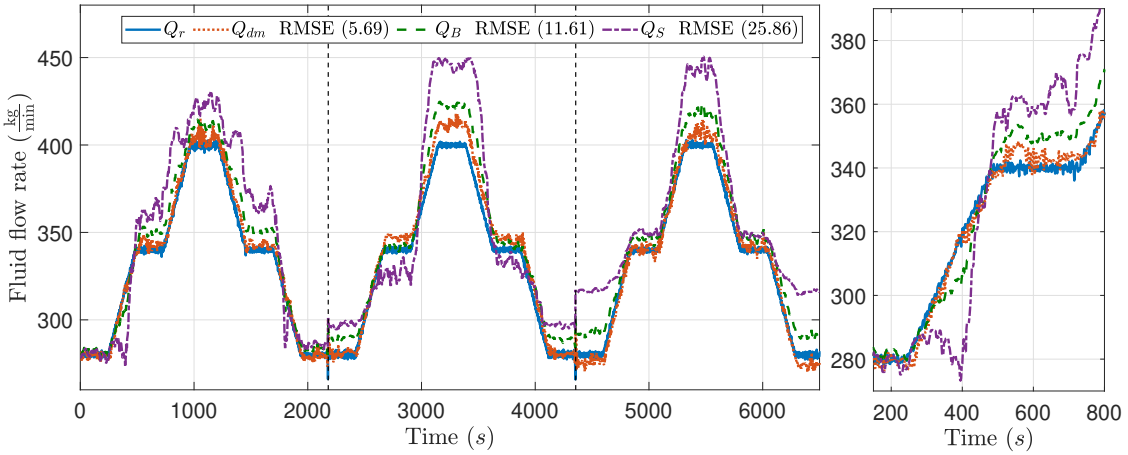

Figure B.2: The dynamic and steady state models with experimental results of different fluid types. Q_r: reference mass flow rate from the experiment, Q_{dm}: mass flow rate from dynamic model, Q_B: mass flow rate from the Bernoulli's equation, Q_S: mass flow rate from steady state equation. The RMSEs are given in $\frac{kg}{min}$. The vertical dashed lines indicate the change of fluid type.

with the result from the dynamic model described in Article B, and the results from the steady state equations (B.1) and (B.2) (see Figure B.2). It can be seen that the steady state model results have a higher RMSE compared to the dynamic model, especially when the fluid type is changed as well as during the transients. The main drawback of the steady state equations is that the tuning parameters cannot be adapted for different fluid types in a continuous operation. Further, a suitable model should have the ability to identify a sudden change in the flow rate as quickly as possible to be useful in a kick detection application. Since the steady state equation is based on the fluid level at the throat, it takes a longer time to identify the change of flow rate as evident in the enlarged section of the Figure B.2.

Additional information on sensitivity analysis

A Bayesian sensitivity analysis results are presented in section 4.2 in Article B. The sensitivity analysis could have been improved by calculating the Fisher information matrix. However, to calculate the Fisher information matrix, the model equations need to be solved analytically. Analytical solving of the equations is quite complex for the model structures used in this article. Therefore, a simpler approach based on the Bayesian analysis on the steady state values has been chosen and applied to perform the sensitivity analysis. This method qualitatively well describes which of the parameters are sensitive to the process output.

Modeling, Identification and Control, Vol. 39, No. 4, 2018, pp. 261–272, ISSN 1890–1328

Modeling and Analysis of Fluid Flow through A Non–Prismatic Open Channel with Application to Drilling

Asanthi Jinasena [1] Ali Ghaderi [2] Roshan Sharma [1]

[1] *Department of Electrical Engineering, IT and Cybernetics, University of South–Eastern Norway, Norway.*
E-mail: {asanthi.jinasena,roshan.sharma}@usn.no

[2] *Department of Mathematics and Science Education, University of South–Eastern Norway, Norway.*
E-mail: ali.ghaderi@usn.no

Abstract

This paper presents the development and validation of a simplified dynamic model of a Venturi channel. The existing dynamic models on open channels are based on the open channel flow principles, which are the shallow water equations. Although there are analytical solutions available for steady state analysis, the numerical solution of these partial differential equations is challenging for dynamic flow conditions. There are many complete and detailed models and numerical methods available for open channel flows, however, these are usually computationally heavy. Hence they are not suitable for online monitoring and control applications, where fast estimations are needed. The orthogonal collocation method could be used to reduce the order of the model and could lead to simple solutions. The orthogonal collocation method has been used in many chemical engineering applications. Further, this has been used in prismatic open channel flow problems for control purposes, but no literature is published about its use for non–prismatic channels as per the author's knowledge. The models for non–prismatic channels have more non–linearity which is interesting to study. Therefore, the possibility of using the collocation method for determining the dynamic flow rate of a non–prismatic open channel using the fluid level measurements is investigated in this paper. The reduced order model is validated by comparing the simulated test case results with a well–developed numerical scheme. Further, a Bayesian sensitivity analysis is discussed to see the effect of parameters on the output flow rate.

Keywords: model reduction, shallow water equation, return flow estimation, Bayesian sensitivity analysis, open channel

1 Background

Kick and loss detection in an oil drilling process is a key requirement to reduce the risk and cost in the drilling industry. In the drilling process, a drilling fluid is circulated from the tanks into the well through the drill bit, up the annulus and then back to the tanks, as shown in Figure 1. This drilling fluid is used to balance the pressure inside the well, to bring the drill cuttings out of the well and also to lubricate the drill bit. If the pressure inside is not well balanced, a kick or a loss can occur. When the pressure inside the well exceeds the formation pressure, the drilling fluids can seep into the formation and commonly known as a loss. When the well pressure is too low than the formation pressure, the formation fluids (air, water, oil or a combination) can flow into the well, producing a kick. A kick or a loss can be catastrophic, if not controlled.

doi:10.4173/mic.2018.4.3

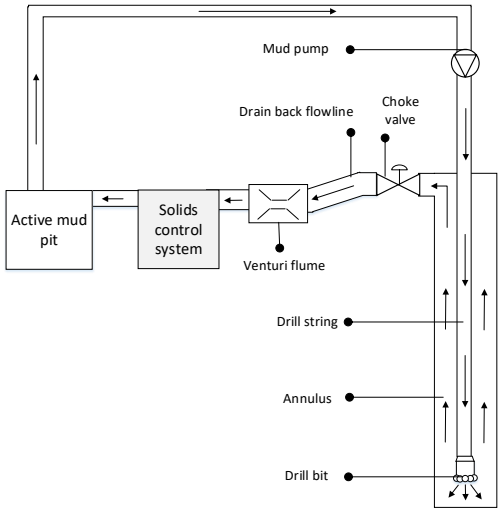

Figure 1: The schematic of a typical drilling fluid circulation process with the inclusion of the proposed Venturi channel

The difference of the fluid flow rate pumped in to the well and the return flow rate coming out of the well is a commonly used indicator of a kick/loss. However, the return flow rate is quite difficult to measure because it contains the drill cuttings as well as dissolved gas. A novel approach of using a Venturi rig for this purpose is proposed in previous studies done by Pirir et al. (2017); Jinasena et al. (2017); Chhantyal et al. (2016). This is a low cost and an easy to maintain solution. The flow rate through the Venturi can be estimated online with the use of mathematical models. However, the modeling and simulation of free surface flows are complex and challenging. Generally, the open channel hydraulics are often modeled by the wellknown and efficient shallow water equations which are also known as SaintVenant equations (Chow, 1959; Chaudhry, 2008; Litrico and Fromion, 2009; Chanson, 2004). These are nonlinear, hyperbolic Partial Differential Equations (PDEs) which are difficult to discretize and solve. The classical finite difference of finite volume methods are usually computationally expensive, hence less suitable for an online estimation application.

Therefore, the use of a model reduction method is explored in this study, to obtain accurate and fast solutions for the shallow water equations. Orthogonal collocation method is used to reduce the PDE model into Ordinary Differential Equations (ODEs) efficiently, and the model results are validated using simulations. For the validation, a well balanced and well developed numerical scheme, which is specifically developed for the shallow water equations by Kurganov and Petrova (2007) is used. The use of collocation method in solving open channel problems has been studied previously by a lot of researchers including Georges et al. (2000); Dulhoste et al. (2004); Jinasena et al. (2017); Layton (2003), but these are limited only to prismatic channels. The Venturi is a non–prismatic channel which gives better fluid level differences along the channel length, therefore the model reduction for the non–prismatic channels is described in this study. Further, a sensitivity analysis is done to find the effect of different input, geometrical and fluid parameters on the model output.

The paper is organized as follows. The development of the mathematical model from the shallow water equations and the model reduction is described in detail in the Section 2. This is followed by the sensitivity analysis in Section 3. Then the simulation results and the discussion based on the results are stated in Section 4. Finally, the conclusions drawn by the results are summarized.

2 The Model

The model is the 1D shallow water equations for a non–prismatic channel, with the following assumptions (Chaudhry, 2008; Litrico and Fromion, 2009).

- The pressure distribution is hydrostatic.
- The channel bed slope is small *i.e.* the cosine of the angle it makes with the horizontal axis may be replaced by unity.
- The head losses in unsteady flow (due to the effect of boundary friction and turbulence) can be calculated through resistance laws analogous to those used for steady flow.

The Equations for a 1D, unsteady, non–prismatic, open channel system, is expressed as,

$$\frac{\partial A}{\partial t} + \frac{\partial Q}{\partial x} = 0, \tag{1}$$

$$\frac{\partial Q}{\partial t} + \frac{\partial (\beta Q^2/A + gI_1)}{\partial x} = gI_2 + gA\left(S_b - S_f\right), \tag{2}$$

where $A(x,h,t)$ is the wetted cross sectional area normal to the flow, $h(x,t)$ is the depth of flow, $Q(x,t)$ is the volumetric flow rate and $S_f(Q,x,h)$ is the friction slope. I_1, the first moment of area represents the hydrostatic pressure term and I_2 represents the pressure forces in the fluid volume, which occur from the longitudinal width and slope variations. g is the gravitational acceleration, t is the time and x is the distance along the flow direction (Chow, 1959; Chaudhry, 2008). β is known as the momentum correction coefficient or

the Boussinesq coefficient and corresponds to the deviations of the local velocity over the mean velocity of the flow. The channel bed slope $S_b(x)$ is calculated by $-\frac{\partial z}{\partial x}$ (z is the absolute fluid level), where it is considered positive when sloping downwards. The friction slope S_f is defined from the Gauckler–Manning–Strickler formulae as follows (Chow, 1959).

$$S_f = \frac{Q\,|Q|\,n_M^2}{A^2 R^{\frac{4}{3}}}, \tag{3}$$

where n_M is the Manning roughness coefficient and R is the hydraulic radius given by $\frac{A}{P}$. Here, P is the wetted perimeter. For a channel with an isosceles trapezoidal cross section I_1 and I_2 can be found as follows,

$$I_1 = \frac{1}{2}h^2 W + \frac{1}{3}h^3 S_s, \quad \text{and} \tag{4}$$

$$I_2 = \frac{1}{2}h^2\frac{dW}{dx} + \frac{1}{3}h^3\frac{dS_s}{dx}. \tag{5}$$

For a channel with a uniform side slope $\frac{dS_s}{dx}$ would be zero. Therefore, the Eqs. 1 and 2 can further be simplified for an isosceles trapezoidal channel with uniform side slope and no lateral inflow rate. This simplified set of equations can be presented in a simpler form as follows,

$$\frac{\partial U}{\partial t} + \frac{\partial F}{\partial x} = S \tag{6}$$

where U vector is the vector of conserved variables as follows,

$$U = (A, Q)^T, \tag{7}$$

$$F = \left(Q, \frac{\beta Q^2}{A} + gI_1\right)^T, \tag{8}$$

and S is the source term as follows,

$$S = (0, \frac{gh^2}{2}\frac{dW}{dx} + gA\,(S_b - S_f))^T. \tag{9}$$

Then the mass flow rate $\dot{m}$ is calculated by multiplying the volumetric flow rate Q with a constant density ρ for a given drilling fluid.

2.1 Model Reduction for Non–Prismatic Channel

The shallow water equations are (as described earlier), a nonlinear hyperbolic system of PDEs. These are commonly known as very complicated systems to solve, because of the non-smooth solutions which could also contain shock and rarefaction waves, and the possible discontinuities (occurs due to discontinuous bottom topography or cross section) (Kurganov, 2018). Further, the numerical solutions could break down even for a system with smooth initial data and no discontinuities. Therefore, solving the shallow water equations in a stable and accurate manner, specially for a non–prismatic channel (with discontinuities) is a difficult task (Kurganov, 2018). There are well–balanced and well–developed numerical schemes available, which address these issues. However, due to the demand of high computational resources these schemes are not suitable for a real time estimation application. Therefore, a model reduction is applied here, in order to obtain fast and accurate enough, application oriented solutions.

The model reduction is done by the use of orthogonal collocation method. The use of the orthogonal collocation method for shallow water equations for a prismatic channel is described in detail in (Jinasena et al., 2017). The construction of ordinary differential equations from orthogonal collocation on the spatial domain, for a non–prismatic channel is briefly described here.

The spatial length x of the channel is divided into $n-1$ non–equidistant spaces between n points, which are known as collocation points (CP). The state vector U of the shallow water model at these specific points can be approximated by polynomial interpolation (Isaacson and Keller, 1966). In this study, the Lagrange interpolating polynomial is used for this purpose. The approximated states vector U_a can be expressed as follows,

$$U_a(x,t) = \sum_{i=1}^{n} L_i(x)U_i(t), \tag{10}$$

Here, the subscript i denotes the i^{th} position along the channel and L_i is a weighted fraction defined as follows,

$$L_i = \prod_{\substack{j=1 \\ j\neq i}}^{n} \frac{x - x_j}{x_i - x_j}, \tag{11}$$

where, x is the entire set of n number of positions. The derivatives of these approximated states can be derived as follows,

$$\frac{\partial U_a}{\partial x} = \sum_{i=1}^{n} L_{ij}^{'} U_i, \tag{12}$$

where $L_{ij}^{'}$ is the element at i^{th} row and j^{th} column of the matrix $L^{'}$,

$$L^{'} = \left(\frac{\partial L_1}{\partial x}, \frac{\partial L_2}{\partial x}, \ldots, \frac{\partial L_n}{\partial x}\right)^T. \tag{13}$$

Similarly, the other functions of x, $\left(\frac{\beta Q^2}{A},\ I_1,\ h \text{ and } W\right)$ can be approximated using the same method and the derivatives can also be found. The equations expanded from the original

Eqs. 6 can be approximated with these approximated functions as follows,

$$\frac{dA_a}{dt} + \sum_{i=1}^{n} L_{ij}^{'} Q_a \approx 0, \tag{14}$$

and

$$\begin{aligned} &\frac{dQ_a}{dt} + \sum_{i=1}^{n} L_{ij}^{'} \frac{\beta Q_a^2}{A_a} + g \sum_{i=1}^{n} L_{ij}^{'} I_{1_a} \\ &- \frac{g h_a^2}{2} \sum_{i=1}^{n} L_{ij}^{'} W_a - g A_a \left(S_b - S_f\right) \approx 0. \end{aligned} \tag{15}$$

Considering the functions at the selected CPs, the approximated value will be the same as the functional value, since the approximation of the function was done at these particular points. Therefore, the approximated Eqs. 14 and 15 would be equal to zero and can be expressed as follows after re–arranging,

$$\frac{dA_i}{dt} = -\sum_{i=1}^{n} L_{ij}^{'} Q_i, \tag{16}$$

and

$$\begin{aligned} \frac{dQ_i}{dt} = &- \sum_{i=1}^{n} L_{ij}^{'} \frac{\beta Q_i^2}{A_i} - g \sum_{i=1}^{n} L_{ij}^{'} I_{1_i} \\ &+ \frac{g h_i^2}{2} \sum_{i=1}^{n} L_{ij}^{'} W_i + g A_i \left(S_b - S_f\right). \end{aligned} \tag{17}$$

The number of CPs in this study are selected as 2, 3 and 4, and the position of these points are selected according to the shifted Legendre polynomials (Jinasena et al., 2017). The corresponding matrices for $L^{'}$ for 2, 3 and 4 CPs are stated below, respectively,

$$L^{'} = \frac{1}{L} \begin{bmatrix} -1 & 1 \\ -1 & 1 \end{bmatrix}, \tag{18}$$

$$L^{'} = \frac{1}{L} \begin{bmatrix} -3 & 4 & -1 \\ -1 & 0 & 1 \\ 1 & -4 & 3 \end{bmatrix}, \tag{19}$$

$$L^{'} = \frac{1}{L} \begin{bmatrix} -7.0005 & 8.1964 & -2.1959 & 1 \\ -2.7326 & 1.7328 & 1.73190 & -0.7321 \\ 0.7321 & -1.7319 & -1.7328 & 2.7326 \\ -1 & 2.1959 & -8.1964 & 7.0005 \end{bmatrix}, \tag{20}$$

where L is the length of the channel. The geometry of the channel that is used for the simulations is shown in Figure 2.

2.2 Kurganov–Petrova (KP) Scheme for Validation

To compare the results from the collocation model, a well developed, semi-discrete, second order and central upwind scheme, which has specifically been used to solve Saint–Venant systems (Bernstein et al., 2016; Bollermann et al., 2013) is used. With the use of the KP scheme by Kurganov and Petrova (2007), the PDE model is discretized in space into a set of ODEs. For a control volume as shown in Figure 3, the ODEs are written as follows,

$$\frac{d}{dt}\overline{U}_j = -\frac{H_{j+\frac{1}{2}} - H_{j-\frac{1}{2}}}{\Delta x} + \overline{S}(t). \tag{21}$$

$\overline{S}$ is the average value of the source term calculated using the average values of the conserved variables. $H_{j\pm\frac{1}{2}}$ represent the fluxes flowing into the cell (minus sign) and out of the cell (plus sign) respectively. Assuming that there are no changes in the bed slope the fluxes are given by,

$$\begin{aligned} H_{j+\frac{1}{2}} = &\frac{a^{+}_{j+\frac{1}{2}} F\left(U^{-}_{j+\frac{1}{2}}\right) - a^{-}_{j+\frac{1}{2}} F\left(U^{+}_{j+\frac{1}{2}}\right)}{a^{+}_{j+\frac{1}{2}} - a^{-}_{j+\frac{1}{2}}} \\ &+ \frac{a^{+}_{j+\frac{1}{2}} a^{-}_{j+\frac{1}{2}}}{a^{+}_{j+\frac{1}{2}} - a^{-}_{j+\frac{1}{2}}} \left[U^{+}_{j+\frac{1}{2}} - U^{-}_{j+\frac{1}{2}}\right] \end{aligned} \tag{22}$$

$$\begin{aligned} H_{j-\frac{1}{2}} = &\frac{a^{+}_{j-\frac{1}{2}} F\left(U^{-}_{j-\frac{1}{2}}\right) - a^{-}_{j-\frac{1}{2}} F\left(U^{+}_{j-\frac{1}{2}}\right)}{a^{+}_{j-\frac{1}{2}} - a^{-}_{j-\frac{1}{2}}} \\ &+ \frac{a^{+}_{j-\frac{1}{2}} a^{-}_{j-\frac{1}{2}}}{a^{+}_{j-\frac{1}{2}} - a^{-}_{j-\frac{1}{2}}} \left[U^{+}_{j-\frac{1}{2}} - U^{-}_{j-\frac{1}{2}}\right] \end{aligned} \tag{23}$$

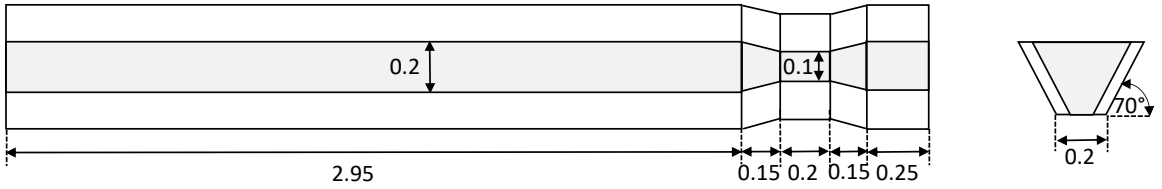

Figure 2: The sketch of the used Venturi channel (measurements are given in meters)

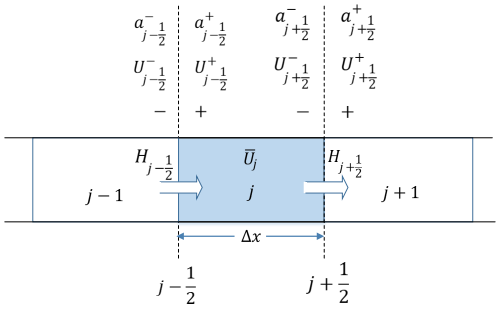

Figure 3: A Control Volume of the KP scheme

where the local speed of wave propagations $a^{\pm}_{j\pm\frac{1}{2}}$ can be calculated as the largest and smallest eigenvalues of the Jacobian of the system.

$$a^+_{j\pm\frac{1}{2}} = \max\left\{u^+_{j+\frac{1}{2}} + \sqrt{gh_{d^+_{j\pm\frac{1}{2}}}}, u^-_{j+\frac{1}{2}} + \sqrt{gh_{d^-_{j\pm\frac{1}{2}}}}, 0\right\} \tag{24}$$

$$a^-_{j\pm\frac{1}{2}} = \max\left\{u^+_{j+\frac{1}{2}} - \sqrt{gh_{d^+_{j\pm\frac{1}{2}}}}, u^-_{j+\frac{1}{2}} - \sqrt{gh_{d^-_{j\pm\frac{1}{2}}}}, 0\right\} \tag{25}$$

Here h_d is the hydraulic depth and is equal to the cross-sectional area of the flow divided by the top width of the flow (T) that is exposed to the atmospheric pressure ($h_d = A/T$).

3 Bayesian Sensitivity Analysis

A sensitivity analysis is a generic method used to evaluate models. This is a way of decomposing the input uncertainty, where we can determine the parameters which are the most influential on the model output. This is done by analyzing the changes in the model output values that happen due to modest changes in the model input values. There are several techniques available for sensitivity analysis, where most approaches determine the effect of changes in one parameter when the others are not changing. However, the combined effect of multiple parameters can also be found. The sensitivities are determined as a percentage variation of the output for a percentage change of each input and/or parameters.

The errors and approximations in the input data measurements, parameter values, model structure and the numerical schemes (model solution algorithm) are the sources of uncertainty in this system. This model highly depends on the values of the parameters, therefore, only the uncertainty in parameters were studied and the analysis of the other sources of uncertainty is out of scope of this study. For this study, all the parameters were tested for sensitivity on the model output flow rate. All the geometrical parameters can be measured directly for a particular system. But the parameters which depend on the fluid properties (n_M and β) cannot be measured always. Therefore a further analysis was done to quantify the effect of uncertainties in these two parameters on the model output and to understand the relationship between these two parameters and the model output.

A Bayesian analysis is used here. The Bayesian method will find the posterior probability with the use of a chosen prior and a likelihood. According to the Bayes theorem,

$$p\left(Y|X\right) = \frac{p\left(X|Y\right) \times p\left(Y\right)}{p\left(X\right)}. \tag{26}$$

The probability of Y given X (posterior $p\left(Y|X\right)$) is found by the probability of X given Y (likelihood $p\left(X|Y\right)$), the probability of Y (prior $p\left(Y\right)$) and the probability of X (model evidence $p\left(X\right)$) (Sivia and Skilling, 2006). Also the marginal likelihood can be obtained by marginalization over the parameters (for example X) as follows,

$$p\left(Y\right) = \int_X p\left(Y|X\right) p\left(X\right) dX. \tag{27}$$

The posterior probability of the output flow rate can be obtained using marginalization for the above mentioned two parameters as follows.

$$p\left(\dot{m}|M,D\right) = \int_a^b \int_c^d p\left(\dot{m}, n_M, \beta|M,D\right) dn_M d\beta \tag{28}$$

Here, $\dot{m}$ is the output of the model *i.e.* mass flow rate (volumetric flow rate Q × density ρ), that we are interested in. The model is denoted by M and the input data is denoted by D, which are considered to be noise free data. a, c, b and d are the minimum and maximum values for the two parameters, respectively. These values are chosen from test simulations, where the full range of values for which the model converges is taken. Further, with use of the product rule and the independence between n_M and β, the right hand side can be expanded as follows,

$$p\left(\dot{m}, n_M, \beta|M,D\right) = p\left(n_M|M,D\right) p\left(\beta|M,D\right) \times p\left(\dot{m}|n_M,\beta,M,D\right), \tag{29}$$

which leads to the following expression.

$$p\left(\dot{m}|M,D\right) = \int_a^b \int_c^d p\left(n_M|M,D\right) p\left(\beta|M,D\right) \times p\left(\dot{m}|n_M,\beta,M,D\right) dn_M d\beta \tag{30}$$

Here, n_M and β are assumed to be random variables with Gaussian distributions of known means and standard deviations. The mean value is decided based on the test simulations, where it will give a certain desired flow rate as the output. The standard deviation is selected to cover the entire range of values that are possible for the simulated flow condition and model convergence. Further, both the data and the model are deterministic, therefore $p\left(\dot{m}|n_M, \beta, M, D\right)$ can be written as a delta function as follows,

$$p\left(\dot{m}|n_M, \beta, M, D\right) = \delta\left\{\dot{m} - M\left(D, n_M, \beta\right)\right\}, \quad (31)$$

which is zero everywhere except at $M\left(D, n_M, \beta\right) = \dot{m}$.

4 Results and Discussion

The models are simulated for the trapezoidal non–prismatic channel geometry using MATLAB (9.2). The initial conditions for the simulation are selected carefully. Runge–Kutta 4^{th} order time integrator is used with a fixed time step. The design of the channel geometry (see Figure 2) ensures trans–critical flow conditions for all conditions at the upstream. For example, if the upstream conditions are sub–critical, the flow becomes critical or super–critical at the throat. And if the upstream is at super–critical conditions, the flow at the throat becomes sub–critical. The trans–critical flows allow the possibility of using one or more boundary conditions. Hence, both of these trans–critical flow conditions are simulated with the inlet fluid level (converted in to the wetted cross sectional area) as the boundary condition for each different model. The different models are the model with KP scheme, and the models with different numbers of CPs. The results and the discussion for these followed by the sensitivity study results are stated below. The position of the collocation points along the channel were selected in a way that always the last point would lie in the middle of the throat, and the rest of the points are at upstream. Both the flow rate and the fluid levels were calculated at all points, except the boundary fluid level.

4.1 Comparison of Different Models

The collocation models were simulated for one boundary condition at the upstream, which is the wetted cross sectional area at the inlet. Step responses were given to check the model responses for changes with time. Figure 4 shows the results obtained for the mass flow rates for the super–critical to sub–critical flow condition using each model. The mass flow rates are calculated from the volumetric flow rates for a given drilling fluid density. The results for the collocation models are compared with the KP scheme in Figure 4. It is worth mentioning that the KP scheme is difficult to implement for super–critical upstream conditions with fluid level as a boundary. Therefore, KP scheme is used with the upstream flow rate as the boundary and the resulting fluid level at upstream is used as the boundary for the collocation models.

The mass flow rates for the super–critical to sub–critical, trans–critical conditions are well comparable in all the models. These are relatively easier simulation

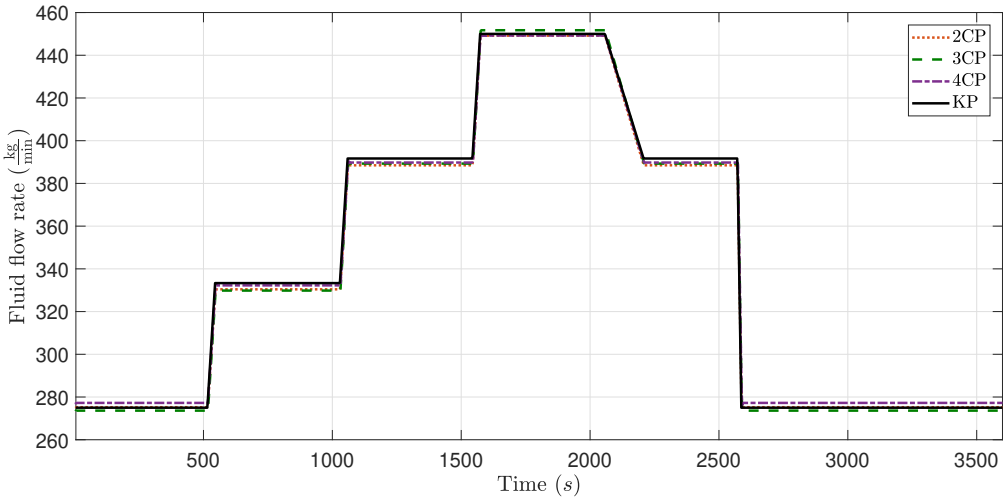

Figure 4: The mass flow rates calculated from different models for super–critical upstream conditions. 'KP': KP scheme and '2, 3 or 4 CP': model with 2, 3 or CPs.

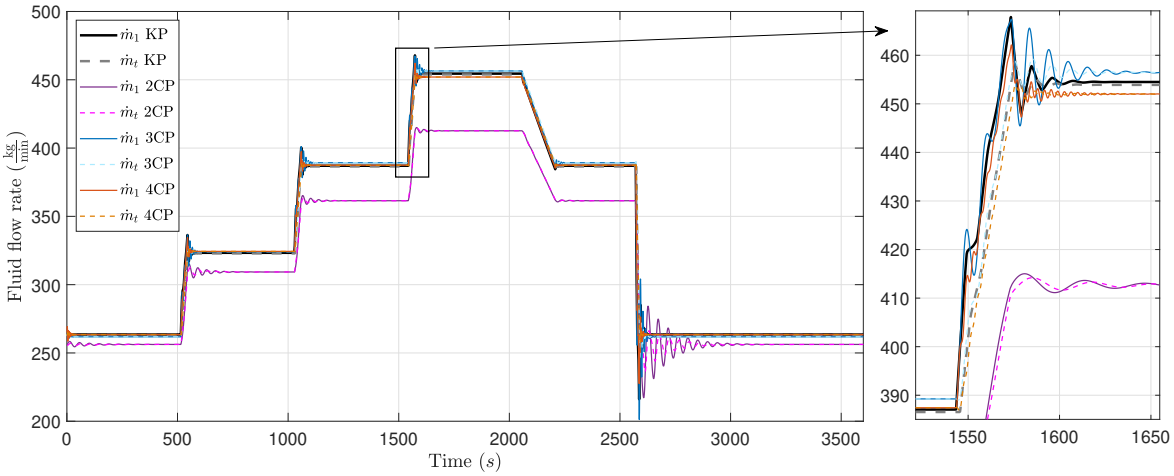

Figure 5: The mass flow rates calculated from different models for sub–critical upstream conditions. 'KP': KP scheme and '2, 3 or 4 CP': model with 2, 3 or CPs. The subscripts 1 and t denote the first and last positions of the collocation points along the channel.

conditions because the interference from waves (oscillations in fluid levels which propagates to the mass flow rate calculations) is less significant due to high velocities of the flow. However, more interesting flow behaviors can be observed with the trans–critical condition from sub–critical to super–critical, which is shown in Figure 5. Here, the KP scheme is also simulated taking the wetted cross sectional area at the upstream as the boundary.

From Figure 5, it can be clearly seen that the model with 3 and 4 CPs is more comparative with the KP results than the model with 2 CPs. Further, the results with 4 CP model is closer to the KP results than the results with 3 CP model. This is expected because the more the CPs, the better the approximation is. However, the number of oscillations that occur due to step changes is higher when the number of CPs are higher. But the time taken to reach steady state is shorter with the increase of number of CPs. Further, the amplitude of the oscillations are bigger, with 3 CP model. This is due to the Runge's phenomenon, which is the occurrence of oscillations when using polynomial interpolation over equi–spaced interpolation points. The 4 CPs are not equi–spaced, therefore, this effect is not seen with 4 CP model.

The shallow water equations, which are used in this study, is presented in the conservative form, so that it preserves the mass conservation along the entire spatial domain at steady state. This mass conservation can be seen in the collocation models, since the mass flow rates at all the CPs are the same.

The 2 CP model was the quickest to simulate and the 3 and 4 CP models take about 10–15 times more simulation time than the 2 CP model. KP scheme usually takes 40–50 times more simulation time than the CP models. The results from the 2 CP model for sub–critical upstream conditions is unsatisfactory. However, the use of 3 or 4 CPs for any flow condition, is enough to obtain similar results to KP scheme. Therefore, in an online estimation application the use of 3 or 4 CP model would give sufficiently accurate results with less computational time. This means that with the 3 or 4 CPs model it is possible to obtain a fast estimate of the flow rate in real–time. Although there are oscillations in the presence of an abrupt step change in a sub–critical flow condition will eventually reach to the steady state in a relatively short period of time.

As a summary, the reduced order model was able to capture the general fluid flow behaviors. Appearance of transient oscillations can be observed in both the models (reduced order model as well as the KP scheme), when a step change is given to the input. The CP models (especially the 2 CP model) show prolonged oscillations before settling down to a steady state value in the presence of sharp step changes in the input/inlet boundary conditions (at $t = 2500$s in Figure 4). Such abrupt step changes in the input is simulated here as this can be expected to occur during a kick or loss in drilling system. When the stepping is done gradually throughout a longer time period (ramping, at $t = 2000$s in Figure 4), the flow comes to a steady state value quickly, with less oscillations. This behav-

ior is expected during the pipe connection procedure in drilling, where the mud pump is stopped and started gradually.

4.2 Sensitivity Analysis Results

The sensitivity analysis was done for all the models (KP scheme and collocation with 2, 3 and 4 CPs) for sub–critical upstream flow conditions. The inlet fluid level and all of the fluid and geometrical parameters are tested for sensitivity of the flow rate.

A spider plot, which shows the sensitivity of the input parameters on the output flow rate for each model is shown in Figure 6. For all the models, the channel bed slope has the highest sensitivity. In addition, the inlet fluid level and the bottom widths of the channel are also sensitive parameters. However, the calculations are done using the nominal fluid levels for bed slope changes. But in reality, when the channel bed slope changes, the fluid levels in the channel also change accordingly, thus may reduce the sensitivity to the flow rate. This is also true for the bottom width W_1. The change of fluid level due to the changes in the bed slope and the bottom width W_1, are not taken into account in the calculations, for simplicity of comparison. Nonetheless, the effect of the channel bed slope should be taken into consideration in a real fluid flow scenario due to its high sensitivity with the flow rate and the fluid flow conditions. A small increase in the channel bed slope of the Venturi channel that is taken into consideration can change the sub–critical upstream conditions into super–critical conditions. Therefore, in this study, the bed slope is changed only within a small range, due to the limitation of the flow conditions based on the used geometry.

Most of the parameters have a bigger impact on the 2 CP model than on the other models.

Even though the effect of geometrical parameters (W_1, W_t, S_s and L) on the 3 and 4 CP models are comparatively lower, the flow rate can still be affected significantly. In order to reduce the effect on the magnitude of the flow rate, the geometrical parameters can be measured accurately for each geometry. The fluid properties such as friction factor n_M and β are tunable parameters, hence can be estimated together with the flow rate, in the context of adaptive estimation. However, the input (Ain) and the channel bed slope may change with time, hence have to be measured with a good accuracy and precision due to their high sensitivity.

For an estimation application, an analysis of the sensitivity of the estimable parameters on the output flow rate will be informative in advance. Therefore, the change of flow rate due to perturbations in the two estimable parameters (n_M and β) is analyzed with the use of the Bayesian sensitivity analysis described in Section 3. In order to determine the marginal posterior distribution of the mass flow rate shown by Eq. 30, a large number of independent samples (10000 pairs), representing n_M and β, were generated from their respective Gaussian distributions. Then for each pair, depending on the model, the corresponding steady

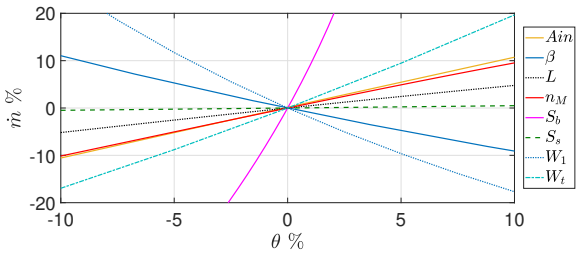

(a) 2 CP

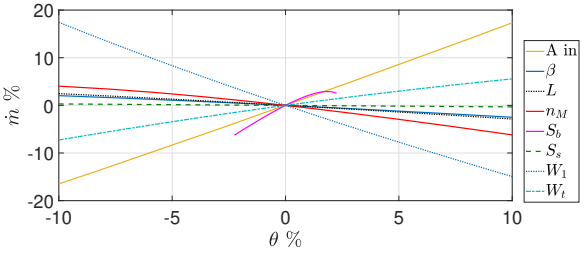

(b) 3 CP

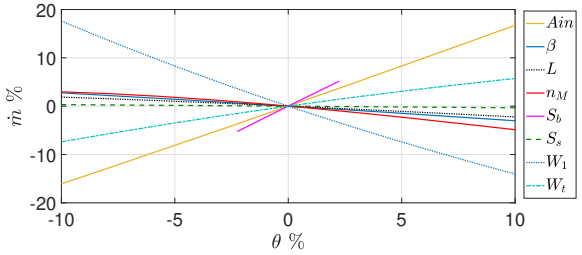

(c) 4 CP

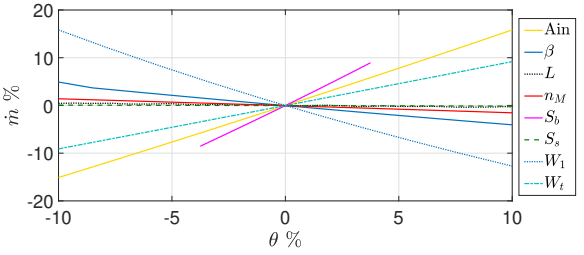

(d) KP

Figure 6: The spider plots showing the relationship of percentage mass flow rate to the percentage deviation of each parameter (θ) from their nominal values.

state mass flow rates were calculated. The histogram of n_M, β and $\dot{m}$ can be considered as an estimate for the joint posterior distribution of these triples, conditional on the appropriate model ($p(n_M, \beta, \dot{m}|M)$). Similarly, the marginal posterior distribution of the mass flow rate ($p(\dot{m}|M)$) can be approximated by considering only the histogram of the mass flow rate of the samples. These posterior distributions for each model are shown in Figure 7. For the sake of comparison, the histograms are vertically scaled so that their highest value is unity. Further, a Gaussian distribution is fitted to the marginal posterior histogram of the output flow rate (shown by red curve in Figure 7).

The two parameters for the models had to be tuned to ensure the model convergence for sub–critical to super–critical flow conditions. Therefore, in some of the models (especially in 3 and 4 CP models) the parameter values may not be meaningful. It is shown that the used Gauckler–Manning–Strickler formulae with a constant n_M is suitable only for uniform flows (Chow, 1959). During the transition the flow is not uniform. Further, it is suggested that the n_M depends on the hydraulic radius and the Froude number, hence could not be a constant (Tullis, 2012). However, it is also shown that at super–critical flow conditions this is relatively constant (Tullis, 2012). This might be the reason that the collocation models had to be tuned for sub–critical flow conditions.

The mean (μ) and the standard deviation (σ) of the estimated mass flow rate distributions together with the values of the chosen parameter distributions for each model are tabulated in Table 1. For comparison, the percentage deviation is shown in Table 2. The full range of possible parameter values for n_M and β are not used here due to the limitation of model convergence. Because of this the distribution could be truncated towards the tails, even though it is approximated with the Gaussian distribution.

As shown in the tables, the 2 CP model has a significant change in flow rate, due to the high sensitivity of the parameters. Further, it can be seen from the tabulated percentage changes, that the perturbations in the two parameters have caused less impact on the flow

Table 1: Details of input parameters and output flow rate for different models

Model	n_M		β		$\dot{m}$	
	μ	σ	μ	σ	μ	σ
2 CP	0.0135	0.0007	0.98	0.039	236.4	10.3
3 CP	0.0305	0.0015	0.6	0.024	283.8	8.1
4 CP	0.0465	0.0023	0.46	0.019	282.7	9.2
KP	0.0133	0.0007	0.98	0.04	283.0	5.4

Table 2: Percentages of Parameters and flow rate

Model	n_M %	β %	$\dot{m}$ %
2 CP	4.96	3.96	4.36
3 CP	5.02	4.04	2.86
4 CP	5.00	4.05	3.25
KP	5.26	4.10	1.91

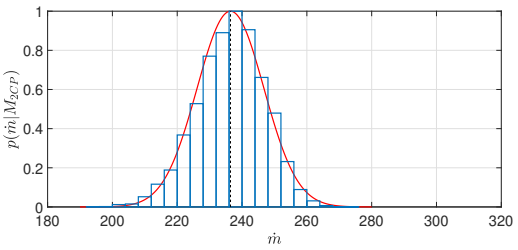

(a) 2 CP model

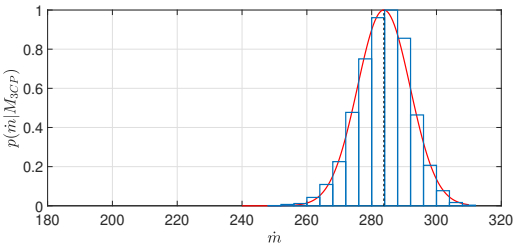

(b) 3 CP model

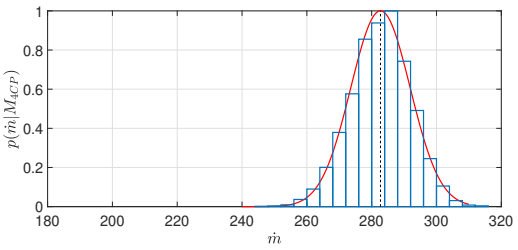

(c) 4 CP model

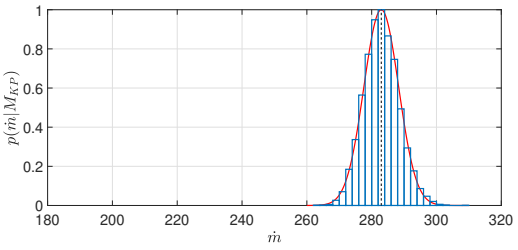

(d) KP model

Figure 7: The probability distributions of the output mass flow rate ($p(\dot{m}|M)$) for different models.

rate, when the number of CPs are 3 or 4. Since there is no significant improvement with the 4 CP model than the 3 CP model, it is a trade off between the slightly better accuracy and the slightly higher computation time.

However, the dominance of the correlation of the two parameters with the output flow rate will strictly depend on the choice of these two parameter values, which then indirectly affects the output flow rate itself. These correlations between the parameters and the flow rate can clearly be seen from the scatter plots obtained from the simulations. The scatter plots and the contours drawn on their densities are shown in Figure 8, for all the models. The 3 and 4 CP models show a dominant correlation of flow rate with n_M, while the KP model shows more dominance with β. This could be due to the choice of the mean values of the parameters for a desired output flow rate. Since the parameters are tuned in order to get a desired flow rate, we cannot decide about the accuracy between the models based on the parameter values. However, we can have an idea about the desired flow rate and the precision. Further, the 3 CP results with β (in Figure 8b) are truncated due to the crossing into the sub–critical region at the throat as oppose to the super–critical region. This further indicates that a careful selection of the values for these two parameters by means of estimation/adaptation will be needed for an accurate flow

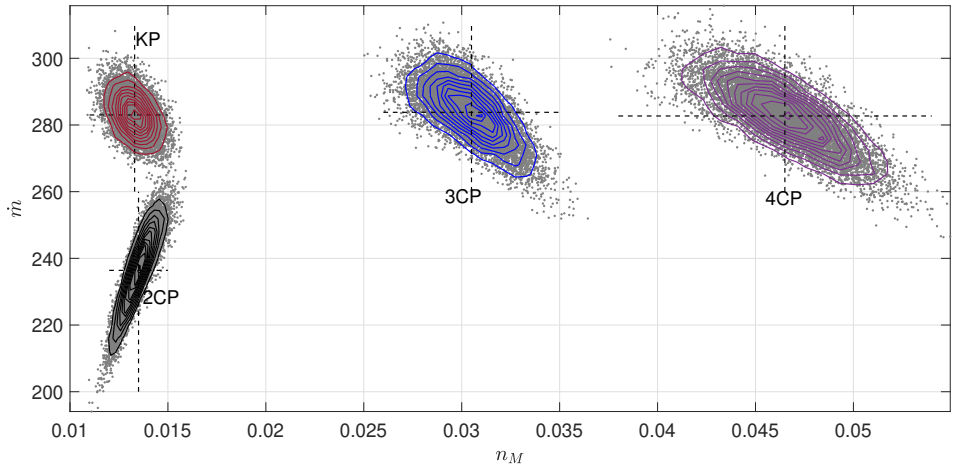

(a)

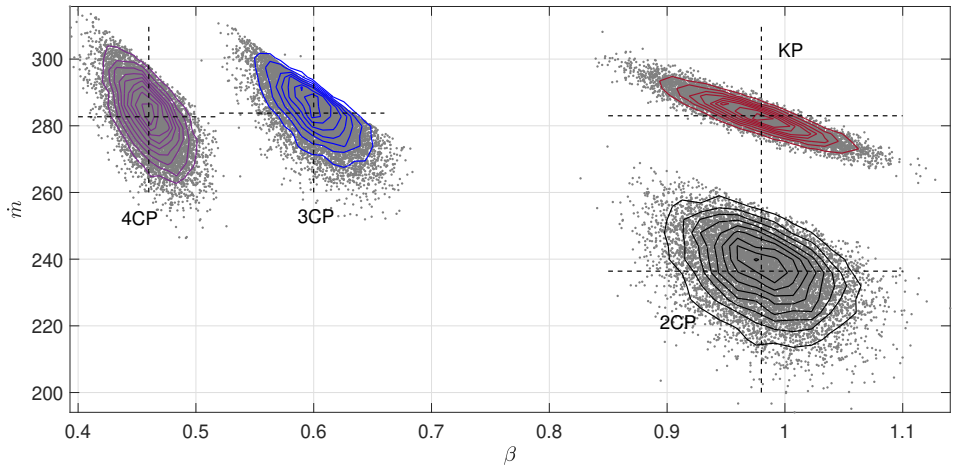

(b)

Figure 8: The scatter plots with the input parameters and output flow rate. (a) for n_M and (b) for β.

rate estimation. This study will be carried out in the future.

Further, the expected relationship of both n_M and β with the flow rate is generally a negative relationship, based on the model structure. This cannot be seen with n_M and the flow rate with the 2 CP model as shown in Figure 8, in fact it shows a complete opposite relationship, which is difficult to interpret according to physical laws. Since the 2 CP model is highly sensitive to most of the parameters, this might have occurred due to improper domination of other parameters over n_M. With 2 CP model the CPs fall on the boundaries, and the information of the states inside the channel between the boundaries is not captured by the model. 2 CP model is faster and simpler but less accurate and less physically sound than the other models. This further implies that the model simplification comes with a cost on accuracy and physical explanation. Although these models are not suitable for estimating the friction factor, it is (3 CP or 4 CP model) accurate and fast enough to estimate the flow rate based on the level measurement.

However, to obtain a better understanding of the model, other uncertainty sources such as the structural uncertainty and numerical uncertainty may also need to be explored. The structural uncertainty which occurs due to the improper approximations of the real system and the numerical uncertainty which occurs due to the discretization and model reduction could be studied in future with a comparison to a real system. Further, a proper selection of the tunable parameters (n_M and β) should be done in order to ensure a good estimation of the flow rate. Due to the high sensitivity of the bed slope and the inlet fluid level in all the models, a careful consideration of the uncertainty in these two measurements should be taken into account in a real world application. The knowledge and results obtained from this study will be beneficial for such studies and applications in the future.

5 Conclusions

This paper highlights a reduced order open channel model which can be used to estimate the flow rate in an open channel. The model is developed to be used for a Venturi channel in the drain back flow line during an oil well drilling to estimate the flow rate of the return fluid. The simplified model is simulated for a non-prismatic open channel Venturi with a throat. The reduced order model is a set of ODEs hence faster and less complex than the shallow water equations. The reduced order models are validated using simulations from a well–developed finite volume method. Two trans–critical conditions (super–critical to sub–critical and sub–critical to super–critical) are simulated using the upstream fluid level as the boundary condition. Three or four collocation points seem to be sufficient to obtain a good accuracy for the determination of the flow rate in both the flow conditions. Further, a parameter sensitivity analysis of all the models is also done to evaluate the reduced order models. This model structure is well suited to be used in process control and state estimation algorithms, where the state estimates have to be computed in real–time. The proposed solution of using a Venturi channel for on–line estimation of return flow rate during drilling seems possible together with the use of a reduced order collocation model.

Acknowledgments

The economic support from The Research Council of Norway and Statoil ASA through project no. 255348/E30 'Sensors and models for improved kick/loss detection in drilling (Semi–kidd)' is gratefully acknowledged.

References

Bernstein, A., Chertock, A., and Kurganov, A. Central-upwind scheme for shallow water equations with discontinuous bottom topography. *Bulletin of the Brazilian Mathematical Society*, 2016. 47(1):91–103. doi:10.1007/s00574-016-0124-3.

Bollermann, A., Chen, G., Kurganov, A., and Noelle, S. A Well-Balanced Reconstruction of Wet/Dry Fronts for the Shallow Water Equations. *Journal of Scientific Computing*, 2013. 56(2):267–290. doi:10.1007/s10915-012-9677-5.

Chanson, H. *The Hydraulics of Open Channel Flow: An Introduction.* Elsevier Butterworth-Heinemann, Burlington, 2nd edition, 2004.

Chaudhry, M. H. *Open-Channel Flow.* Springer, New York, 2nd edition, 2008.

Chhantyal, K., Viumdal, H., Mylvaganam, S., and Elseth, G. Ultrasonic Level Sensors for Flowmetering of non- Newtonian Fluids in Open Venturi Channels: Using Data Fusion based on Artificial Neural Network and Support Vector Machines. In *2016 IEEE Sensors Applications Symposium (SAS)*. Catania, pages 1–6, 2016. doi:10.1109/SAS.2016.7479829.

Chow, V. T. *Open-Channel Hydraulics.* McGraw-Hill, New York, 1959.

Dulhoste, J.-F., Georges, D., and Besançon, G. Nonlinear Control of Open-Channel Water Flow

Based on Collocation Control Model. *Journal of Hydraulic Engineering*, 2004. 130(3):254–266. doi:10.1061/(ASCE)0733-9429(2004)130:3(254).

Georges, D., Dulhoste, J.-f., and Besançon, G. Modelling and Control of Water Flow Dynamics via a Collocation Method. In *Math. Theory of Networks and Systems*. 2000.

Isaacson, E. and Keller, H. B. *Analysis of Numerical Methods*. John Wiley & Sons, New York, 2nd edition, 1966.

Jinasena, A., Kaasa, G.-O., and Sharma, R. Use of Orthogonal Collocation Method for a Dynamic Model of the Flow in a Prismatic Open Channel : For Estimation Purposes. In *Proceedings of the 58th Conference on Simulation and Modelling (SIMS 58)*, 138. Linköping University Electronic Press, Linköpings universitet, Reykjavik, Iceland, pages 90–96, 2017. doi:10.3384/ecp1713890.

Kurganov, A. Finite-volume schemes for shallow-water equations. *Acta Numerica*, 2018. 27:289–351. doi:10.1017/S0962492918000028.

Kurganov, A. and Petrova, G. A second-order well-balanced positivity preserving central-upwind scheme for the Saint-Venant system. *Communications in Mathematical Sciences*, 2007. 5(1):133–160. doi:10.4310/CMS.2007.v5.n1.a6.

Layton, A. T. A Semi-Lagrangian Collocation Method for the Shallow Water Equations on the Sphere. *SIAM Journal on Scientific Computing*, 2003. 24(4):1433–1449. doi:10.1137/S1064827501395021.

Litrico, X. and Fromion, V. *Modeling and Control of Hydrosystems*. Springer, 2009.

Pirir, I., Jinasena, A., and Sharma, R. Model based flow measurement using venturi flumes for return flow during drilling. *Modeling, Identification and Control: A Norwegian Research Bulletin*, 2017. 38(3):135–142. doi:10.4173/mic.2017.3.3.

Sivia, D. and Skilling, J. *Data Analysis: A Bayesian Tutorial*. Data Analysis: A Bayesian Tutorial. OUP Oxford, 2006.

Tullis, B. P. Hydraulic Loss Coefficients for Culverts: NCHRP REPORT 734. Technical report, National Cooperative Highway Research Program, Utah, 2012.

Article C

Model based Real–Time Flow Rate Estimation in Open Channels with Application to Conventional Drilling

Jinasena, A. and Sharma, R. (2018). Model based Real-Time Flow Rate Estimation in Open Channels with Application to Conventional Drilling. In 18th International Conference on Control, Automation and Systems (ICCAS 2018), pages 546–551, PyeongChang, GangWon, Korea. http://www.dbpia.co.kr/Journal/ArticleDetail/NODE07549683

Overview

The article presents the estimation of flow rate using different estimators based on the reduced order model stated in Article B. A reduced order linear observer has been designed and tested in simulations. Further, a linear Kalman filter, an extended Kalman filter and an unscented Kalman filter are tested and compared. The paper is presented at the 18th International Conference on Control, Automation and Systems (ICCAS 2018) held at PyeongChang, GangWon, Korea from 17th to 20th October 2018. The article is published in the conference proceedings and the student best paper award was received.

Additional Information for Article C

Linearization of the orthogonal collocation model

The system of equations for the model with 3 collocation points is defined as follows,

$$f_1 := \dot{Q}_1 = -\frac{\beta}{l}\left(-3\frac{Q_1^2}{A_1}+4\frac{Q_2^2}{A_2}-\frac{Q_3^2}{A_3}\right)-g\frac{Q_1^2 n_M^2}{A_1 R_1^{\frac{4}{3}}}-\frac{g}{2l}\left(-3h_1^2W_1+4h_2^2W_2-h_3^2W_3\right)$$
$$-\frac{gS_s}{3l}\left(-3h_1^3+4h_2^3-h_3^3\right)+gA_1S_b+\frac{gh_1^2}{2l}(-3W_1+4W_2-W_3), \quad \text{(C.1)}$$

$$f_2 := \dot{Q}_2 = -\frac{\beta}{l}\left(-\frac{Q_1^2}{A_1}+\frac{Q_3^2}{A_3}\right)-g\frac{Q_2^2 n_M^2}{A_2 R_2^{\frac{4}{3}}}-\frac{g}{2l}\left(-h_1^2W_1+h_3^2W_3\right)-\frac{gS_s}{3l}\left(-h_1^3+h_3^3\right)$$
$$+gA_2S_b+\frac{gh_2^2}{2l}(-W_1+W_3), \quad \text{(C.2)}$$

$$f_3 := \dot{Q}_3 = -\frac{\beta}{l}\left(\frac{Q_1^2}{A_1}-4\frac{Q_2^2}{A_2}+3\frac{Q_3^2}{A_3}\right)-g\frac{Q_3^2 n_M^2}{A_3 R_3^{\frac{4}{3}}}-\frac{g}{2l}\left(h_1^2W_1-4h_2^2W_2+3h_3^2W_3\right)$$
$$-\frac{gS_s}{3l}\left(h_1^3-4h_2^3+3h_3^3\right)+gA_3S_b+\frac{gh_3^2}{2l}(W_1-4W_2+3W_3), \quad \text{(C.3)}$$

$$f_4 := \dot{h}_1 = -\frac{(-3Q_1+4Q_2-Q_3)}{l(W_1+2S_sh_1)}, \quad \text{(C.4)}$$

$$f_5 := \dot{h}_2 = -\frac{(-Q_1+Q_3)}{l(W_2+2S_sh_2)}, \quad \text{(C.5)}$$

$$f_6 := \dot{h}_3 = -\frac{(Q_1-4Q_2+3Q_3)}{l(W_3+2S_sh_3)}. \quad \text{(C.6)}$$

The linearized system with states $x=[Q_1\ Q_2\ Q_3\ h_1\ h_2\ h_3]^T$ around their operating points $\bar{x}=[\bar{Q}_1\ \bar{Q}_2\ \bar{Q}_3\ \bar{h}_1\ \bar{h}_2\ \bar{h}_3]^T$, can be expressed as follows,

$$\dot{X}=AX, \quad \text{(C.7)}$$

where, $\dot{X}=[\dot{Q}_1^\delta\ \dot{Q}_2^\delta\ \dot{Q}_3^\delta\ \dot{h}_1^\delta\ \dot{h}_2^\delta\ \dot{h}_3^\delta]^T$ and $X=[\delta_1\ \delta_2\ \delta_3\ \delta_4\ \delta_5\ \delta_6]^T$. δ is the difference between the actual states and the operating points ($\delta=x-\bar{x}$). An element in matrix A can be expressed as follows,

$$A_{ij}=\left.\frac{\partial f_i}{\partial x_j}\right|_{\bar{x}}, \quad i=j=[1,2,\ldots,6]. \quad \text{(C.8)}$$

A system with h_1 as input (due to the upstream boundary condition) can be written in deviation form as follows,

$$\dot{X} = A^* X + Bu, \tag{C.9}$$

where $X = [\delta_1 \ \delta_2 \ \delta_3 \ \delta_5 \ \delta_6]^T$ and $u = \delta_4 = (h_1 - \bar{h}_1)$. A^* and B can be expressed using A as follows,

$$A^* = \begin{bmatrix} A_{(1:3,1:3)} & A_{(1:3,5:6)} \\ A_{(5:6,1:3)} & A_{(5:6,5:6)} \end{bmatrix}, \tag{C.10}$$

and

$$B = \begin{bmatrix} A_{(4,1:3)} & A_{(4,5:6)} \end{bmatrix}^T. \tag{C.11}$$

The following terms are defined for $k = [1,2,3]$, for the clarity in presentation,

$$T_{1_k} := \quad \frac{\beta Q_k}{l(W_k h_k + S_s h_k^2)} \tag{C.12}$$

$$T_{2_k} := \quad \frac{g Q_k n_M^2}{W_k h_k + S_s h_k^2 \left(\frac{W_k h_k + S_s h_k^2}{W_k + 2h_k\sqrt{1+S_s^2}}\right)^{\frac{4}{3}}} \tag{C.13}$$

$$T_{3_k} := \quad \frac{g S_s h_k^2}{l} + \frac{g h_k W_k}{l} - \frac{\beta Q_k^2 (W_k + 2S_s h_k)}{l(W_k h_k + S_s h_k^2)^2} \tag{C.14}$$

$$T_{4_k} := \quad \frac{4 g Q_k^2 n_M^2 \left(\frac{W_k + 2S_s h_k}{W_k + 2h_k\sqrt{1+S_s^2}} - \frac{2(W_k h_k + S_s h_k^2)\sqrt{1+S_s^2}}{(W_k + 2h_k\sqrt{1+S_s^2})^2}\right)}{3(W_k h_k + S_s h_k^2)\left(\frac{W_k h_k + S_s h_k^2}{W_k + 2h_k\sqrt{1+S_s^2}}\right)^{\frac{7}{3}}} \tag{C.15}$$

$$T_{5_k} := \quad \frac{g Q_k^2 n_M^2 (W_k + 2S_s h_k)}{\left(W_k h_k + S_s h_k^2\right)^2 \left(\frac{W_k h_k + S_s h_k^2}{W_k + 2h_k\sqrt{1+S_s^2}}\right)^{\frac{4}{3}}} \tag{C.16}$$

$$T_{6_k} := \frac{1}{l(W_k + 2S_s h_k)} \tag{C.17}$$

$$T_{7_k} := gS_b(W_k + 2S_s h_k) \tag{C.18}$$

$$T_8 := \frac{gh_1(3W_1 - 4W_2 + W_3)}{l} \tag{C.19}$$

$$T_9 := \frac{gh_2(W_1 - W_3)}{l} \tag{C.20}$$

$$T_{10} := \frac{gh_3(W_1 - 4W_2 + 3W_3)}{l} \tag{C.21}$$

$$T_{11} := \frac{2S_s(3Q_1 - 4Q_2 + Q_3)}{W_1 + 2S_s h_1} \tag{C.22}$$

$$T_{12} := \frac{2S_s(Q_1 - Q_3)}{W_2 + 2S_s h_2} \tag{C.23}$$

$$T_{13} := \frac{2S_s(Q_1 - 4Q_2 + 3Q_3)}{W_3 + 2S_s h_3} \tag{C.24}$$

Each element A_{ij} in A is expressed as follows.

$$A = \begin{bmatrix} 6T_{1_1} - 2T_{2_1} & -8T_{1_2} & 2T_{1_3} & T_{14} & -4T_{3_2} & T_{3_3} \\ 2T_{1_1} & -T_{2_2} & -2T_{1_3} & T_{3_1} & T_{15} & -T_{3_3} \\ -2T_{1_1} & -8T_{1_2} & -6T_{1_3} - 2T_{2_3} & -T_{3_1} & 4T_{3_2} & T_{16} \\ 3T_{6_1} & -4T_{6_1} & T_{6_1} & -T_{6_1}T_{11} & 0 & 0 \\ T_{6_2} & 0 & T_{6_2} & 0 & -T_{6_2}T_{12} & 0 \\ -T_{6_3} & 4T_{6_3} & -3T_{6_3} & 0 & 0 & T_{6_3}T_{13}, \end{bmatrix} \tag{C.25}$$

Here,

$$T_{14} := 3T_{3_1} + T_{7_1} + T_{4_1} + T_{5_1} - T_8, \tag{C.26}$$

$$T_{15} := T_{4_2} + T_{5_2} + T_{7_2} - T_9, \tag{C.27}$$

$$T_{16} := -3T_{3_3} + T_{4_3} + T_{5_3} + T_{7_3} + T_{10}. \tag{C.28}$$

The linearized system is used for the linear observability analysis of the system and is found to be observable.

The results of EKF

The plot shown in Figure C.1 are the simulation results for the same conditions as for Fig. 3 in Article C, but without the noise in the reference flow rate for clarity.

The EKF showed a slight offset at higher flow rates than the UKF, both with simulation results and experimental data. Although the EKF is not an optimal estimator for non-linear systems in general, it is one of the most used estimators

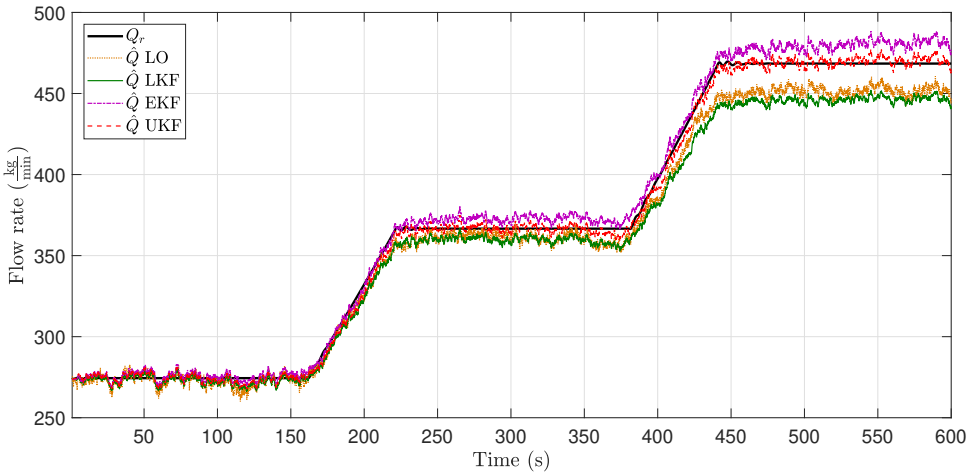

Figure C.1: The estimated out flow rates for various estimators. Q_r: target mass flow rate from the reference model, $\hat{Q}$: estimated mass flow rate from various estimators.

in nonlinear systems (Kolås et al., 2009). However, several authors have reported certain shortcomings/flaws with EKF in nonlinear systems (Haseltine and Rawlings, 2005; Wan and Merwe, 2000; Romanenko et al., 2004; Chang and Chen, 1995). These flaws are associated with the problems in calculating the Jacobians, errors introduced by linearization and/or problems dealing with multimodal or asymmetric probability density functions (Kolås et al., 2009). The most common problem is based on the errors induced by the first order linearization in highly non-linear systems, which could also be the reason for the offset in this study. In EKF algorithm the a priori state mean can be estimated by directly propagating the nonlinear system. However, the covariance estimate needs the calculation of the state transitions matrix, which needs to be obtained by linearization of the system model. This could introduce significant errors depending on the nonlinearity of the system model, and when the initial state estimation error is not sufficiently small (Zarei and Poshtan, 2010).

2018 18th International Conference on Control, Automation and Systems (ICCAS 2018)
Oct. 17–20, 2018; YongPyong Resort, PyeongChang, GangWon, Korea

Model based Real–Time Flow Rate Estimation in Open Channels with Application to Conventional Drilling

Asanthi Jinasena* and Roshan Sharma

Department of Electrical Engineering, IT and Cybernetics,
University of South–Eastern Norway, Norway
(asanthi.jinasena@usn.no; roshan.sharma@usn.no)* Corresponding author

Abstract: Improvements in kick/loss detection are a key research interest in the drilling industry. Cost–effective, accurate and advanced online return flow sensors play a vital role in this regard. We have proposed the use of a Venturi channel in the return flow line with the possibility of developing it into an online soft sensor. A mechanistic model based online estimator would possibly estimate the flow rate with a reasonable accuracy. A reduced order mathematical model for this purpose has been developed by the authors [4]. In this paper, we study the possibility of estimation of flow rate using different estimators based on this reduced order model. A reduced order linear observer has been designed and tested in simulations. Further, a linear Kalman filter, an extended Kalman filter and an unscented Kalman filter are tested and compared. The extended and unscented Kalman filters are further tested with experimental results. The estimations are accurate enough with a mean absolute error of 2% and 1.9%, respectively. The proposed model based flow estimation idea has a promising potential of developing into an online soft sensor in kick–loss detection algorithms.

Keywords: flow estimation, observer, Kalman filter, open channel flow, kick loss detection, drilling.

1. BACKGROUND

Oil well drilling operations are prone to high risks. Especially, the high risks are associated with the offshore and deepwater drilling operations. Dealing with high operational pressures and temperatures is one of the main factors which makes drilling very risky. Generally, pressure related problems in drilling are high contributors for both risk and cost. Hence, reduction of risk and cost in oil drilling is a key research interest in oil and gas industry. The early detection of kick and loss is crucial part in safe well control operations. A recent study done in the Norwegian Continental Shelf shows that 13% of the triggering causes for well control incidents are due to technical failures of, or imperfect kick detection [1].

The kick and loss detection methods that are used today, can be divided into three main categories as; measuring the flow difference between the inlet and outlet (also known as delta flow measurement), monitoring free gas in the annulus and mud logging [2]. The most common method used in the industry, specially in conventional drilling rigs, is the delta flow measurements together with the mud pit gain, due to the direct relationship of the delta flow with the well pressure (see Fig. 1). There are advanced flow measurement techniques available for the clean flow going into the well, which is comparatively easy to measure. On the contrary, the return flow consists of drill cuttings and gases which makes flow measurement difficult and inaccurate. There are advanced flow-metering technologies available for accurate measurements of flow, such as Coriolis flow meters. These are expensive and may not be accurate enough for return flow in the presence of gasses. Although there are advanced technologies available such as managed pressure drilling incorporated with the Coriolis flow meters as return flow meters, most of the on-shore and off-shore oil rigs still use conventional drilling systems. These conventional drilling processes use intermittent or online return flow rate and density measurements together with mud pit levels for kick and loss detection. There are various flow meters used in these processes, but most of the time paddle flow sensors are used. These have comparatively less accuracy as well as repeatability. In most of the conventional oil rigs, this is just an indicator rather than a real-time flow meter, thus early kick and loss detection can not be expected. Advances in flow metering technology will provide accurate differential flow measurements. Therefore, development of cost-effective, accurate and online sensors for early kick and loss detection is vital.

Real–time estimation of the return fluid (coming out of the well) is important for kick and loss detection algorithms. Equally it is important to study the dynamics of the fluid flow in the return line. The possibility of developing an online flow soft sensor with the use of Venturi effect in open channel flow has been studied recently by [3], [4]. This work is focused on developing model based estimators for estimating the flow rate of the fluid coming out of the well on the top side using a Venturi channel. Two non–intrusive level sensors are used to measure the fluid level at different points along the Venturi channel. A suitable reduced order model of the fluid flow through the channel is used together with these level measurements in order to estimate the flow rate.

The paper is organized as follows. An introduction to the used mathematical model is given in section 2. A detailed description of the observer design followed by a

978-89-93215-15-1/18/$31.00

brief introduction to other estimators is stated in section 3. The results and discussion, followed by the conclusions which are drawn based on the results are shown in sections 4 and 5, respectively.

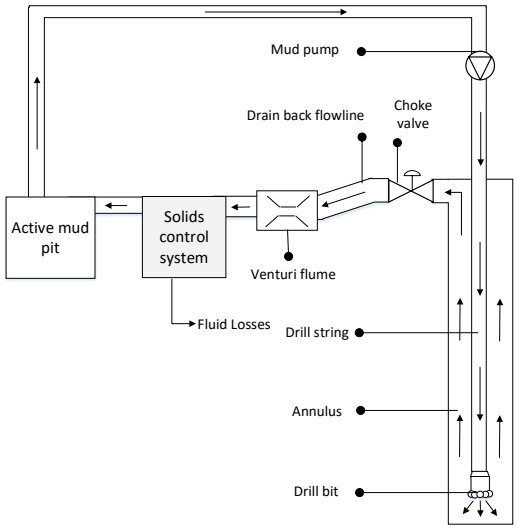

Fig. 1 Illustration of a simplified drilling process with the proposed Venturi flume on the drain back flow line

2. MATHEMATICAL MODEL

The model is developed by using the orthogonal collocation method to discretize the 1D shallow water equations for a non–prismatic, trapezoidal channel, along the spatial direction [4]. Three spatial points (n) are selected along the length l of the Venturi channel. At each point (i = 1, 2 and 3), the levels h_i and volumetric flow rates Q_i are given by the Eqs. $1 \sim 3$. The three points are chosen such that the last point lies on the middle of the Venturi section and the rest is equally distributed towards the upstream channel section.

$$\dot{h}_i = -\sum_{i=1}^{n} L_{ij}^{'} Q_i \frac{1}{W_i + 2S_s h_i}, \tag{1}$$

and

$$\begin{aligned} \dot{Q}_i \quad &= -\sum_{i=1}^{n} L_{ij}^{'} \frac{\beta Q_i \left|Q_i\right|}{A_i} - g\frac{Q_i \left|Q_i\right| n_M^2}{A_i R_i^{\frac{4}{3}}} \\ &-g\sum_{i=1}^{n} L_{ij}^{'} \left(\frac{h_i^2 W_i}{2} + \frac{h_i^3 S_s}{3}\right) + gA_i S_b \\ &+\frac{gh_i^2}{2}\sum_{i=1}^{n} L_{ij}^{'} W_i, \end{aligned} \tag{2}$$

where,

$$L^{'} = \frac{1}{l}\begin{bmatrix} -3 & 4 & -1 \\ -1 & 0 & 1 \\ 1 & -4 & 3 \end{bmatrix}. \tag{3}$$

Here, W_i is the bottom width of the channel at the specific position, S_s is the side slope of the channel, β is the momentum correction coefficient and A_i is the wetted cross sectional area at the specific point. g is the gravitational constant, n_M is the Manning roughness coefficient, S_b is the channel slope and R_i is the hydraulic radius.

3. ESTIMATORS FOR FLOW RATE THROUGH THE VENTURI CHANNEL

The system is considered to have two level measurements at the first and third collocation points of the channel and the purpose of the estimator is to estimate the flow rate though the channel. The following linear system with no inputs is taken into consideration for designing linear estimators by linearizing the Eqs. $1 \sim 3$.

$$\dot{x} = Ax \tag{4}$$

$$y = Cx \tag{5}$$

Here, $x = [Q_1\ Q_2\ Q_3\ h_1\ h_2\ h_3]^T$ and $y = [h_1\ h_3]^T$.

A linear observer (LO), a linear Kalman filer (LKF), an extended Kalman filter (EKF) and an unscented Kalman filter (UKF) are used as estimators. For the UKF, the system is described as shown by the Eqs. $6 \sim 7$, where f represents the nonlinear model given by the Eqs. 2 and 1.

$$\dot{x} = f(x,t) \tag{6}$$

$$y = g(x,t) = Cx \tag{7}$$

All the estimators are used in discrete form. The design of the linear observer is stated below. The other estimators are not stated in detail here for simplicity.

3.1 Linear Observer Design

A reduced order LO is designed with the general recipe of injection of the measurements into the observer dynamics equation. The states are divided in to measured (x_1) and unmeasured (x_2) states as follows,

$$x = \begin{bmatrix} x_1 \\ x_2 \end{bmatrix}, \tag{8}$$

where, $x_1 = [h_1\ h_3]^T$ and $x_2 = [Q_1\ Q_2\ Q_3\ h_2]^T$. The system equations Eqs. $4 \sim 5$ are changed accordingly in to Eqs. $9 \sim 10$.

$$\begin{bmatrix} \dot{x}_1 \\ \dot{x}_2 \end{bmatrix} = \begin{bmatrix} A_{11} & A_{12} \\ A_{21} & A_{22} \end{bmatrix} \begin{bmatrix} x_1 \\ x_2 \end{bmatrix} \tag{9}$$

$$y = x_1 \tag{10}$$

The transformation variable ζ for observing the vector x_2 is defined as follows,

$$\zeta = x_2 + Kx_1, \tag{11}$$

where K is the gain matrix (4×2). Similarly, the dynamics of ζ can be derived as follows,

$$\dot{\zeta} = \dot{x}_2 + K\dot{x}_1. \tag{12}$$

Combining Eq. 12 with the system equation (Eq. 9),

$$\dot{\zeta} = A_{21}x_1 + A_{22}x_2 + K\left(A_{11}x_1 + A_{12}x_2\right). \tag{13}$$

The re–arranged Eq. 13 is as follows,

$$\dot{\zeta} = \left(A_{21} + KA_{11}\right)x_1 + \left(A_{22} + KA_{12}\right)x_2. \tag{14}$$

Similarly the estimate of ζ can be written as follows,

$$\dot{\hat{\zeta}} = \left(A_{21} + KA_{11}\right)x_1 + \left(A_{22} + KA_{12}\right)\hat{x}_2. \tag{15}$$

Now, the observation error dynamics (for observation error vector $\tilde{\zeta} = \zeta - \hat{\zeta} = x_2 - \hat{x}_2$) can be written as follows,

$$\dot{\tilde{\zeta}} = \dot{\zeta} - \dot{\hat{\zeta}} = \left(A_{22} + KA_{12}\right)\tilde{\zeta}. \tag{16}$$

A candidate Lyapunov function (Eq. 17) is chosen, such that the observation error dynamics will be asymptotically stable.

$$V = \frac{1}{2}\tilde{\zeta}^\top\tilde{\zeta} \tag{17}$$

By taking the time derivative of the Eq. 17 and substituting the observation error dynamics (Eq. 16) the equation is as follows,

$$\dot{V} = \tilde{\zeta}^\top\dot{\tilde{\zeta}} = \tilde{\zeta}^\top\left(A_{22} + KA_{12}\right)\tilde{\zeta}. \tag{18}$$

The following condition is to be satisfied for asymptotic stability,
$\dot{V} < 0 \iff \left(A_{22} + KA_{12}\right) < 0$
The values of A_{22} and A_{12} depends on the model parameters and the linearization point. Therefore, a careful consideration of the choice of K will lead to a better estimate with asymptotic convergence.

3.2 Implementation of Various Kalman Filters

Some of the versions of Kalman filters are also tested with the above stated LO for a comparison. A LKF, an EKF and an UKF are selected. The algorithm for the LKF in discrete form is shown in Eqs. 19 $\sim$ 23 and described in detail in [5]. The process and measurement noise covariance matrices are denoted as Q and R.

$$P_k^- = AP_{k-1}^+A^\top + Q \tag{19}$$

$$K_k = P_k^-C^\top\left(CP_k^-C^\top + R\right)^{-1} \tag{20}$$

$$P_k^+ = \left(I - K_kC\right)P_k^-\left(I - K_kC\right)^\top + K_kRK_k \tag{21}$$

$$\hat{x}_k^- = A\hat{x}_{k-1}^+ \tag{22}$$

$$\hat{x}_k^+ = \hat{x}_k^- + K_k\left(y_k - C\hat{x}_k^-\right) \tag{23}$$

The EKF follows the same algorithm of Eqs. 19 $\sim$ 23, except that the system matrix A is calculated at each time step k [5]. The UKF algorithm is also presented in detail in [5]. In this paper, only the final equations given by Eqs. 24 $\sim$ 37 are listed for presentation. The non–linear state equations (Eqs. 1 $\sim$ 2) are denoted as $g(x_k, t_k)$ and $f(x_k, t_k)$, respectively.

$$\hat{x}_{k-1}^{(j)} = \hat{x}_{k-1}^+ + \left(\sqrt{nP_{k-1}^+}\right)_j^\top \quad j = 1, \ldots, n \tag{24}$$

$$\hat{x}_{k-1}^{(j)} = \hat{x}_{k-1}^+ - \left(\sqrt{nP_{k-1}^+}\right)_j^\top \quad j = n+1, \ldots, 2n \tag{25}$$

$$\hat{x}_k^{(j)} = f(\hat{x}_{k-1}^{(j)}, t_k) \tag{26}$$

$$\hat{x}_k^- = \frac{1}{2n}\sum_{j=1}^{n}\hat{x}_k^{(j)} \tag{27}$$

$$P_k^- = \frac{1}{2n}\sum_{j=1}^{n}\left(\hat{x}_k^{(j)} - \hat{x}_k^-\right)\left(\hat{x}_k^{(j)} - \hat{x}_k^-\right)^\top + Q \tag{28}$$

$$\hat{x}_k^{(j)} = \hat{x}_{k-1}^+ + \left(\sqrt{nP_k^-}\right)_j^\top \quad j = 1, \ldots, n \tag{29}$$

$$\hat{x}_k^{(j)} = \hat{x}_{k-1}^+ - \left(\sqrt{nP_k^-}\right)_j^\top \quad j = n+1, \ldots, 2n \tag{30}$$

$$\hat{y}_k^{(j)} = g(\hat{x}_k^{(j)}, t_k) \tag{31}$$

$$\hat{y}_k = \frac{1}{2n}\sum_{j=1}^{n}\hat{y}_k^{(j)} \tag{32}$$

$$P_y = \frac{1}{2n}\sum_{j=1}^{n}\left(\hat{y}_k^{(j)} - \hat{y}_k\right)\left(\hat{y}_k^{(j)} - \hat{y}_k\right)^\top + R \tag{33}$$

$$P_{xy} = \frac{1}{2n}\sum_{j=1}^{n}\left(\hat{x}_k^{(j)} - \hat{x}_k^-\right)\left(\hat{y}_k^{(j)} - \hat{y}_k\right)^\top \tag{34}$$

$$K_k = P_{xy}P_y^{-1} \tag{35}$$

$$P_k^+ = P_k^- - K_kP_yK_k^\top \tag{36}$$

$$\hat{x}_k^+ = \hat{x}_k^- + K_k\left(y_k - \hat{y}_k\right) \tag{37}$$

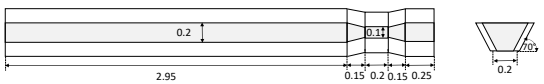

Fig. 2 The plan and front views of the channel geometry. The values are given in meters.

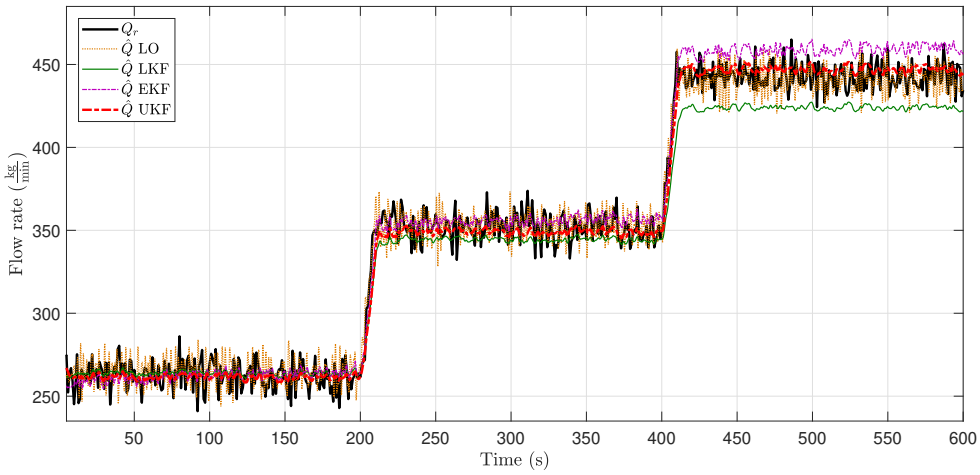

Fig. 3 The estimated outlet flow rates from different estimators against the model results

4. RESULTS AND DISCUSSION

The estimators are tested both by simulations as well as experiments. The geometry of the channel is shown in Fig. 2. The type of fluid is taken to be a water based synthetic drilling fluid. The details of the simulation and experimental validation are stated below.

4.1 Simulation Results

First the estimators are simulated for synthetic data to check the performance of the estimators. The two level measurements are generated with two step changes of $\sim$ 10 mm each. Then a random Gaussian noise is added to the data. The main model is also simulated with the same data for the reference flow rate Q_r.

The simulation results are shown in Fig. 3. All the flow rates at the three spatial points gave the same value at steady state conditions. For the clarity of presentation, only the flow rate estimated at the Venturi section (third point) is shown in the Fig. 3. The volumetric flow rates are converted into mass flow rates after the estimation, for a better presentation. The main model is non–linear. Therefore, we expect that the non–linear estimators to behave better in this application, which is also clearly seen in the figure. Further, the various Kalman filters have filtered out the noise, while the observer has not, which we expect. The linear estimators are good around the linearization point. Here, the models are linearized around the mean value of the data range 0–200 s. Away from the linearization point, both the LO and the LKF deviates from the reference values as expected. However, the estimations of the LO is closer to the reference values than the other linear estimator (LKF). Between the two non–linear estimators, the UKF performs better than the EKF.

The UKF and EKF take more computational time than the rest of the estimators. Further, EKF takes the longest computational time. Generally the time taken to perform the entire time series simulation (with .01s fixed time step) for LO, LKF, EKF and UKF are around 0.3, 1, 55 and 15 s of CPU time, respectively. Nonetheless, the EKF and UKF showed better performance than the rest of the estimators in terms of accuracy and noise.

4.2 Experimental Results

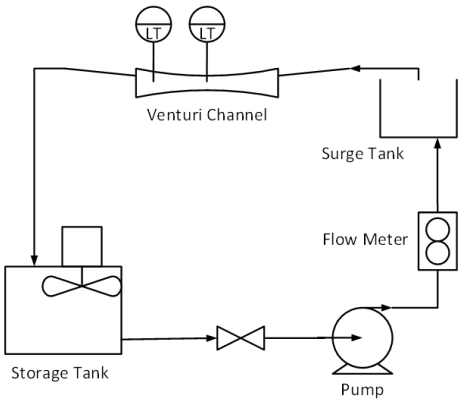

Fig. 4 The experimental setup

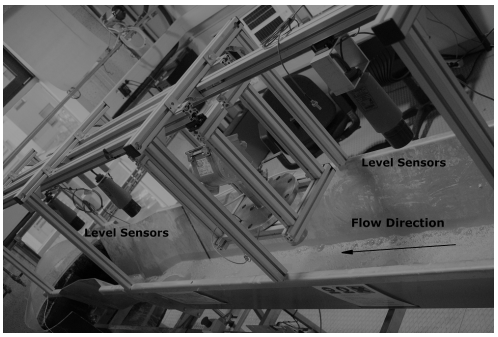

Fig. 5 A picture of the Venturi channel with level sensors

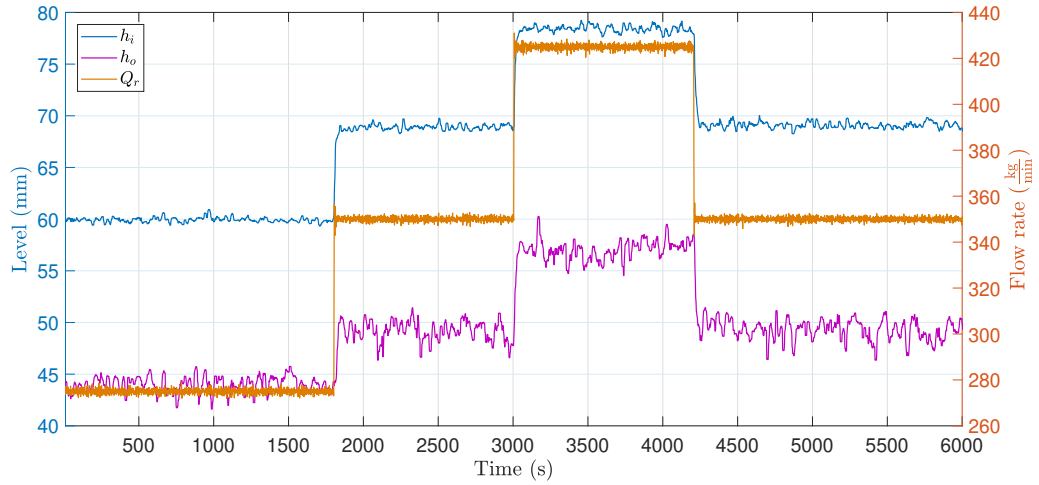

Fig. 6 The inlet, outlet fluid levels and the flow rate into the channel, measured from the experiments

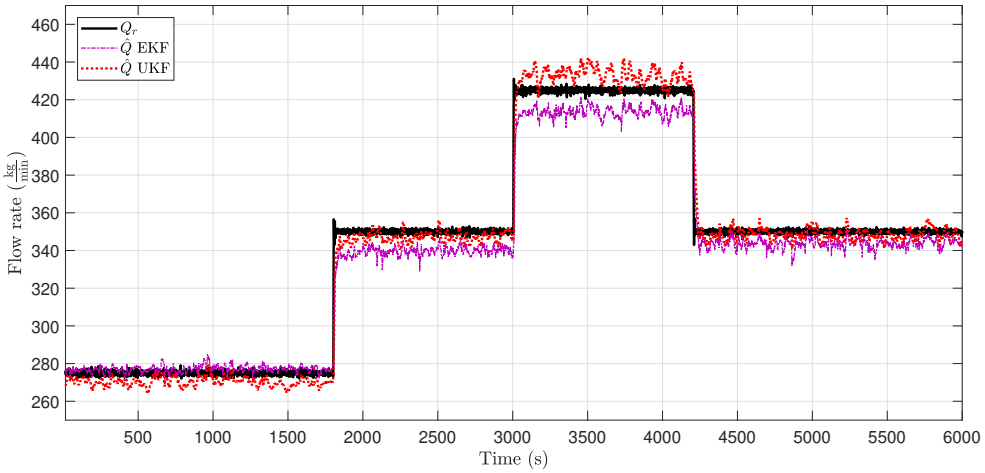

Fig. 7 The estimated outlet flow rates of the channel against the experimental results

An experimental setup of a Venturi channel with two level measurements and a pump flow rate measurement is available at the University of South–Eastern Norway. The simplified diagram of the experimental setup is shown in Fig. 4. For different set points of the pump flow rate, two level measurements from the channel is recorded together with the flow meter measurements from the Coriolis flow meter. A photograph of the channel at the experimental rig is shown in Fig. 5. The level and flow rate measurements taken from the experiments under sub–critical flow conditions are shown in Fig. 6.

Since we observed that the non–linear estimators are superior than the linear estimators in the simulations, the experimental data is tested only for the EKF and the UKF (see Fig. 7). The level measurements are noisy and the flow rate measurements are relatively less noisy due to full piped flow. (The flow rate measurement from the Coriolis meter is used only as the reference flow for comparison in this paper.) Therefore, the estimations are more noisy than the reference data, even though the noise in the estimations are filtered out by the estimators. The fluid levels are measured in an open channel (the venturi channel) where foams are formed when the fluid enters (falls into) the channel from a small height. Due to these foams and waves formed in the open channel, the level measurements are very noisy. From the Fig. 7 it can be seen that the UKF performs better than the EKF. Further, the mean absolute error (MAE) for each set point is calculated. The maximum MAE given by the UKF is 1.91% (8.1 at 425 $\frac{\text{kg}}{\text{min}}$) whereas for EKF the maximum MAE is 2.02% (7.1 at 350 $\frac{\text{kg}}{\text{min}}$).

To summarize, the non–linear estimators performed better in accuracy. The best performance out of the tested estimators is given by the UKF. The UKF is also fast

enough to be implemented in a real–time estimation application where the sensor measurements are taken at 1s time intervals.

5. CONCLUSIONS

The given mathematical model is used with different estimators to estimate the flow rate through an open Venturi channel using only two level measurements. A reduced order linear observer is designed and used in comparison with the other estimators. First, the estimators have been compared through simulations. Then the best performing estimators in simulations (EKF and UKF) are selected and used to estimate the flow rate through an experimental Venturi channel. The estimations are well comparable with the experimental data. The proposed model based flow estimation shows a promising potential as an online soft sensor which can be used in kick–loss detection algorithms.

ACKNOWLEDGMENTS

The economic support from The Research Council of Norway and Equinor ASA through project no. 255348/E30 'Sensors and models for improved kick/loss detection in drilling (Semi–kidd)' is gratefully acknowledged.

REFERENCES

[1] I. I. Carlsen, S. Hauge, R. K. Tinmannsvik and E. Okstad, "Causes and Measures Related to Well Control Incidents in Norwegian Petroleum Activities," *Risikonivå i Petroleumsvirksomheten Hovedrapport 2011, Norsk Sokkel*, Petroleum Safety Authority Norway, 2011.

[2] F. Jianhong, S. Yu, J. Wei and X. Liangbin, "Development and Testing of Kick Detection System at Mud Line in Deepwater Drilling," *Journal of Petroleum Science and Engineering*, Vol. 135, pp. 452 - 460, 2015.

[3] K. Chhantyal, H. Viumdal, S. Mylvaganam and G. Elseth, "Ultrasonic Level Sensors for Flowmetering of non- Newtonian Fluids in Open Venturi Channels: Using Data Fusion based on Artificial Neural Network and Support Vector Machines," *2016 IEEE Sensors Applications Symposium (SAS)*, pp. 1–6, 2016.

[4] A. Jinasena, G–O. Kaasa and R. Sharma, "Use of Orthogonal Collocation Method for a Dynamic Model of the Flow in a Prismatic Open Channel : For Estimation Purposes," *Proceedings of the 58th Conference on Simulation and Modelling (SIMS 58)*, pp. 90–96, 2017.

[5] D. Simon, *Optimal State Estimation: Kalman, H Infinity, and Nonlinear Approaches*, John Wiley & Sons, New Jersey, 2006.

Article D

Improved Real–Time Estimation of Return Flow Rate of Drilling Fluids by Model Adaptation for Friction Parameter

Jinasena, A., Kaasa, G.-O., and Sharma, R. (2019). Improved Real–Time Estimation of Return Flow Rate of Drilling Fluids by Model Adaptation for Friction Parameter. IEEE Sensors Journal, 19(20):9314–9323. https://doi.org/10.1109/JSEN.2019.2923854

Overview

The article presents the real-time estimation of states and parameters of the reduced order model that is stated in Article B and C. The model is modified with various non–Newtonian friction models available in the literature, and a fit–for–purpose friction model has been developed by the authors. In order to improve the fluid flow rate estimation, the model is adapted to some of the rheological parameters in real-time. The paper is published at the IEEE Sensors Journal. However, due to the copyrights, only the accepted version of the article is included here. The published version can be found at https://doi.org/10.1109/JSEN.2019.2923854.

Additional Information for Article D

Linearization of the system

The linearized system shown in (C.7) and (C.8) is augmented with the parameters for the friction term for the linear system observability analysis of each friction model. For augmentation, the parameters are considered to be slowly varying with time. The linear augmented system with different friction parameters is found to be observable. For example, for the model with Manning's friction factor, the linearized system is as follows.

$$\begin{aligned} \dot{X_{n_M}} &= A_{n_M} X_{n_M} \\ &= \begin{bmatrix} & & & & & & -T_{17_1} \\ & & & & & & -T_{17_2} \\ & & & A_{(1:6,1:6)} & & & -T_{17_3} \\ & & & & & & 0 \\ & & & & & & 0 \\ & & & & & & 0 \\ 0 & 0 & 0 & 0 & 0 & 0 & 0 \end{bmatrix} \end{aligned} \tag{D.1}$$

where

$$T_{17_k} := \frac{2gQ_k^2 n_M}{\left(W_k h_k + S_s h_k^2\right)\left(\frac{W_k h_k + S_s h_k^2}{W_k + 2h_k\sqrt{1+S_s^2}}\right)^{\frac{4}{3}}}. \tag{D.2}$$

Estimation error

The estimation errors associated with different models are discussed in Article D using figures. The dynamics of the flow travel through the Venturi channel fast and the steady state conditions can be quickly achieved. Therefore, the transient behaviors are hard to recognize in the plots for the presented time scale. Since a dynamic model is used for the estimation, the RMSE values are presented for the entire time duration including both dynamic and steady state conditions. However, if the steady state error or transient error is desired that can also be calculated separately, as shown in Figure D.1.

A more detailed (enlarged) plot during a transient is shown in Figure D.2. It is briefly stated in the article that the transport delay between the Coriolis flowmeter and the channel has contributed to a higher total error. The estimators were able to identify the change of flow rate as soon as it is indicated by the level measurements of the channel. But the Coriolis flow rate was placed upstream of the channel and when the change of flow rate is indicated by the Coriolis meter, it has not reached the channel.

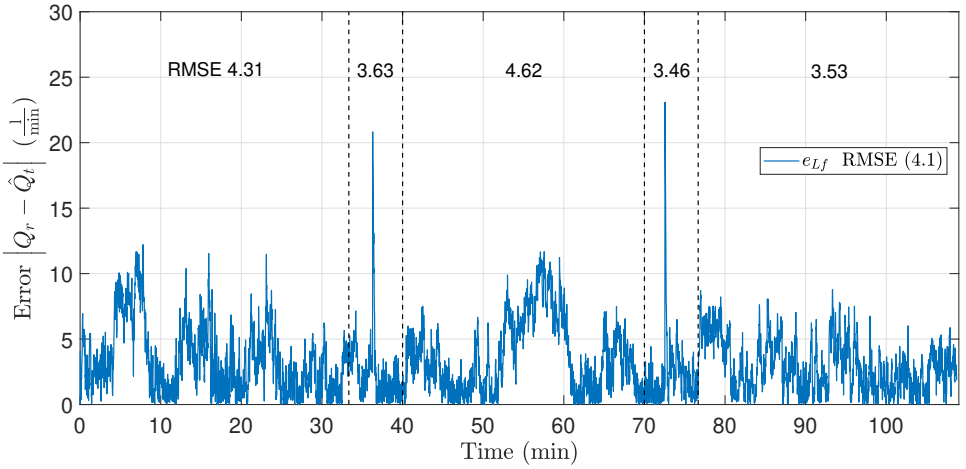

Figure D.1: The estimation error e_{Lf} for the fit-for-purpose model. The RMSE value for the entire time domain is given in the legend. RMSE for each steady state and transient period is also stated for comparison.

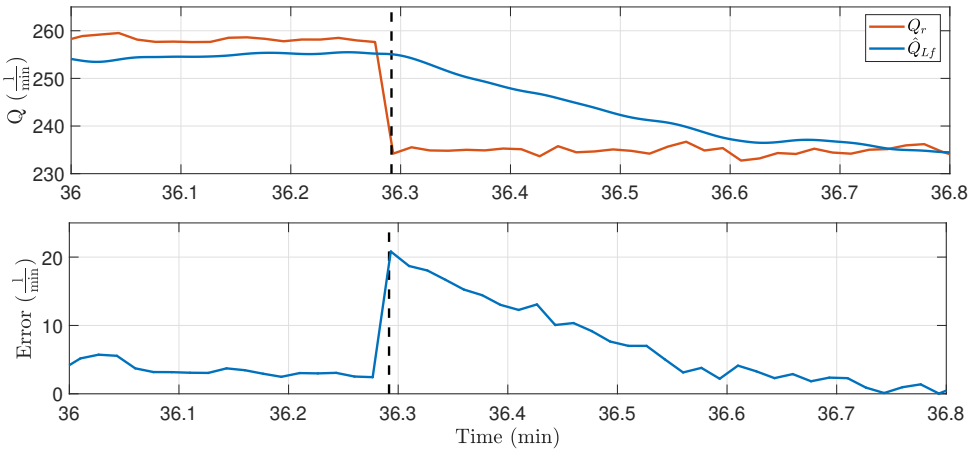

Figure D.2: The estimation error during transient conditions. The estimation error and the estimated flow rate $\hat{Q}_{Lf}$ using the fit-for-purpose model are shown here. Q_r: reference flow rate from the Coriolis meter

Improved Real–Time Estimation of Return Flow Rate of Drilling Fluids by Model Adaptation for Friction Parameter

Asanthi Jinasena, Glenn–Ole Kaasa, and Roshan Sharma

***Abstract*—Early kick and loss detection is a major concern in any drilling operation. A real-time return flow rate measurement would be an added advantage for the early kick and loss detection for conventional drilling systems. In this paper, the real-time estimation of the return flow rate during drilling is studied, using a Venturi channel. A reduced order, 1D, mathematical equation for the shallow water flow/open flow in the Venturi channel is investigated with various non–Newtonian friction models. The volumetric fluid flow rate is estimated online using an unscented Kalman filter. In order to improve the fluid flow rate estimation, the model is adapted to some of the rheological parameters in real time. A simple and effective fit–for–purpose friction model is developed and compared with the other friction models from literature. The fit–for–purpose model has the least estimation error (RMSE 1.465%) and requires less information as inputs. The proposed method exhibits promising potential to be used as an online return flow rate measurement for early kick and loss detection in conventional drilling.**

***Index Terms*—adaptive estimation, conventional drilling, drilling fluid, fit–for–purpose, flow estimation, friction model, non-Newtonian, open flow, trapezoidal channel, unscented Kalman filter**

I. Introduction

THE delta flow which is the difference between the inflow and outflow of a drilling well, is one of the kick and loss detection method used in the industry. Proper delta flow monitoring would allow early problem detection including kick/loss, and reduce non-productive time in drilling operations. In order to monitor the delta flow in real-time, the in and out flows of the well need to be measured using reliable and accurate flow meters. There exists many novel and advanced flow metering techniques for petroleum industry, specially for multiphase flow metering [1]. The inflow is a comparatively clean fluid with known rheological properties, thus many flow meter types can be used to measure the inflow rate accurately. However, the outflow or the return fluid is contaminated with drill cuttings, wear material and sometimes even gasses and other formation fluids. Due to this harsh condition only a limited number of flow meter types can be used such as Coriolis, electromagnetic, ultrasonic and open channel flow meters.

A. Jinasena and R. Sharma are with Department of Electrical Engineering, IT and Cybernetics, University of South–Eastern Norway, Norway e-mail: asanthi.jinasena@usn.no; roshan.sharma@usn.no

G. Kaasa is with Kelda Drilling Controls A/S, Porsgrunn, Norway e-mail: gok@kelda.no

Manuscript received ...

Since most of the current operating drilling rigs are still conventional, the popular industry standard for outflow meter is the flow paddle [2], [3]. The flow paddle is only an indicator which requires human interpretation to convert into flow rate, thus cannot be used for online monitoring. Instead of a flow paddle, a more precise magnetic flow meter can be used. However, it can only be used with electrically conductive fluids such as water based drilling mud [4], [5]. On the other hand, Coriolis meters are highly accurate and the current state–of-the–art for pressure controlled systems such as managed pressure drilling. However, the high footprint (large size, need for bypass lines and pressure limitations) and cost make this less feasible for conventional drilling systems. Further, these have shown certain systematic bias during pipe connections [6], and inaccurate measurements in the presence of gasses [7]. Out of the ultrasonic flow meters, the most suitable type for outflow is Doppler ultrasonic flow meters. This type is suitable for conventional drilling systems, however it is less accurate than the Coriolis or magnetic flow meters and the accuracy is affected by the mechanical and electrical noise in the drilling environment [4], [8].

The open channel flow meters are low in cost, easy to install and specially the Venturi flow meters are easy to maintain because of the non-intrusive nature of the level sensors [3], [4]. The main disadvantage of this Venturi meter is that the temperature and the composition of air in the return flow line can affect the echo time of the level sensors, thus the measurement needs to be corrected [4]. Typical Venturi flumes are designed according to the ISO 4359:2013 standards and performs best for steady or slowly varying flow conditions. These flume equations need one level measurement and empirical coefficients based on the geometry [9]. Therefore, these flume equations are not suitable for a rapidly changing fluid flow environment such as a return flow during drilling.

Various studies have been done to improve the use of Venturi channels for return flow measurement, by using two or more fluid levels [7], [10]–[12]. Different methods based on both mechanistic models and machine learning algorithms are investigated in these studies. However, the effects of the non–Newtonian fluid rheology, the cross-sectional shape of the channel, and the variation of the cross–sectional area along the channel are some of the factors that have not been fully investigated.

Therefore, the motivation for this work is to improve the real–time estimation of return flow rate by studying the effect of non–Newtonian fluid properties in terms of friction. Differ-

ent friction models based on the fluid type, channel type and the flow regime are investigated. Suitable friction models are selected and tested with experimental results. Further, a simple and effective fit–for–purpose friction model is developed and compared with the selected friction models from literature. Moreover, the rheological properties of the return fluid can vary over time, due to the variation of the formation that is being drilled. Therefore, the parameters for these friction models are estimated online together with the flow rate, for an improved estimation of the drilling fluid flow rate.

The paper is organized as follows. The mathematical model and estimator of the return flow rate is stated in detail in section II and the relevant theory and literature for the friction parameters in drilling fluids are discussed in section III. Then the experimental set up is summarized in section IV, followed by detailed results and discussion in section V. Finally, the conclusions drawn from the results and discussion are summarized in section VI.

II. Modeling and Estimation of Return Fluid Flow

An open Venturi channel can be placed in the return flow-line of a conventional drilling system, to measure the return flow rate. The mathematical model and the model based estimator are described in detail here.

A. Mathematical Model for Return Fluid Flow

The flow through the open Venturi channel is a free surface flow. Generally, these open channel hydraulics are modeled by the well–known and efficient shallow water equations. The shallow water equations for a 1D, unsteady, open channel system, is expressed as follows [13], [14],

$$\frac{\partial U}{\partial t} + \frac{\partial F}{\partial x} = S. \tag{1}$$

Here U is a vector of conserved variables A and Q, where $A(x,h,t)$ is the wetted cross–sectional area normal to the flow and $Q(x,t)$ is the volumetric flow rate. Further, $h(x,t)$ is the fluid level of the flow in the channel, x is the distance along the flow direction and t is the time. F, the conservative flux vector consists of the force terms and S is the source term.

The geometry of the channel used in this study is non–prismatic *i. e.* the cross–sectional area changes with the flow direction (along the length of the channel). Further, it is a Venturi channel with an isosceles trapezoidal cross–section (See Fig. 1). For this geometry, these U, F and S terms can be expressed as follows [11],

$$U = \begin{bmatrix} A \\ Q \end{bmatrix}, \tag{2}$$

$$F = \begin{bmatrix} Q \\ \frac{\beta Q^2}{A} + gI_1 \end{bmatrix}, \tag{3}$$

$$S = \begin{bmatrix} 0 \\ \frac{gh^2}{2}\frac{dW}{dx} + gAS_b - T \end{bmatrix}. \tag{4}$$

Here, g is the gravitational acceleration and β is known as the momentum correction coefficient or the Boussinesq coefficient which corresponds to the deviations of the local velocity over the mean velocity of the flow. $W(x)$ is the bottom width of the channel and the channel bed slope $S_b(x)$ is calculated by $-\frac{\partial z}{\partial x}$ (z is the absolute fluid level), where it is considered positive when sloping downwards. I_1 is the first moment of area which represents the hydrostatic pressure term, and is expressed as follows for a channel with an isosceles trapezoidal cross–section,

$$I_1 = \frac{1}{2}h^2W + \frac{1}{3}h^3S_s, \tag{5}$$

where, S_s is the side slope of the channel. T is the frictional stress due to fluid flow. This friction terms T will be discussed in detail in section III.

The relationship $A = hW + h^2S_s$, can be used to replace the term A in (2) by the term h, so that the partial differential equations are expressed in terms of h and Q. To simplify this complex model, these partial differential equations are then converted into ordinary differential equations by a model reduction method. This model reduction by the orthogonal collocation method is described in detail in [11], [12]. The simplified model described by ordinary differential equations are stated as follows,

$$\dot{h}_i = -\sum_{i=1}^{3} L_{ij}^{'} Q_i \frac{1}{W_i + 2S_s h_i}, \tag{6}$$

and

$$\dot{Q}_i = -\sum_{i=1}^{3} L_{ij}^{'} \frac{\beta Q_i |Q_i|}{A_i} + \frac{gh_i^2}{2}\sum_{i=1}^{3} L_{ij}^{'} W_i - g\sum_{i=1}^{3} L_{ij}^{'}\left(\frac{h_i^2 W_i}{2} + \frac{h_i^3 S_s}{3}\right) + gA_iS_b - T_i, \tag{7}$$

for 3 collocation points ($i = 1,2,3$). Here, subscript i represents the corresponding variable at the i^{th} specific position along the channel. $L_{ij}^{'}$ refers to an element in $L^{'}$ matrix at i^{th} row and j^{th} column, where,

$$L^{'} = \frac{1}{l}\begin{bmatrix} -3 & 4 & -1 \\ -1 & 0 & 1 \\ 1 & -4 & 3 \end{bmatrix}. \tag{8}$$

Here, l is the length of the channel.

Jinasena, Ghaderi, and Sharma [11] have successfully tested this simplified model in simulations for different flow conditions. However, it is also shown that this model is highly sensitive to the noise in the upstream level measurement [11]. Further, the values of the model parameters are not exactly known. In addition, these parameters can vary with time. This causes a model-mismatch. Under such conditions, simulating the model with measured inputs is inadequate and may produce an incorrect estimation of the return flow rate. Therefore, an estimator which can estimate the return flow rate and adapt to changes in the parameters is needed to get an accurate result.

B. State and Parameter Estimation

Jinasena and Sharma [10] have tested several linear and non–linear estimators and proposed that an extended Kalman filter (EKF) or an unscented Kalman filter (UKF) is adequate

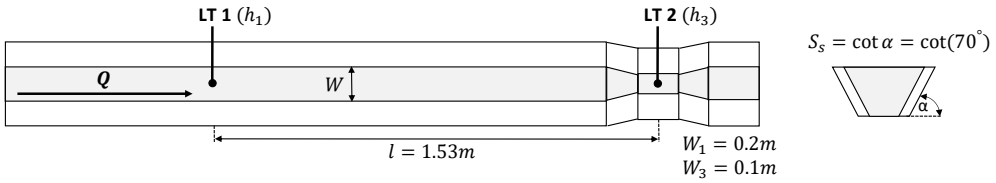

Fig. 1: Plan view and end view of the Venturi channel. The placement of level sensors (LT 1 and LT 2) and the dimensions are also shown here.

for the estimation of fluid flow rate through the Venturi channel. Further, the UKF has given better results than the EKF when the boundary conditions are noisy [10]. Therefore, for this study, a UKF with uniformly distributed sigma points is used to estimate the return flow rate and parameters, for both simulations and experimental data.

The system of equations for the estimation is taken as follows, where the parameters are augmented with states.

$$\dot{x} = f_n(x,t) \tag{9}$$

$$y = Cx \tag{10}$$

Here, $x = [Q_1\ Q_2\ Q_3\ h_1\ h_2\ h_3\ \theta]^T$ is the augmented state vector and $y = [h_1\ h_3]^T$ is the measurement vector. $f_n(x,t)$ represents the nonlinear model given by (7) and (6) for $\dot{Q}_i$ and $\dot{h_i}$, respectively. Further, $\dot{\theta}$ is taken as zero *i.e.* the parameters are considered to be constant or slowly varying with time. θ for different friction models *i.e.* Newtonian, Haldenwang and fit–for–purpose models is either n_M, $[k\ n]^T$ or F, respectively. These parameters are explained in detail in sections III-B and III-C. The observability is checked for all linearized systems with different friction models.

III. Literature and Theory on Friction Parameters

Most of the drilling fluids that are used in the industry are non–Newtonian in nature *i. e.* the viscosity of the fluid depends on the stress applied on the fluid. As viscosity is related to fluid friction, this non-Newtonian behavior is represented by the friction stress term T in the model stated in section II. This can be modeled using different friction models with various parameters. Therefore, the estimation of the return flow rate and friction parameters requires a proper model selection. There are various models which based on fluid rheological properties, channel type, and flow regimes. Therefore, a theoretical insight based on the available literature is summarized in this section.

A. Mathematical Modeling of Drilling Fluids

Most of the drilling fluids are non–Newtonian and exhibit shear–thinning (pseudoplastic) behavior. Generally, non–Newtonian models which use two or three parameters are used to model these fluids. Commonly used three–parameter models in the drilling industry are Robertson– Stiff, Collins–Graves, and Herschel–Bulkley models [15]–[17]. However, other models such as the Newtonian model, the Bingham plastic model, the power law or Ostwald–de Waele model are also being used by drilling engineers to approximate the drilling fluid behavior [18]. There is no general rheological model which will suit for all types of drilling fluids. However, the Herschel-Bulkley model has a wide acceptance throughout the industry and have the American Petroleum Institute recommendation (API RP 13D) [15].

Widely used fluid models *i. e.* Newtonian, power law, Bingham plastic, and Herschel-Bulkley models, can be expressed as shown in (11), (12), (13) and (14), respectively [19].

$$\tau = \mu\dot{\gamma} \tag{11}$$

$$\tau = k\dot{\gamma}^n \tag{12}$$

$$\tau = \tau_B + \eta\dot{\gamma} \tag{13}$$

$$\tau = \tau_{HB} + k\dot{\gamma}^n \tag{14}$$

Here, τ is the shear stress, $\dot{\gamma}$ is the shear rate. μ is the dynamic viscosity of the Newtonian fluid. τ_B and τ_{HB} are the Bingham yield stress and the Herschel–Bulkley yield stress. η, k and n are known as plastic viscosity, the fluid consistency coefficient, and the flow behavior index, respectively. Usually, the non–Newtonian friction models are expressed with these friction parameters corresponding to each fluid model *i. e.* either with k and n or with η and τ_B or with k, n and τ_{HB}.

Although the Herschel–Bulkley model is widely used for drilling fluids, it is a complex, three parameter model. The system considered in this study is not observable to estimate three parameters by taking only two fluid flow levels as the known measurements. Further, the drilling fluids that are used in this study can be modeled by the power law (see Fig. 4). Therefore, the power law model is used to approximate the behavior of synthetic drilling fluids in this study.

Further, drilling fluids are usually dependent on shear time (thixotropic) [18]. The thixotropic behavior of drilling fluids is rarely modeled mathematically. Livescu [20] has reviewed the mathematical modeling done on thixotropic drilling fluids so far. However, these studies are based on well conditions and/or pipe flow [15], [18], [20]–[22], and there are no explicit models developed for open flow. Usually, complex rheological models are accepted as more accurate when predicting the rheological behavior of drilling fluids [20]. However, these complex models are hard to use because of the difficulties in obtaining the analytical solutions to the fluid flow equations and finding the Reynolds number and friction factor. On the other hand, drilling fluid models contain empirical correlations together with major simplifications to easily identify the

TABLE I: Newtonian friction models

Model	Friction factor	Equation	
Gauckler–Manning [13], [14]	Manning's friction coefficient n_M	$S_f = \frac{n_M^2 Q\|Q\|}{A^2 R^{\frac{4}{3}}}$	(16)
Darcy-Weisbach [23]	Darcy-Weisbach friction factor f_D	$S_f = \frac{f_D Q\|Q\|}{8gRA^2}$	(17)
Kellerhals* [23]	Kellerhals roughness coefficient r_K	$S_f = \frac{r_K^2 Q\|Q\|}{A^2 R^{\frac{3}{2}}}$	(18)
model for irregular or compound sections [23]	cross–sectional discharge factor** ψ	$S_f = \frac{Q\|Q\|}{\psi^2}$	(19)

Q: volumetric flow rate. R: hydraulic radius.
* mostly used for gravel–bed rivers.
** ψ depends on the maximum fluid depth and the spatial position along the channel

laminar, turbulent or transition flow regimes [20]. Therefore, a compromise between the accuracy and the simplicity is needed in the mathematical modeling of drilling fluids. Hence, the general Newtonian and non–Newtonian models for open channels are focused in the following sections.

B. Newtonian Friction Models

A Newtonian fluid has a linear relationship between the shear stress and the shear rate as shown in (11). Usually, non–Newtonian drilling fluids are approximated using the Newtonian models in laminar flow conditions. Most of these models are expressed as a friction slope S_f, where the relationship between S_f and the friction stress T in the shallow water equations in (4) is given as follows,

$$T = gAS_f. \tag{15}$$

Some of the friction models that are used for Newtonian fluids are summarized in Table I. From these models, the Gauckler–Manning friction model in (16) is selected for analysis. Here, the parameter θ to be estimated is the Manning's friction coefficient n_M.

C. Non–Newtonian Friction Models

Usually, in pipe flow, the flow conditions and the frictional relationship is presented in the form of a Moody chart. This is a plot of Fanning friction factor f against the Reynolds number at different flow regimes laminar, transitional, or turbulent. For the channel flow, the Fanning friction factor can be used in analogous to the pipe flow friction stress. The friction stress over the channel solid surface (T) is given as follows [19],

$$T = \frac{fPu\,|u|}{2}, \tag{23}$$

where P is the wetted perimeter.

Some of the non–Newtonian friction models that have been developed for open channel flows are summarized in Table II. Out of the non–Newtonian friction models listed in Table II, the Haldenwang models are selected due to the fact that those were developed for trapezoidal channels (shown in (20), (21) and (22) in Table II). Haldenwang, Slatter, and Chhabra [29] have developed these friction factor–Reynolds number relationships for open channels, in parallel to the pipe flow [19], [31], [32]. These models are based on a new Reynolds number known as Re_H, which is introduced based on the Herschel–Bulkley model,

$$Re_H = \frac{8\rho u^2}{\tau_{HB} + k\left(\frac{2u}{R}\right)^n}. \tag{24}$$

This Reynolds number is in general form, therefore, can be applicable for power law fluids and Bingham plastic fluids as well [19].

Based on this Re_H, the Fanning friction factor (f) is expressed for different flow conditions and various uniform channel geometries.

The a, b, c, d, e and k coefficients in the equations depend on the channel shape and are found empirically. For a uniform trapezoidal channel of 60° sides (side slope of 1.732), the values for a, b, c, d, e, k are 17.6, 0.0851, –0.2655, 911, 15 and 0.06, respectively [30].

The channel used in this study is a trapezoidal channel of 70° sides (side slope of 2.747) with varying base width along the length of the channel (non–prismatic). Further, the Venturi section in the channel (the narrowest section in the channel, see Fig. 1 and Fig. 2a), ensures that the flow conditions obtain critical or supercritical conditions at the throat, thus always having transcritical conditions. It is also unclear whether the flow conditions are laminar, turbulent or transitional, without knowing the non–Newtonian fluid properties in advance. Further, the factors such as the changes in drilling conditions and operations with time, the type of fluid and the flow rate influence the return flow conditions. Therefore, the flow condition in the channel changes over time and the spatial direction. This makes it difficult to choose a specific model and requires additional information such as density, to estimate the flow rate of the fluid in real–time.

To overcome this problem, a fit–for–purpose model is developed such that no additional data is needed except the fluid level along the channel. Here, the friction stress over the channel solid surface (T) is described by the use of a dimensionless lumped friction factor F as follows.

$$T = FRu\,|u| \tag{25}$$

This is analogous to the Fanning friction factor ($f = F\frac{2A}{P^2}$). F compensates for the friction in the compound channel and acts as a lumped friction factor. However, this does not directly provide any rheological information of the fluid. The main purpose of the model is to aid the flow rate estimation with minimum information input together with the adaptation of the lumped friction factor parameter.

In this study, the non–Newtonian relationships (assuming power law) for all flow conditions in (20), (21) and (22) is tested and compared with the fit–for–purpose friction model in (25). The parameter θ to be estimated for the fit–for–purpose friction model is the dimensionless lumped friction factor F, while the θ for the other selected non–Newtonian models are both the fluid consistency coefficient k and the flow behavior index n.

TABLE II: Non–Newtonian friction models for open channel flows

Authors	Channel type	Flow condition	Fluid type	Model
Kozicki and Tiu [24]	rectangular, triangular, semicircular	laminar, turbulent	P, B	$f = \frac{16}{Re^*},\ Re^* = \frac{\rho u^{2-n} R^n}{2^{n-3} k}$
Coussot [25]	rectangular, trapezoidal	steady laminar flow	HB	$\tau = \tau_{HB}(1 + \alpha_s H_B^{-0.9}),\ H_B = \frac{\tau_{HB} h^n}{k u^n},$ $n = 1/3$
Slatter [26] cited in [27], p. 9	rectangular	laminar , turbulent	P, B,HB	$f = \frac{2Rg \sin\theta}{u^2},\ Re^* = \frac{8\rho u^2}{\tau + k\left(\frac{8u}{d_{85}}\right)^n}$
Abulnaga [28]	rectangular	laminar f_L, turbulent f_T	B	$f_T = 10^a (Re^*)^b,\ Re^* = \frac{4\rho u R}{\eta},$ $f_L = \frac{16}{Re^*}\left\{1 + \frac{He}{6Re^*} + \frac{He^4}{3 f_L (Re^*)^2}\right\}$
Haldenwang, Slatter, and Chhabra [29]	rectangular, triangular, semicircular, trapezoidal	laminar f_L [19], turbulent f_T [19], transition f_{Ts} [30]	P, B, HB	$f_L = \frac{a}{Re_H}$ (20), $f_T = bRe_H^c$ (21), $f_{Ts} = bRe_H^c + \frac{\frac{a}{Re_H} - bRe_H^c}{\left\{1 + \left(\frac{Re_H}{d}\right)^e\right\}^k}$ (22),

P – power law, B – Bingham plastic, HB – Herschel–Bulkley, ρ: density of the fluid, u: average velocity of the flow, h: flow depth, α_s: shape factor, d_{85}: particle diameter of 85% distribution, He: Hedström number, Re_H: Haldenwang Reynolds number shown in (24)

IV. Experimental Setup

Experimental setup of a Venturi channel with two level measurements and a pump flow rate measurement is available at the University of South–Eastern Norway. The block diagram of the test flow loop and a picture of the channel at the experimental rig is shown in Fig. 2 and the level sensors in the channel are shown in the picture. The system consists of a fluid tank, a pump, an open channel with Venturi constriction and flow and level sensors (LT 1 and LT 2 in Fig. 2). The fluid in the tank is pumped through the pipelines into a surge tank and then the fluid flows into the non–prismatic channel with a Venturi section towards the end. The channel has a uniform trapezoidal cross section. The fluid then flows back to the tank. Two radar sensors are used for fluid level measurements at two positions along the channel, and a Coriolis mass flow meter is used to record the mass flow rate and the density of the fluid. The volumetric flow rate calculated from the Coriolis meter recordings is used only as a reference for comparison with the model output. The density measurements taken from the Coriolis meter is used in the Haldenwang models. The pump flow rate is changed to mimic the transient flow conditions. The channel was kept horizontal throughout the experiments and the flow condition of the channel is transcritical. The level sensor used at the upstream of the flow (LT 1 in Fig. 2) is a Krohne Optiwave 7500 radar sensor of W–band 80 GHz frequency range with a $\pm$ 2 mm accuracy and a $\pm$ 1 mm repeatability. The level sensor at throat section (LT 2) is a Krohne Optiwave 8300 C radar sensor of 24 GHz frequency range with a $<$ 2 mm accuracy and repeatability of $\leq$ 0.5$\times$measurement error. The Coriolis mass flow meter is a Promass 63F (Endress+Hauser) with a measuring range of 0–1000 l/min with an uncertainty of $\pm$ 0.1%.

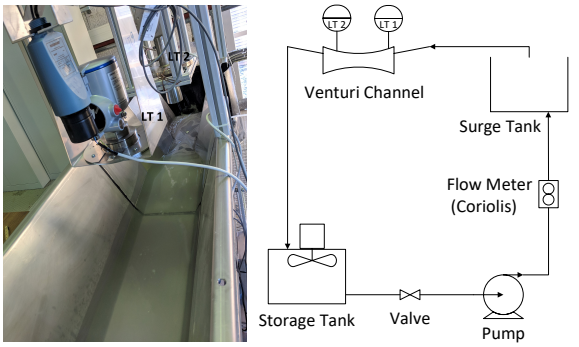

(a) (b)

Fig. 2: (a) The Venturi channel with the placement of level sensors (LT 1 and LT 2). (b) The block diagram of the test flow loop

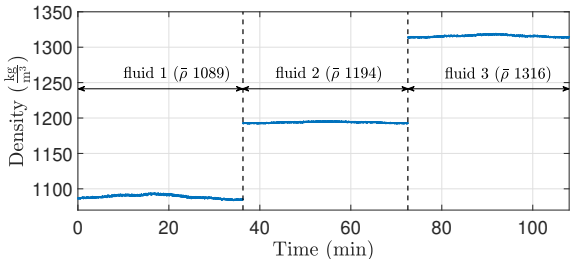

Fig. 3: Density of the three synthetic drilling fluids used in the experiments. $\bar{\rho}$ is the average density of the fluid.

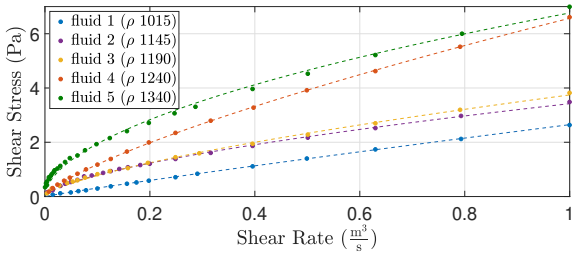

Fig. 4: Shear stress and rate relationships of similar synthetic drilling fluids. (Dots represent the experimental data from Fig. 2(a) in [7], p. 5005 and the dashed lines represents the fitted power law relationships). The density (ρ) is given in $\frac{kg}{m^3}$.

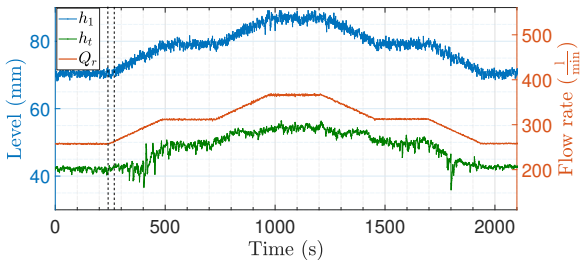

Fig. 5: Fluid levels and the flow rate over time for one of the synthetic drilling fluids.

For the experiments, different types of synthetic drilling fluids are available. These fluids are a mixer of potassium and calcium carbonates and xanthan gum dissolved in water. Three different fluids were tested and they are identified based on their densities. Only one type of fluid can be circulated through this experimental rig, at a time. Therefore, three different fluid types were circulated separately and the data is combined afterward, into a single time scale. The density of the three fluid types is shown in Fig. 3. These fluids are non-Newtonian and shear thinning in nature [7]. Based on a study done by Chhantyal, Jondahl, Viumdal, *et al.* [7] on similar fluids, it is clear that these fluids can be approximated by the power law (see Fig. 4).

As an illustration, the flow rate from the Coriolis meter is shown in Fig. 5 along with the upstream (h_1) and throat (h_t) level measurements. The delay between flow meter increment and the upstream level increment can be clearly seen here. This is due to the transportation of liquid through the pipeline into the surge tank and then to the channel, which at least takes approximately 20 s.

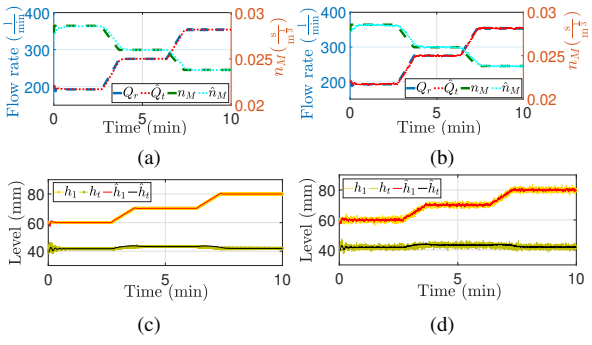

Fig. 6: (a) and (b): The simulation results for estimation of flow rate ($\hat{Q}_t$) and Manning's friction coefficient ($\hat{n}_M$) together with their true values (Q_r and n_M) for fluid level measurements without and with noise, respectively. (c) and (d): The noise free and noisy fluid levels (h_1: input and h_t: measurement) with the estimated fluid levels ($\hat{h}_1$: filtered input and $\hat{h}_t$: estimated level). Subscript *1* stands for the upstream position, *t* stands for the throat section.

V. Results and Discussion

The estimations of volumetric flow rate by adaptation of different friction parameters by the UKF is described here. The process covariance matrix was not changed for different fluid types in order to keep the practicality of the application. Further, the measurement covariance matrix which is based on the level sensors is the same for different models and fluid types. All the simulations and the estimations are done in MATLAB2018b. The details of the simulation and experimental validation are stated below.

A. Simulation Test Results

The estimation was done for simulated data and compared with the model itself. Random Gaussian noise was added to the measurements to reflect reality. The model with Newtonian fluid approximation is analyzed here, to estimate the Manning's friction coefficient (n_M). The reference model needs a boundary condition to simulate the transient conditions. Therefore, the upstream level (h_1) is used as the boundary condition (input to the system) while the throat level (h_t) is used as the measurement. The simulation results together with the inputs and measurements are shown in Fig. 6. (a) and (b) in Fig. 6 are the Q and n_M estimations for noise free and noisy level measurements. The respective level measurements are shown in (c) and (d) together with the level estimations.

Both the states (Q and h) and the parameter (n_M) quickly converged to their true values, in less than 60 seconds. The simulation results show that a UKF can be successfully used to estimate combined state and parameters, by simply considering the parameters as slowly varying or constant variable. Since the estimation seems possible and accurate, the estimator is then tested with various friction models for experimental data.

B. Experimental Test Results

The fluid level measurements from the experimental data is taken as the measurements to the system and both the flow rates and the required parameters are estimated using the UKF. As mentioned in section IV, the experiments were performed for three types of non–Newtonian fluids which have different rheological properties. The three sets of data were then combined together to form a single set of data. This mimics the sudden change of fluid properties (for example due to an occurrence of a kick). However, the analysis of the single data set is done in a continuous manner *i.e.* the experimental test results for these three fluid types are considered as continuous in nature and the results for the estimations are not merged plots.

For various friction models the corresponding parameters were estimated for all three types of fluids. The results for Newtonian approximation, power law approximation with Haldenwang models and the fit–for–purpose model are described in the following sections, separately.

1) Newtonian Friction Model: The n_M in the Gauckler–Manning friction model (16) is estimated and adapted together with the flow rates and levels. The flow rate estimations are shown in Fig. 7 followed by the estimation of fluid levels in

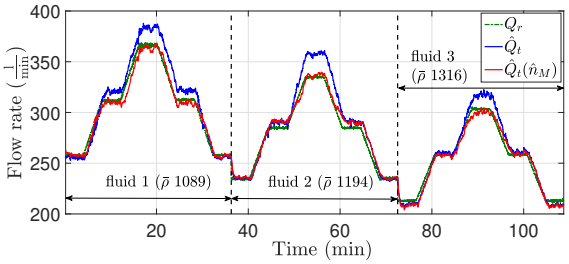

Fig. 7: Estimated flow rates ($\hat{Q}_t$) using the Newtonian friction model. The Coriolis flow measurements (Q_r) are also plotted for reference. $\hat{Q}_t$ is from state estimation only (without adaptation) and $\hat{Q}_t(\hat{n}_M)$ is with adaptation of n_M. Subscript *t* stands for the throat section and *r* is for the reference data (Coriolis meter).

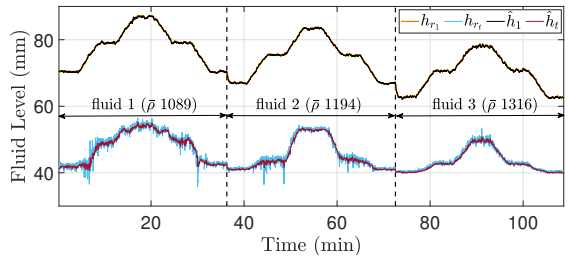

Fig. 8: The real and estimated fluid levels. Subscript *1* stands for the upstream position, *t* stands for the throat section and *r* is for the reference data.

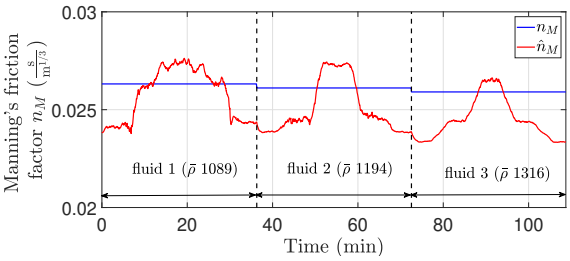

Fig. 9: The estimated $\hat{n}_M$ and the constant n_M used for different fluids.

Fig. 8. The effect of adaptation of friction parameter (n_M) is clearly seen at higher flow rates. In this case, with the adaptation of the friction factor, the estimate of the fluid flow rate (at higher rates) is significantly improved.

The estimated Manning's friction factor is shown in Fig. 9. n_M has increased considerably with high flow rates rather than with different fluid types. Manning equation was originally developed for steady flows [33]. Usually, the values of n_M are available based on the roughness of the channel surface [13]. However, Chow [13] has identified several factors affecting the numerical value of n_M stressing that the roughness should not be considered as the only factor. Further, it is reported to change with the change of depth and flow rate [34], [35].

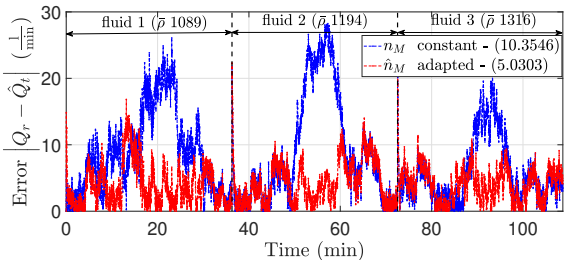

Fig. 10: The absolute error between the real and estimated flow rates with and without n_M adaptation. The root mean square error (RMSE) values are also given within brackets in $\mathrm{l/min}$.

Further, it depends on the physical conditions, such as bed geology and cross-sectional geometry, and also is affected by flow conditions, such as the flow turbulence intensity [36]. Since the n_M is calculated for the entire channel here, it can be considered as a composite value contributed by all factors. It is stated that the composite or compound roughness on the wall and the shape of the channel alters the velocity distribution across the cross section, and thereby changes the resistance coefficient [37]. A complete 2D or 3D analysis is needed to examine this problem. However, for a 1D case, generally, the composite roughness resistance coefficient is expressed by the Manning coefficient together with a weighted sum of the local resistance. Thereby, the calculation of Manning's coefficient based on these estimated composite values is possible [37]. However, the convergence of the estimated n_M to its true value cannot be guaranteed by this method. This is also not the main aim of the paper, since the primary objective is to improve the fluid flow rate estimation. The online estimation of friction factor improves the estimation of flow rates by considerably reducing the estimation error as shown in Fig. 10, where the RMSE value has reduced from 10.35 to 5.03 $\mathrm{l/min}$ when n_M is adapted.

2) Power Law with Haldenwang Friction Models: The synthetic drilling fluids are assumed as power law fluids and the 3 friction models based on the Re_H for laminar (20), turbulent (21) and transition (22) flow conditions are used for estimation of flow rates and parameters. The parameters that were adapted are the fluid consistency coefficient k and the flow behavior index n.

The estimated flow rates based on these three models, and their estimation errors are shown in Figs. 11 and 12, respectively. The friction model estimations based on the laminar conditions have significantly deviated from the real value for the third fluid type. Further, there is not a significant difference between the turbulent and transition friction models as evident from similar RMSE values (4.56 and 4.59 $\mathrm{l/min}$) in Fig. 12. The similar behavior between these two models is also seen in k and n estimations (Fig. 13). The n values for all the models are above 1, which indicates that these fluids are shear–thickening fluids. However, in reality, they are considered as shear–thinning fluids ($n < 1$) [7], thus the values of n are inaccurate. Also, in this case, the convergence of

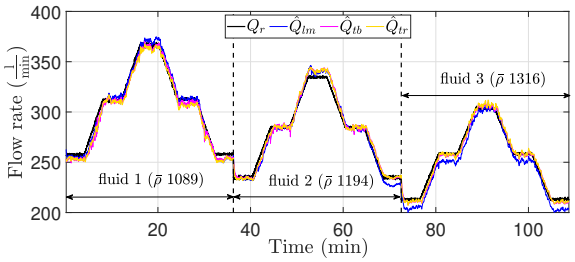

Fig. 11: Flow rate estimations for power law fluids. Subscripts *lm*, *tb* and *tr* stand for the laminar, turbulent and transition friction models, respectively.

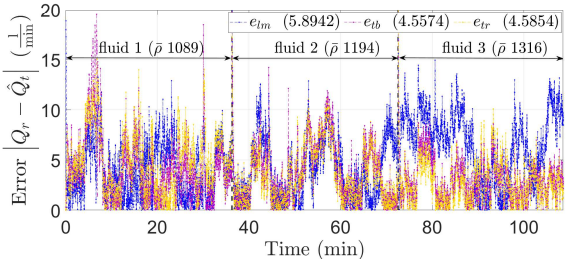

Fig. 12: The absolute error between the real and estimated flow rates using the laminar e_{lm}, turbulent e_{tb} and transition e_{tr} friction models. The RMSE values are also given within brackets in $\mathrm{l/min}$.

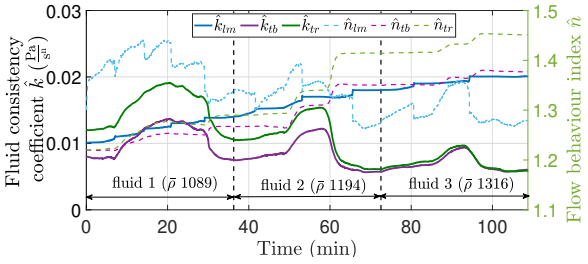

Fig. 13: Estimated fluid consistency coefficients $\hat{k}$ and flow behavior indexes $\hat{n}$ for laminar lm, turbulent tb and transition tr friction models.

the estimated parameters to their true value is not guaranteed. However, being able to estimate parameters online and using it further for state estimation, has produced a better estimation of the fluid flow rate. Nonetheless, the k values are in the range of similar fluids in the literature [19], [38].

Further, the calculated Haldenwang Reynolds numbers (Re_H) based on this estimated $\hat{k}$ and $\hat{n}$ seems to be in accordance with the Newtonian Reynolds number regions in pipe flow (Fig. 14). Also, there are no specific Haldenwang Reynolds numbers given for this specific channel type, except for the Reynolds numbers given for prismatic channel types [27], [31]. It suggests the region is closer to a transition region, although there is no clear margin to define laminar or turbulent. Based on the Froude number, the flow in this channel is

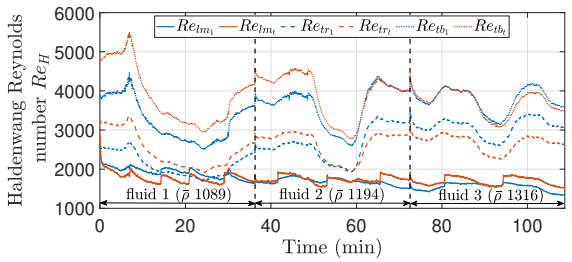

Fig. 14: The calculated Haldenwang Reynolds numbers (Re_H) based on the estimated $\hat{k}$ and $\hat{n}$ values. Subscripts *lm*, *tb* and *tr* stand for the laminar, turbulent and transition friction models, respectively. Subscript *1* stands for the upstream position, *t* stands for the throat section

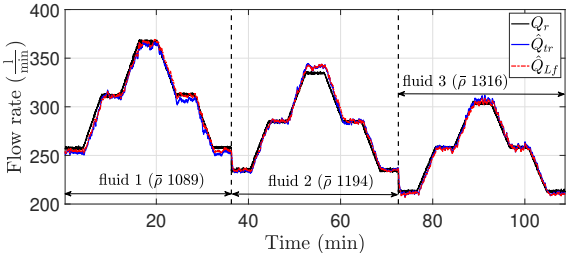

Fig. 15: The estimated flow rate ($\hat{Q}_{Lf}$) using the fit–for–purpose friction model. Subscripts *tr* and *r* stand for the Haldenwang transition friction model and the reference Coriolis meter, respectively.

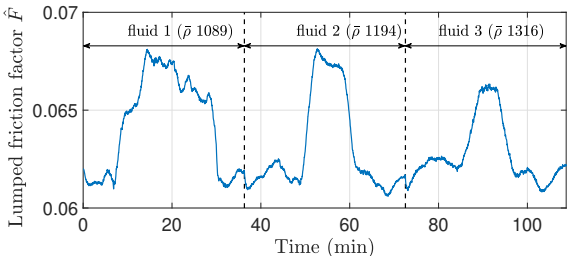

Fig. 16: The estimated dimensionless lumped friction factor ($\hat{F}$).

transcritical, where upstream is at subcritical conditions and the throat is at supercritical conditions. This is analogous to the transition region based on the Reynolds number. Therefore, the reason that the estimated $\hat{n}$ is not accurate could be due to the reason that the flow conditions change with the spatial position and cannot be known in advance to select the proper friction model. Another reason could be the fact that this is a compound non–prismatic channel where the selected empirical friction models deviate. Nonetheless, the flow rate estimations are slightly improved with turbulent or transition non–Newtonian friction models compared to the Newtonian friction models.

3) Fit–for–purpose Friction Model: The dimensionless lumped friction factor F is estimated online together with the flow rate, using only the fit–for–purpose model (25). The flow rate estimations are plotted in Fig. 15 together with the transition Haldenwang model for comparison. The lumped friction model is well comparable with the accurate and detailed Haldenwang model. Further, the estimation error between the real and estimated flow rates using the lumped friction model is (RMSE 4.1 $\frac{\mathrm{l}}{\mathrm{min}}$) slightly lower than that of the Haldenwang models. The estimated lumped friction factor is shown in Fig. 16. This lumped friction factor in itself does not convey any direct information on the rheological properties of the fluid. However, for the online estimation of fluid flow rate and the parameters, this model is simple to use with an accuracy similar to the other tested models.

VI. Conclusions

The reduced order shallow water model is used for improved estimation of non–Newtonian fluid flow rate by online estimation of fluid parameters. Different friction models are used in the shallow water equations for comparison. The process covariance matrix does not need to be changed for different fluids, hence this is suitable for real–time estimation where the incoming fluid properties can change at any time. However, the momentum correction coefficient (β) acts as a fitting parameter based on the position of the second level sensor in the throat section. Hence, this parameter needs to be changed, if the sensor position is changed. Therefore, a one–time calibration is needed to find out β, the process and measurement covariance matrices at the beginning.

The non–Newtonian friction models showed better estimations over the Newtonian friction model. However, the convergence of the estimated parameters to their true values cannot be guaranteed. Nevertheless, the online estimation of the parameters produces a better estimation of the fluid flow rate. In terms of the flow rate estimation, the more accurate models out of the selected models are the lumped friction model and the Haldenwang transition model. However, the lumped friction model is preferred based on the simplicity and the fact that it requires less information. It also has the least RMSE value out of the tested models which is 4.1 $\frac{\mathrm{l}}{\mathrm{min}}$ (=1.465 % = 0.068 $\frac{\mathrm{l}}{\mathrm{s}}$) and the MAPE (Mean Absolute Percentage Error) is 0.1655. This has a better performance compared to the different machine learning models used by Chhantyal, Jondahl, Viumdal, *et al.* [7], for the same experimental set up using similar synthetic drilling fluids (Table II in [7], p. 5008). The transport delay between the Coriolis flow meter and the channel also contributes to higher error calculations during transitions in both the studies. So the estimation error can be slightly lower in reality.

According to Orban, Zanner, and Orban [39], a flow meter for kick loss detection in drilling should have an accuracy of 1.5–3 $\mathrm{l/s}$ for flow rates up to 75 $\mathrm{l/s}$ in a normal drilling operational environment. Further, it requires the reliability and accuracy of measurements over the full range of flow and the accuracy should be maintained for any type of drilling fluid in a viscosity range of 1–200 cP and a density range of 1000–2160 $\frac{\mathrm{kg}}{\mathrm{m}^3}$ [39]. Although the estimation error is well below the required range, the tested experimental set up has a limited range of 3.3–7 $\mathrm{l/s}$. Therefore, the model needs to be tested on an industrial scale to further confirm that it can be used in early kick and loss detection during oil well drilling. Nevertheless, the lab tests show that it holds tremendous potential for real-time estimation of drill mud flowing out of the well during oil well drilling.

Acknowledgment

This work is supported by the Research Council of Norway and Equinor ASA through project no. 255348/E30 ‘Sensors and models for improved kick/loss detection in drilling (Semi–kidd)’.

References

[1] G. Falcone, G. Hewitt, C. Alimonti, and B. Harrison, “Multiphase Flow Metering: Current Trends and Future Developments,” *Journal of Petroleum Technology*, vol. 54, no. 04, pp. 77–84, 2014. DOI: 10.2118/74689-jpt.

[2] E. Cayeux and B. Daireaux, “Insights Into the Physical Phenomena That Influence Automatic Gain/Loss Detection During Drilling Operations,” *SPE Drilling & Completion*, vol. 32, no. 01, pp. 13–24, 2016. DOI: 10.2118/166801-pa.

[3] B. Brezina, “Analysis of Flow Behavior in Mud Return Lines of Open System Drilling Rigs,” MSc Thesis, University of Leoben, Austria, 2016, pp. 1–101.

[4] D. Schafer, G. Loeppke, D. Glowka, D. Scott, and E. Wright, “An Evaluation of Flowmeters for the Detection of Kicks and Lost Circulation During Drilling,” in *IADC/SPE Drilling Conference*, New Orleans, 1992, pp. 783–792. DOI: 10.2118/23935-MS.

[5] F. Le Blay, E. Villard, S. C. Hilliard, and T. Gronas, “A New Generation of Well Surveillance for Early Detection of Gains and Losses When Drilling Very High Profile Ultradeepwater Wells, Improving Safety, and Optimizing Operating Procedures,” in *SPETT 2012 Energy Conference and Exhibition*, Trinidad: Society of Petroleum Engineers, 2012, pp. 1–10. DOI: 10.2118/158374-ms.

[6] E. Cayeux and B. Daireaux, “Precise Gain and Loss Detection Using a Transient Hydraulic Model of the Return Flow to the Pit,” in *SPE/IADC Middle East Drilling Technology Conference and Exhibition*, Dubai, UAE: Society of Petroleum Engineers, 2013, pp. 1–24. DOI: 10.2118/166801-MS.

[7] K. Chhantyal, M. H. Jondahl, H. Viumdal, and S. Mylvaganam, “Upstream Ultrasonic Level Based Soft Sensing of Volumetric Flow of non-Newtonian Fluids in Open Venturi Channels,” *IEEE Sensors Journal*, vol. 18, no. 12, pp. 5002–5013, 2018. DOI: 10.1109/JSEN.2018.2831445.

[8] Q. Zhou, H. Zhao, Y. He, S. Li, S. Jiang, and H. Zhang, “Research on Mud Flow Rate Measurement Method Based on Continuous Doppler Ultrasonic Wave,” *International Journal of Optics*, vol. 2017, pp. 1–12, 2017. DOI: 10.1155/2017/4750290.

[9] S. Basu, “Open-Channel Flow Measurement,” in *Plant Flow Measurement and Control Handbook*, S. Basu, Ed., Academic Press, 2019, ch. III, pp. 257–331, ISBN: 978-0-12-812437-6.

[10] A. Jinasena and R. Sharma, “Model based Real–Time Flow Rate Estimation in Open Channels with Application to Conventional Drilling,” in *18th International Conference on Control, Automation and Systems (ICCAS 2018)*, PyeongChang, GangWon, Korea, 2018, pp. 546–551. [Online]. Available: http://www.dbpia.co.kr/Journal/ArticleDetail/NODE07549683.

[11] A. Jinasena, A. Ghaderi, and R. Sharma, “Modeling and Analysis of Fluid Flow through A Non-Prismatic Open Channel with Application to Drilling,” *Modeling, Identification and Control*, vol. 39, no. 4, pp. 261–272, 2018. DOI: 10.4173/mic.2018.4.3.

[12] A. Jinasena, G.-O. Kaasa, and R. Sharma, “Use of Orthogonal Collocation Method for a Dynamic Model of the Flow in a Prismatic Open Channel : For Estimation Purposes,” in *Proceedings of the 58th Conference on Simulation and Modelling (SIMS 58)*, Reykjavik, Iceland: Linköping University Electronic Press, 2017, pp. 90–96. DOI: 10.3384/ecp1713890.

[13] V. T. Chow, *Open-Channel Hydraulics*. New York: McGraw-Hill, 1959, pp. 1–728. DOI: ISBN07-010776-9.

[14] M. H. Chaudhry, *Open-Channel Flow*, 2nd. New York: Springer, 2008, p. 528, ISBN: 9780387301747.

[15] K. Gjerstad and R. Time, "Simplified Explicit Flow Equations for Herschel-Bulkley Fluids in Couette-Poiseuille Flow – For Real-Time Surge and Swab Modeling in Drilling," *SPE Journal*, vol. 20, no. 03, pp. 610–627, 2015. DOI: 10.2118/170246-PA.

[16] I. S. Weir and W. J. Bailey, "A Statistical Study of Rheological Models for Drilling Fluids," *SPE Journal*, vol. 1, pp. 473–486, 1996. DOI: 10.2118/36359-PA.

[17] W. J. Bailey and I. S. Weir, "Investigation of methods for direct rheological model parameters estimation," *Journal of Petroleum Science and Engineering*, vol. 21, pp. 1–13, 1998. DOI: 10.1016/S0920-4105(98)00040-0.

[18] R. F. Mitchell and S. Z. Miska, *Fundamentals of Drilling Engineering*, R. F. Mitchell and S. Z. Miska, Eds. Texas, USA: Society of Petroleum Engineers, 2011, vol. 12, p. 691, ISBN: 9781555632076.

[19] J. H. Burger, R Haldenwang, and N. J. Alderman, "Laminar and Turbulent Flow of Non-Newtonian Fluids in Open Channels for Different Cross-Sectional Shapes," *Journal of Hydraulic Engineering*, vol. 141, no. 4, pp. 04 014 084–1–12, 2015. DOI: 10.1061/(ASCE)HY.1943-7900.0000968..

[20] S. Livescu, "Mathematical modeling of thixotropic drilling mud and crude oil flow in wells and pipelines-A review," *Journal of Petroleum Science and Engineering*, vol. 98-99, pp. 174–184, 2012. DOI: 10.1016/j.petrol.2012.04.026.

[21] T. D. Reed and A. A. Pilehvari, "A New Model for Laminar, Transitional, and Turbulent Flow of Drilling Muds," *SPE Production Operations Symposium*, pp. 469–482, 1993. DOI: 10.2118/25456-MS.

[22] C. O. Negrão, A. T. Franco, and L. L. Rocha, "A weakly compressible flow model for the restart of thixotropic drilling fluids," *Journal of Non-Newtonian Fluid Mechanics*, vol. 166, pp. 1369–1381, 2011. DOI: 10.1016/j.jnnfm.2011.09.001.

[23] J. Burguete, P. Garcia-Navarro, J. Murillo, and I. Garcia-Palacin, "Analysis of the friction term in the one-dimensional shallow-water model," *Journal of Hydraulic Engineering*, vol. 133, no. 4, pp. 440–450, 2007. DOI: 10.1061/(ASCE)0733-9429(2007)133.

[24] W. Kozicki and C. Tiu, "Non-Newtonian flow through open channels," *The Canadian Journal of Chemical Engineering*, vol. 45, no. 3, pp. 127–134, 1967. DOI: 10.1002/cjce.5450450302.

[25] P. Coussot, "Steady, laminar, flow of concentrated mud suspensions in open channel: Ecoulements à surface libre permanents et laminaires de suspensions boueuses concentrées," *Journal of Hydraulic Research*, vol. 32, no. 4, pp. 535–559, 1994. DOI: 10.1080/00221686.1994.9728354.

[26] P. T. Slatter, "Transitional and turbulent flow of non-Newtonian slurries in pipes," PhD, University of Cape Town, 1995, p. 314.

[27] N. J. Alderman and R. Haldenwang, "A review of Newtonian and non-Newtonian flow in rectangular open channels," in *Hydrotransport 17: The 17th International Conference on the Hydraulic Transport of Solids*, 2007, pp. 1–20.

[28] B. Abulnaga, *Slurry systems handbook*. New York: McGraw-Hill, 2002, pp. 1–800, ISBN: 0071375082.

[29] R. Haldenwang, P. Slatter, and R. Chhabra, "Laminar and transitional flow in open channels for non-newtonian fluids," in *Hydrotransport 15: 15th international conference on the hydraulic transport of solids in pipes*, Banff, Jun. 2002, pp. 755–768.

[30] J. H. Burger, R. Haldenwang, R. P. Chhabra, and N. J. Alderman, "Power law and composite power law friction factor correlations for laminar and turbulent non-Newtonian open channel flow," *Journal of the Brazilian Society of Mechanical Sciences and Engineering*, vol. 37, no. 2, pp. 601–612, 2015. DOI: 10.1007/s40430-014-0188-1.

[31] R. Haldenwang and P. Slatter, "Experimental procedure and database for non-Newtonian open channel flow," *Journal of Hydraulic Research*, vol. 44, no. 2, pp. 283–287, 2006. DOI: 10.1080/00221686.2006.9521682.

[32] J. Burger, R. Haldenwang, and N. Alderman, "Friction factor-Reynolds number relationship for laminar flow of non-Newtonian fluids in open channels of different cross-sectional shapes," *Chemical Engineering Science*, vol. 65, no. 11, pp. 3549–3556, 2010. DOI: 10.1016/j.ces.2010.02.040.

[33] P. Garcia-Navarro, E. Playan, and N. Zapata, "Solute Transport Modeling in Overland Flow applied to Fertigation," *Journal of Irrigation and Drainage Engineering*, vol. 126, pp. 33–40, 2000.

[34] O. J. Schmidt, "Measurement of Manning's Roughness Coefficient," *Sewage and Industrial Wastes*, vol. 31, no. 9, pp. 995–1003, 1959. DOI: 10.1017/s0140525x17000048.

[35] H. Damangir and M. J. Abedini, "System identification and subsequent discharge estimation based on level data alone-Gradually varied flow condition," *Flow Measurement and Instrumentation*, vol. 36, pp. 24–31, 2014. DOI: 10.1016/j.flowmeasinst.2014.01.002.

[36] X. Xu, X. Zhang, H. Fang, R. Lai, Y. Zhang, L. Huang, and X. Liu, "A real-time probabilistic channel flood-forecasting model based on the Bayesian particle filter approach," *Environmental Modelling and Software*, vol. 88, pp. 151–167, 2017. DOI: 10.1016/j.envsoft.2016.11.010.

[37] B. C. Yen, "Open Channel Flow Resistance," *Journal of Hydraulic Engineering*, vol. 128, no. 1, pp. 20–39, 2002. DOI: 10.1061/(ASCE)0733-9429(2002)128:1(20).

[38] R Haldenwang, P. T. Slatter, R. P. Chhabra, R Haldenwang, P Slatter, and R Chhabra, "An experimental study of non-Newtonian fluid flow in rectangular flumes in laminar, transition and turbulent flow regimes," *Journal of the South African Institution of Civil Engineering*, vol. 52, no. 1, pp. 11–19, 2010.

[39] J. Orban, K. Zanner, and A. Orban, "New Flowmeters for Kick and Loss Detection During Drilling," in *62nd Annual Technical Conference and Exhibition of the Society of Petroleum Engineers*, Dallas, Texas: Society of Petroleum Engineers, 1987, pp. 151–161. DOI: 10.2118/16665-MS.

Asanthi Jinasena received a B.Sc. Engineering degree in chemical and process engineering from University of Moratuwa, Sri Lanka and a M.Sc. degree in process technology from University of South–Eastern Norway, Norway.

She is a PhD student at the Institute of Electrical Engineering, IT and Cybernetics at the University of South–Eastern Norway, Norway. She is currently working on developing models and estimators for the top side of a drilling process. Her research interests include state and parameter estimation, fluid dynamics and mathematical modeling of dynamic systems.

Glenn–Ole Kaasa received the B.Eng. degree from Telemark University–College, Porsgrunn, Norway, in 1997, and the M.Sc. degree in mechanical engineering from the Norwegian University of Science and Technology (NTNU), Norway, in 1999. He was a Fulbright visiting fellow at University of California, Santa Barbara in 2002, and received the Ph.D. degree from NTNU in 2006.

From 2003 through 2006, he was with Kongsberg Automotive in positions as Lead Specialist and Research Manager. In 2006 he moved to Statoil Research Centre, as Principal Researcher and later Head of department of Intelligent Drilling. In this period he also held an Adjunct Professorship at NTNU in adaptive control theory. From 2013 he has been CEO of Kelda Drilling Controls, developing software systems for pressure control in drilling. His research interests include mathematical modeling and applied nonlinear control and estimation.

Roshan Sharma is an Associate Professor at the University of South–Eastern Norway, Norway. He received a Ph.D. degree in Process, Energy and Automation from Telemark University College in 2014.

His areas of expertise are mathematical modeling of dynamic systems, advance process control and optimization, state and parameter estimation. He has been actively working as a researcher within oil and gas processes since 2011.

Article F

A Dynamic Model for Drain Back to Active Mud Pit Combined with a Well Model during Drilling

Pirir, I., Jinasena, A., and Sharma, R. (2018). A Dynamic Model for Drain Back to Active Mud Pit Combined with a Well Model During Drilling. Journal of Petroleum Science and Engineering, 167:803–818. https://doi.org/10.1016/j.petrol.2018.04.057

Overview

A combined model for a complete, closed-loop drilling process, which captures the dynamics of the return flow of the topside and the dynamics of the bottom side of the well is presented in this article. The model is simulated for common operational scenarios during drilling such as pipe connection, movements of the drill string and reservoir influx. The combined model can be used for studying the pressure dynamics as well as for return flow estimation, thus to detect kicks and losses occurring in the well. To the best of the authors' knowledge, such a single combined model for both the topside and the bottomside dynamics is neither published nor available in the literature.

Journal of Petroleum Science and Engineering 167 (2018) 803–818

Contents lists available at ScienceDirect

Journal of Petroleum Science and Engineering

journal homepage: www.elsevier.com/locate/petrol

A dynamic model for drain back to active mud pit combined with a well model during drilling

Ivan Pirir, Asanthi Jinasena*, Roshan Sharma**

Department of Electrical Engineering, IT, and Cybernetics, University College of Southeast Norway, Porsgrunn, Norway

ARTICLE INFO

Keywords:
Well drilling
Combined model
Open channel flow
Saint–Venant equations
Kurganov-Petrova scheme

ABSTRACT

There are no published mathematical models that combine the dynamics of the returned fluid flow to the active mud pit (top side drilling) and the dynamics of the bottom side of the well being drilled. In this paper a simple dynamic model that combines the top and the bottom side drilling operations is provided. The model has been simulated for various operational scenarios during drilling including pipe connection, movements of drill string and reservoir influx. This combined model can be used for studying not only the pressure dynamics but also to estimate the return fluid flow rate and hence to detect kicks and losses occurring in the well.

1. Introduction

During oil well drilling, the drill bit connected to a drill string is lowered and rotated using a drive system at the top side and used to cut rocks, soil etc. At the same time drilling fluid is pumped through the drill string and into the annulus through a non return valve. The drill mud will then flow upwards through the annulus and through the choke valve to a return line. After this, the mud is filtered and stored in mud pits before being pumped back into the well again. The mud circulation has multiple purposes, the two most important being to retrieve the cuttings from the bottom of the well and to exert hydrostatic pressure against the walls of the well to prevent fluids from flowing into the well (Bourgoyne et al., 1986). Fig. 1 shows a simplified schematic of such a system.

In an overbalanced drilling, the pressure in the well is kept at a high enough level (higher than the pore pressure) so it will stop fluids from the reservoir from entering the annulus. An unwanted flow of reservoir fluid into the annulus is commonly referred to as a kick. If the occurrence of a kick is not regulated, it can cause a blowout where the fluids from the reservoir rise uncontrolled to the surface (Grace, 1994). In the other hand if the pressure in the well is too high, it will cause the drilling fluids to penetrate the reservoir formation which will result in a loss of the circulating drill mud.

It is challenging to correctly estimate the reservoir pore pressure, so the discharge from the flow-line is constantly measured to estimate the fluids flowing in and out of the annulus. This is currently done by measuring the flow rate coming from the choke valve directly using Coriolis meters. However, this type of equipment is both expensive and presents many challenges. For instance there is a risk of blockage due to drill cuttings while measuring the discharge. The presence of gas and cuttings in the drilling fluid will also have a negative effect in the measurement *i.e.* for multi-phase fluid, the readings from Coriolis meters may not be accurate. These are some of the reasons why there is an interest in the research community for developing cheaper and more efficient methods to replace the Coriolis meter.

One possibility is the development of a full mathematical model that describe the entire mud circulation *i.e.* a complete model for describing both the bottom side and the top side dynamics during drilling of an oil well. To the best of the author's knowledge, a combined model of such a type has not been published. This paper provides a simple yet a complete model for an oil well drilling dynamics.

The model for the drain back to the active mud pit can be used in combination with cheaper sensors to estimate the flow rate of the returned drill mud. Proper online estimation of the return fluid flow rate aids in early kick and loss detection. Thus the model presented in this paper can be used for the estimation of bottom hole pressure and at the same time for the estimation of the return fluid flow rate to the active mud pit.

The paper is organized as follows: In section 2, a widely used model for the bottom side dynamics during drilling is presented. Section 3 describes the top side operations while the model of the active mud pit is developed in Section 4. In section 5, the model for the drain back flow-line is developed. The numerical solution of the top side drilling dynamics is provided in Section 6. Three important drilling scenario are simulated and discussed in Section 7 and finally conclusion are made in Section 8.

* Corresponding author.
** Corresponding author.
E-mail addresses: asanthi.jinasena@usn.no (A. Jinasena), roshan.sharma@usn.no (R. Sharma).

https://doi.org/10.1016/j.petrol.2018.04.057
Received 1 August 2017; Received in revised form 27 February 2018; Accepted 25 April 2018
Available online 28 April 2018
0920-4105/

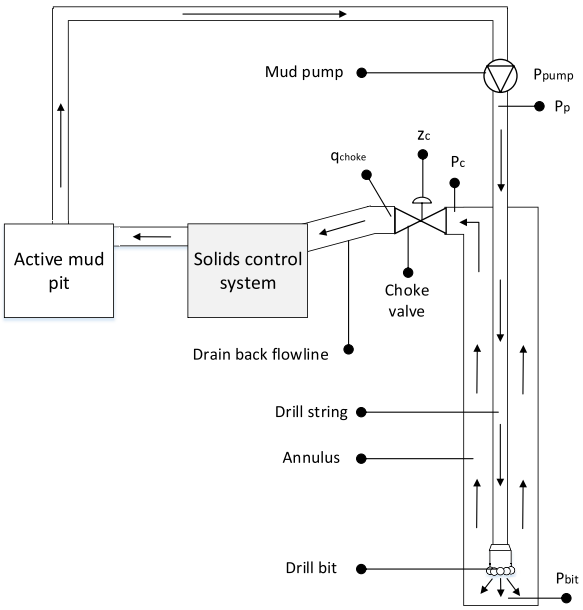

Fig. 1. Drilling fluid circulating system.

2. Model of the bottom side of a drilling operation

Different types of models with different complexities are available in order to describe the dynamics of the mud circulation through the well being drilled. For this paper a simple dynamic model developed by (Kaasa, 2007) was implemented to simulate the circulation of drill mud pumped into the well by the mud pumps and flowing out of the well through the choke valve. The following assumptions are used in the development of the model (Kaasa, 2007; Kaasa et al., 2012).

- Flow can be considered as 1D along the main flow direction
- Flow is radially homogeneous
- The spatial time variance of the density in the momentum equation is neglected.
- Time variance of the viscosity is negligible in the momentum equation**Remark on third assumption:** The transient spatial density effects are insignificant for flows that has Mach numbers less than 0.3 (White, 2011). However, the error that can cause by not taking the compressibility into consideration when calculating the hydrostatic pressure and friction forces could be considerable. For a general drilling fluid, this error in bottom hole pressure at a depth of about 3000 m could be a few bars (less than 0.25%) (Kaasa et al., 2012). However, the incompressibility is assumed only in the momentum equation. The main compressibility effects of the fluid are considered in terms of an equation of state incorporated with the mass balance. A linear equation of state is used for the density as follows,

$$\rho = \rho_r + \frac{\rho_r}{\beta}(p - p_r) - \rho_r \alpha (T - T_r), \tag{1}$$

because the changes in density (ρ) as a function of pressure (p) and temperature (T) is small for a liquid. (Subscript r stands for the property at a reference point.) Further, the temperature effects on the density is also ignored, because of the small thermal expansion coefficients (α) of liquids and the pressure transients are fast compared to the temperature transients in drilling fluids. (However, special cases where faster temperature transients occur, are not considered in this study.) Therefore, the pressure transients are expressed as follows for this study,

$$\frac{d\rho}{\rho_r} = \frac{dp}{\beta}, \tag{2}$$

with the use of β, the bulk modulus. Although, the linearized equation of state can deviate from reality with increasing pressure and temperature, this deviation is not significant for most drilling fluids within the range of 0–500 bars of pressure and 0–200°C of temperature (Kaasa et al., 2012). Even though, the model is simplified with the third assumption, it is shown that this model can approximate the pressure at any point of the well quite accurately by the dynamics of the average pressure in the entire well; with an offset with the hydrostatic pressure and friction drop relative to a reference point. More details are included in (Kaasa et al., 2012).

To give a general understanding of the model, this model utilizes two control volumes: the drill string as the first control volume and the annulus as the second control volume.

For each control volume, the continuity equation can be written using the pressure and the volumetric flow rates as variables, which is a form commonly used to describe incompressible pipe flows. Here, the pressure is taken as an average pressure in the entire control volume. It is shown that the dynamics of the average pressure is capable of capturing the dynamics of the pressure at any point, due to the relatively fast transients of the flow dynamics (Kaasa et al., 2012). The mass balance for the control volume can be written as follows,

$$\frac{d}{dt}(\rho V) = \rho_{in} q_{in} - \rho_{out} q_{out}, \tag{3}$$

where q is the volumetric flow rate, V is the volume of the control volume and the subscripts *in* and *out* stand for the inlet and outlet of the control volume. This can further be expanded and expressed in pressure using the Equation (2) as follows,

$$\frac{\rho_r V}{\beta}\frac{dp}{dt} = \rho_{in} q_{in} - \rho_{out} q_{out} - \rho \frac{dV}{dt}, \tag{4}$$

and further,

$$\dot{p} = \frac{\beta}{\rho_r V}\left(\rho_{in} q_{in} - \rho_{out} q_{out} - \rho \frac{dV}{dt}\right). \tag{5}$$

Therefore, in the drill string, the mass balance can be simplified further to find the pressure at the top, using the volumetric flow rates of drilling fluid through the mud pump (q_{pump}) and through a non-return valve at the drill bit (q_{bit}).

$$\dot{p}_p = \frac{\beta_d}{V_d}(q_{pump} - q_{bit}) \tag{6}$$

Here β_d denotes the bulk modulus of the drilling mud at the drill string and V_d the volume of the drill string which is updated every time a new pipe section is connected.

Similarly, in the annulus, the pressure at the top is expressed using the volumetric flow rates passing through the drill bit, going out of the annulus through the choke valve (q_{choke}), through the back-pressure pump (q_{back}) and the volumetric flow rate going into or out of the reservoir (q_{res}). Also the effects which can occur due to the change of volume of the annulus depending on the drilling rate ($\dot{V}_a$) is included.

$$\dot{p}_c = \frac{\beta_a}{V_a}(q_{bit} + q_{back} - q_{choke} + q_{res} - \dot{V}_a) \tag{7}$$

Here, β_a is the bulk modulus of the drilling mud at the annulus. The volumetric flow rate through the choke valve can be modeled by a standard orifice equation.

$$q_{choke} = K_c z_c \sqrt{\frac{2}{\rho_a}(p_c - p_0)} \tag{8}$$

where K_c is the valve constant and the normalized valve opening.

From the momentum balance and assuming that the average density of the drilling mud is constant, one can calculate the volumetric flow

rate through the drill bit as follows,

$$M\dot{q}_{bit} = \begin{cases} p_p - p_c - F_d|q_{bit}|q_{bit} - F_a|q_{bit} + q_{res}|(q_{bit} + q_{res}) \\ \quad +(\bar{\rho}_d - \bar{\rho}_a)gh_{bit} & q_{bit} > 0 \\ max\{0,\ p_p - p_c + (\bar{\rho}_d - \bar{\rho}_a)gh_{bit}\} & q_{bit} = 0 \end{cases} \tag{9}$$

Here $\bar{\rho}$ is the average density and h_{bit} is the depth of the drill bit. F_a and F_d are lumped friction terms and the detailed derivation is given in Appendix. The subscript d denotes the drill string and the subscript a denotes the annulus. The mass matrix M is defined as the integrated density per cross section over the flow path,

$$M_a = \bar{\rho}_a \int_0^{l_w} \frac{1}{A_a} dx\ , \tag{10}$$

$$M_d = \bar{\rho}_d \int_0^{l_d} \frac{1}{A_d} dx\ , \tag{11}$$

$$M = M_a + M_d. \tag{12}$$

Here l_w is the length of the well, l_d the length of the drill string and A_a, A_d are the cross-sectional areas of the annulus and the drill string, respectively.

Further, the bottom hole pressure p_{bit} can be calculated as follows,

$$p_{bit} = p_c + M_a\dot{q}_{bit} + F_a|q_{bit} + q_{res}|(q_{bit} + q_{res}) + \bar{\rho}_a g h_{bit}. \tag{13}$$

The left hand side of the Equation (9) represents the average (integrated along the flow path) flow dynamics under the assumption that the fluid accelerates homogeneously as a stiff mass. The derivation of the Equation (9) is shown in the Appendix in detail. The lumped friction terms depend on the conditions of the flow. These terms include all frictional losses that happen due to the viscous dissipation, turbulence, swirl flow and non ideal conditions caused by the geometry (Kaasa et al., 2012). However, in the simulations of this study, the friction terms are considered to be a constant value for the simplicity, but estimation of the friction terms is recommended for a better accuracy.

Further, the effect of the movement of the drill string with a given velocity (v_{drill}) on the depth of the drill bit and the volume of the annulus are given by the following equations,

$$\frac{dh_{bit}}{dt} = v_{drill}, \tag{14}$$

$$\frac{dV_a}{dt} = -A_d v_{drill}. \tag{15}$$

The change of the pressures in the well and the fluid flow rates due to movements of the drill string is found using the Equations (14) and (15) together with the expressions for pressures and fluid flow rates (Equations (6)–(8)). The dynamics due to the movements of the drill string is discussed in Section 7.2.

3. Description of the top side of a drilling operation

The top side of a drilling operation consist of a return line or drain back flow-line, a solid control system to remove the cuttings from the drill mud retrieved from the well and mud pits to store the drilling fluid at each section of the solid control system. The removal of solids is needed as the presence of cuttings in the drill mud can have adverse effects, for example: reduced penetrated rate caused by the formation of mud cakes near the drill bit, decreased bit life and increased rate of wear pump parts, greater difficulty in maintaining optimum rheological properties etc (Growcock and Harvey, 2005).

The setup of the solid control system is a step by step system where the return drill mud will be pumped into different equipment in order to remove the cuttings depending on their size. There are no standards for the arrangement of these equipment and they will change depending on the type of drill fluid in use and the type and size of the cuttings expected from the well-bore. In general, a shale shaker is situated at the beginning of the system and will remove most of the large to medium sized cuttings. The drilling fluid from the well may also contain entrained gas bubbles. To separate the gas from the drilling fluid, a degasser is installed after the main shale shakers.

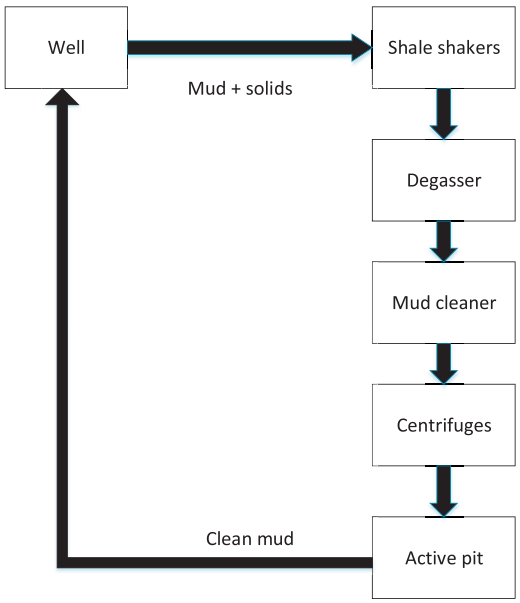

Fig. 2. A simplified block diagram of the top side flow loop.

Gumbo may be present in some wells, which are sticky drilled solids that hydrate as they move up the annulus forming groups of cuttings. The presence of gumbo will decrease the efficiency of the shale shakers, therefore some setups will include some type of gumbo removal equipment e. g. scalper shakers or gumbo traps before the main shale shakers.

The smallest cuttings that are less than two microns in size are removed using centrifuges, most commonly the decanting centrifuges. They are removed since these particles can increase the viscosity of the mud, thus making it difficult to maintain the desired value. Other equipment like mud cleaners, distillers and de-sanders are also commonly used to remove medium-size cuttings.

One common setup for the solid control system is shown in Fig. 2. Here the term active pit is used to refer to that partition of the mud pit (usually the last partition) where the drilling fluid is considered clean and connected to the intake line of the mud pump. After the shale shaker and between every equipment, the mud will be placed into different partitions of the mud pit setup. Each of these partitions are connected to each other through equalizers to avoid synchronization problems when turning the pumps on and off.

As the drill mud is processed by the solid control system, fluid losses will occur due to leakages and fluid retention on the cuttings disposed by the system. The amount of drill fluid loss depends on the efficiency of the solid removal system, the type of drilling fluid used and the size of the cuttings. The API has published guidelines on how to measure the drill fluid content from cuttings by retort analysis (API RP 13B-2). This value is normally between 5 and 15 percent by weight depending on the equipment (Johnston and Rubin, 2000). Note that since the density of the cuttings is usually higher than the density of the drill mud, the percentage of loses by volume will be higher.

Since the solid control system is both complex and has no standard arrangement, the system can be simplified to neglect the delay of the fluid though the solid control system. In cases where the delay is too big to be neglected, a delay model based on measurements is possibly the

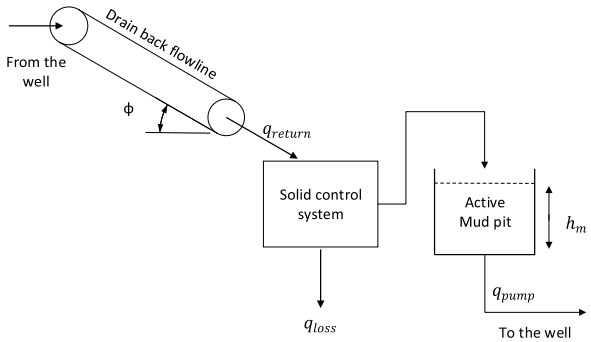

Fig. 3. Simplified model for the drain back.

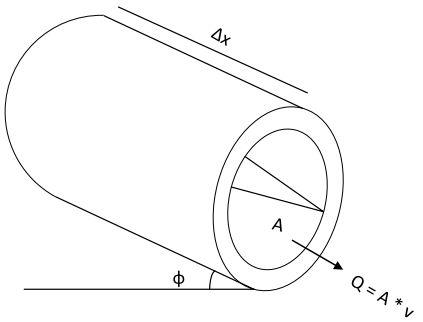

Fig. 4. Flow through a circular pipe.

best alternative to account for this delay. Fig. 3 shows a simplified block diagram of the top side operation during drilling. Different equipment used for cleaning the mud are lumped together as a single block and denoted as solid control system. The detailed dynamics of the fluid flow through the solid control system are too complex to be considered in the development of a simplified model for control and estimation and thus have been neglected. The fluid losses of the entire solid removal system is considered instead of each individual equipment and is denoted by q_{loss} in Fig. 3.

4. Mass balance and fluid losses in the top side

From the mass balance and considering the volumetric flow rates going in (q_{in}) and out (q_{out}) of the active pit, one can derive the following equation:

$$A_m\left(h_m\frac{d\rho_m}{dt}+\rho_m\frac{dh_m}{dt}\right)=\rho_{in}q_{in}-\rho_{out}q_{out} \tag{16}$$

Here A_m is the base area of the active mud pit, h_m is the level of the fluid inside the active mud pit and ρ_m is the density of fluid in the active mud pit. The outlet stream of the active pit goes through the mud pump and the back-pressure pump. Also, the tank agitators, mud guns and/or blenders are used to homogenize the drilling fluid inside the mud pits (Growcock and Harvey, 2005) so the contents of these can be assumed to be well mixed. Therefore, assuming a similar density ρ_d, the mass flow rate $\rho_{out}q_{out}$ can be expressed as follows,

$$\rho_{out}q_{out}=\rho_d(q_{pump}+q_{back}). \tag{17}$$

Some amount of fluid is lost from the return flow, at the drill cuttings removal processes. This happens due to three main reasons, one is the fluid loss with the discarded cuttings and the other two are the fluid losses by the mud retention and the losses due to the leakages. The rest of the return flow goes into the mid pit. Assuming the same density ρ_d, this can be written as follows,

$$\rho_d q_{return}=\rho_d(q_{in}+q_{loss}). \tag{18}$$

Inserting (17) and (18) into (16) gives

$$A_m\left(\rho_d\frac{dh_m}{dt}\right)=\rho_d q_{return}-\rho_d q_{loss}-\rho_d q_{pump}-\rho_d q_{back}. \tag{19}$$

Simplified equation:

$$\frac{dh_m}{dt}=\frac{1}{A_m}(q_{return}-q_{loss}-q_{pump}-q_{back}). \tag{20}$$

In practice, the solid control system will not be able to remove all the cuttings from the drilling fluid. This will cause the density of the mud to gradually increase inside the active pit. However, this can be expected to have very little impact to the fluid level inside the active mud pit. A better solution will be to update the value of the density at the active pit at time intervals. The fluid losses due to retention on cuttings would still need to be estimated.

5. Model of the drain back flow-line

The return line or drain back flow-line is the connector between the choke valve and the solid control system (see Fig. 3). The flow through the return line is at atmospheric pressure and is gravity driven. For modeling the flow rate flowing through the return line, it is assumed that the flow is an open channel flow. The cross-sectional area and length of the flow-line can vary depending on the installation. For this model, the flow-line is assumed to be a circular pipe with a given length, diameter and a small inclination. The most common way to represent the flow through such a pipeline is by using the Saint–Venant equations. These are a set of partial differential equations derived by the French engineer Adhémar Jean Claude Barré de Saint–Venant in 1871 (Chaudhry, 2008).

Consider an incompressible pipe flow through a prismatic channel with a wetted cross-sectional area A and a volumetric flow rate Q as shown in Fig. 4. The length of the channel is taken as Δx and the angle of inclination is ϕ. Both the wetted cross sectional area and the volumetric flow rate will change with time and position along the channel. Assuming no lateral inflow rates, the continuity equation can be written for the channel as follows,

$$\frac{\partial Q}{\partial x}+\frac{\partial A}{\partial t}=0. \tag{21}$$

For the momentum equation, the forces acting on the fluid are a frictional resistance of the channel acting along the channel, a force due to the change in static pressure acting horizontally and a gravitational force acting downwards. Applying momentum balance,

$$\rho A\Delta x\frac{dv}{dt}=\sum F \tag{22}$$

$$\rho A\Delta x\left(v\frac{\partial v}{\partial x}+\frac{\partial v}{\partial t}\right)=-\rho g\Delta x I\cos(\phi)-\rho g\Delta x A S_f+\rho g\Delta x A\sin(\phi) \tag{23}$$

Here, v is the velocity of fluid flowing through the channel, ρ is the density of the fluid, g is the gravitational constant S_f is the friction slope and I represents the first moment of area. Simplifying this will give the momentum balance of the Saint–Venant equations

$$\frac{\partial Q}{\partial t}+\frac{\partial}{\partial x}\left(\frac{Q^2}{A}+gI\cos(\phi)\right)=gA\sin(\phi)-gAS_f \tag{24}$$

The first moment of area term I for a channel can be written as

$$I(A)=\int_0^{h(A)}(h(A)-\tilde{z})w(\tilde{z})d\tilde{z} \tag{25}$$

where $w(\tilde{z})$ is the top width of the channel at an arbitrary position $\tilde{z}$ from a datum and h is the fluid level. In the case of a circular channel of diameter D, the top width can be written as

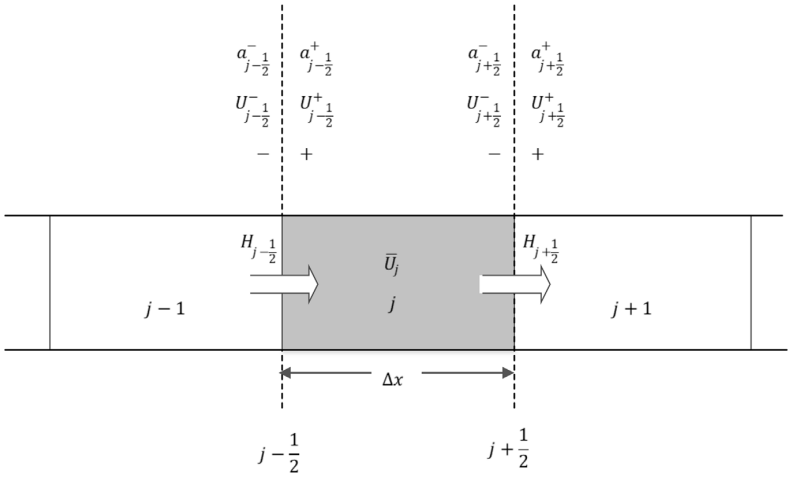

Fig. 5. Control volumes/cells.

$$w(\tilde{z}) = D\sin\frac{\theta}{2} = 2\sqrt{\tilde{z}D - \tilde{z}^2}, \tag{26}$$

where $\theta = 2\cos^{-1}\left(\frac{D-2\tilde{z}}{D}\right)$. By substituting the expression of $w(\tilde{z})$ in Equation (25) and solving could lead to the expression for I for a circular pipe in terms of its diameter (D) and the level of fluid in the pipe (h).

$$I = \int_h^h 2(h-\tilde{z})\sqrt{\tilde{z}D - \tilde{z}^2}\,d\tilde{z} \tag{27}$$

$$= \frac{1}{12}[\sqrt{\tilde{z}(D-\tilde{z})}(3D^2 - 6Dh + 2D\tilde{z} + 12h\tilde{z} - 8\tilde{z}^2)]_0^h$$
$$- \frac{1}{12}\left[3D^2(D-2h)\tan^{-1}\left(\sqrt{\frac{\tilde{z}}{D-\tilde{z}}}\right)\right]_0^h \tag{28}$$

$$I = \frac{1}{12}[(3D^2 - 4Dh + 4h^2)\sqrt{h(D-h)}]$$
$$- \frac{1}{12}\left[3D^2(D-2h)\arctan\frac{\sqrt{h}}{\sqrt{D-h}}\right] \tag{29}$$

For uniform flow of Newtonian fluids in channels of uniform cross section, the friction slope S_f can be represented by using the Mannings equation (Chow, 1959).

$$S_f = \frac{Q|Q|n_M^2 P_w^{\frac{4}{3}}}{A^{\frac{10}{3}}} \tag{30}$$

Here n_M is the Manning's roughness coefficient and P_w is the wetted perimeter. In the case of a circular channel, the wetted perimeter can be calculated in terms of the diameter of the channel and the fluid level (Chaudhry, 2008).

$$P_w = \frac{\theta D}{2} = D\cos^{-1}\left(\frac{D-2h}{D}\right) \tag{31}$$

To calculate the fluid level from the cross-sectional area of the flow, the non-linear equation (33) can be used (Chaudhry, 2008).

$$A = \frac{D^2}{8}(\theta - \sin\theta)$$
$$A = \left(\frac{D}{2}\right)^2\cos^{-1}\left(\frac{D-2h}{D}\right) - \left(\frac{D}{2} - h\right)\sqrt{h(D-h)} \tag{32}$$

In reality, the drilling fluids are non-Newtonian, but to simplify the model, the Manning's equation is used. The friction can also be estimated by using more complex models such as the Herschel-Buckley model.

In a compact form, equations (21) and (24) can be written as follows

$$\frac{\partial U}{\partial t} + \frac{\partial \mathcal{F}}{\partial x} = S \tag{33}$$

where U vector is the vector of conserved variables

$$U = (A, Q)^T \tag{34}$$

$\mathcal{F}$ is the vector of fluxes

$$\mathcal{F} = \left(Q, \frac{Q^2}{A} + gI\cos(\phi)\right)^T \tag{35}$$

And S is the source term

$$S = (0, gAsin(\phi) - gAS_f)^T \tag{36}$$

6. Numerical solution for the drain back flow-line model

The well model explained in Section 5 consists of a set of partial differential equations (PDEs). In particular, the Saint-Venant equation is a set of non-linear hyperbolic PDEs for which an analytical solution may be difficult to obtain. Therefore, the general practice is to use numerical methods for solving these PDEs. Some of the commonly used numerical methods are the method of characteristics, finite difference, finite element or finite volume methods. In this work, a finite volume method developed by Kurganov and Petrova (KP07 for short) (Kurganov and Petrova, 2007) is selected. This is a well developed, semi-discrete, second order and central upwind scheme, which has specifically been used to solve Saint–Venant systems (Bernstein et al., 2016; Bollermann et al., 2013). The scheme is based on the local speed of discontinuity propagation and it is able to preserve the positivity of the fluid levels. For more information about the development of this scheme refer to (Kurganov and Petrova, 2007) and (Sharma, 2015).

For implementing the numerical scheme, the return flow pipeline is divided into a number of control volumes or cells as shown in Fig. 5. The average value of the conserved variables at the center of each cell are calculated by applying the Reconstruct–Evolve–Average (known as REA) algorithm. With j representing the j^{th} control volume, the average of the conserved variables $\overline{U}$ at a time $t = t_n$ can be written as

$$\overline{U}_j^n = \frac{1}{\Delta x}\int_{x_{j-\frac{1}{2}}}^{x_{j+\frac{1}{2}}} U(x, t_n)dx. \tag{37}$$

With the use of the KP07 scheme the PDE model of equation (33) is discretized in space into a set of ordinary differential equations (ODEs) of equation (38).

$$\frac{d}{dt}\overline{U}_j = -\frac{H_{j+\frac{1}{2}} - H_{j-\frac{1}{2}}}{\Delta x} + \overline{S}(t) \tag{38}$$

$\overline{S}$ is the average value of the source term (36) calculated using the average values of the conserved variables. $H_{j\pm\frac{1}{2}}$ represent the fluxes flowing into the cell (minus sign) and out of the cell (plus sign) respectively. Assuming that there are no changes in the bed slope the fluxes are given by,

$$H_{j+\frac{1}{2}} = \frac{a^+_{j+\frac{1}{2}} \mathscr{F}\left(U^-_{j+\frac{1}{2}}\right) - a^-_{j+\frac{1}{2}} \mathscr{F}\left(U^+_{j+\frac{1}{2}}\right)}{a^+_{j+\frac{1}{2}} - a^-_{j+\frac{1}{2}}} + \frac{a^+_{j+\frac{1}{2}} a^-_{j+\frac{1}{2}}}{a^+_{j+\frac{1}{2}} - a^-_{j+\frac{1}{2}}}\left[U^+_{j+\frac{1}{2}} - U^-_{j+\frac{1}{2}}\right] \tag{39}$$

$$H_{j-\frac{1}{2}} = \frac{a^+_{j-\frac{1}{2}} \mathscr{F}\left(U^-_{j-\frac{1}{2}}\right) - a^-_{j-\frac{1}{2}} \mathscr{F}\left(U^+_{j-\frac{1}{2}}\right)}{a^+_{j-\frac{1}{2}} - a^-_{j-\frac{1}{2}}} + \frac{a^+_{j-\frac{1}{2}} a^-_{j-\frac{1}{2}}}{a^+_{j-\frac{1}{2}} - a^-_{j-\frac{1}{2}}}\left[U^+_{j-\frac{1}{2}} - U^-_{j-\frac{1}{2}}\right] \tag{40}$$

where the local speed of wave propagations $a^{\pm}_{j\pm\frac{1}{2}}$ can be calculated as the largest and smallest eigenvalues of the Jacobian of the system.

$$a^+_{j\pm\frac{1}{2}} = \max\left\{u^+_{j+\frac{1}{2}} + \sqrt{gh^+_{dj\pm\frac{1}{2}}}, u^-_{j+\frac{1}{2}} + \sqrt{gh^-_{dj\pm\frac{1}{2}}}, 0\right\} \tag{41}$$

$$a^-_{j\pm\frac{1}{2}} = \max\left\{u^+_{j+\frac{1}{2}} - \sqrt{gh^+_{dj\pm\frac{1}{2}}}, u^-_{j+\frac{1}{2}} - \sqrt{gh^-_{dj\pm\frac{1}{2}}}, 0\right\} \tag{42}$$

Here h_d is the hydraulic depth and is equal to the cross-sectional area of the flow divided by the top width of the flow (T) that is exposed to the atmospheric pressure ($h_d = A/T$). For circular channels

$$h_d = \frac{A}{2\sqrt{hD - h^2}} \tag{43}$$

7. Simulation results and discussion

The combined model *i.e.* the model for the bottom side drilling, model for the active mud pit level and the model of the drain back flow-line was simulated as a complete closed loop drilling system. The main motive for performing the simulations is to observe the complete system's (top side and the bottom side) dynamics simultaneously under common drilling operations.

During the drilling operation, different disturbances that affect the bottom hole pressure will occur. One such disturbance is the change in the hydrostatic pressure of the well caused by the changes in length of the well, by raising and lowering the drill string and during tripping. Another big disturbance occurs during a pipe connection procedure when extending the length of the drill string. During pipe connections, the mud pump is temporarily stopped to connect a new section of the drill string. If the pressure is not controlled, it can reach dangerously low levels resulting in a blowout.

The combined model was simulated for three drilling scenarios: (1) Movements of the drill string, (2) pipe connection, (3) a sudden influx of fluid from the reservoir. The parameters used for the simulations are listed in Table 1. For these scenarios, the density at the active mud pit was assume to be constant i. e. considering 100% efficiency of the solid control system and no fluid losses were taken into account. All simulations were done in MATLAB and Runge-kutta 4^{th} order integrator was used to solve the differential equations (6), (7), (9), (20) and (38).

Table 1
Parameters for simulation.

Parameter	Value	Description
V_d	42	Volume drill string $[m^3]$
β_d	14000	Bulk modulus drill string [bar]
β_a	14000	Bulk modulus annulus [bar]
$\overline{\rho}_d$	0.0121	Density annulus $[10^5 \times \frac{kg}{m^3}]$
$\overline{\rho}_a$	0.0124	Density drill string $[10^5 \times \frac{kg}{m^3}]$
F_d	0.16	Lumped friction term drill string $[10^6 \times \frac{bars^2}{m^6}]$
F_a	0.003	Lumped friction term annulus $[10^6 \times \frac{bars^2}{m^6}]$
M_a	1.5	$[10^8 \times \frac{kg}{m^4}]$
M_d	4.2	$[10^8 \times \frac{kg}{m^4}]$
h^0_{bit}	1825	Vertical depth at $t = 0$ $[m]$
L	15	Length flow-line $[m]$
D	0.5	Diameter flow-line $[m]$
$V_{pit} = A_m h_{m_0}$	8	Volume mud-pit at $t = 0$ $[m]$
ϕ	7	inclination flow-line [°]
n_M	0.02	Manning's roughness coefficient $\left[\frac{s}{\sqrt[3]{m}}\right]$
h_{m_0}	2	Initial level of the active mud pit $[m]$

7.1. Boundary conditions for the simulation of the drain back flow-line

In an open channel flow, different kinds of flow conditions can be defined depending on the flow velocity. If the flow velocity is equal to the velocity of a gravity wave with a small amplitude, the flow is called critical and the respective velocity is called the critical velocity. When the flow velocity is lower or higher than the critical velocity, the flow is called sub-critical or super-critical, respectively (Chaudhry, 2008).

During a normal drilling operation, the mud pumps will be pumping drill fluid into the well and these will normally have a high discharge rate. This might induce a high velocity in the flow through the open channel. It is therefore safe to assume that the flow through the drain back flow-line will be either super-critical or trans-critical (The KP07 scheme is capable of solving trans-critical flow). For trans-critical flows, one, two or three boundary conditions are needed depending on the flow situation. On the other hand, super-critical flows need two boundary conditions at the left boundary of the first control volume and none at the right boundary of the last control volume. In this case, boundary values for the discharge and the cross-sectional area of the flow are needed. Knowledge about the cross-sectional area of the flow at the start of the flow-line can be difficult and challenging. For simplifying the simulations, the discharge at the inlet of the drain back flow-line is selected as the only boundary condition which is considered to be finite. This means that the simulation has only one boundary condition at the upstream which is the value for the discharge from the choke valve calculated from equation (8). In a real operation, it is recommended to have a level sensor at the inlet of the drain back flow-line to precisely measure the fluid level and thus the wetted cross sectional area of the flow.

7.2. Movements of the drill string

One of the primary reasons behind simulating the movements of the drill string is to see how the flow rate of the fluid coming out of the well changes when drill string is moved either up or down with a given velocity. Furthermore, this changed flow rate will cause changes in the fluid level in the active mud pit (after certain transport delay captured by the distributed model *i.e.* open channel flow model). It is also of

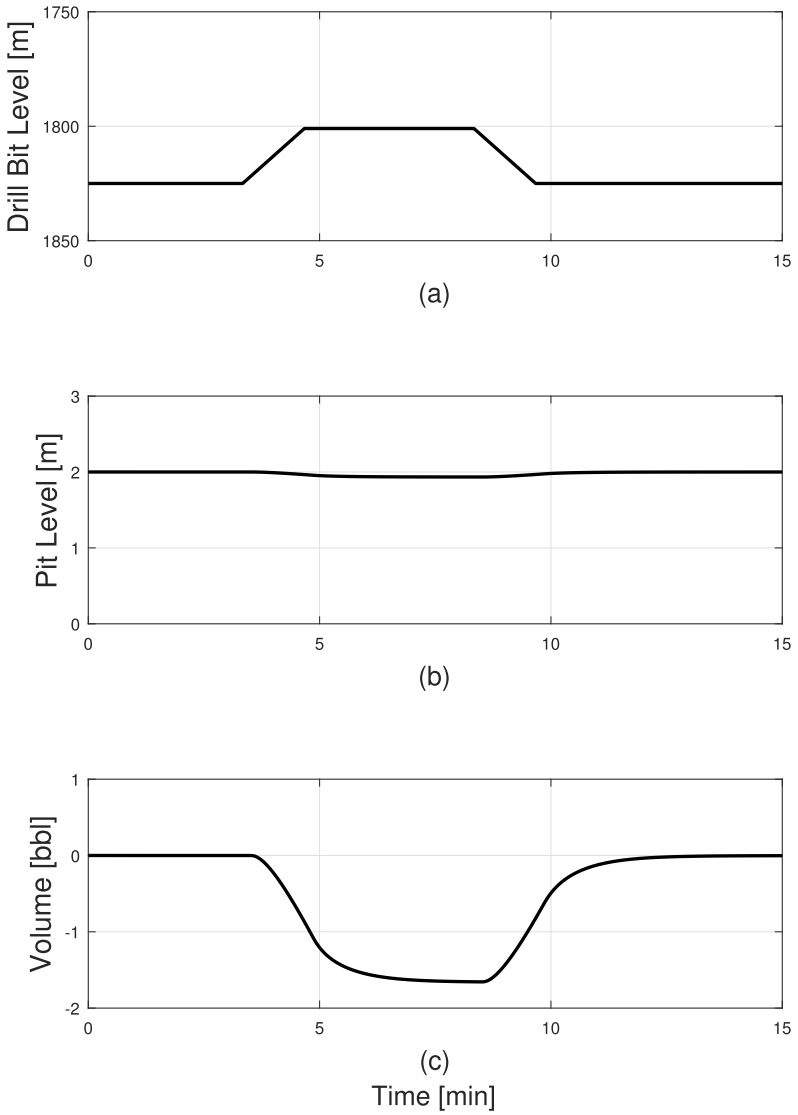

Fig. 6. Changes in the mud pit level (b) and volume (c) due to the movement of the drill string (a).

interest to see how the bottom hole pressure changes due to the drill string movement.

Movements of the drill string will cause the discharge from the well and thus from the choke valve to change. During swab the drill string is moved upwards from the well. This will decrease the discharge from the choke valve momentarily until the increased annulus volume is filled with drill mud. In contrast during surge, the drill string will be pushed downwards and into the well. This will cause a momentarily rise in the discharge from the choke valve as the excess liquid is squeezed out from the reduced annulus volume.

To observe the response of the average flow dynamics of the model to these two scenarios, the following two cases were simulated. The drill string was pulled from the well (swab) with a constant velocity of 18 m per minute at 200 s (3.33 min) and continued for 80 s as shown in Fig. 6(a). At 500 s (8.33 min), the drill string was pushed back into the well (surge) with the same constant velocity of 18 m per minute for 80 s. The discharge from the mud pump, the back-pressure pump and the opening of the choke valve were all kept constant during the simulation. Therefore, any changes in the simulations will happen only due to the variations in the annulus volume. The dynamics of the level of the fluid inside the mud pit under the two scenarios are shown in Fig. 6(b) and the changes in the drill mud volume of the active mud pit is shown in Fig. 6(c).

The simulation results showed that the level of the mud pit decreased while pulling the drill string from the well and the mud pit level increased when the drill string is pushed back into the well. The changes in the mud pit level will happen after a delay depending on the length and the friction of the drain back flow-line. This delay can be observed while looking at the changes in the discharge at the inlet and at the outlet of the drain back flow-line as shown in Fig. 7. The discharge at the first cell is the volumetric flow rate entering the flow-line from the choke valve and the discharge at the last cell is the volumetric flow rate exiting the pipe to the solid control system.

As the drill string is pulled from the well, the bottom hole pressure will decrease (see Fig. 8(b)). At the same time, the drilling fluid flowing through the bit will increase to fill the space left by the drill string (see Fig. 8(a)). The opposite happens when the drill string is pushed back into the well. The pressure at the bottom of the well will increase and

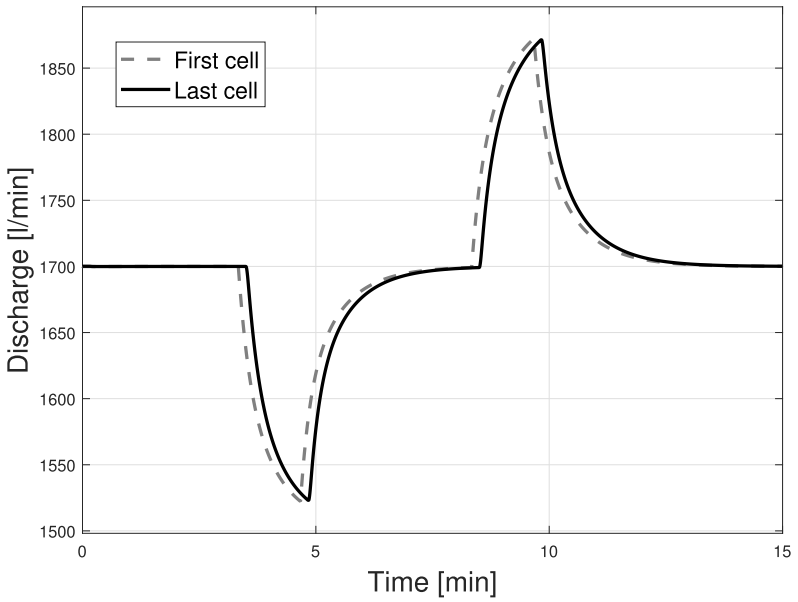

Fig. 7. Changes in the discharge of the flow-line (first and last cell) during the movement of the drill string.

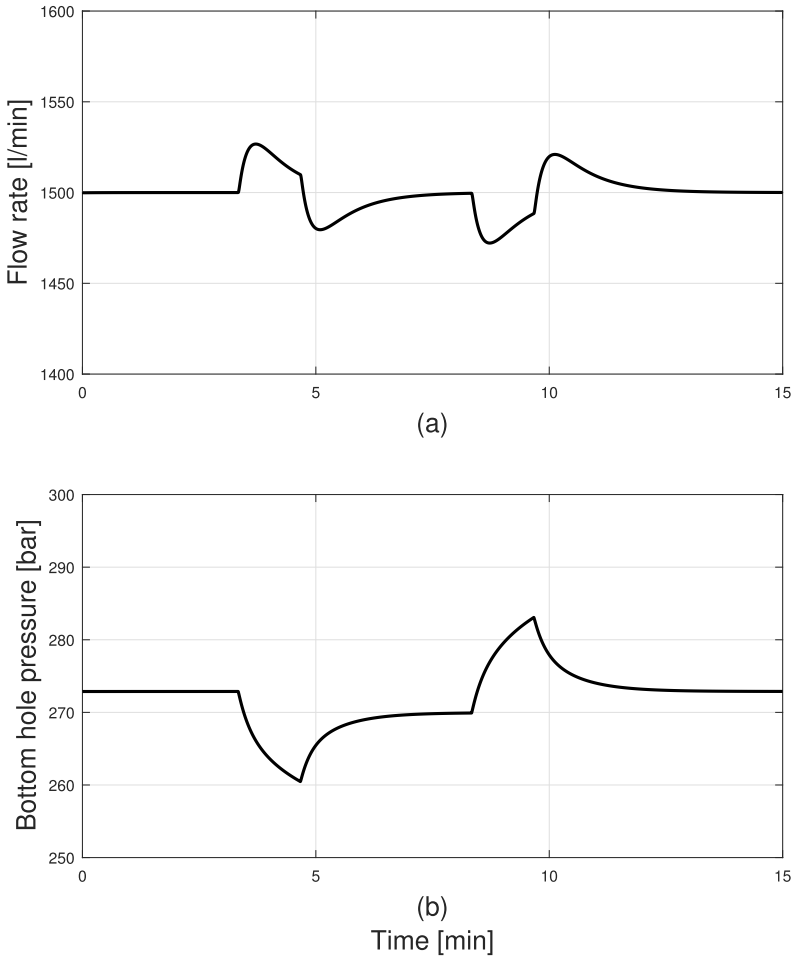

Fig. 8. Changes in the volumetric flow rate through the drill bit (a) the bottom hole pressure (b) during the movement of the drill string.

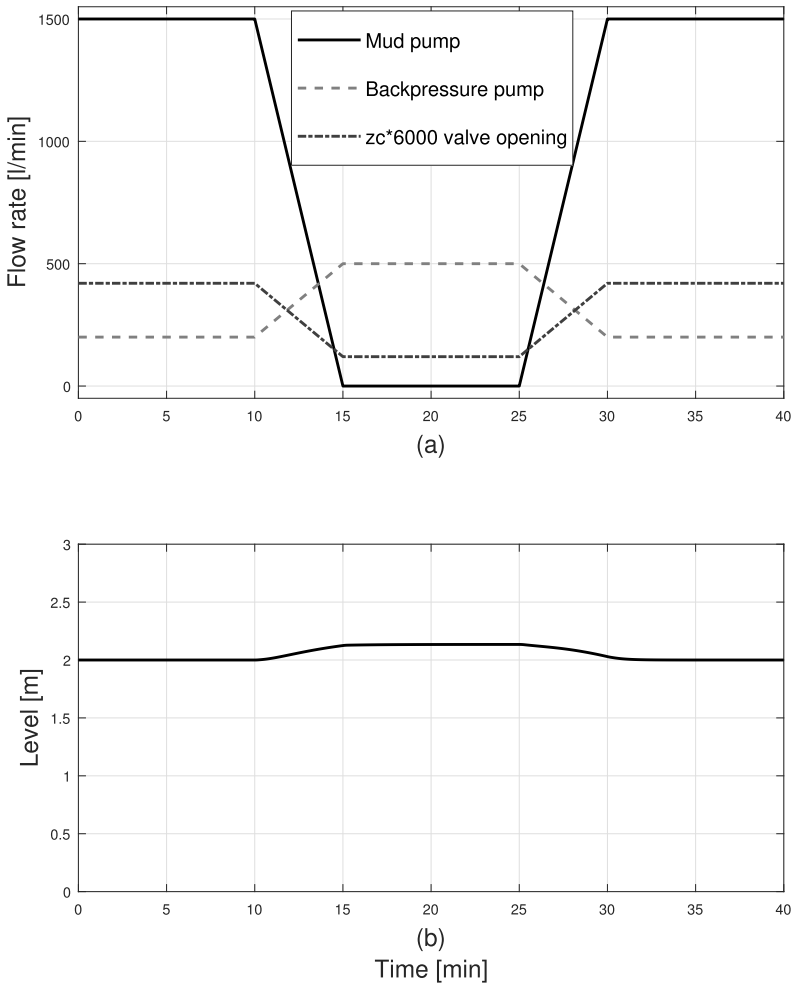

Fig. 9. Changes in the volumetric flow rates (a) and the mud pit level (b) during a pipe connection procedure.

the flow rate from the drill bit into the annulus will decrease as shown in Fig. 8.

7.3. Pipe connection scenario

The drill strings are manufactured as segments of ca. 27–30 feet length. When this length has been drilled, a new segment of the drill string has to be added to make it longer. The procedure of adding a new segment of the drill string is called pipe connection.

During a pipe connection, the bottom hole pressure has the risk to be reduced to dangerously low levels if it is not controlled properly. Because of this, it is important to have a good measure of the discharge from the drain back flow-line to detect if a kick has occurred. For connecting an extra segment of the drill string, the mud pump is ramped down to a zero flow rate to stop pumping the drill fluid into the annulus. This will decrease the discharge from the choke valve and consequentially the discharge to the drain back flow-line. The KP scheme does not work with a zero-flow rate *i.e.* complete dry channel, thus the back-pressure pump is used to have a non-zero flow rate in the flow-line an also to manually maintain the bottom hole pressure. In addition, the choke valve is also used for maintaining the pressure at the bottom of the well during pipe connection.

For simulating this scenario, the values for the opening of the choke valve, the back-pressure pump and the mud pump flow rates were set manually as shown in Fig. 9(a). The dynamics of the active mud pit level during a pipe connection procedure is shown in Fig. 9(b). It can be seen that the level of the mud pit will increase slightly as the mud pump is ramped down to zero flow rate. This is due to the difference in the inflow rate and the outflow rate of the active mud pit as shown in Fig. 10.

During a pipe connection, the bottom hole pressure will start decreasing when the mud pump stops pumping drill mud into the well if it is not controlled. To maintain the bottom hole pressure at a desired stable value and thus to avoid the reservoir fluid from entering the annulus, the flow rate from the back-pressure is increased and the opening of the choke valve is reduced as shown in Fig. 11(a). The changes in the bottom hole pressure during a pipe connection procedure are shown in Fig. 11(b). By manually manipulating the flow rates through back pressure pump and the choke valve as the control inputs, the resultant bottom hole pressure is maintained to lie between a chosen upper limit (fracture pressure) and a lower limit (collapse pressure).

7.4. Influx from the reservoir scenario

As the reservoir pore pressure is an uncertain value that can only be estimated, the risk for the occurrence of a kick cannot be neglected even in a well controlled environment. The value of the volumetric flow rate

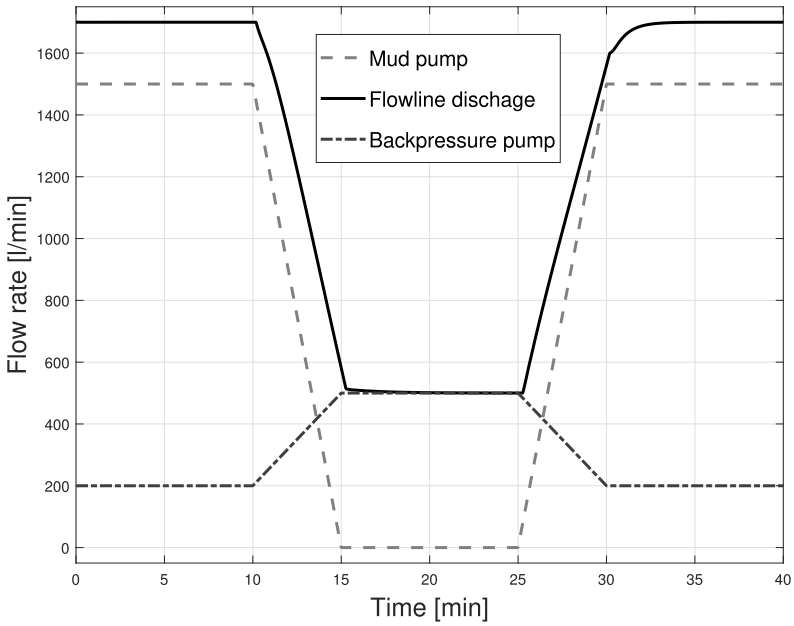

Fig. 10. Changes in the volumetric flow rates in and out of the active mud pit during a pipe connection procedure.

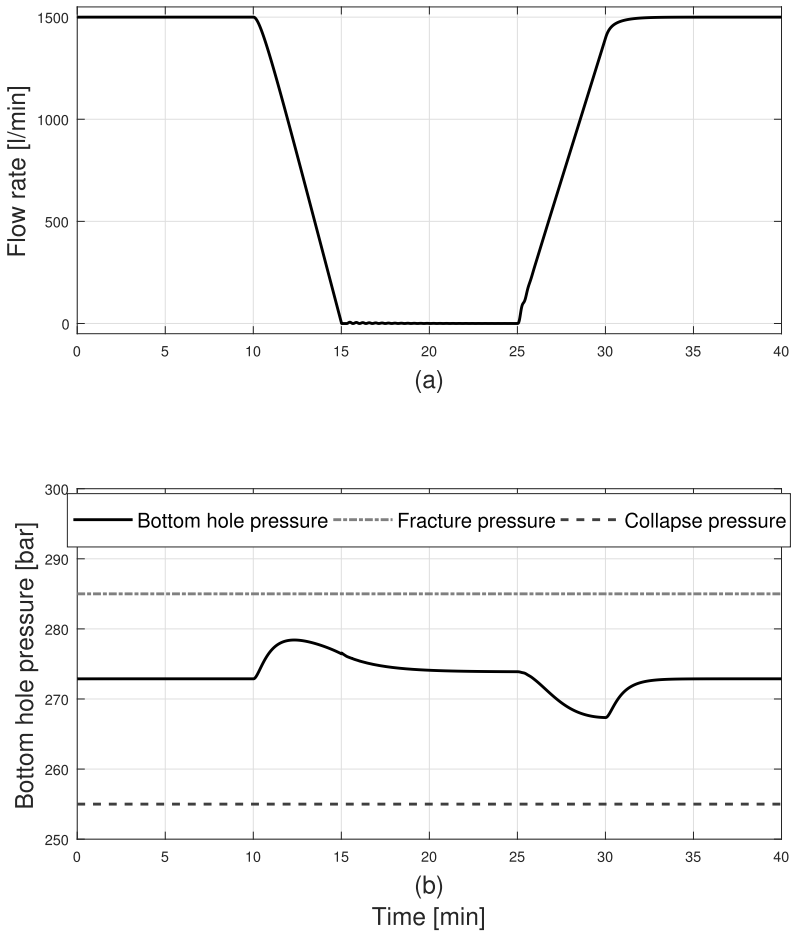

Fig. 11. Changes in the volumetric flow rates (a) and the bottom hole pressure (b) during a pipe connection procedure.

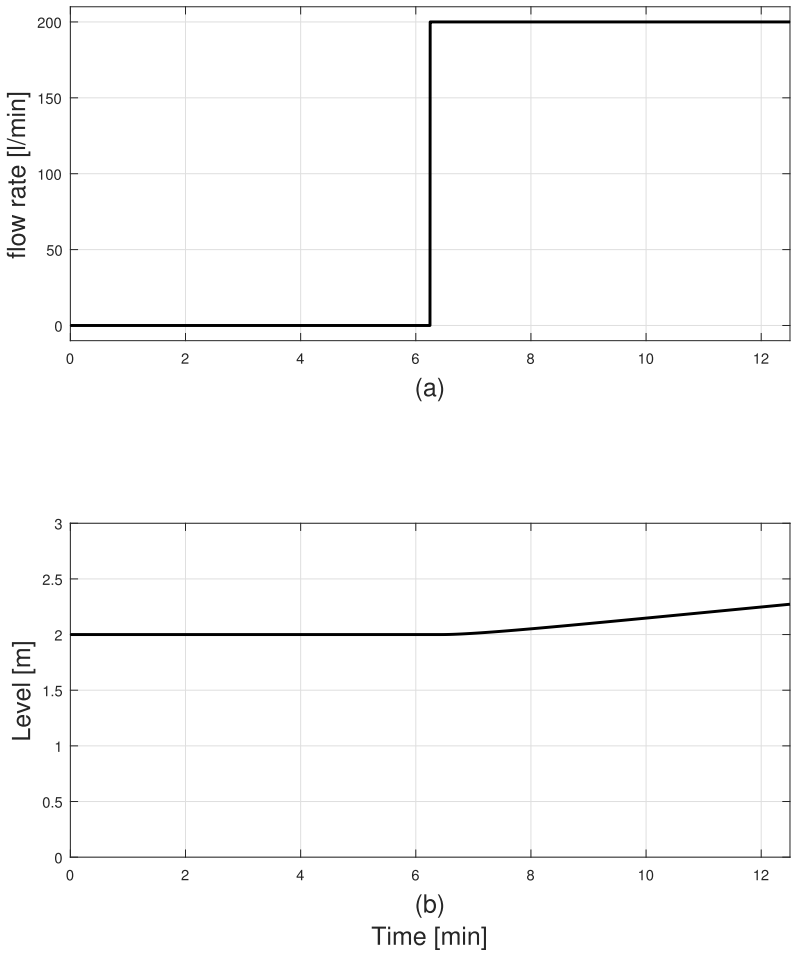

Fig. 12. Changes in the mud pit level (b) after an immediate influx from the reservoir(a).

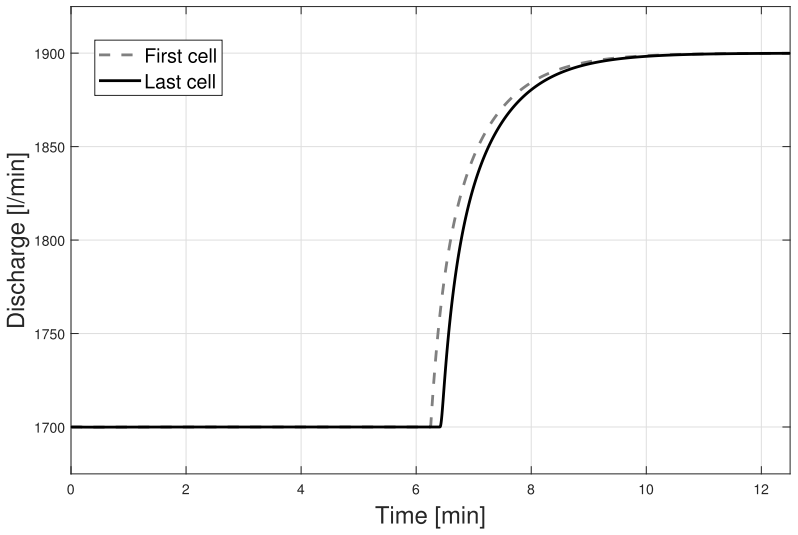

Fig. 13. Changes in the discharge of the flow-line (first and last cell) after an immediate influx from the reservoir.

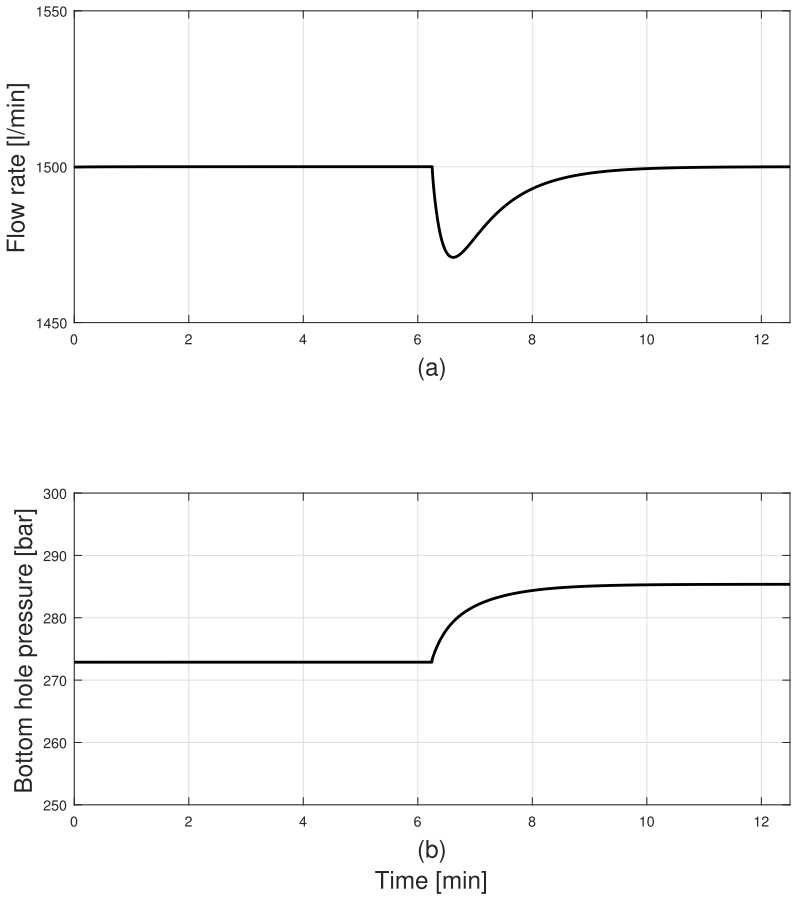

Fig. 14. Changes in the volumetric flow rate through the drill bit (a) and the bottom hole pressure (b) after an immediate influx from the reservoir.

from the reservoir following a kick are highly uncertain and can vary greatly. To simulate the combined model for a kick, a positive step change on the reservoir volumetric flow rate (q_{res}) equal to 200 l/min was applied as shown in Fig. 12(a). The dynamics of the active mud pit level under a kick is shown in Fig. 12(b). An important observation is the delay from the time the kick occurs to the time when the change in the level inside the active mud pit is noticed. It can be argued that if the active mud pit level alone is used for the detection of kick, then due to the delay in the observation of the level change, it may prove to be too late for the prevention of a blowout. Fig. 13 shows the delay through the drain back flow-line.

After a kick, the bottom hole pressure will quickly increase as shown in Fig. 14(b). Due to the increase in pressure at the bottom of the well, the flow rate through the drill bit into the annulus will immediately decrease as shown in Fig. 14(a). Assuming that the volumetric flow rate from the reservoir is constant, the flow rate through the drill bit will go back to its original value when the flow rate through the choke valve reaches steady state.

8. Conclusion

A dynamic model for the closed loop circulation of drilling mud from the mud pumps into the well and back again to the mud pits was developed. The model is based on conservation principles. It is simple and easy to implement. More importantly, it shows the dynamic behavior of both the bottom side and the top side of a drilling operation simultaneously. The combined model is described by a set of ODEs which makes it suitable for designing control systems. Furthermore, the model can also be used for states and parameter estimation and observer designs. In particular, the model can be used to estimate both the bottom hole pressure and the fluid losses through the solid removal system due to retention on cuttings. Accurate and fast estimation of the flow rate of fluid through the drain back pipeline and the changes in the mud pit volume probably is useful for early detection of a kick or loss.

Acknowledgment

The economic support from The Research Council of Norway and Statoil ASA through project no. 255348/E30 ‘Sensors and models for improved kick/loss detection in drilling (Semi–kidd)' is gratefully acknowledged.

Greek symbols

β_a Bulk modulus of the drilling mud at the annulus
β_d Bulk modulus of the drilling mud at the drill string

ϕ	Angle of inclination of the channel
ρ	Average density of the fluid in the channel
$\bar{\rho}$	Average density of the fluid in the main control volume
$\bar{\rho}_a$	Average density of the fluid at annulus
ρ_{cv}	Density of the fluid in the differential control volume
ρ_r	Density at the reference point
$\bar{\rho}_d$	Average density of the fluid at drill string
ρ_{in}	Fluid density of the inlet stream of active mud pit
ρ_m	density of fluid in the active mud pit
ρ_{out}	Fluid density of the outlet stream of active mud pit
θ	Angle made by the free surface on the center of the cross section of the channel

Roman symbols

A	Wetted cross sectional area of flow in the channel
A_a	Cross-sectional area of annulus
A_{cv}	Cross sectional area in the differential control volume
A_d	Cross-sectional area of drill string
$a^{\pm}_{j\pm\frac{1}{2}}$	Local speed of wave propagation into the cell (subscript minus sign) and out of the cell (subscript plus sign)
A_m	Base area of the active mud pit
D	Diameter of the circular pipe
F	General Forces acting on the flow
f	Darcy friction factor
$\mathcal{F}$	A vector of fluxes
F_a	Lumped frictional term at annulus
F_d	Lumped frictional term at drill string
F_f	Friction force acting on the differential control volume
F_g	Gravitation forces acting on the differential control volume
F_L	A lumped friction term for the main control volume
F_s	Forces acting on the surfaces of the differential control volume
g	Gravitational constant
h	Fluid level of the channel
h_{bit}	Depth of the drill bit
$H_{j\pm\frac{1}{2}}$	Fluxes flowing into the cell (minus sign) and out of the cell (plus sign)
h_d	Hydraulic depth of the flow
h_m	Fluid level inside the active mud pit
h_p	Depth (vertical) of the flow in the differential control volume
I	First moment of area on x direction
i	An arbitrary number
j	An arbitrary control volume
K	A dimensionless loss coefficient
k	An arbitrary number
K_c	Valve constant
l	Length of the main control volume
l_d	Length of the drill string
l_w	Length of the well
M	Mass matrix
m	Number of major losses
M_a	Mass matrix for annulus
M_b	Mass matrix for drill string
n	An arbitrary time
n_M	Manning's roughness coefficient
p	pressure in the differential control volume
Δp_f	Total pressure loss due to friction
Δp_{maj}	Major pressure loss inside a pipe
Δp_{min}	Minor pressure loss
p_0	Atmospheric pressure
p_{bit}	Bottom hole pressure
p_c	Choke pressure
p_p	Pump pressure
p_r	Pressure at the reference point
P_w	Wetted perimeter of the channel
Q	Volumetric flow rate in the channel
q	Volumetric flow rate of the main control volume
q_{back}	Volumetric flow rate through the back pressure pump
q_{bit}	Volumetric flow rate through the drill bit

q_{choke}	Volumetric flow rate through the choke valve
q_{in}	Volumetric flow rate going into the active mud pit
q_{loss}	Losses of volumetric flow rates from the solid control system
q_{out}	Volumetric flow rate going out of the active mud pit
q_{pump}	Volumetric flow rate through the mud pump
q_{res}	Volumetric flow rate of the reservoir influx/outflux
q_{return}	Return flow rate
r	Number of minor losses
S	A vector of source terms
$\overline{S}$	Average value of the source terms
S_f	Friction slope in the channel
T	Top width of the flow
t	Time
T	Temperature of the fluid
T_r	Temperature at the reference point
U	A vector of conserved variables
u	Velocity of the fluid in the differential control volume
$\overline{U}$	Average value of the conserved variables
V	Volume of the main control volume
v	Velocity of fluid in the channel
V_a	Volume in the annulus
v_{drill}	Velocity of the drill string
V_d	Volume in the drill string
w	Top width of the fluid surface at any vertical position in the channel
x	Differential length along the flow direction
$\tilde{z}$	An arbitrary vertical position from the datum, in the channel
	Normalized valve opening

Appendix

The derivation of the Equation (9) which is described in detail in (Stamnes, 2007; Kaasa, 2007; Kaasa et al., 2012) is summarized here. A differential control volume of the drill string/annulus is taken as shown in Figure A.1.

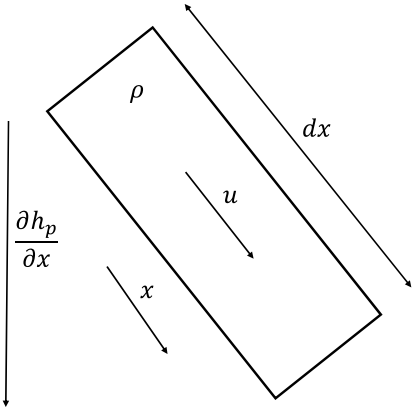

Fig. A.1. A differential control volume.The momentum balance along the x direction for the differential control volume can be written as follows,

$$\sum F = \rho_{cv} \frac{du}{dt} A_{cv} dx, \tag{A.1}$$

where F is the general forces acting on the differential control volume, u is the velocity and A_{cv} is the cross sectional area of the differential control volume. The density of the fluid in the differential control volume ρ_{cv} is taken as constant inside the control volume, neglecting the spatial time variance of the density in the momentum equation. The assumption of incompressibility is considered valid for fluid flows which have a Mach number less than 0.3 (White, 2011). The forces acting on the differential control volume are the surface stresses (F_s which include the hydrostatic pressure gradient and the friction) and the gravity forces (F_g). Therefore, the sum of forces can be written as follows,

$$\sum F = F_s + F_g, \tag{A.2}$$

where

$$F_s = -\frac{\partial p}{\partial x} A_{cv} dx - \frac{\partial F_f}{\partial x} dx, \tag{A.3}$$

and

$$F_g = \rho_{cv} g \frac{\partial h_p}{\partial x} A_{cv} dx. \tag{A.4}$$

Here, p is the pressure inside the differential control volume, h_p is the depth (vertical) of the differential control volume and F_f is the friction force. Combining these expressions with Equation (A.1) the following equation can be obtained.

$$\rho_{cv} \frac{du}{dt} dx = -\frac{\partial p}{\partial x} dx - \frac{1}{A_{cv}} \frac{\partial F_f}{\partial x} dx + \rho_{cv} g \frac{\partial h_p}{\partial x} dx \tag{A.5}$$

Interpreting the velocity in terms of volumetric flow rate (q) and then integrating over the flow path *i.e.* one of the main control volumes, drill string or the annulus, the equation becomes as follows,

$$\int_0^l \frac{\rho_{cv}}{A_{cv}} \frac{dq}{dt} dx = -\int_{p(0)}^{p(l)} dp - \int_0^l \frac{1}{A_{cv}} \frac{\partial F_f}{\partial x} dx + \int_{h_p(0)}^{h_p(l)} \rho_{cv} g \, dh_p, \tag{A.6}$$

where l is the length of the flow path/main control volume. Average density ($\bar{\rho}$) is defined as follows,

$$\bar{\rho} = \frac{1}{V} \int_0^l \rho_{cv} A_{cv} dx, \tag{A.7}$$

and used in the Equation (A.6).

$$\int_0^l \frac{\bar{\rho}}{A_{cv}} \frac{dq}{dt} dx = p(0) - p(l) - \int_0^l \frac{1}{A_{cv}} \frac{\partial F_f}{\partial x} dx + \bar{\rho} g \{h_p(l) - h_p(0)\} \tag{A.8}$$

The pressure loss due to the friction (Δp_f) is expressed by the term $\int_0^l \frac{1}{A_{cv}} \frac{\partial F_f}{\partial x} dx$ in the Equation (A.8) and the $\frac{\partial F_f}{\partial x}$ can be identified as a friction gradient, which depends on the Reynolds number, density and the geometry (White, 2011). Since the drilling fluid flow inside the well is dynamic, this friction gradient will also be dynamic, hence complex and difficult to evaluate. To avoid this complexity, the pressure loss due to friction is expressed using a lumped friction term which consists of the major and minor losses as stated by (Merrit, 1967; Manring, 2005). Major or minor losses are not representative of the magnitudes by any means. Major losses are the frictional losses that could occur over a straight sections of pipe due to viscous dissipation, turbulence or/and swirl flow. Whereas the minor losses accounts for all frictional losses that can occur due to non–ideal flow conditions at restrictions, section changes, bends and valves (Kaasa et al., 2012). A major pressure loss inside a pipe (Δp_{maj}) can be expressed using the Darcy friction factor (f) as follows (Manring, 2005),

$$\Delta p_{maj} = \frac{fl}{2D} \bar{\rho} |u| u. \tag{A.9}$$

Similarly, the minor losses (Δp_{min}) are expressed using a dimensionless loss coefficient (K) as follows (Merrit, 1967; Manring, 2005),

$$\Delta p_{min} = \frac{K}{2} \bar{\rho} |u| u. \tag{A.10}$$

Now, the total pressure drop due to friction inside the drill string/annulus is the sum of all major and minor losses.

$$\Delta p_f = \sum_{i=1}^{m} \frac{f_i l_i}{2D_i} \bar{\rho} |u_i| u_i + \sum_{k=1}^{r} \frac{K_k}{2} \bar{\rho} |u_k| u_k \tag{A.11}$$

Here, m number of major losses and r number of minor losses are assumed and i, k are arbitrary numbers where $i = 1, 2, \ldots, m$ and $k = 1, 2, \ldots, r$, respectively. Using the volumetric flow rate, the Equation (A.11) can be re–written as follows,

$$\Delta p_f = \left[\sum_{i=1}^{m} \frac{f_i l_i}{A_i^2 D_i} + \sum_{k=1}^{r} \frac{K_k}{A_k^2} \right] \frac{\bar{\rho} |q| q}{2}, \tag{A.12}$$

where q is the respective volumetric flow rate either in drill string or annulus, and A_i, A_k are the cross sectional areas of the respective pipe sections. A lumped friction term (F_L) can be defined from Equation (A.13) as follows,

$$F_L = \left[\sum_{i=1}^{m} \frac{f_i l_i}{A_i^2 D_i} + \sum_{k=1}^{r} \frac{K_k}{A_k^2} \right] \frac{\bar{\rho}}{2}, \tag{A.13}$$

which is a dynamic friction term that depends on the operating conditions. For the drill string this lumped friction term is introduced as F_d and for the annulus as F_a, with their respective diameters and cross sectional areas. The values for F_a and F_d (in Table 1) are taken from the calibrated parameters using both top and bottom side measurements by (Stamnes, 2007; Kaasa et al., 2012), further in (Kaasa et al., 2012), an adaptive observer has been used to estimate these friction terms and they were compared with experimental data.

The pressure loss due to friction can now be written in simple terms as follows,

$$\Delta p_f = F_L |q| q. \tag{A.14}$$

Now replacing the pressure loss due to friction in Equation (A.8) by the new term, the following equation can be obtained.

$$\int_0^l \frac{\bar{\rho}}{A_{cv}} \frac{dq}{dt} dx = p(0) - p(l) - F_L |q| q + \bar{\rho} g \{h_p(l) - h_p(0)\} \tag{A.15}$$

For the drill string the equation is as follows,

$$\int_0^{l_d} \frac{\overline{\rho_d}}{A_d} \frac{dq}{dt} dx = p_p - p_{bit} - F_d |q_{bit}| q_{bit} + \overline{\rho_d} g h_{bit}. \tag{A.16}$$

Similarly, for the annulus,

$$\int_0^{l_w} \frac{\overline{\rho_d}}{A_d}\frac{dq}{dt}dx = p_{bit} - p_c - F_a|q_{bit} + q_{res}|(q_{bit} + q_{res}) - \overline{\rho_a}gh_{bit}. \tag{A.17}$$

With the definitions in Equations (10) and (11) the following equations can be obtained.

$$M_d\dot{q}_{bit} = p_p - p_{bit} - F_d|q_{bit}|q_{bit} + \overline{\rho_d}gh_{bit} \tag{A.18}$$

$$M_a(\dot{q}_{bit} + \dot{q}_{res}) = p_{bit} - p_c - F_a|q_{bit} + q_{res}|(q_{bit} + q_{res}) - \overline{\rho_a}gh_{bit} \tag{A.19}$$

Assuming that q_{res} is a constant and combining with the Equation (12), the two equations (Equation A.18 and A.19) can be summed up as follows,

$$M\dot{q}_{bit} = p_p - p_c - F_d|q_{bit}|q_{bit} - F_a|q_{bit} + q_{res}|(q_{bit} + q_{res}) + (\overline{\rho_d} - \overline{\rho_a})gh_{bit}, \tag{A.20}$$

to obtain the Equation (9) mentioned in the main section.

References

Bernstein, A., Chertock, A., Kurganov, A., 2016. Central-upwind scheme for shallow water equations with discontinuous bottom topography. Bull. Braz. Math. Soc. 47 (1), 91–103. http://dx.doi.org/10.1007/s00574-016-0124-3.

Bollermann, A., Chen, G., Kurganov, A., Noelle, S., 2013. A well-balanced reconstruction of wet/dry fronts for the shallow water equations. J. Sci. Comput. 56 (2), 267–290. http://dx.doi.org/10.1007/s10915-012-9677-5.

Bourgoyne, A., Millheim, K., Chevevert, M., Young, F., 1986. Applied Drilling Engineering, first ed. vol. 2 Society of Petroleum Engineers.

Chaudhry, M.H., 2008. Open-channel Flow, second ed. Springer.

Chow, V.T., 1959. Open-channel Hydraulics. McGraw-Hill, New York.

Grace, R., 1994. Advanced Blowout & Well Control, first ed. Gulf Publishing Company.

Growcock, F., Harvey, T., 2005. Drilling Fluids Processing Handbook, first ed. Gulf Professional Publishing.

Johnston, C.A., Rubin, M., 2000. Development document for final effluent limitations guidelines and standards for synthetic-based drilling fluids and other non-aqueous drilling fluids in the oil and gas extraction point source category. Tech. Rep Enviromental Protection Agency.

Kaasa, G.O., 2007. A simple dynamic model of drilling for control. Tech. Rep Statoil hydro Research center.

Kaasa, G.-O., Stamnes, Ø.N., Aamo, O.M., Imsland, L., 2012. Simplified hydraulics model used for intelligent estimation of downhole pressure for a managed-pressure-drilling control system. SPE Drill. Complet. 27 (01), 127–138. http://dx.doi.org/10.2118/143097-PA.

Kurganov, A., Petrova, G., 2007. A second-order well-balanced positivity preserving central-upwind scheme for the saint-venant system. Commun. Math. Sci. 5 (1), 133–160.

Manring, N., 2005. Hydraulic Control Systems. Wiley.

Merrit, H.E., 1967. Hydraulic Control Systems. John Wiley & Sons, New York.

Sharma, R., 2015. Second Order Scheme for Open Channel Flow, Technical Report, Telemark Open Research Archive (TEORA). University college of Souteast Norway, Porsgrunn, Norway. http://hdl.handle.net/2282/2575.

Stamnes, Ø.N., 2007. Adaptive Observer for Bottomhole Pressure during Drilling. Msc thesis. Norwegian University of Science and Technology.

White, F.M., 2011. Fluid Mechanics, seventh ed. McGraw-Hill,New York.

Doctoral dissertation no. 44
2019
—

Models and Estimators for Flow of Topside Drilling Fluid

Dissertation for the degree of Ph.D

—

Asanthi Jinasena

—

ISBN: 978-82-7206-529-3 (print)
ISBN: 978-82-7206-530-9 (online)

usn.no